Evaluation of Raman Spectroscopy for Fracture Resistance Assessment

By

Alexander James Makowski

Dissertation

Submitted to the Faculty of the

Graduate School of Vanderbilt University

in partial fulfillment of the requirements

for the degree of

DOCTOR OF PHILOSOPHY

in

Biomedical Engineering

December, 2014

Nashville, Tennessee

Approved:

Jeffry S. Nyman, Ph.D.

Anita Mahadevan-Jansen, Ph.D.

E. Duco Jansen, Ph.D.

Florent Elefteriou, Ph.D.

Jeffrey M. Davidson, Ph.D.

To Johanna, my wife, my muse, and my one true love,

without whose support this would not have been possible.

ACKNOWLEDGEMENTS

This work was made possible by the financial support of Department of Veteran's Affairs Research Service, as well as grants from the National Institutes of Health, the National Science Foundation, and the Department of Defense. Funds and equipment from the Biophotonics Laboratories, the Vanderbilt Center for Bone Biology, the Vanderbilt Institute of Imaging Science, and the Vanderbilt University Medical Center Department of Orthopaedic Surgery and Rehabilitation were also instrumental in the completion of this dissertation.

I would like to thank my advisor Dr. Jeffry S. Nyman for his help and guidance over the last 4 years. My committee members Dr. Anita Mahadevan-Jansen, Dr. E. Duco Jansen, Dr. Florent Elefteriou, and Dr. Jeffrey M. Davidson each welcomed me into their laboratories and took the time to train me in their individual fields, beyond guiding me through the dissertation process. Other members of Vanderbilt Center for Bone Biology: Dan Perrien, Xiangli Yang, and Julie Sterling took great interest in my training and helped me overcome the difficulties of intertwining biological research with my engineering training. Dr. Jon Schoenecker and Dr. Ginger Holt took special interest in my dissertation and the potential application of my research to orthopaedic surgery, helping me to guide the work towards the interest of the surgical audience. My mentors have become like a second family.

I was fortunate to be trained as an undergraduate at the Vanderbilt Institute for Integrated Biosystems Research and Education. My thanks to Dr. John Wikswo, Dr. Franz Baudenbacher, Dr. Kevin Seale, Ron Reiserer, Phil Samson and Dmitri Markov, for training me in instrumentation, laboratory skills, and prototyping techniques, as well as consistently providing

access to the facilities(and their expert brains) to build, repair, and customize equipment throughout my thesis studies.

I was fortunate to work with excellent postdoctoral scholars and staff who have become close friends. Dr. Chetan Patil and Isaac Pence are excellent researchers and friends. I am truly blessed to have such friends that would come at night in bad weather to help you work underground in the dark, often with either dangerous equipment or biohazard samples. Sasidhar Uppuganti and Dr. Mathilde Granke have been a constant source of reliable support both in the lab and personally. I was also fortunate to train dedicated and committed undergraduate volunteers in Ahbid Zein-Sabatto and Meredith Huszagh, who were eager and willing to learn as well as put in the hours to truly contribute to a research project.

Finally, I would like to thank my family for their love and support throughout my education and my graduate studies. Specifically, my loving wife Johanna has supported me financially, emotionally, and even in the lab. She moved away from a great job and a supportive environment to Nashville to support me. I would not have had the success I do today without her undying support and love. She has listened to countless presentations, proofread documents, labeled samples, operated machines, made delicious meals and consoled grumpy scientists (not just me) when experiments weren't working. She provides unending motivation and drive to succeed by example and I am lucky to have made this journey with her at my side.

TABLE OF CONTENTS

LIST OF FIGURES

LIST OF TABLES

CHAPTER 1

INTRODUCTION

1.1 Goals

This thesis seeks to determine whether Raman Spectroscopy (RS) can assess biochemical changes that help explain differences in the fracture resistance of bone among different laboratory models of disease. Identifying spectral signatures will later determine the potential of RS as a fracture risk assessment tool. The work measures bone mechanical properties a rigorous universal standard of mechanical testing to determine fracture resistance for both animal models of genetic disease and donated human tissue across genders and all decades of adulthood. Specific studies will detail the discrimination between, and ultimately isolation of the different sources of RS signal contrast in bone tissue as they relate to tissue organization and composition. These sources of contrast are then evaluated side-by-side as well as combined to demonstrate consistency in the RS signatures of decreased bone mechanical quality across unrelated models of brittle bone. Finally, the results of these studies are applied to the complex organizational hierarchy of human bone tissue to determine if RS detects any driving factors in the age-related decrease in fracture resistance. Ultimately this dissertation will provide the groundwork to determine the feasibility of RS for clinical use in fracture resistance assessment, yielding optimized outcome metrics and suggestions for instrumentation and data collection parameters.

1.2 Motivation

Bone health deteriorates as we age, and the subsequent loss of tissue mechanical properties leads to an increased risk of fracture. Ultimately developing into osteoporosis, the age-related loss in fracture resistance results in over 9 million annual osteoporotic fractures worldwide [1]. Although incident rates alone are not as significant as other major diseases including atherosclerosis and diabetes, the World Health Organization places osteoporotic fracture as the 6th largest source of disease burden in number of years lost [1]. The most worrisome statistic, however, is that the many patients die within one year of hip fracture, with estimates as high as 30%[2]. Current clinical analyses are largely limited to X-ray based mineral density scans[3] and patient history for concomitant risk factors including diabetes[4, 5], neither of which fully captures age-related trends in fracture risk[6]. The idea of "bone quality" [7]was invented to encompass these factors beyond mineral density. The ability of Raman Spectroscopy(RS) to concurrently measure both the mineral and collagen phases of bone, coupled with nondestructive and non-invasive potential as shown in other clinical applications, makes the technique a strong candidate to complement mineral density and help explain bone quality to improve our understanding of fracture risk. Therefore, the overall objective of this doctoral dissertation is to define the mechanisms by which Raman Spectroscopy can optically diagnose decreased bone quality: first by identifying the sources of signal contrast, then by establishing the consistency and nature of RS signatures in controlled animal models, and finally by applying those findings to the study of age-related changes in fracture resistance.

1.3 Specific Aims

The current milieu of inconsistent instrument designs, outcome metrics, and disease conditions in many of the prominent studies of Raman Spectroscopy for bone [8-10] leaves an inconsistent picture of the role of RS for detection of fracture resistance. Can Raman Spectroscopy help the field gain a better understanding of the elusive factors underlying fracture resistance? If so, could the diagnostic mechanism of contrast between "good" and "bad" bone quality be translated into a clinical instrument? What is responsible for the apparent inconsistency between studies using RS to discriminate decreased bone quality? To fully answer any of these questions could result in more than a lifetime of dedicated study; therefore, to better delineate the first and most significant steps, I drew up the following specific aims:

1. **Establish RS sensitivity to differences in composition with respect to organization.by correlating polarization effects to bone orientation effects on relative peak intensities.** At the outset of this dissertation, there were significant questions regarding the best way to acquire RS data for the proper characterization of bone quality, including specimen preparation techniques, RS processing techniques, and the validity of established RS outcomes in the field. Moreover, RS techniques in our lab could not explain differences in multiple available models of brittle bone. Finally, the concurrent reports that polarization in the Raman spectrum highlighted lamellar structures [11] cast doubt upon the validity of RS peak ratios. This goal of this aim (written as Chapter 3) was to resolve these seeming conflicts in light of polarization theory, establishing whether RS measures of composition could be separated from RS metrics that are also sensitive to polarization and therefore organization. Success of this aim was defined qualitatively as the optimization of RS metrics

for either organization or composition, such that compositional metrics minimize the coefficient of variation under different polarizations or rotation.

2. **Assess RS capability to explain fracture resistance differences due to genetic manipulation (mice) and aging (human).**

   a. **Characterize RS correlation to downstream biomechanics as a function of transcription factor deletion.**

Numerous environmental factors combine with lifestyle choices, concomitant disease[4], and genetic predisposition [5]to determine human fracture risk, making the study human risk nontrivial. To better understand the mechanisms underlying disease progression, the study of rare genetic diseases that present with musculoskeletal defects offers unique insights into the biological underpinnings of bone quality. Genetically altered animal models offer scientific control, while recapitulating one specific aspect of the human condition.

Having optimized the polarization sensitivity of RS to organization and composition, this aim focuses on re-evaluating the potential of RS to characterize toughness loss in animal models. The goal of Aim 2a is to identify the Raman metrics that explain brittleness (peak intensities, ratios, and multivariate signatures) in animal models of compromised bone mechanical quality. Since RS of composition alone had failed to explain toughness loss at the time of proposal, success was defined as any significant explanation of the variance in toughness, with greater than 25% variance explained meriting further experimentation. Success in the original transcription factor deletion model (Atf4 or activation transcription factor 4, written in Chapter 4) led to application of the methods to another model of brittleness (deletion of theMmp9 gene) for which compositional RS metrics alone had been

insufficient (Chapter 5). This aim also extends the polarization analysis to a multivariate expression of the complete spectrum in order to include all polarization and spectral information, instead of just specific peaks and peak ratios, since these original outcomes used by the field were established for their stability in measuring composition.

b. Correlate microstructure fracture resistance to RS property mapping.

With established metrics and methods, it became important to determine if polarization in RS properties could distinguish natural microstructural differences in bone beyond what was previously shown[11], and if so, to what extent did this microstructural contrast correspond to the age-related decrease in fracture resistance (Chapter 6). Fracture toughness was implemented as part of these studies to ensure state-of-the-art physiologically relevant laboratory analogues to quantify fracture resistance. RS mapping of microstructural components provided a strong measure of tissue heterogeneity which is under debate as a potential mechanism underlying fracture resistance [12], but until now, little quantitative evidence has been demonstrated. Thus the goal of Aim 2b was to quantify RS metrics that explain the age-related decrease in human fracture toughness, using both point measures and RS mapping. Because concurrent analyses of mineral density and novel modalities including NMR and micro-indentation were concurrently conducted on these samples, success of this aim was defined as the significant correlation to fracture outcomes, with performance in excess of the variance explained by mineral density.

1.4 Dissertation Outline

This dissertation has been organized with the following structure:

Chapter 1 provides a brief introduction to the main problem addressed by the research, while establishing the motivation to conduct the included studies and larger goals of the research project. The specific research aims are defined and explained.

Chapter 2 provides background information including bone and its roles in systems physiology; the engineering perspective of bone as a structural material; current clinical diagnostics for fracture risk; biomechanical testing and its relationship to fracture mechanics; and Raman spectroscopy for the diagnosis of bone quality, with a specific emphasis on the use of polarization to determine tissue organization.

Chapter 3 entails the work accomplished in Specific Aim 1, detailing the experimental procedure and results behind isolating the impact of composition and organization in Raman spectroscopy with respect to the inherent polarization of commercial instruments and the optical theory of light transport through birefringent materials.

Chapter 4 applies the use of polarization Raman spectroscopy in order to identify the underlying mechanism behind bone brittleness due to the loss of activation transcription factor 4 (Atf4), detailing how organization-sensitive metrics show associated changes, while traditional compositional metrics were limited in explanation.

Chapter 5 extends the analyses accomplished in Chapter 4 to complete Specific Aim 2a, by applying the multivariate analysis analytical techniques of Principal Components Analysis (PCA) and Sparse Multinomial Logistic Regression (SMLR) in order to establish the impact of polarization and a spectral signature of bone brittleness. A detailed analysis suggests how consistencies between principal components that explain toughness imply the possibility of a universal Raman spectroscopy signature for bone toughness, despite the fundamental difference

in the genetic of animal models included. Specificity of the technique is validated by comparing results to those with a model of bone maturation, where only strength and not toughness is affected.

Chapter 6 applies the techniques and metric established in Chapters 3-6 to the complex hierarchical organization of donated human tissue. Raman Spectroscopy (with and without the organizational information from polarization) is assessed for its ability to explain the age-related decrease in fracture toughness of human cortical bone, a leading laboratory surrogate for fracture resistance. RS maps of microstructure implicate tissue heterogeneity of both composition and organization as a driving force behind fracture toughness loss.

Chapter 7 summarizes the result of Chapters 3-6 with respect to the specific aims as well as the overall goals of the project. The greater implications of the dissertation work and contributions to the field are discussed.

1.5 References

1. Johnell, O. and Kanis, J.A., "An estimate of the worldwide prevalence and disability associated with osteoporotic fractures," Osteoporos Int **17**(12), 1726-1733 (2006)
2. Wolinsky, F.D., Fitzgerald, J.F. and Stump, T.E., "The effect of hip fracture on mortality, hospitalization, and functional status: a prospective study," American journal of public health **87**(3), 398-403 (1997)
3. Johnell, O., Kanis, J.A., Oden, A., Johansson, H., De Laet, C., Delmas, P., Eisman, J.A., Fujiwara, S., Kroger, H., Mellstrom, D., Meunier, P.J., Melton, L.J., 3rd, O'Neill, T., Pols, H., Reeve, J., Silman, A. and Tenenhouse, A., "Predictive value of BMD for hip and other fractures," J Bone Miner Res **20**(7), 1185-1194 (2005)
4. Giangregorio, L.M., Leslie, W.D., Lix, L.M., Johansson, H., Oden, A., McCloskey, E. and Kanis, J.A., "FRAX underestimates fracture risk in patients with diabetes," J Bone Miner Res **27**(2), 301-308 (2012)

5. Kanis, J.A., McCloskey, E., Johansson, H., Oden, A. and Leslie, W.D., "FRAX((R)) with and without bone mineral density," Calcif Tissue Int **90**(1), 1-13 (2012)

6. Kanis, J.A., Johnell, O., Oden, A., Dawson, A., De Laet, C. and Jonsson, B., "Ten year probabilities of osteoporotic fractures according to BMD and diagnostic thresholds," Osteoporos Int **12**(12), 989-995 (2001)

7. Boskey, A.L., Donnelly, E. and Kinnett, J.G., "Bone quality: from bench to bedside: opening editorial comment," Clinical orthopaedics and related research **469**(8), 2087-2089 (2011)

8. McCreadie, B.R., Morris, M.D., Chen, T.C., Sudhaker Rao, D., Finney, W.F., Widjaja, E. and Goldstein, S.A., "Bone tissue compositional differences in women with and without osteoporotic fracture," Bone **39**(6), 1190-1195 (2006)

9. Maher, J.R., Takahata, M., Awad, H.A. and Berger, A.J., "Raman spectroscopy detects deterioration in biomechanical properties of bone in a glucocorticoid-treated mouse model of rheumatoid arthritis," Journal of biomedical optics **16**(8), 087012 (2011)

10. Donnelly, E., Boskey, A.L., Baker, S.P. and van der Meulen, M.C., "Effects of tissue age on bone tissue material composition and nanomechanical properties in the rat cortex," Journal of biomedical materials research **92**(3), 1048-1056 (2010)

11. Kazanci, M., Roschger, P., Paschalis, E.P., Klaushofer, K. and Fratzl, P., "Bone osteonal tissues by Raman spectral mapping: orientation-composition," Journal of structural biology **156**(3), 489-496 (2006)

12. Currey, J., "Structural heterogeneity in bone: good or bad?," Journal of Musculoskeletal and Neuronal Interactions **5**(4), 317 (2005)

CHAPTER 2

BACKGROUND

Some of the work discussed in this Chapter has also been published in the following:

Nyman, J.S., Makowski, A.J., Patil, C.A., Masui, T.P., O'Quinn, E.C., Bi, X., Guelcher, S.A., Nicollela, D.P. and Mahadevan-Jansen, A., "Measuring differences in compositional properties of bone tissue by confocal Raman spectroscopy," Calcif Tissue Int 89(2), 111-122 (2011)

Nyman, J.S. and Makowski, A.J., "The contribution of the extracellular matrix to the fracture resistance of bone," Current osteoporosis reports 10(2), 169-177 (2012)

2.1 The Growing Statistical Incidence of Bone Disease

Bone is more than just a structural support system for the body; it is also an endocrine organ participating in calcium and phosphate homeostasis. However, when bones fail structurally the results are catastrophic. Numerous diseases increase the likelihood of a fracture of bone, and the one with the largest impact in terms of morbidity and cost is arguably osteoporosis. The World Health Organization (WHO) study on disease burden measured the disability-adjusted life-years in diseases across America and Europe, listing osteoporotic fracture at 6th and hip fracture separately as 11th. Worldwide data indicated that nearly 9,000,000 osteoporotic fractures occurred in the year 2011[1]. Unfortunately, the aging of the US population, largely from the baby boomer era, means that the burden and morbidity of this disease will only rise. By 2020,

the US Census Bureau estimates that 28.7% of the US population (97.8 million) will reach the age range associated with osteoporosis onset[2]. Of the many issues that hinder fracture as diagnosis and prevention, the most concerning is the lack of a definitive mechanism behind the clinical development and progression of osteoporosis. In fact osteoporosis as a disease itself has defied accurate definition. The word itself is literally Greek for "porous bone" being first coined in the 1820s by French pathologist Jean Lobstein, but it was not until years later when Astley Cooper related the disease to aging[3]. Since then, the disease is gradually been defined by diagnosis of exclusion, separating it from rickets, scurvy, and various genetic disorders. The WHO defines a practical operating definition for osteoporosis by clinical measurement of areal bone mineral density (aBMD)[1, 4, 5]. Specifically, the dual energy X-ray absorptiometry measure of aBMD via projection is used to calculate a T-score, such that a diagnosis of osteoporosis is given at a T-score less than -2.5 or 2.5 standard deviations below the population mean value [6, 7]. However, the WHO definition of "established osteoporosis" also usually includes a diagnosed fragility fracture[1]. Fragility fractures are defined by the low amount of energy required to cause bone failure, specifically energy equivalent to or less than "falling from less than a standing height". This type of diagnosis after morbid presentation not only limits the potential for treatment, but also the study of disease progression. In a shift away from this paradigm, this thesis focuses on obtaining a better understanding of the underlying fracture mechanisms behind bone disease, while pushing towards better diagnostic criteria and methods.

Although osteoporosis is the most prominent bone disease by incidents and morbidity, there are a surprising number of genetic conditions that display skeletal phenotypes, not all of which are rare in incidence. As one example, the Genetics Home Reference of the NIH cites the

incidence of neurofibromatosis type I at as many as 1 in 3000 live human births[8]. Osteoegenesis Imperfecta is an example of a group of genetic disorders in which mutations affect the structure of collagen, affecting as many as 6 to7 people per 100,000 worldwide [9]. Beyond the potential to help patients with these genetic maladies, the study of genetic disease offers unique opportunities to examine specifically altered cellular pathways to gain insight into the mechanisms underlying bone function disease.

In addition to diseases defined by their skeletal symptoms, systemic diseases often have adverse effects on bone function. Type 2 diabetes is associated with an increased risk of fracture[10], though the mechanisms behind this are not entirely clear. Clinical epidemiology programs that aid X-ray based measurements in diagnosing fracture risk often underestimate the fracture risk of patients with type 2 diabetes[11], and research has shown that calculations require a multiplicative factor to correct for the risk associated with diabetes[11], independently of age, height, smoking, alcohol use, and other known risk factors. One theory behind the increased risk proposes that higher circulating glucose leads to increased glycation of collagen which affects normal fracture resistance[12]. These advanced glycation end-products or AGEs are found in higher concentrations in postmenopausal women with type 2 diabetes and vertebral body fractures associated with osteoporosis[12], and the concentrations of AGEs are also higher in general among the older adults with diabetes. These advanced glycation end products alter collagen in bone[13] and have been associated with increased microdamage accumulation in bone[14, 15].

Cancer can also have catastrophic effects on bone tissue. Numerous cancers metastasize to bone, theoretically due to some combination of the numerous growth factors in this region

(Paget's seed-to-soil hypothesis)[16] and by the increased likelihood that cancer cells circulating will simply become lodged into bone marrow due to the complex circulatory network by which bone supplies blood cells to the body. Cancers can make use of the local cellular remodeling in what has been termed a "vicious cycle"[17, 18]. The cancer secretes growth factors that hijack bone remodeling, the coupled actions of osteoblasts (bone forming cell) and osteoclasts (bone resorption cells), as described later in Section 2.3. Osteoclasts digest bone matrix releasing growth factors that stimulate the cancer cells and the cycle continues. Eventually lesions of missing bone (osteolytic) or improperly grown bone tissue (osteoblastic) impact the fracture resistance of the bone, requiring surgical resection and reconstruction with implants.

Complicated traumatic fracture is also on the rise. An increase in improvised explosive devices since the Gulf War in military theaters including Afghanistan, have led to an increased number of survivable but crippling fractures[19]. The competitions of physical, chemical, and burn trauma, as well as infection, make it difficult to diagnose tissue quality in the fracture when making surgical decisions[20]. Understanding the driving forces of bone tissue quality could help make an accurate diagnosis of tissue viability, load-bearing capability, and healing potential. An accurate assessment of tissue biomechanics could also help the design of better, even patient-tailored, implants and materials[21-24] preventing excessive wear while still avoiding stress shielding[25], phenomena where the presence of an implant leads to bone degradation and surrounding area.

2.2 Physiological Functions of Bone

Bone is a highly organized composite tissue that is alive with cells that are active in repair and involved in several physiological systems. Aside from its obvious support and motility functions at the core of the musculoskeletal system, bone is crucial to the circulatory and endocrine systems. In the circulatory system, bone marrow serves as the site of differentiation of both red blood cells and lymphocytes from progenitor stem cells[26]. Bone also has numerous endocrine functions, including regulation of phosphate metabolism by fibroblast growth factor (FGF-23) activity on kidney reabsorption [27], as well as the fact that bone degradation itself releases phosphate. Bone secretes osteocalcin, regulates blood sugar, and fat deposition by influencing insulin secretion and sensitivity[26]. Bone is also the major source for regulation of serum calcium. Parathyroid hormone (PTH) acts on bone osteoblasts to stimulate the remodeling cycle to resorb bone tissue and release calcium into the bloodstream. Briefly, PTH binding to osteoblasts increases RANKL expression and inhibits osteoprotegerin (OPG). Since OPG competitively binds RANKL, these combined effects of PTH result in increased RANKL to bind with osteoclast precursors, inducing their fusion into mature osteoclasts and increasing bone resorption. [26]

Thoroughly understanding the biochemical pathways behind bone's function in normal physiology and the role that each cell population plays in maintaining that function is crucial to the understanding of the disease states that arise when normal physiology is not preserved, or worse yet when it is hijacked by diseases like cancer. Even in normal physiology, milk production depletes calcium, initiating remodeling, therefore lactating women may be at a higher risk of fracture[28]. To use NF1 as one example, we recently showed that the targeted knockout of

the gene encoding for neurofibromin (*NF1*) leads to an increase in local pyrophosphate (PPi)[29]. Since pyrophosphate is the body's fundamental inhibitor of calcification, and phosphate is necessary for the formation of calcium hydroxyapatite crystals that mineralize the type I collagen of bone, this accumulation of PPi explained the hypomineralization seen in this disease model and biopsies from NF1 patients. Knowing that pyrophosphate was also implicated in hypophosphatasia, a rare genetic disease in which osteoblasts are deficient in alkaline phosphatase, we were able to apply an experimental hypophosphatasia drug to partially rescue the hypomineralization phenotype (as measured by Raman Spectroscopy) and the skeletal dwarfism that it caused [29].

2.3 A Brief Overview of the Cellular Biology of Bone

A more detailed understanding of the roles each cell type in bone is crucial to the understanding of disease. For the sake of this engineering thesis, the review of bone cells will be limited to the 3 major cell types and their roles in material regulation of bone's skeletal function. The osteoblast is the major synthetic cell type in bone, differentiated from the mesenchymal stem cell lineage. Osteoblasts are not only responsible for the synthesis of the matrix protein type I collagen, but also for key non-collagenous proteins like osteocalcin and osteopontin, each of which has various biological functions but together help form structural dilatational bands that protect bone for microdamage[30]. Osteoblasts usually form groups and work in conjunction with osteoclasts to form basic multicellular units (BMUs; see Figure 2.1), responsible for replacing damaged bone tissue with healthy new osteons. When osteoblasts are embedded in the matrix during this process, they form small pores called lacunae and terminally differentiate into

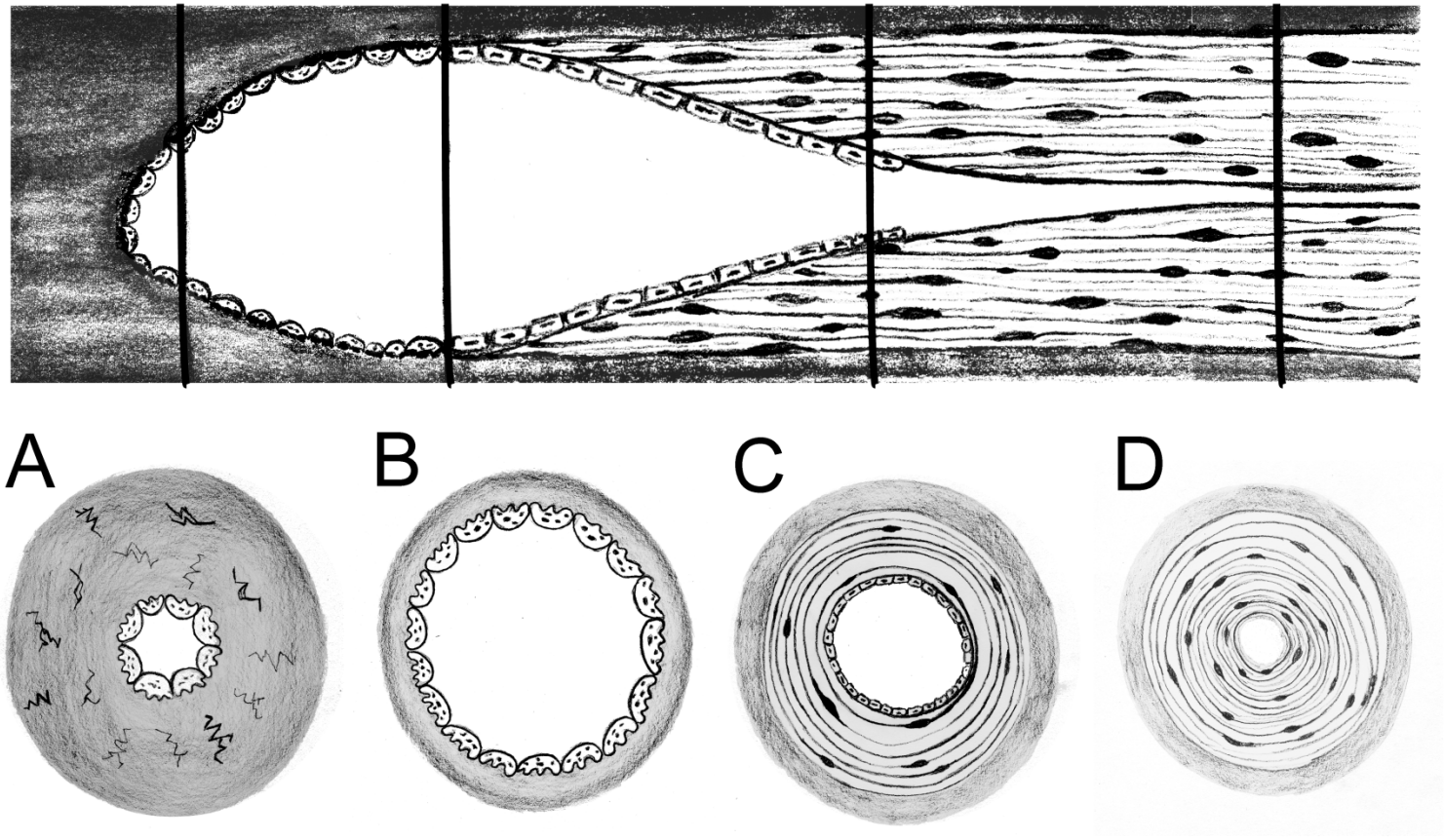

Figure 2.1 Basic Multicellular Unit is comprised of a cutting cone of osteoclasts that digest damaged tissue **(A&B)**, followed by a closing cone of osteoblasts **(C)** that deposits new tissue in organized lamellae, eventually leading to the creation of a new osteon with embedded osteocytes **(D)**.

osteocytes. While the osteoblast builds bone, the osteoclast, as the name implies, breaks it down in the process of resorption. Osteoclasts are large multi-nucleated cells formed through the fusion of monocytic progenitor cells. Osteoclasts are thought to anchor to the bone matrix using osteopontin, creating a ruffled border that subsequently generates pockets for the release of carbonic anhydrase to digest calcium hydroxyapatite mineral. Subsequently osteoclasts are often found in resorption pits, known as Howship's lacunae. After mineral degradation is complete, the release of cathepsin K and byproducts of tartrate resistant acid phosphatase (TRAP) degrade the type I collagen. Because osteoclasts are multinucleated, it is often difficult to quantify their number relative to their activity, although TRAP staining allows for quantification of total bone surface in contact with mature active osteoclasts.

Osteocytes are an interesting part of bone biology. Thought to be osteoblasts embedded into the matrix during remodeling, these unique cells live in tombs called lacunae. Recent research has shown that they play an active role in bone signaling and remodeling. Osteocytes extend processes through a network of tiny spindle like pores called canaliculi extending off of their lacunae. Canaliculi are thought to be used for intercellular signaling and the sensation of mechanical forces (mechanotransduction) through fluid flow or direct deformation. Recent findings suggest that osteocytes undergo apoptosis when damage occurs in the surrounding matrix to actively signal the need for local remodeling. Although the precise mechanism behind the signal generation is yet unclear, it has a significant impact on osteoporotic disease and osteocyte death-related complications from glucocorticoid use. [31]

2.4 Bone is a Tri-phasic Organic Composite

Now that a rudimentary understanding of major bone cell populations has been discussed as it relates to the remodeling of bone material and structure, a more detailed analysis of the bone as a biological organic composite material is merited. Analyzing bone by weight, it is composed of 3 major chemical phases, namely mineral, collagen, and water. The mineral phase makes up approximately 60% of bone by weight, and is composed largely of carbonated calcium apatites either deposited directly upon the collagen scaffold by osteoblasts or accumulated over time. Interestingly, research has shown that this deposition is not uniform across the bone matrix and tends to occur more frequently in pockets at the C and N terminals of the collagen molecules within a fiber, though it is also bound directly along the length of the molecules[26]. The mineral phase of bone is responsible for most of bones material strength and resistance to compressive loading forces[32]. As time goes on and bone tissue ages, carbonate substitution into the crystal lattice increases, replacing phosphate groups in the apatitic crystals[33, 34]. There is also significant evidence to suggest that crystals grow longer and thinner as tissue ages[35, 36].

Type I fibrillar collagen composes 30% of bone by weight, and is thought to be responsible for bones mechanical toughness, and its resistance to bending and tensile forces. Collagen is deposited by osteoblasts organized into highly oriented lamellar structures. Briefly, type I collagen is synthesized as a triple helical trimer composed of two α-1 and one α-2 procollagen molecules, each comprised of a typical Gly – X – Y repeating amino acid structure, where X or Y is usually either proline or hydroxyproline, respectively. Assembly of collagen occurs according to oxidation by prolyl and lysyl hydroxylases. After oligosaccharide post-translational modifications, peptidases cleave the molecule at both the C and N terminals to form

tropocollagen. Finally, lysyl oxidase aids in forming covalent crosslinks between α -chains to form collagen fibrils. Collagen cross-links are also formed between molecules resulting in a large fibrillar network.

The last and perhaps least explored major component of bone by weight is water, comprising approximately 10% of bone's weight. Water can be found in all levels of bone pores from Haversian canals to canaliculi (pore water), but is also found between molecules and directly incorporated into bonds between mineral and collagen molecules (bound water). Nuclear magnetic resonance (NMR) differentiates between bound and pore water, and has been found to show significant correlation between bound water content and bone bending strength, pre-yield toughness[37] and fracture toughness[38].

In spite of a relatively small contribution to the overall weight of bone tissue, a number of non-collagenous proteins including osteopontin, osteonectin, and osteocalcin have a significant impact on the mechanical integrity and biological function of bone. These proteins are secreted from osteoblasts and used as regulators of remodeling both locally and systemically. Because of its pro-osteoblastic nature, osteocalcin is associated with bone mineralization and calcium ion homeostasis. Outside of bone, osteocalcin is a hormone intricately involved in the body's metabolic functions, believed to be acting upon pancreatic beta cells to regulate insulin release[39], and upon adipocytes to release adiponectin, thereby increasing insulin sensitivity[39](so far demonstrated only in mice). Osteonectin is an extracellular matrix glycoprotein that is capable of so separately binding both collagen and the mineral phase of bone, promoting mineralization in immature tissue [40]. Interestingly, osteonectin also has a promoting effect on matrix metalloproteinases, and is therefore implicated in the metastasis of cancer to bone [40].

Osteopontin, which is also known as bone sialoprotein, is another glycoprotein that forms a small but crucial part of the bone's extracellular matrix. Osteopontin strongly binds available calcium ions inhibiting further mineralization. Osteopontin is also implicated as an anchor for osteoclasts to begin the remodeling process of bone [40]. Although these proteins are small and make up only a minor portion of bone's total volume, they are potent and the information presented here only represents a small portion of the known functions that they can have when released into the serum to interact with other physiological systems. Beyond the three prominent non-collagenous proteins described, and it is notable that bone also serves as a significant reservoir for growth factors including members of the TGF-β family [17].

More recently non-collagenous proteins have also been found to be incorporated in the matrix. As embedded cues, matrix remodeling or damage could result in their release and initiation of associated signaling pathways. Moreover, Poundarik et al. showed these non-collagenous proteins have a crucial role in the mechanical integrity of bone as they form small but important dilatational bands surrounding larger fibrillar structures of collagen and protecting them from microdamage[30].

2.5 Formation, Adaptation, and the Aging of Bone

As a highly organized tissue undergoing constant damage from repeated loading as well as chemical strains due to bone's other roles in the homeostasis of physiology, bone's material properties would readily degrade not for complex highly orchestrated processes for formation, growth, adaptation, and repair. Because investigation of the processes of endochondral bone

formation and fracture repair are not investigated in this thesis, they will only be described briefly for the sake of contrast to modeling and remodeling processes.

Long bones in the body are formed by the process known as endochondral ossification. Briefly, the body forms a hyaline cartilage scaffold surrounded by a dense connective tissue layer which becomes the periosteum, rich with osteoprogenitor cells. Once osteoprogenitors differentiate into osteoblasts, bone formation around the cartilage leads to formation of a collar of bone resulting in appositional growth. Osteoblasts form more bone, while osteoclasts digest tissue to form the medullary cavity. Secondary ossification at epiphyseal plates (at each end of the bone) continues a similar mechanism of cartilage growth followed by replacement by bone while appositional growth beneath the periosteum increases bone diameter.

Even as bone is being formed, it is undergoing stress and strain sensed by cells. Our understanding of how bone grows and adapts in response to changing forces is one of the oldest stories in the collaboration between engineering and orthopedics. Carl Culmann, a civil engineer researching crane designs, was visiting the anatomist Georg Hermann von Meyer when he was shocked to find that a cross section of a femoral head contained trabecular and cortical structures that closely mimicked the force vectors (stress trajectories) in his latest crane design[41]. Published transcriptions on their subsequent discussion of the biological meaning of this observation eventually became the motivation behind Julius Wolff's work on bone adaptation, which we now know as Wolff's Law: the theory that healthy bone actively adapts to the forces under which it is placed[42]. We now know that bone has diverse and complex mechanisms to accomplish these adaptations[43].

Bone undergoes modeling processes as a method to withstand greater forces often sustained due to growth[43, 44]. Modeling happens on opposite surfaces of the bone such that osteoclasts are resorbing bone on one surface, usually the endocortical surface, while osteoblasts are depositing new bone tissue on the opposite surface (usually periosteal; see Figure 2.2). In the case where this results in increased cortical thickness, it is also known as appositional growth; however, modeling can also be uneven on the two surfaces resulting in a net loss of tissue. Because bone responds to forces in this way, setting broken bones is important for proper healing. Moreover, in situations where bones are malformed, like bowed tibia encountered with mutations in neurofibromatosis[45], improper modeling in response to unusual forces may lead to progressive downward spiral that requires surgical intervention.

Because modeling happens on opposing surfaces of the bone, such that it is unlikely that the cell populations are in direct communication, significant efforts have been placed into engineering models to better understand the possible role of mechanosensation in this adaptation. Modern analytical models to explain bone modeling are often more complex analogues of Harold Frost's original mechanostat theory[46]. This theory postulated that excessive sensation of force indicated the need for more bone tissue and would stimulate growth, while a lack of force sensation indicated excess of tissue and would stimulate resorption. The model also accounts for a range of homeostasis in which normal force sensation leads to no net change in tissue volume. The development of adaptive elasticity theory by Cowin et al. suggested a surface model that depends upon the difference in strain between what the cell observed and a theoretical target value representative of tissue homeostasis[47]. With increases in computing power, these models

have grown into adaptive finite element models with increasingly complex algorithms, even including the presence of cell populations in calculations.

While modeling is thought to handle bone growth, remodeling is responsible for bone's mechanisms of damage repair[43, 44]. Unlike modeling, remodeling occurs on one surface or more frequently within tissue volumes, in which osteoblasts and osteoclasts work in close physical proximity as a cone-shaped basic multicellular unit (BMU) to remove and replace damaged tissue (Figure 2.1). Osteoclasts form a cutting cone at the leading edge of the BMU resorbing damaged tissue, followed by osteoblasts that gradually fill in the void, resulting in the circular lamellar pattern of matrix layers we know at osteon. The mechanisms initiating the formation in guiding the movement of the BMU are not fully understood; however, leading theories suggest the signal might originate from osteocytes undergoing apoptosis after mechanosensation of damage.

Significant problems arise when the rate of remodeling becomes imbalanced. In normal remodeling, osteoblasts and osteoclasts are inherently linked through local cellular mechanisms already described. In situations like glucocorticoid-induced osteocyte death, the accumulation of damage [31]or excessive osteocyte signaling leads to the formation of a large pores instead of proper osteons with Haversian canals. Subsequently, compromised local mechanical properties cause further increases in tissue damage accumulation, and it becomes easy to envision a downward spiral of bone loss. One of the most significant questions that remains unanswered about the remodeling process is the mechanism by which osteoblasts know to lay down new lamellar structures with the proper orientation to resist the forces encountered.

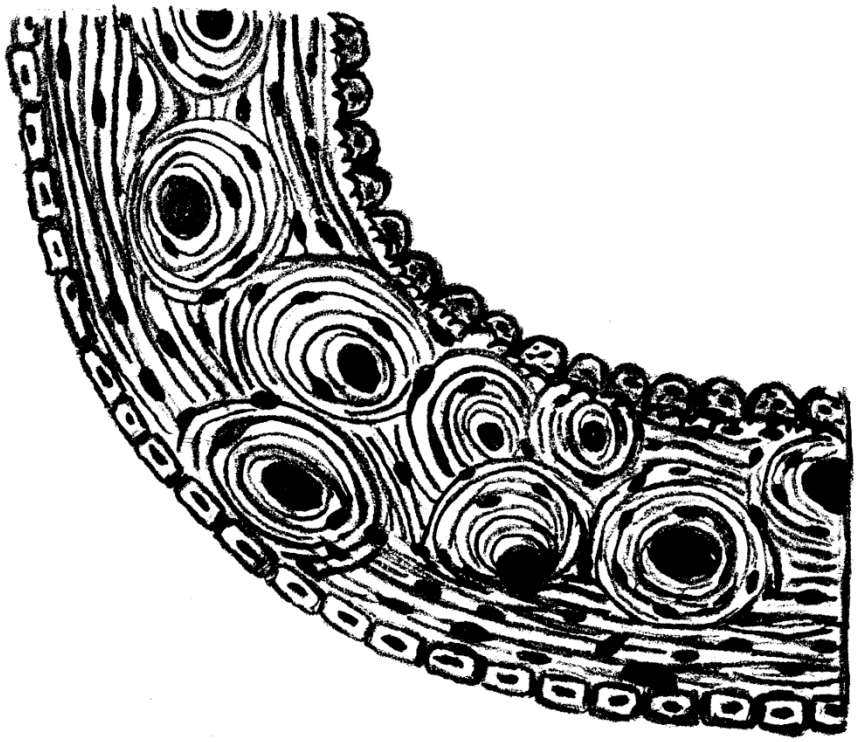

Figure 2.2 Idealized diagram of bone modeling: Osteoclasts on the endocortical surface resorb bone , while osteoblasts on the periosteal surface lay down more bone. In appositional growth in response to force increases, imbalance favors greater osteoblast activity and increased bone tissue.

While it is unclear how the process begins, one of the leading theories behind the progression of osteoporosis is the uncoupling of proper behavior in modeling and remodeling processes leading to decreased bone growth and net resorption of tissue. Hypothesized mechanisms vary greatly, and research is currently underway to determine how these processes deteriorate during aging. Load-bearing exercise may play an important role, wherein insufficient physical activity could lead to a decrease in mechanosensation. Any change in the cell death mechanisms of osteocytes with aging including autophagy instead of apoptosis[31], could impact the initiation of remodeling. Alternatively, decoupling of the relative activity of osteoblasts and osteoclasts could shift the actions of remodeling away from the normal homeostasis of bone volume, as in lytic cancer[17]. If the rate of remodeling is inherently insufficient to repair all bone damage, gradual entropy would lead to increased damage accumulation and incomplete tissue replacement.

To help us better understand the natural course of modeling and remodeling mechanisms in bone, diseases associated with genetic defects can be viewed in terms of their improper modeling and remodeling, and by isolating a single aspect of the complex process, directed hypotheses may be evaluated. The following are possible example interpretations of how the phenotypes of genetically altered animal models could be related to deficits in bone adaptation mechanisms. The genetic knockout of activation transcription factor 4 (Atf4), a signaling molecule required for the proper differentiation and function of mature osteoblasts that has been associated with Coffin-Lowry syndrome[48], results in dwarfism and decreased bone mechanical toughness as well as fracture toughness. A surprising lack of change in bulk bone tissue composition implies a possible difference in organization; therefore, changes in osteoblasts may

result in improper organization during lamellar remodeling. MMP9 or matrix metalloproteinase 9 is an enzyme used by osteoclasts to break down the collagen in bone. When MMP9 is removed using genetic knockout in mouse model, a phenotype of dwarfism and bone brittleness is observed[49]. Because of the role of osteoclasts in the resorption of damaged bone tissue during adaptation, the brittle phenotype could be the result of microdamage accumulation that is not fully cleared in this deficient system. Thus, one can see how it is important to analyze bone comprehensively in terms of its systems biology and biochemistry in order to glean a greater understanding of the mechanisms underlying age and disease-related loss of fracture resistance.

2.6 The Complex Organizational Hierarchy of Bone: an Engineering Perspective

From an engineering perspective, bone is a complex organic composite with a discrete organizational hierarchy spanning several length scales. For the sake of this review, the organizational hierarchy of bone is limited to the cortical compartment analyzed throughout this thesis; however, trabecular bone exhibits a similar organizational structure. At the nanoscale (~0.5μm), type I collagen fibrils are formed and covalently cross-linked to one another at lysine and hydroxylysine residues, forming parallel sheets with staggered ends, resulting in gaps on the order of 10s of nanometers. Mineral crystals of semi-crystalline hydroxyapatite with carbonated substitutions are deposited onto the matrix and nucleate in the gaps between fibers[44]. At the submicron level (~3-7μm), lamellar structures of ordered collagen orientation are formed. Sequential lamellae are known to have different concentrations of mineral and staggered collagen orientation[50-53].

Concentric circles of lamellae around the central Haversian canal form the bone's primary microstructural (10-500μm) unit, the osteon. Osteons vary in structure based on anatomical location, and 3 major types of osteons have been identified based on the collagen orientation within their lamellae[51, 54-58]. Type I osteons are characterized by collagen orientation in all lamellae running transverse to the direction of the Haversian canal. These osteons are mostly associated with anatomical regions of predominant compression forces[59]. In the femoral midshaft this trend can be seen in the medial quadrant of the tissue. Type II osteons are comprised of lamellae that alternate sequentially with collagen orientation running either longitudinal or transverse with respect to the Haversian canal. These osteons are associated with mixed-mode forces. Type III osteons are comprised of lamellae with predominantly longitudinal collagen orientation, are considered to be resistant to tensile forces, and are frequent in the lateral femoral midshaft[59].

The other dominant microstructural tissue type is called interstitial space. Interstitial spaces are effectively defined by exclusion, such that they encompass all tissue that can no longer be classified as a complete osteon. Because of the constant remodeling of bone, interstitial space is considered to be the older tissue that remains from previous remodeling processes. This tissue has a higher degree of mineralization and increased markers of tissue age, including carbonate substitution[33, 60, 61]. Cortical bone at the microstructural length scale is effectively composed of a network of osteons in their surrounding interstitial space. At the macro length scale (> 1 mm), the whole bone can then be seen as a structure with an organized cortical shell filled with trabecular bone, the structures in which are shaped to resist the primary of loading.

Just as the mineralized matrix of bone has its hierarchy of organization, so too is the network of pores that is responsible for circulation and innervation in bone. Fluid flow through the pores is responsible for nutrient supply, waste removal, and mechanosensation of tissue damage. At the nanoscale, there's a network of canaliculi, tiny pores surrounding transverse processes that connect neighboring osteocytes. Thought to be responsible for mechanosensation, osteocytes reside in slightly larger pores called lacunae, residing at the lower end of the microstructural length scale. Recent evidence shows that osteocytes have the capability to gradually remodel their lacunae[62]. At the microstructural level, the dominant feature is the Haversian canal, the main pore in the center of osteons that contains blood vessels and or nerves. Another network of pores called Volkmann's canals, running transverse to the axes of the osteons, connects Haversian canals[63]. Note that in materials like bone[64], pores and flaws act as stress risers[65-67].

Improper changes at any level of the organizational hierarchy can result in to an imbalance of structure and function, leading to functional inequivalence. Such changes could result in a decrease in heterogeneity, an imbalance between mass and strength, a change in the resistance to the dominant force profile, or an imbalance in the relative composition of mineral and collagen. As biomedical engineers, before we can effectively evaluate why bone fails as a material, we first need to isolate where bone fails. Specifically, it is crucial to determine where bone fails <u>first</u>, and then backtrack to isolate the underlying mechanism of the failure. Therefore, it is necessary to be able to measure bone at all of its length scales.

2.7 The Clinical Inadequacy of Current Diagnostics

The clinical gold standard for the measurement of fracture risk is DXA, dual energy x-ray absorptiometry, a technique where the acquisition of x-ray projections at two separate energies removes the soft tissue signal from the measurement of bone, effectively yielding projection-based measures of mineral termed areal bone mineral density (aBMD). Note that this is not the true bone mineral density, which would be a volumetric measurement, because it is flattened in one dimension by the projection based acquisition. High resolution, state-of-the-art images for tracking bone loss and evaluating treatment efficacy measure patients at the lumbar spine and femoral neck. Higher throughput screening at a low resolution is often conducted on the calcaneus, phalanges, and distal radius. Scans frequently last 10 to 30 minutes, with manufacturers listing radiation exposure at less than that of a cross-country domestic flight. The outcome of the DXA test is termed the T-score, a measure of the number of standard deviations of the individual from a population mean, where the population is determined by age, race, gender, and geographic location[6, 7]. However DXA is fundamentally limited to the mineral phase of bone. This makes DXA a strong predictor of bone strength[68], but a relatively poor predictor of other material properties, including fracture toughness[69]. Kanis and collaborators have tracked and developed DXA for osteoporosis screening, showing the aBMD alone does not fully explain fracture risk[6, 7, 70, 71]. In a 10 year post hoc study of fracture risk probability versus T-score measurement[7], the T-score was not linear relative to fracture risk, and a different curve was determined for each age decade. Effectively people of different age receive the same T-score for significantly different fracture risk, meaning there is a significant population of undiagnosed people who could potentially benefit from treatment. Therefore there has been significant effort

in the development of the fracture risk calculator by the World Health Organization entitled FRAX, which uses epidemiological factors including family history, concomitant health risk (smoking, drinking) and geographic location[72-74]. Because of the long lead time required to collect sufficient data to develop such a large population-based model, specific risk factors like diabetes are still under development[11, 75]. Despite significant increases in the accuracy of patient estimates, fracture risk is still not fully explained.

Many research groups have therefore focused on developing more advanced analogues of X-ray based techniques. Laboratory investigation often makes use of micro-computed tomography (μCT) which utilizes higher radiation to achieve resolutions as well as one micron with the added benefit of 3-D reconstruction to yield true tissue mineral density and a separate measurement of tissue porosity. However the machines function by reconstruction of a high number of planar projections, and their resolution is directly proportional to the distance between the excitation source and the detector, effectively limiting maximum sample volume. This often means that the level of radiation involved in μCT scanning is too high for clinical use. To circumvent radiation exposure while preserving 3-D reconstruction and measurements of porosity, a new technique named peripheral quantitative computed tomography or pQCT has been designed for application to distal limbs[76, 77]. The technique allows for detailed descriptions of porosity in trabecular structure; however, this is again achieved through close source detector spacing, significantly limiting the technique to applications of the distal radius, calcaneus, and other peripheral sites. Investigations in the use of this technique have applied engineering finite element modeling to the 3-D reconstructions to achieve patient specific estimates of mechanical properties and failure criteria [76, 78, 79].

Given our knowledge that bone microstructure varies among anatomical sites[54, 55, 57] and load bearing profiles, the potential of this technique may be limited by the assumption that distant anatomical sites are indicative of fracture risk throughout the body. Indeed the distal radius suffers from Colle's fracture, but this is not the most significant source of nonunion, nor morbidity and mortality among osteoporotic fractures[1]. Jepsen et al. showed that anatomical changes are often local and not global such that certain subpopulations have differences in skeletal traits[80, 81]. Specifically citing slenderness, or the ratio between cortical thickness and bone length, his findings imply that different sets of skeletal traits will result in different relationship between varying anatomical site, such that the distal radius might be representative of hip fracture for certain subpopulations, but not for others[80].

Despite all advances, the relationship between age-related fracture risk and diagnostic criteria remain nonlinear, leading to the hypothesis that there are unexplained factors of "bone quality" beyond areal bone mineral density that are essential for the complete explanation of fracture risk[82]. The immediate goal of improving fracture risk assessment is to achieve an accurate diagnosis of osteoporosis prior to presentation with fragility fracture. As simple as this may seem, for many patients, the diagnosis of osteoporosis is a self-fulfilling prophecy, since they are only diagnosed after they are already suffering from fragility fractures. This is crucial considering that the current treatment for osteoporosis is bisphosphonate therapy (a chemical analog to diphosphonates or pyrophosphate), which effectively inhibits and kills the osteoclast population. This prevents tissue resorption and subsequently tips remodeling and modeling processes towards increasing bone mass. This treatment may be much more effective if applied early in the degradation of bone tissue. However, recent evidence linking atypical femoral

fractures to bisphosphonate treatment[83] suggests decreased tissue heterogeneity[84] and therefore a likely increase in the accumulation of microdamage allowing for unstable crack propagation and brittle failure[85, 86]. Therefore physicians are now revisiting bisphosphonate treatment regimens[87], as well as the prophylactic use of bisphosphonates on a patient by patient basis.

However, before the role of tissue heterogeneity on fracture risk can be established, there is a need to better understand the underlying mechanisms of bone failure. Because DXA measures the mineral phase of bone, it is well accepted that it offers a powerful assessment of bone strength[68], but examining age-related trends in biomechanical properties indicates that the loss of bone toughness per decade age is significantly greater than the loss of bone strength[88]. By modeling results from pQCT, it may be possible to achieve better predictors of bone quality including criteria for stress, strain, and failure mode. However, the diagnostic modalities are still ignoring the crucial contribution of the collagen and water phases of bone to its fracture resistance. Therefore other techniques must be applied to establish the role of mechanical properties beyond strength as they relate to clinical fracture. Subsequently, a multimodal expression of bone mechanical quality could provide a better expression of fracture risk.

Among the diagnostic modalities being evaluated for the assessment of fracture risk, nuclear magnetic resonance shows promise due to its clinical relevance via MRI as well as its unique ability to directly measure the water content of bone, separating chemically bound water from water in pores using differences in the relaxation time of hydrogen ions. Horch et al. established the contribution of each chemical peak[89] and successfully related the contribution of water to bone strength[90, 91]. He then translated the technique to clinical machines by developing a unique pulse sequence[92, 93], allowing for the volumetric clinical imaging of bone water content.

Nanoindentation, although not clinically relevant, measures nanoscale mechanical properties directly using a diamond tipped probe[94, 95]. After the precise shape of the probe has been characterized (sphere, pyramidal Berkovich tip, etc.), it is depressed slowly into the tissue, held for a defined time, and then gradually unloaded. The resulting force-displacement curve is convolved with the probe geometry to reach an analytical solution for nanoindentation hardness, modulus, and stiffness derived from the unloading slope of the curve[96, 97]. It is important to note that these nanoindentation properties are not direct analogues for macro scale properties of the same name. While this technique allows for precise quantification of nanoscale material properties, it is extremely sensitive to sampling conditions, including temperature, surface roughness, and device frame stiffness. Furthermore, any minor changes in the tip geometry require regular calibration to plastic standards.

In a prototype device directly measuring bone mechanical properties at the microscale level, Hansma et al. applied the theories of the Rockwell micro-hardness test and nanoindentation to develop clinical reference point micro-indentation (RPI) system[98]. After a small incision and local anesthesia, the device engages the bone at a superficial site (anterior tibia) with a hypodermic needle. When the needle is securely pressed against the bone, the device cyclically drives a conical indenter head deeper into the tissue. The measurement of indentation distance increase (IDI) relative to the hypodermic needle reference point was associated with osteoporotic fragility fracture[99] as well as bisphosphonate related atypical femoral fractures in small cohorts of patients[100]. While the precise mechanical meaning of this outcome metric has not been fully established, several users have suggested that the test itself create microcracks (data not published). The same group has also developed another instrument

(OsteoProbe™) for the direct measure of mechanical properties based off of a small-scale impact test, rather than the cyclic indentation increase[101]. These techniques show promise as potential measurements of bone quality beyond mineral density that could help to complement current clinical protocols and better explain fracture risk.

2.8 The Mechanical Failure of Bone: Advanced Laboratory Tests Approach Reality

Association between clinical diagnostics and laboratory mechanical tests of structure and material properties help determine mechanisms of action and driving forces of human pathology. However the goal of statistical correlation doesn't necessarily indicate that fracture risk prediction. Bone can fail in many ways including tensile failure, compressive failure, mixed-mode bending, torsion, buckling, fatigue failure, and crack propagation[102]. For each of these failure modes, there are unique tests and outcome metrics. An idealized stress-strain curve from a three-point bend test is included as a frame of reference in Figure 2.3, illustrating the calculation of the Young's modulus, bending strength, and toughness. Young's modulus is calculated as the slope of the linear elastic portion of the force displacement curve, and it represents the relationship between elastic stress and strain. Bending or flexural strength, is calculated as the maximum stress undergone by the material at the time of failure, and is representative of a material's ability to withstand loading. Toughness was measured as the area beneath the force displacement curve, and is defined as the ability of material to deform (undergo work) without permanent damage or failure. Strength and toughness are often normalized to cross-sectional area to minimize the influence of structure, and better represent properties of the material itself.

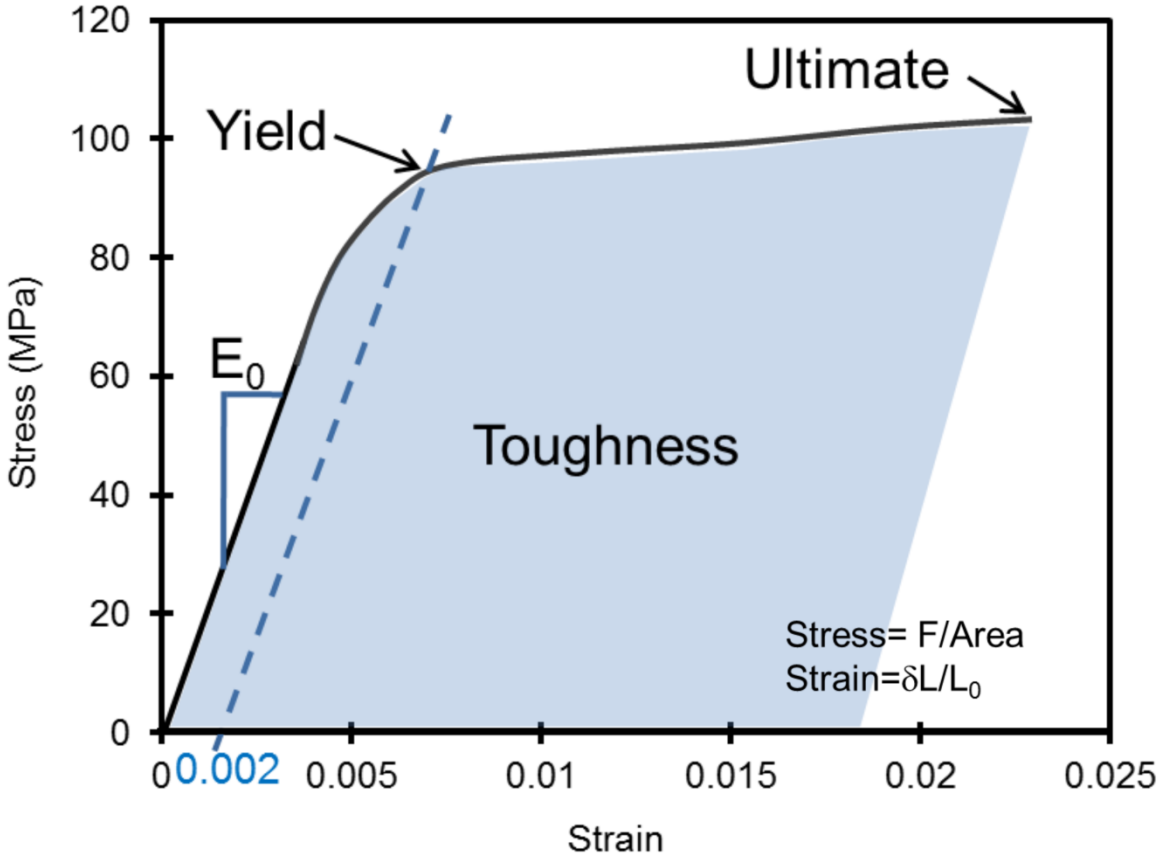

Figure 2.3 Idealized stress-strain curve conceptually demonstrates, bending strength, yield point, toughness and Young's modulus.

In many natural materials, including for some scenarios with bone, there is an inherent conflict between strength and toughness[103]. For example, polymer materials like rubber bands exhibit high toughness but low strength (weakness), whereas glass exhibits very high strength, but remarkably low toughness. All of these material properties are useful in the evaluation of bone quality; however, they all effectively exclude the presence of pores and flaws in the material. Bone, like all materials, has inherent flaws. The ability of a material to resist the generation of damage accumulation, crack initiation, and failure by crack propagation is termed its "fracture toughness". In pure homogeneous materials, fracture toughness often follows reasonably simplistic equations because the material usually exhibits linear elastic behavior. As an organic heterogeneous porous composite, bone exhibits non-linear elastic fracture toughness properties, termed elasto-plastic fracture toughness. As the name implies, crack growth is no longer linearly based only upon stress intensity induced because of crack toughening mechanisms.

A brief history of fracture mechanics is included here to discuss relevant applications and technical advances as they apply to the methods utilized in this thesis. Fracture toughness became crucial to our understanding of the mechanical behavior of materials in 1921, when Griffith showed that the failure criteria of glass was significantly lower than the theoretical predicted failure from the energy of the atomic bonds[104], generating a theory that failure occurred along the weakest link in the material (damaged regions, cracks, pores). When welded steel plate warship designs in World War II famously split in half at the welds under their own weight, this theory gained attention. Irwin extended this theory to include the coalescing of cracks in the damage region, resulting in gradual crack propagation testing, subsequently relating stress

intensity to the length of crack growth in a resistance curve or R-curve[105]. Rice formulated the J-integral which in linear elastic fracture mechanics is equivalent to the strain energy release rate[106, 107], explaining resistance to overall crack growth with an area-under-the-curve measurement that can also be used to incorporate nonlinearity in elasto-plastic materials. In heterogeneous organic composites like bone, nonlinear elastic behavior, also known as elasto-plastic behavior, violates some of the traditional assumptions of these original fracture mechanics equations, necessitating modification of calculation and testing techniques. The calculation of R-curves is practically tested by generating a defined defect using guidelines in ASTM standard E1820[108]. Because the fracture mechanics of materials is often anisotropic with respect to organization, there are numerous methods for the generation of samples depending upon the fracture mode to be analyzed. Because bone is often analyzed in mode I (opening; see Figure 2.4) relative to the orientation of osteons, the discussion in this thesis is subsequently limited to the three-point bend of a single edge notched beam (SENB) specimen in mode I opening. In the case of this thesis, all fracture toughness tests were conducted in mode I opening with the notch orientation transverse to the long axis of the bone sample and therefore the majority of microstructural features.

The fracture toughness specimen dimensions are also critical for the appropriate measure of fracture toughness. Specifically, a specific ratio of dimensions is necessary to ensure adequate thickness relative total crack propagation length, so that the sample achieves plane-strain conditions. Subsequently, the calculations of stress intensity factor K becomes relatively constant, thereby representing the maximum stress intensity the material can withstand before failure by crack instability. This occurs because the region of sheering at the edges of the sample

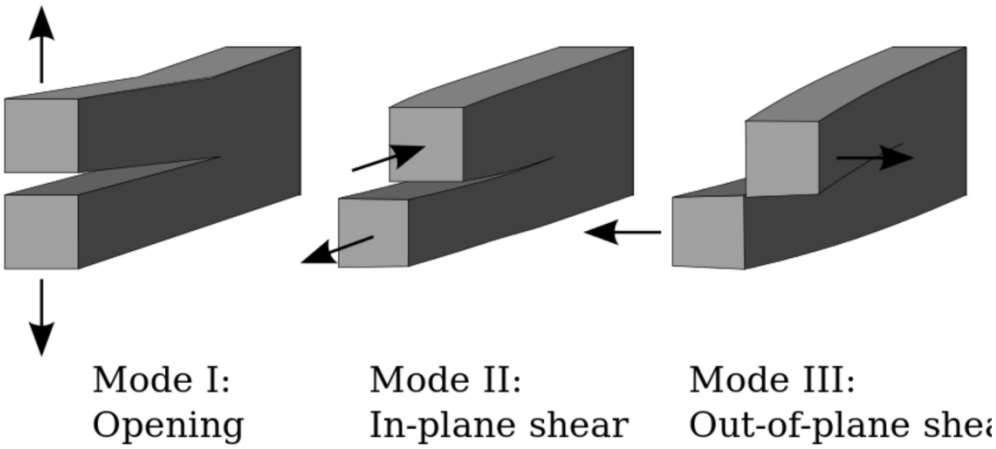

Figure 2.4 Example Fracture modes demonstrating opening, in-plane shear, and out-of-plane shear. Credit: "Fracture modes v2" by Twisp - self-made,This vector image was created with Inkscape.. Licensed under Public domain via Wikimedia Commons - http://commons.wikimedia.org/wiki/File:Fracture_modes_v2.svg#mediaviewer/File:Fracture_modes_v2.svg

no longer occupies a significant percentage of the total sample volume. Thus the value of the critical stress intensity for crack initiation K_{Ic} can be calculated. Under cyclic loading conditions, the crack will gradually grow and the relationship between the critical stress intensity observed for each crack growth can be defined in proportion to the increase in crack length, generating the critical stress intensity for crack propagation K_{grow} from the R-curve. Conducting R-curve fracture toughness testing on bones is effectively pushing the limit of the method due to the small volume of available cortical bone relative to the size of structural features (osteons and pores). The fit of the linear regression necessary to generate K_{grow} requires a finite number of crack propagation events. For example, with exceptionally poor material properties or extraordinarily high porosities, the crack can become instantly instable and these assumptions are violated, precluding the calculation of K_{grow}[38]. Finally, because the exact crack length in a three-dimensional material cannot be accurately measured during the test without tomographic imaging[109], most protocols require the estimation of crack length using a mechanical compliance-based equivalent.

Moreover the use of fracture toughness testing in small rodent bone is limited by the inability to machine the samples to defined dimensions. Rather, the Richie lab developed a method that modifies the equations assume the condition of a uniform pipe, allowing for geometry factors that explain the non-cylindrical shape of mouse femurs[110]. However the method is derived from the analytical solution of finite element model for the design of nuclear steam pipes[111] which assumes a homogeneous thin-walled pipe. Given the relatively thick cortical walls of the murine femur, the assumption may not be valid for all samples. Stability of the method

also depends upon the critical angle of the notch generated through the cross-section of the pipe, requiring exacting standards to generate consistent results between samples.

Despite various shortcomings of fracture toughness testing for the analysis of bone, the method allows significant insights into physiological mechanisms of material failure. Bone has a rising R-curve, such that as the crack progresses, various mechanisms cause crack toughening; therefore, more energy is needed for continued progression of the crack. Damage in the peritubular plastic zone preceding the crack tip (including pores and microcracks) leads to mechanisms of intrinsic toughening[112-114]. Bone has also been observed to demonstrate ligament crack bridging[115, 116], such that unbroken collagen fibers span the gradually growing crack and impeded opening. Bone also displayed significant time-dependent crack blunting[117], and propagating cracks have been observed to deflect around microstructural features like osteons[118]. These findings imply that there are more mechanisms at play in the fracture resistance of bone than mineral composition and the strength that it imparts. Therefore, bone quality investigations now include expressions of water and collagen content, composition, structure, porosity, collagen packing, and the interplay between mineral and collagen phases, in an effort to capture more physiologically and clinically relevant expressions of fracture risk.

Examining bone quality with state-of-the-art fracture mechanics and clinically relevant novel diagnostics allows us to quantify how each material phase of bone contributes differently to fundamental mechanical properties. It was already established that the mineral phase was responsible for bones material strength[68], and bound water correlates to toughness and fracture toughness[37, 38]. It is widely accepted that collagen is responsible for the toughness of bone[119, 120], and this has been measured by FTIR[121]; however, ideally a diagnostic to complement clinical

DXA would be able to measure all 3 phases at once, providing an avenue for the investigation of the interplay between the material components.

2.9 Raman Spectroscopy Concurrently Measures the Mineral and Collagen in Bone

Raman scattering is an inelastic process by which a small percentage of the light impinging on chemical bonds in a material undergoes a slight shift in wavelength. That shift is a relative to the input wavelength and based upon the energy of the chemical bond encountered. Although the exact physical mechanisms of Raman scattering are still under debate, current theory is delineated here; briefly, a photon excites the chemical bond to a metastable state, and when the molecule relaxes, it releases a photon with either one vibrational energy level more or less energy than the original photon (see Jablonski Diagram, Figure 2.5). A Stokes shift or increase in wavelength results from the loss of energy from the individual photon to the chemical bond encountered. While probabilistically less likely, anti-Stokes shift results in a decrease in wavelength due to an increase in photon energy imparted by the molecule. The percentage of light distributed by wavelength shift produces a spectrum of relative composition of dipolar covalent bonds. Because the shift in wavelength is relative to the input wavelength, it can be converted into a wavenumber shifts such that Raman Spectroscopy (RS) is inherently independent of the excitation wavelength.

This was first discovered by C.V. Raman in 1928 as part of a series of investigations into the nature of light diffraction. Using sunlight and a pair of tuned monochromatic photographic filters, he observed that a small portion of the light had shifted in wavelength and was therefore not blocked by the second filter in the optical path. Placzek pioneered the use of Raman between

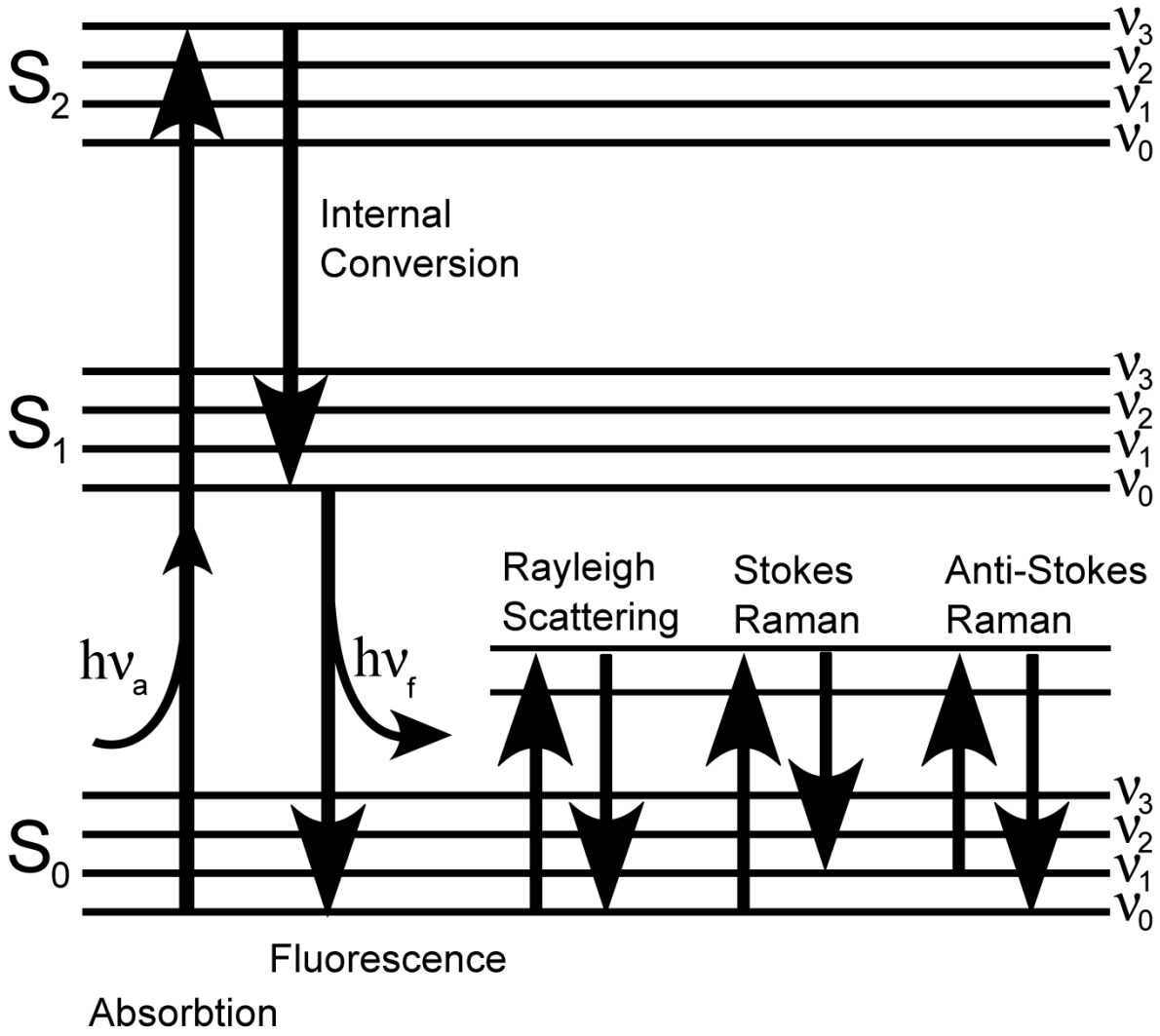

Figure 2.5 Jablonski energy diagram demonstrates absorption and release of photons by matter for fluorescence, elastic Rayleigh scattering, and Raman scattering (for both Stokes and Anti-Stokes shift). Note that Raman spectra in this thesis are acquired for Stokes shifts.

1930 and 1934, also discovering the inherent polarizability of the Raman bands based upon the chirality and birefringence of the molecules studied. Unfortunately, a lack of available RS sources resulted in few applications, and instead, infrared spectroscopy was used to test the vibrational energy of chemical bonds. However, the advent of lasers in 1960 [122, 123] later provided a convenient monochromatic source allowing for greater flexibility in the use of Raman spectroscopy. Unlike infrared spectroscopy, Raman spectroscopy is possible on wet, thick samples without destructive preparation methods. Moreover, the fact that the wavenumber shift occurs with respect to the input allows for the same Raman spectra for all excitation wavelengths, subsequently allowing the user to choose the wavelength contextually to avoid absorption in the target material. In biological tissue, this range is known as the "Optical Window", where a decrease in protein absorption coefficients coincides with a decrease in water's absorption coefficient, resulting in less heating in the near infrared range[124]. This flexibility allows for applications in tissue when using near infrared laser diodes. In the early applications to the analysis of bone quality, the biochemical assignments of peaks in Raman spectroscopy were validated by known shifts in the infrared spectrum; however, infrared spectroscopy (IR) and Raman spectroscopy (RS) are fundamentally sensitive to different molecules. Because of the physical nature RS (the theory of which involves phonons and group theory), RS is fundamentally more sensitive asymmetric bonds with dipole moment; however, IR is sensitive to symmetric bonds[125]. The mode of data collection is also fundamentally different between the two technologies, such that IR spectroscopy is driven by absorption and measured in transmission through thin sections, while RS is driven by scattering and measured in reflection; therefore, results between two modalities do not always align. Unfortunately, between the two

technologies, RS instrumentation usually have a significantly lower signal to noise ratio of 30:1 as compared to the IR signal to noise ratio on the order of 1000:1 [126]. Nonetheless, RS retains the distinct advantage of clinical relevance. Near infrared probe-based instrumentation allows for minimal heating and nondestructive data acquisition without chemical drying or the need to create thin samples. RS also has disadvantages, namely the noise of concurrent tissue florescence that can obstruct the signal, requiring careful algorithmic subtraction to isolate the true Raman spectrum[127]. Finally, the most significant recent development in RS that is utilized in this thesis is the manipulation of inherent polarization sensitivity that allows RS to be sensitive to the organization of birefringent tissues[128-131].

2.10 The Polarization of Light Affects its Interaction with Materials

Light can be fundamentally viewed as an electromagnetic wave, such that each wave has its own oscillating orthogonal electric and magnetic fields. In this sense, all light is essentially polarized in the direction of its electric field. When light is viewed as a photon using the particle theory of light, any photon that impinges upon matter is either scattered or absorbed[132]. For this discussion of polarization, I will focus on scattering and assume that no significant absorption occurs as light interacts with the materials. When light impinges upon or makes contact with the new material, the subsequent direction of light travel is determined by Snell's law, based upon the angle between the light and the surface of contact, as well as the index of refraction. Index of a fraction is a measure the relative velocity of light within the material[132]. The amount of light transmitted into the material as opposed to the percentage which is reflected back is determined by Fresnel's Laws and also depends upon the angle of incidence and the difference in the index

of refraction between the two materials through which the light is traveling[132]. Once the light enters the material, the probabilistic likelihood of a scattering event that changes the trajectory of the light is expressed by the tissue scattering coefficient (μ_s), while the angle of most probable scattering is expressed by the scattering anisotropy (g)[124]. It is important to know that each of these three material properties is dependent upon light wavelength. However, certain materials display birefringence, an anisotropy of the index of refraction based upon material orientation[132]. Essentially, light polarized at different orientations relative to the material structure will travel at different speeds through the material. Birefringent materials are often quite chiral or crystalline in nature. Not surprisingly, the collagen and mineral in bone are both birefringent, and this property has been used to measure the orientation of collagen and mineral within the osteon since as early as 1949[59, 133]. While the precise measure of orientation using Raman spectroscopy is convolved with inherent sensitivity to composition, it is possible to measure organization by comparing changes in how peaks vary as a function of polarization.

Light polarization and the birefringence of materials also play significant roles in the function of the modern Raman instrument. Because of the nature of laser light, an amplified stimulated emission, most lasers emit light that is not only monochromatic but also polarized. Therefore, laser-based Raman instrumentation inherently uses polarized light and is sensitive to chemical organization. In optics, the purification of light wavelength (as needed in RS) is often accomplished utilizing dichroics, which effectively manipulate wavelength-specific birefringence to eliminate undesired wavelengths. Moreover, the holographic grating often employed in Raman spectroscopy utilizes polarization to help disperse the light (based upon the slight shifts in wavelength) onto a detector to create the final Raman spectrum. The collection

and delivery method of light in the instrument will also affect the ability to detect polarization in the Raman spectrum. Light undergoing scattering may not preserve its polarization, and this is more likely in turbid media like bone. Therefore confocal microscopy can be used to limit the sample volume and subsequently the number of scattering events encountered by collected light, effectively preserving polarization[134]. Ultimately, commercial RS instrument often have polarization sensitivity when utilizing an open beam. Importantly, probe-based instruments based upon standard fiber optics effectively scatter the polarization state of the illumination; however, if polarization preservation is desired, special polarization-maintaining fibers can be implemented. In summary, both the instrument and the sample must be carefully analyzed to determine system polarization and sensitivity. Since bone is birefringent and organized, polarization in Raman instrumentation logically impacts the Raman measurements of bone composition. The empirical support for this statement is located in Chapter 3[135]. However, it is important to note that the sensitivity of polarization to bone organization, if controlled, is not necessarily an impedance to the assessment of fracture risk. Measuring organization and composition, separately by manipulating polarization, or concurrently using inherent system polarization allows for a new dimension of tissue analysis.

2.11 Raman Sensitivity to Material Changes is Not Limited to Composition

The Raman spectrum of bone could be thought of as existing on 3 axes: polarization, wavenumber, and intensity. As such, five different measures can be extracted from RS when used to characterize a material:

- RS identifies the presence of specific chemical bonds using wavenumber shift, based upon vibrational energy. However, it is important to note that some peaks inherently overlap in energy; therefore, context is often important in interpreting the Raman spectrum. As one example in bone, phenylalanine and hydroxy phosphate both exist in the small range between 1000-1008 cm^{-1}.[136]
- The concept can be extended to relative composition, such that the relative intensity and ratio of defined peaks can be used to determine the percent composition of the material. With a given biochemical assignment for each peak, this can be a powerful tool for the interpretation of biological meaning. As an example in bone, we often measure the mineral to collagen ratio as a function of overall mineralization, the ratio of carbonate peak height to phosphate peak height as the measure of carbonate substitution into the crystal lattice[60]; however, it was important to note that these interpretations required empirical validation prior to reliable use[33].
- Raman spectroscopy can also detect mechanical strain and damage as a wavenumber shift, largely due to the influence of our group changes on the dipole moment of the chemical bond. As an example in bone Timlin et al. demonstrated specific signatures for bone microdamage[137]. One caveat to the use of this method is that slightly different biochemical species also have different dipole moments, causing differences in wavenumber shift without damage. Therefore, this method is often used to distinguish the presence of damage with time course measurements before and after mechanical loading.

- Molecular orientation can be detected as a function of bond polarization; therefore, RS is sensitive to static orientation and repeating structures in materials. This can be seen in the quantification of collagen fiber orientation in mouse bone[138, 139] validated by the known collagen orientation in turkey tendon. Important caveats include the influence of intrinsic RS polarization[128, 129] as well as birefringence, such that organized chiral or handed materials like carbon tetrachloride display polarization sensitivity even without organization when the input and collection arms of the instrument contain crossed polarizers[130]. Therefore, care in experimental design and instrument setup, as well as attention to the degree of sample scattering, is crucial in utilizing this sensitivity.
- Crystal size and perfection can be measured using the observed width (effectively the distribution of slightly different chemical species) within the peak. This is accomplished by measuring the inverse full-with-at-half-maximum intensity of the peak, and is often used to describe the mineral crystallinity of bone in both RS and IR measure of the ν1 phosphate peak. In tissue, this method has limited application because it requires the absence of conflicting peaks and a large degree of inherent crystal purity. Moreover, it effectively convolves the influence of crystal defects and size with RS system wavenumber resolution.

These five outcomes of Raman spectroscopy are often used for material science analysis, and have previously been employed to characterize crystalline and fibrous organic materials including the quality of silkworm silk and the orientation distribution of spider silk[140]. Dental enamel is highly organized and pure in crystal composition. It is known that enamel alternates crystal orientation between sequential layers, applications of polarization Raman spectroscopy

have used this knowledge to study the organization of enamel[141-143] and for the early detection of caries[144], in which the breakdown of enamel into disorganized tissue results in a loss of polarization sensitivity. Polarization RS has also been used to diagnose wound biopsies wounds as a function of scar severity and tissue organization[145], known metrics of wound healing quality. In bone, the sequential lamellae of human osteon and the osteonal-interstitial border have been imaged by the contrast in polarization RS[52, 146, 147]. Subsequently this is been used to demonstrate the uniform thickness of osteonal lamellae, and the distribution of osteon size in the tissue[147]. Using the mouse model of osteogenesis imperfecta (*oim*-/-), the ability to characterize Raman polarization in turbid tissue was tested for different instrument configurations[148]. Because the mouse model demonstrates severe heterogeneity (random collagen orientation) that is associated with decreased material toughness, instrument sensitivity was characterized by the ability to distinguish this disorganization from the collagen fiber organization seen in wild type mice. Although the article focused on the finer points of instrument design for polarization RS and no direct measure of mechanical properties was correlated to RS outcomes, this was the first evidence that suggested polarization RS could be used in turbid media like bone to nondestructively assess organization and its impact on toughness[148].

2.12 Goals for the Usage of Raman Spectroscopy in and Beyond This Thesis

The immediate goal of this thesis is to evaluate the use of Raman spectroscopy as noninvasive and nondestructive tool for bone quality diagnosis, with an emphasis on statistical explanation of the physiological decreases in mechanical quality with human aging and animal models of genetic disease. Specific emphasis will be placed on the ability of RS to explain bone

toughness and fracture toughness. To our knowledge neither of these two mechanical properties has been significantly explained by a noninvasive, clinically relevant diagnostic to date. In addition to the use of Raman spectroscopy, other nascent technologies with clinical potential and established metrics for laboratory investigation will be concurrently evaluated for comparison of explanatory power (μCT, NMR, RPI, nanoindentation).

Because the use of Raman spectroscopy has already been established for *in vivo* applications of optical diagnosis including cancer of the skin[149], cervix[150-152], and breast[153], as well as the time course of altered wound healing[154], this thesis will determine the mechanism by which Raman spectroscopy can best diagnose tissue mechanical properties. The versatility in tailored instrument design for RS necessitates the early determination of the mechanisms of signal contrast in order to best guide device design for optimal diagnostic application. Evaluation of RS alongside other developmental tools also implicitly assesses whether it is efficient to invest the time and resources necessary to optimize RS tools for the clinical assessment of bone at this juncture.

The original aims of the thesis work as defined at the proposal were as follows:

1) Establish RS sensitivity to differences in composition with respect to organization. Correlate polarization effects to bone orientation effects on relative peak intensities.
2) Assess RS capability to explain fracture resistance differences due to genetic manipulation (mice) and aging (human).
    a) Characterize RS correlation to downstream biomechanics as a function of transcription factor deletion.
    b) Correlate microstructure fracture resistance to RS property mapping.

Since then, the specific aims were expanded and adapted to include multivariate analysis of RS to determine how the interplay between composition and organization assist in the explanation of bone mechanical quality, expanding aim 2a to include multiple animal models in which genetic knockout resulted in bone brittleness (Chapter 5). Furthermore, early observations about data variation in human bone lead to the hypothesis that fracture toughness may be driven more by the microstructural heterogeneity in bone than its average composition, now emphasized in aim 2b (Chapter 6).

In addition to laboratory applications in investigating the mechanisms underlying human fracture risk, the 10 year goals for the project were outlined to include a two-pronged approach to clinical assessment. First, an intraoperative probe will be optimized to extract quantitative measurements of bone quality in seconds to aid in clinical fracture fixation decisions. Specifically, it will be necessary to diagnose whether the quality of bone is sufficient to retain surgical hardware. The second goal would be development of a high throughput screening tool for osteoporosis related fracture risk assessment. This requires a library of signals to determine a fracture risk score, as well as assessing the anatomical concerns of where the patient should be best scanned, and whether transcutaneous recovery of signal through layers of skin and muscle is tractable while preserving RS signatures of fracture risk. The following chapters outline the advances made in these respects by completing the outlined aims while keeping these ultimate goals in mind.

2.13 References

1. Johnell, O. and Kanis, J.A., "An estimate of the worldwide prevalence and disability associated with osteoporotic fractures," Osteoporos Int **17**(12), 1726-1733 (2006)
2. Toossi, M., "Century of Change: The US Labor Force, 1950-2050, A," Monthly Lab. Rev. **125**(15 (2002)
3. Grob, G.N., Aging Bones: A Short History of Osteoporosis, Johns Hopkins University Press (2014).
4. Kanis, J.A., Melton, L.J., 3rd, Christiansen, C., Johnston, C.C. and Khaltaev, N., "The diagnosis of osteoporosis," J Bone Miner Res **9**(8), 1137-1141 (1994)
5. Kanis, J.A., Johnell, O., Oden, A., De Laet, C. and Mellstrom, D., "Diagnosis of osteoporosis and fracture threshold in men," Calcif Tissue Int **69**(4), 218-221 (2001)
6. Johnell, O., Kanis, J.A., Oden, A., Johansson, H., De Laet, C., Delmas, P., Eisman, J.A., Fujiwara, S., Kroger, H., Mellstrom, D., Meunier, P.J., Melton, L.J., 3rd, O'Neill, T., Pols, H., Reeve, J., Silman, A. and Tenenhouse, A., "Predictive value of BMD for hip and other fractures," J Bone Miner Res **20**(7), 1185-1194 (2005)
7. Kanis, J.A., Johnell, O., Oden, A., Dawson, A., De Laet, C. and Jonsson, B., "Ten year probabilities of osteoporotic fractures according to BMD and diagnostic thresholds," Osteoporos Int **12**(12), 989-995 (2001)
8. (US), N.L.o.M., "Neurofibromatosis type 1," in Genetics Home Reference N. L. o. M. (US), Ed., The Library, Bethesda, MD.
9. (US), N.L.o.M., "Osteogenesis Imperfecta," in Genetics Home Reference N. L. o. M. (US), Ed., The Library, Bethesda, MD.
10. Yamaguchi, T. and Sugimoto, T., "Bone metabolism and fracture risk in type 2 diabetes mellitus," BoneKEy reports **1**(36 (2012)
11. Giangregorio, L.M., Leslie, W.D., Lix, L.M., Johansson, H., Oden, A., McCloskey, E. and Kanis, J.A., "FRAX underestimates fracture risk in patients with diabetes," J Bone Miner Res **27**(2), 301-308 (2012)
12. Yamamoto, M., Yamaguchi, T., Yamauchi, M., Yano, S. and Sugimoto, T., "Serum pentosidine levels are positively associated with the presence of vertebral fractures in postmenopausal women with type 2 diabetes," The Journal of clinical endocrinology and metabolism **93**(3), 1013-1019 (2008)
13. Viguet-Carrin, S., Roux, J.P., Arlot, M.E., Merabet, Z., Leeming, D.J., Byrjalsen, I., Delmas, P.D. and Bouxsein, M.L., "Contribution of the advanced glycation end product pentosidine and of maturation of type I collagen to compressive biomechanical properties of human lumbar vertebrae," Bone **39**(5), 1073-1079 (2006)

14. Tang, S.Y. and Vashishth, D., "Non-enzymatic glycation alters microdamage formation in human cancellous bone," Bone **46**(1), 148-154 (2010)

15. Tang, S.Y. and Vashishth, D., "The relative contributions of non-enzymatic glycation and cortical porosity on the fracture toughness of aging bone," Journal of biomechanics **44**(2), 330-336 (2011)

16. Paget, S., "The distribution of secondary growths in cancer of the breast," The Lancet **133**(3421), 571-573 (1889)

17. Mundy, G.R., "Mechanisms of bone metastasis," Cancer **80**(8 Suppl), 1546-1556 (1997)

18. Mundy, G.R., "Metastasis: Metastasis to bone: causes, consequences and therapeutic opportunities," Nature Reviews Cancer **2**(8), 584-593 (2002)

19. Owens, B.D., Kragh Jr, J.F., Wenke, J.C., Macaitis, J., Wade, C.E. and Holcomb, J.B., "Combat wounds in operation Iraqi Freedom and operation Enduring Freedom," The Journal of Trauma and Acute Care Surgery **64**(2), 295-299 (2008)

20. Murray, C.K., Obremskey, W.T., Hsu, J.R., Andersen, R.C., Calhoun, J.H., Clasper, J.C., Whitman, T.J., Curry, T.K., Fleming, M.E., Wenke, J.C. and Ficke, J.R., "Prevention of infections associated with combat-related extremity injuries," The Journal of trauma **71**(2 Suppl 2), S235-257 (2011)

21. Kolednik, O., Predan, J., Fischer, F.D. and Fratzl, P., "Bioinspired Design Criteria for Damage-Resistant Materials with Periodically Varying Microstructure," Advanced Functional Materials **21**(19), 3634-3641 (2011)

22. Fratzl, P. and Weiner, S., "Bio-Inspired Materials – Mining the Old Literature for New Ideas," Advanced Materials **22**(41), 4547-4550 (2010)

23. Aizenberg, J. and Fratzl, P., "Biological and Biomimetic Materials," Advanced Materials **21**(4), 387-388 (2009)

24. Dunlop, J.W. and Fratzl, P., "Biological composites," Annual Review of Materials Research **40**(1-24 (2010)

25. Kim, H.W., Knowles, J.C. and Kim, H.E., "Hydroxyapatite porous scaffold engineered with biological polymer hybrid coating for antibiotic Vancomycin release," Journal of materials science. Materials in medicine **16**(3), 189-195 (2005)

26. Hall, J.E., Guyton and Hall Textbook of Medical Physiology: Enhanced E-book, Elsevier Health Sciences (2010).

27. NCBI, "FGF23 fibroblast growth factor 23," in Entrez (2014).

28. Cross, N.A., Hillman, L.S., Allen, S.H. and Krause, G.F., "Changes in bone mineral density and markers of bone remodeling during lactation and postweaning in women consuming high amounts of calcium," Journal of Bone and Mineral Research **10**(9), 1312-1320 (1995)

29. de la Croix Ndong, J., Makowski, A.J., Uppuganti, S., Vignaux, G., Ono, K., Perrien, D.S., Joubert, S., Baglio, S.R., Granchi, D., Stevenson, D.A., Rios, J.J., Nyman, J.S. and Elefteriou, F., "Asfotase-alpha improves bone growth, mineralization and strength in mouse models of neurofibromatosis type-1," Nature medicine **20**(8), 904-910 (2014)

30. Poundarik, A.A., Diab, T., Sroga, G.E., Ural, A., Boskey, A.L., Gundberg, C.M. and Vashishth, D., "Dilatational band formation in bone," Proceedings of the National Academy of Sciences **109**(47), 19178-19183 (2012)

31. Manolagas, S.C. and Parfitt, A.M., "For whom the bell tolls: Distress signals from long-lived osteocytes and the pathogenesis of metabolic bone diseases," Bone **54**(2), 272-278

32. Guo, X., "Mechanical properties of cortical bone and cancellous bone tissue," Bone mechanics handbook **2**(10 (2001)

33. Awonusi, A., Morris, M.D. and Tecklenburg, M.M., "Carbonate assignment and calibration in the Raman spectrum of apatite," Calcif Tissue Int **81**(1), 46-52 (2007)

34. Penel, G., Pottier, E.C. and Leroy, G., "Raman investigation of calcium carbonate bone substitutes and related biomaterials," Bulletin du Groupement international pour la recherche scientifique en stomatologie & odontologie **45**(2-3), 56-59 (2003)

35. Blank, R.D., Baldini, T.H., Kaufman, M., Bailey, S., Gupta, R., Yershov, Y., Boskey, A.L., Coppersmith, S.N., Demant, P. and Paschalis, E.P., "Spectroscopically determined collagen Pyr/deH-DHLNL cross-link ratio and crystallinity indices differ markedly in recombinant congenic mice with divergent calculated bone tissue strength," Connect Tissue Res **44**(3-4), 134-142 (2003)

36. Miller, L.M., Vairavamurthy, V., Chance, M.R., Mendelsohn, R., Paschalis, E.P., Betts, F. and Boskey, A.L., "In situ analysis of mineral content and crystallinity in bone using infrared micro-spectroscopy of the nu(4) PO(4)(3-) vibration," Biochimica et biophysica acta **1527**(1-2), 11-19 (2001)

37. Horch, R.A., Gochberg, D.F., Nyman, J.S. and Does, M.D., "Non-invasive predictors of human cortical bone mechanical properties: T(2)-discriminated H NMR compared with high resolution X-ray," PLoS One **6**(1), e16359 (2011)

38. Granke, M., Makowski, A.J., Uppuganti, S., Does, M.D. and Nyman, J.S., "Identifying novel clinical surrogates to assess human bone fracture toughness," Journal of Bone and Mineral Research **(Under Review)**((2014)

39. Lee, N.K., Sowa, H., Hinoi, E., Ferron, M., Ahn, J.D., Confavreux, C., Dacquin, R., Mee, P.J., McKee, M.D., Jung, D.Y., Zhang, Z., Kim, J.K., Mauvais-Jarvis, F., Ducy, P. and Karsenty, G., "Endocrine regulation of energy metabolism by the skeleton," Cell **130**(3), 456-469 (2007)

40. NCBI, "SPARC secreted protein, acidic, cysteine-rich (osteonectin)," in Entrez (2014).

41. Skedros, J.G. and Brand, R.A., "Biographical sketch: Georg Hermann von Meyer (1815-1892)," Clinical orthopaedics and related research **469**(11), 3072-3076 (2011)

42. Wolff, J., Das Gesetz der Transformation der Knochen, von Dr Julius Wolff, A. Hirschwald, Berlin (1892).

43. Currey, J.D., "The many adaptations of bone," J Biomech **36**(10), 1487-1495 (2003)

44. Ross, M.H. and Pawlina, W., Histology, Lippincott Williams & Wilkins (2006).

45. Wang, W., Nyman, J.S., Ono, K., Stevenson, D.A., Yang, X. and Elefteriou, F., "Mice lacking Nf1 in osteochondroprogenitor cells display skeletal dysplasia similar to patients with neurofibromatosis type I," Human molecular genetics **20**(20), 3910-3924 (2011)

46. Frost, H., "Bone “mass” and the “mechanostat”: a proposal," The Anatomical Record **219**(1), 1-9 (1987)

47. Cowin, S. and Hegedus, D., "Bone remodeling I: theory of adaptive elasticity," Journal of Elasticity **6**(3), 313-326 (1976)

48. Yang, X., Matsuda, K., Bialek, P., Jacquot, S., Masuoka, H.C., Schinke, T., Li, L., Brancorsini, S., Sassone-Corsi, P., Townes, T.M., Hanauer, A. and Karsenty, G., "ATF4 is a substrate of RSK2 and an essential regulator of osteoblast biology; implication for Coffin-Lowry Syndrome," Cell **117**(3), 387-398 (2004)

49. Nyman, J.S., Lynch, C.C., Perrien, D.S., Thiolloy, S., O'Quinn, E.C., Patil, C.A., Bi, X., Pharr, G.M., Mahadevan-Jansen, A. and Mundy, G.R., "Differential effects between the loss of MMP-2 and MMP-9 on structural and tissue-level properties of bone," J Bone Miner Res **26**(6), 1252-1260 (2011)

50. Pathak, S., Vachhani, S.J., Jepsen, K.J., Goldman, H.M. and Kalidindi, S.R., "Assessment of lamellar level properties in mouse bone utilizing a novel spherical nanoindentation data analysis method," Journal of the mechanical behavior of biomedical materials **13**(102-117 (2012)

51. Carando, S., Portigliatti-Barbos, M., Ascenzi, A., Riggs, C.M. and Boyde, A., "Macroscopic shape of, and lamellar distribution within, the upper limb shafts, allowing inferences about mechanical properties," Bone **12**(4), 265-269 (1991)

52. Falgayrac, G., Facq, S., Leroy, G., Cortet, B. and Penel, G., "New method for Raman investigation of the orientation of collagen fibrils and crystallites in the Haversian system of bone," Applied spectroscopy **64**(7), 775-780 (2010)

53. Reznikov, N., Almany-Magal, R., Shahar, R. and Weiner, S., "Three-dimensional imaging of collagen fibril organization in rat circumferential lamellar bone using a dual beam electron microscope reveals ordered and disordered sub-lamellar structures," Bone **52**(2), 676-683 (2013)

54. Boyde, A., Bianco, P., Portigliatti Barbos, M. and Ascenzi, A., "Collagen orientation in compact bone: I. A new method for the determination of the proportion of collagen parallel to the plane of compact bone sections," Metabolic Bone Disease and Related Research **5**(6), 299-307 (1984)

55. Portigliatti Barbos, M., Bianco, P., Ascenzi, A. and Boyde, A., "Collagen orientation in compact bone: II. Distribution of lamellae in the whole of the human femoral shaft with reference to its mechanical properties," Metabolic Bone Disease and Related Research **5**(6), 309-315 (1984)

56. Ascenzi, M.G. and Lomovtsev, A., "Collagen orientation patterns in human secondary osteons, quantified in the radial direction by confocal microscopy," Journal of structural biology **153**(1), 14-30 (2006)

57. Carando, S., Barbos, M.P., Ascenzi, A. and Boyde, A., "Orientation of collagen in human tibial and fibular shaft and possible correlation with mechanical properties," Bone **10**(2), 139-142 (1989)

58. Ascenzi, A. and Bonucci, E., "The tensile properties of single osteons," Anat Rec **158**(4), 375-386 (1967)

59. Bromage, T.G., Goldman, H.M., McFarlin, S.C., Warshaw, J., Boyde, A. and Riggs, C.M., "Circularly polarized light standards for investigations of collagen fiber orientation in bone," Anatomical record **274**(1), 157-168 (2003)

60. Nyman, J.S., Makowski, A.J., Patil, C.A., Masui, T.P., O'Quinn, E.C., Bi, X., Guelcher, S.A., Nicollela, D.P. and Mahadevan-Jansen, A., "Measuring differences in compositional properties of bone tissue by confocal Raman spectroscopy," Calcif Tissue Int **89**(2), 111-122 (2011)

61. Makowski, A.J., Patil, C.A., Gorochow, L., Mahadevan-Jansen, A. and Nyman, J.S., "Polarization Control of Raman Spectroscopy Optimizes Measures of Bone Quality," in American Society for Bone and Mineral Research: Annual Conference, San Diego, CA USA (2011).

62. Tang, S.Y., Herber, R.-P., Ho, S.P. and Alliston, T., "Matrix metalloproteinase–13 is required for osteocytic perilacunar remodeling and maintains bone fracture resistance," Journal of Bone and Mineral Research **27**(9), 1936-1950 (2012)

63. Standring, S., Gray's Anatomy: The Anatomical Basis of Clinical Practice, Elsevier Health Sciences UK (2008).

64. Inoue, K., Ohgushi, H., Yoshikawa, T., Okumura, M., Sempuku, T., Tamai, S. and Dohi, Y., "The effect of aging on bone formation in porous hydroxyapatite: biochemical and histological analysis," J Bone Miner Res **12**(6), 989-994 (1997)

65. Zioupos, P. and Currey, J., "The extent of microcracking and the morphology of microcracks in damaged bone," Journal of materials science **29**(4), 978-986 (1994)

66. Hernandez, C.J., Gupta, A. and Keaveny, T.M., "A biomechanical analysis of the effects of resorption cavities on cancellous bone strength," J Bone Miner Res **21**(8), 1248-1255 (2006)

67. Slyfield, C., Tkachenko, E., Fischer, S., Ehlert, K., Yi, I., Jekir, M., O'Brien, R., Keaveny, T. and Hernandez, C., "Mechanical failure begins preferentially near resorption

cavities in human vertebral cancellous bone under compression," Bone **50**(6), 1281-1287 (2012)

68. Ammann, P. and Rizzoli, R., "Bone strength and its determinants," Osteoporosis International **14**(3), 13-18 (2003)

69. Phelps, J.B., Hubbard, G.B., Wang, X. and Agrawal, C.M., "Microstructural heterogeneity and the fracture toughness of bone," J Biomed Mater Res **51**(4), 735-741 (2000)

70. Kanis, J.A., Oden, A., Johnell, O., Jonsson, B., de Laet, C. and Dawson, A., "The burden of osteoporotic fractures: a method for setting intervention thresholds," Osteoporos Int **12**(5), 417-427 (2001)

71. Leslie, W.D., Morin, S., Lix, L.M., Johansson, H., Oden, A., McCloskey, E., Kanis, J.A. and Manitoba Bone Density, P., "Fracture risk assessment without bone density measurement in routine clinical practice," Osteoporos Int **23**(1), 75-85 (2012)

72. Ettinger, B., Black, D.M., Dawson-Hughes, B., Pressman, A.R. and Melton, L.J., 3rd, "Updated fracture incidence rates for the US version of FRAX," Osteoporos Int **21**(1), 25-33 (2010)

73. Pressman, A.R., Lo, J.C., Chandra, M. and Ettinger, B., "Methods for assessing fracture risk prediction models: experience with FRAX in a large integrated health care delivery system," J Clin Densitom **14**(4), 407-415 (2011)

74. Kanis, J.A., McCloskey, E., Johansson, H., Oden, A. and Leslie, W.D., "FRAX((R)) with and without bone mineral density," Calcif Tissue Int **90**(1), 1-13 (2012)

75. Leslie, W.D., Rubin, M.R., Schwartz, A.V. and Kanis, J.A., "Type 2 diabetes and bone," J Bone Miner Res **27**(11), 2231-2237 (2012)

76. Liu, X.S., Stein, E.M., Zhou, B., Zhang, C.A., Nickolas, T.L., Cohen, A., Thomas, V., McMahon, D.J., Cosman, F., Nieves, J., Shane, E. and Guo, X.E., "Individual trabecula segmentation (ITS)-based morphological analyses and microfinite element analysis of HR-pQCT images discriminate postmenopausal fragility fractures independent of DXA measurements," J Bone Miner Res **27**(2), 263-272 (2012)

77. Vilayphiou, N., Boutroy, S., Szulc, P., van Rietbergen, B., Munoz, F., Delmas, P.D. and Chapurlat, R., "Finite element analysis performed on radius and tibia HR-pQCT images and fragility fractures at all sites in men," J Bone Miner Res **26**(5), 965-973 (2011)

78. Orwoll, E.S., Marshall, L.M., Nielson, C.M., Cummings, S.R., Lapidus, J., Cauley, J.A., Ensrud, K., Lane, N., Hoffmann, P.R., Kopperdahl, D.L. and Keaveny, T.M., "Finite Element Analysis of the Proximal Femur and Hip Fracture Risk in Older Men," Journal of Bone and Mineral Research **24**(3), 475-483 (2009)

79. Wang, X., Sanyal, A., Cawthon, P.M., Palermo, L., Jekir, M., Christensen, J., Ensrud, K.E., Cummings, S.R., Orwoll, E., Black, D.M., Osteoporotic Fractures in Men Research,

G. and Keaveny, T.M., "Prediction of new clinical vertebral fractures in elderly men using finite element analysis of CT scans," J Bone Miner Res **27**(4), 808-816 (2012)

80. Jepsen, K.J., Centi, A., Duarte, G.F., Galloway, K., Goldman, H., Hampson, N., Lappe, J.M., Cullen, D.M., Greeves, J. and Izard, R., "Biological constraints that limit compensation of a common skeletal trait variant lead to inequivalence of tibial function among healthy young adults," Journal of Bone and Mineral Research **26**(12), 2872-2885 (2011)

81. Jepsen, K.J., Pennington, D.E., Lee, Y.L., Warman, M. and Nadeau, J., "Bone brittleness varies with genetic background in A/J and C57BL/6J inbred mice," J Bone Miner Res **16**(10), 1854-1862 (2001)

82. Donnelly, E., Lane, J.M. and Boskey, A.L., "Research perspectives: The 2013 AAOS/ORS research symposium on Bone Quality and Fracture Prevention," Journal of Orthopaedic Research **32**(7), 855-864 (2014)

83. Black, D.M., Kelly, M.P., Genant, H.K., Palermo, L., Eastell, R., Bucci-Rechtweg, C., Cauley, J., Leung, P.C., Boonen, S., Santora, A., de Papp, A., Bauer, D.C., Fracture Intervention Trial Steering, C. and Committee, H.P.F.T.S., "Bisphosphonates and fractures of the subtrochanteric or diaphyseal femur," The New England journal of medicine **362**(19), 1761-1771 (2010)

84. Donnelly, E., Meredith, D.S., Nguyen, J.T., Gladnick, B.P., Rebolledo, B.J., Shaffer, A.D., Lorich, D.G., Lane, J.M. and Boskey, A.L., "Reduced cortical bone compositional heterogeneity with bisphosphonate treatment in postmenopausal women with intertrochanteric and subtrochanteric fractures," J Bone Miner Res **27**(3), 672-678 (2012)

85. Ettinger, B., Burr, D.B. and Ritchie, R.O., "Proposed pathogenesis for atypical femoral fractures: Lessons from materials research," Bone **55**(2), 495-500 (2013)

86. van der Meulen, M.C. and Boskey, A.L., "Atypical subtrochanteric femoral shaft fractures: role for mechanics and bone quality," Arthritis research & therapy **14**(4), 220 (2012)

87. Donnelly, E., Lane, J.M. and Boskey, A.L., "Research perspectives: The 2013 AAOS/ORS research symposium on Bone Quality and Fracture Prevention," J Orthop Res **32**(7), 855-864 (2014)

88. Burstein, A.H., Reilly, D.T. and Martens, M., "Aging of bone tissue: mechanical properties," J Bone Joint Surg Am **58**(1), 82-86 (1976)

89. Horch, R.A., Nyman, J.S., Gochberg, D.F., Dortch, R.D. and Does, M.D., "Characterization of 1H NMR signal in human cortical bone for magnetic resonance imaging," Magn Reson Med **64**(3), 680-687 (2010)

90. Nyman, J.S., Gorochow, L.E., Adam Horch, R., Uppuganti, S., Zein-Sabatto, A., Manhard, M.K. and Does, M.D., "Partial removal of pore and loosely bound water by

low-energy drying decreases cortical bone toughness in young and old donors," J Mech Behav Biomed Mater **22**(136-145 (2013)

91. Horch, R.A., Gochberg, D.F., Nyman, J.S. and Does, M.D., "Non-invasive predictors of human cortical bone mechanical properties: T2-discriminated 1H NMR compared with high resolution X-ray," PLoS One **6**(1), e16359 (2011)

92. Manhard, M.K., Horch, R.A., Harkins, K.D., Gochberg, D.F., Nyman, J.S. and Does, M.D., "Validation of quantitative bound- and pore-water imaging in cortical bone," Magn Reson Med **71**(6), 2166-2171 (2014)

93. Horch, R.A., Gochberg, D.F., Nyman, J.S. and Does, M.D., "Clinically compatible MRI strategies for discriminating bound and pore water in cortical bone," Magn Reson Med **In press**((2012)

94. Oliver, W. and Pharr, G., "Measurement of hardness and elastic modulus by instrumented indentation: advances in understanding and refinements to methodology," J Mater Res **19**(3-20 (2004)

95. Oliver, W.C. and Pharr, G.M., "An improved technique for determining hardness and elastic modulus using load and displacement sensing indentation experiments," Journal Name: Journal of Materials Research; (United States); Journal Volume: 7:6 Medium: X; Size: Pages: 1564-1583 (1992)

96. Silva, M.J., Brodt, M.D., Fan, Z. and Rho, J.Y., "Nanoindentation and whole-bone bending estimates of material properties in bones from the senescence accelerated mouse SAMP6," J Biomech **37**(11), 1639-1646 (2004)

97. Rho, J.Y., Roy, M.E., 2nd, Tsui, T.Y. and Pharr, G.M., "Elastic properties of microstructural components of human bone tissue as measured by nanoindentation," J Biomed Mater Res **45**(1), 48-54 (1999)

98. Hansma, P., Turner, P., Drake, B., Yurtsev, E., Proctor, A., Mathews, P., Lulejian, J., Randall, C., Adams, J., Jungmann, R., Garza-de-Leon, F., Fantner, G., Mkrtchyan, H., Pontin, M., Weaver, A., Brown, M.B., Sahar, N., Rossello, R. and Kohn, D., "The bone diagnostic instrument II: indentation distance increase," Rev Sci Instrum **79**(6), 064303 (2008)

99. Diez-Perez, A., Guerri, R., Nogues, X., Caceres, E., Pena, M.J., Mellibovsky, L., Randall, C., Bridges, D., Weaver, J.C., Proctor, A., Brimer, D., Koester, K.J., Ritchie, R.O. and Hansma, P.K., "Microindentation for in vivo measurement of bone tissue mechanical properties in humans," J Bone Miner Res **25**(8), 1877-1885 (2010)

100. Guerri-Fernandez, R.C., Nogues, X., Quesada Gomez, J.M., Torres Del Pliego, E., Puig, L., Garcia-Giralt, N., Yoskovitz, G., Mellibovsky, L., Hansma, P.K. and Diez-Perez, A., "Microindentation for in vivo measurement of bone tissue material properties in atypical femoral fracture patients and controls," J Bone Miner Res **28**(1), 162-168 (2013)

101. Randall, C., Bridges, D., Guerri, R., Nogues, X., Puig, L., Torres, E., Mellibovsky, L., Hoffseth, K., Stalbaum, T., Srikanth, A., Weaver, J.C., Rosen, S., Barnard, H., Brimer, D., Proctor, A., Candy, J., Saldana, C., Chandrasekar, S., Lescun, T., Nielson, C.M., Orwoll, E., Herthel, D., Kopeikin, H., Yang, H.T.Y., Farr, J.N., McCready, L., Khosla, S., Diez-Perez, A. and Hansma, P.K., "Applications of a New Handheld Reference Point Indentation Instrument Measuring Bone Material Strength," Journal of Medical Devices **7**(4), 041005-041005 (2013)

102. Turner, C.H. and Burr, D.B., "Basic biomechanical measurements of bone: a tutorial," Bone **14**(4), 595-608 (1993)

103. Ritchie, R.O., "The conflicts between strength and toughness," Nature materials **10**(11), 817-822 (2011)

104. Griffith, A.A., "The Phenomena of Rupture and Flow in Solids," Philosophical Transactions of the Royal Society of London. Series A, Containing Papers of a Mathematical or Physical Character **221**(582-593), 163-198 (1921)

105. Irwin, G., "Analysis of stresses and strains near the end of a crack traversing a plate," Journal of Applied Mechanics **24**(361-364 (1957)

106. Rice, J. and Rosengren, G., "Plane strain deformation near a crack tip in a power-law hardening material," Journal of the Mechanics and Physics of Solids **16**(1), 1-12 (1968)

107. Rice, J.R., "A Path Independent Integral and the Approximate Analysis of Strain Concentration by Notches and Cracks," Journal of Applied Mechanics **35**(2), 379-386 (1968)

108. "ASTM E 1820-05a. Standard Test Method for Measurement of Fracture Toughness," American Society for Testing and Materials International (2005).

109. Nalla, R.K., Kruzic, J.J., Kinney, J.H. and Ritchie, R.O., "Effect of aging on the toughness of human cortical bone: evaluation by R-curves," Bone **35**(6), 1240-1246 (2004)

110. Ritchie, R.O., Koester, K.J., Ionova, S., Yao, W., Lane, N.E. and Ager, J.W., 3rd, "Measurement of the toughness of bone: a tutorial with special reference to small animal studies," Bone **43**(5), 798-812 (2008)

111. Takahashi, Y., "Evaluation of leak-before-break assessment methodology for pipes with a circumferential through-wall crack. Part I: stress intensity factor and limit load solutions," International journal of pressure vessels and piping **79**(6), 385-392 (2002)

112. Vashishth, D., Behiri, J.C. and Bonfield, W., "Crack growth resistance in cortical bone: Concept of microcrack toughening," Journal of Biomechanics **30**(8), 763-769 (1997)

113. Vashishth, D., Tanner, K.E. and Bonfield, W., "Contribution, development and morphology of microcracking in cortical bone during crack propagation," Journal of Biomechanics **33**(9), 1169-1174 (2000)

114. Vashishth, D., "Rising crack-growth-resistance behavior in cortical bone:: implications for toughness measurements," Journal of Biomechanics **37**(6), 943-946 (2004)

115. Nalla, R.K., Kinney, J.H. and Ritchie, R.O., "Mechanistic fracture criteria for the failure of human cortical bone," Nature materials **2**(3), 164-168 (2003)

116. Nalla, R.K., Kruzic, J.J. and Ritchie, R.O., "On the origin of the toughness of mineralized tissue: microcracking or crack bridging?," Bone **34**(5), 790-798 (2004)

117. Nalla, R.K., Kruzic, J.J., Kinney, J.H. and Ritchie, R.O., "Aspects of in vitro fatigue in human cortical bone: time and cycle dependent crack growth," Biomaterials **26**(14), 2183-2195 (2005)

118. Nalla, R.K., Stolken, J.S., Kinney, J.H. and Ritchie, R.O., "Fracture in human cortical bone: local fracture criteria and toughening mechanisms," J Biomech **38**(7), 1517-1525 (2005)

119. Nyman, J.S. and Makowski, A.J., "The contribution of the extracellular matrix to the fracture resistance of bone," Current osteoporosis reports **10**(2), 169-177 (2012)

120. Carriero, A., Zimmermann, E.A., Paluszny, A., Tang, S.Y., Bale, H., Busse, B., Alliston, T., Kazakia, G., Ritchie, R.O. and Shefelbine, S.J., "How Tough Is Brittle Bone? Investigating Osteogenesis Imperfecta in Mouse Bone," Journal of Bone and Mineral Research **29**(6), 1392-1401 (2014)

121. Courtland, H.W., Spevak, M., Boskey, A.L. and Jepsen, K.J., "Genetic variation in mouse femoral tissue-level mineral content underlies differences in whole bone mechanical properties," Cells, tissues, organs **189**(1-4), 237-240 (2009)

122. Maiman, T.H., "Stimulated Optical Radiation in Ruby," Nature **187**(4736), 493-494 (1960)

123. Garwin, L. and Lincoln, T., A Century of Nature: Twenty-One Discoveries that Changed Science and the World, University of Chicago Press (2010).

124. Welch, A.J. and van Gemert, M.J.C., Optical-Thermal Response of Laser-Irradiated Tissue, Springer (2011).

125. Walton, A.G., Deveney, M.J. and Koenig, J.L., "Raman spectroscopy of calcified tissue," Calcified tissue research **6**(2), 162-167 (1970)

126. Morris, M.D. and Mandair, G.S., "Raman assessment of bone quality," Clinical orthopaedics and related research **469**(8), 2160-2169 (2011)

127. Lieber, C.A. and Mahadevan-Jansen, A., "Automated method for subtraction of fluorescence from biological Raman spectra," Applied spectroscopy **57**(11), 1363-1367 (2003)

128. Placzek, G., "Rayleigh-Streuung und Raman-Effekt," in Handbuch der Radiologie E. Marx, Ed., pp. 205-374, Akademische Verlagsgesellschaft, Leipzig, Germany (1934).

129. Long, D.A., "Intensities in Raman Spectra. I. A Bond Polarizability Theory," Proceedings of the Royal Society of London. Series A, Mathematical and Physical Sciences **217**(1129), 203-221 (1953)

130. Porto, S., Giordmaine, J. and Damen, T., "Depolarization of Raman Scattering in Calcite," Physical Review **147**(2), 608-611 (1966)

131. Levenson, M.D., "Polarization techniques in coherent Raman spectroscopy," J Raman Spec **10**(1), 9-23 (1981)

132. Hecht, E., Optics, Addison-Wesley, Reading, Mass. (2002).

133. Antonio, A., "Quantitative researches on the optical properties of human bone," Nature **163**(4146), 604-604 (1949)

134. Juang, C.B., Finzi, L. and Bustamante, C.J., "Design and application of a computer-controlled confocal scanning differential polarization microscope," Rev. Sci. Instr. **59**(11), 2399-2408 (1988)

135. Makowski, A.J., Patil, C.A., Mahadevan-Jansen, A. and Nyman, J.S., "Polarization control of Raman spectroscopy optimizes the assessment of bone tissue," Journal of biomedical optics **18**(5), 55005 (2013)

136. Penel, G., Delfosse, C., Descamps, M. and Leroy, G., "Composition of bone and apatitic biomaterials as revealed by intravital Raman microspectroscopy," Bone **36**(5), 893-901 (2005)

137. Timlin, J.A., Carden, A., Morris, M.D., Rajachar, R.M. and Kohn, D.H., "Raman spectroscopic imaging markers for fatigue-related microdamage in bovine bone," Anal Chem **72**(10), 2229-2236 (2000)

138. Gevorkian, B.Z., Arnotskaia, N.E. and Fedorova, E.N., "[Study of bone tissue structure using polarized Raman spectra]," Biofizika **29**(6), 1046-1052 (1984)

139. Gamsjaeger, S., Masic, A., Roschger, P., Kazanci, M., Dunlop, J.W., Klaushofer, K., Paschalis, E.P. and Fratzl, P., "Cortical bone composition and orientation as a function of animal and tissue age in mice by Raman spectroscopy," Bone **47**(2), 392-399 (2010)

140. Rousseau, M.E., Lefevre, T., Beaulieu, L., Asakura, T. and Pezolet, M., "Study of protein conformation and orientation in silkworm and spider silk fibers using Raman microspectroscopy," Biomacromolecules **5**(6), 2247-2257 (2004)

141. Leroy, G., Penel, G., Leroy, N. and Brès, E., "Human Tooth Enamel: A Raman Polarized Approach," Applied spectroscopy **56**(8), 1030-1034 (2002)

142. Penel, G., Leroy, G., Leroy, N., Behin, P., Langlois, J.M., Libersa, J.C. and Dupas, P.H., "[Raman spectrometry applied to calcified tissue and calcium-phosphorus biomaterials]," Bulletin du Groupement international pour la recherche scientifique en stomatologie & odontologie **42**(2-3), 55-63 (2000)

143. Penel, G., Leroy, G., Rey, C. and Bres, E., "MicroRaman Spectral Study of the PO4 and CO3 Vibrational Modes in Synthetic and Biological Apatites," Calcified tissue international **63**(6), 475-481 (1998)

144. Ko, A.C.T., Choo-Smith, L.-P.i., Hewko, M., Sowa, M.G., Dong, C.C.S. and Cleghorn, B., "Detection of early dental caries using polarized Raman spectroscopy," Opt. Express **14**(1), 203-215 (2006)

145. Crane, N., Brown, T., Hawksworth, J., Gage, F., Tadaki, D., Perdue, P., Dunne, J., DeNobile, J. and Elster, E., "Raman spectroscopic analysis of warrior wound biopsies: What happens when good wounds go bad," Proc Fed Anal Chem Spectrosc Soc (2008)

146. Kazanci, M., Wagner, H.D., Manjubala, N.I., Gupta, H.S., Paschalis, E., Roschger, P. and Fratzl, P., "Raman imaging of two orthogonal planes within cortical bone," Bone **41**(3), 456-461 (2007)

147. Kazanci, M., Roschger, P., Paschalis, E.P., Klaushofer, K. and Fratzl, P., "Bone osteonal tissues by Raman spectral mapping: orientation-composition," Journal of structural biology **156**(3), 489-496 (2006)

148. Raghavan, M., Sahar, N.D., Wilson, R.H., Mycek, M.A., Pleshko, N., Kohn, D.H. and Morris, M.D., "Quantitative polarized Raman spectroscopy in highly turbid bone tissue," Journal of biomedical optics **15**(3), 037001 (2010)

149. Patil, C.A., Kirshnamoorthi, H., Ellis, D.L., van Leeuwen, T.G. and Mahadevan-Jansen, A., "A clinical instrument for combined raman spectroscopy-optical coherence tomography of skin cancers," Lasers in surgery and medicine **43**(2), 143-151 (2011)

150. Keller, M.D., Kanter, E.M., Lieber, C.A., Majumder, S.K., Hutchings, J., Ellis, D.L., Beaven, R.B., Stone, N. and Mahadevan-Jansen, A., "Detecting temporal and spatial effects of epithelial cancers with Raman spectroscopy," Disease markers **25**(6), 323-337 (2008)

151. Robichaux-Viehoever, A., Kanter, E., Shappell, H., Billheimer, D., Jones, H. and Mahadevan-Jansen, A., "Characterization of Raman Spectra Measured in Vivo for the Detection of Cervical Dysplasia," Applied spectroscopy **61**(9), 986-993 (2007)

152. Mahadevan-Jansen, A., Mitchell, M.F., Ramanujam, N., Malpica, A., Thomsen, S., Utzinger, U. and Richards-Kortum, R., "Near-infrared Raman spectroscopy for in vitro detection of cervical precancers," Photochemistry and photobiology **68**(1), 123-132 (1998)

153. Keller, M.D., Vargis, E., de Matos Granja, N., Wilson, R.H., Mycek, M.A., Kelley, M.C. and Mahadevan-Jansen, A., "Development of a spatially offset Raman spectroscopy probe for breast tumor surgical margin evaluation," Journal of biomedical optics **16**(7), 077006 (2011)

154. Makowski, A.J., Davidson, J.M., Mahadevan-Jansen, A. and Jansen, E.D., "In vivo analysis of laser preconditioning in incisional wound healing of wild-type and HSP70

knockout mice with Raman spectroscopy," Lasers in surgery and medicine **44**(3), 233-244 (2012)

CHAPTER 3

POLARIZATION CONTROL OF RAMAN SPECTROSCOPY OPTIMIZES THE ASSESSMENT OF BONE TISSUE

Work comprised in this Chapter is published in:
Makowski, A. J., C. A. Patil, A. Mahadevan-Jansen and J. S. Nyman (2013). "Polarization control of Raman spectroscopy optimizes the assessment of bone tissue." J Biomed Opt 18(5): 55005.

3.1 Abstract

There is potential for Raman Spectroscopy (RS) to complement clinical tools for bone diagnosis due to its ability to assess compositional and organizational characteristics of both collagen and mineral. To aid this potential, the present study assessed specificity of multiple RS peaks to the composition of bone, a birefringent material, for different degrees of instrument polarization. Specifically, relative changes in peaks were quantified as the incident light rotated relative to the orientation of osteonal and interstitial tissue, acquired from cadaveric femurs. In a highly polarized instrument (106:1 extinction ratio), the most prominent mineral peak (v1 Phosphate at 961 cm^{-1}) displayed phase similarity with the Proline peak at 856 cm^{-1}. This sensitivity to relative orientation between bone and light observed in the highly polarized regime persisted for certain sensitive peaks (e.g., Amide I at 1666 cm^{-1}) in unaltered instrumentation (200:1 extinction ratio). Though Proline intensity changed with bone rotation, the phase of

Proline matched that of ν1 Phosphate. Moreover, when mapping ν1 Phosphate/Proline across osteonal-interstitial borders, the mineralization difference between the tissue types was evident whether using a 20x or 50x objective. Thus, the polarization bias inherent in commercial RS systems does not preclude the assessment of bone composition when using phase-matched peaks.

3.2 Introduction

Despite recent advances in the ability to assess fracture risk [1, 2], definitive metrics do not yet exist to identify individuals in need of an intervention that lowers fracture risk. Complementary to established X-ray based diagnostics of bone, Raman Spectroscopy (RS) is an emerging technology that offers non-destructive [3-7] measures of the biochemical nature of tissue. As an indication of its potential to assess fracture risk, RS detected differences in carbonate concentration relative to phosphate between bone samples from non-fracture patients and bones from osteoporotic fracture cases [8]. In addition to quantifying the amount of carbonate in calcified tissue [9], RS is sensitive to local changes in mineral accumulation through mineral to collagen peak ratios, as well as local changes in mineral maturation through measurements of crystallinity [10]. These properties become less heterogeneous with aging [11], change in response to tissue damage [12], and correlate to mechanical strength of rodent bones [13, 14] as well as human cortical bone [10].

While these attributes make RS a candidate for clinical diagnosis of bone quality and disease states, unresolved issues regarding instrument polarization and its impact on analysis hamper unambiguous derivation of quantities reflecting the biochemical properties of bone tissue, referred to henceforth as biomarkers. For example, probe-based instruments have been

developed to acquire Raman spectra from bone through the overlying tissue [15-17]. However, most RS studies assessing bone use laser confocal microscopes [18] in which the laser is polarized [19, 20]. Since most fiber optic instruments do not preserve polarization, there is potential for significant discrepancy between the relevant biomarkers of fracture resistance as obtained from RS microscopes and those obtained from existing clinically relevant instruments.

Earlier studies in FTIR identified that vibrational spectroscopy markers for mineralization, crystallinity, carbonation, and collagen cross-linking all significantly associate with fragility fracture [21], and while the influence of polarization on FTIR was previously characterized [22, 23], the polarization state for this instrument was not reported. FTIR and RS are linked as vibrational spectroscopy methods, but fundamental differences give RS an apparent clinical advantage that has fueled cross-correlation and validation in RS.

Recent correlation studies linking RS to the fracture resistance of bone have reported different biomarker sensitivity of RS to the biomechanical properties of bone, possibly due to instrument polarization differences. In one RS study involving a commercial confocal system, differences in v1 Phosphate / CH2-wag between trabecular and cortical bone were related to differences in nanomechanical properties between the tissue types [24]. In another study analyzing cortical bone from genetic mouse models (MMP2-/- and MMP9-/-) and using a similar commercial instrument, correlations among nanoindentation modulus, bending strength, and RS were reported for several mineral-to-collagen ratios, but not v1 Phosphate / Amide I [25]. On the other hand, strength of bone from vehicle- and glucocorticoid-treated mice was correlated to various RS peaks when normalized to Amide I in a fiber optic system [26]. Despite differences in

modes of biomechanical testing among these studies, the polarization state of the instrument likely influences which RS biomarkers are sensitive to experimental groups.

Even though bone is a birefringent material, only a few investigations have intentionally examined the effect of polarization on RS peaks of bone [27-30]. The vast majority of polarization RS studies of mineralized tissues utilized isolator and analyzer polarizers to "fully polarize" both the input light and collection arm of the Raman system (Table 3.1). To the best of our knowledge, the extent to which polarization may affect various peak ratios used to assess composition of bone is not well understood for RS instruments without these added optics. Addressing this is important because Raman scattering bands are inherently and differentially affected by polarization due to vibrational modes that give rise to the Raman effect [31, 32]. Even though Legendre polynomials can be used to extract the distribution of collagen and mineral orientation by modulating polarization [30], inherent polarization within the instrument can affect bands even in the absence of molecular organization (e.g., analyzing carbon tetrachloride) [33]. Because sample volume, molecular organization, scattering anisotropy, and tissue turbidity influence the scattered light [30], it is difficult to predict how polarization affects RS spectra of bone tissue (which is both turbid and organized), especially when the input laser light is unaltered (Table 3.1). In the context of RS instrumentation, we refer to changes in Raman peak intensities due to bone rotation (relative to light polarization) as a "polarization bias". Rather than intentionally polarizing Raman collection, the present study compares RS biomarkers of human cortical bone with respect to inherent system polarization using commercial instrumentation. The hypothesis of this study was that the intensity of polarization-sensitive Raman bands would oscillate relative to input polarization. Thus, optimization of the

relative phase of these Raman bands oscillations could yield biomarkers that are better suited for the study of either composition (phase matched and less polarization sensitive) or structure (phase mismatched and polarization sensitive). This study uses polarization theory to quantify the phase and amplitude for a number of Raman peaks of bone, and in doing so, identifies phase matching as the source of polarization insensitivity in known and newly characterized peak ratios of bone composition. Whereas other studies have observed the intensity change of specific peak ratios (Table 3.1), the present work establishes phase profiles for many of the prominent peaks arising from bone with and without added polarization optics.

Table 3.1: Previous polarized Raman Studies used altered instrumentation to analyze mineralized tissues and collagen

Tissue	Instrumentation	Polarization	Laser (nm)	Factor(s)	Raman Property	Reported trends	Ref.
Human tooth enamel	Spectrophotometer coupled to Microscope with 100x and 50x objectives	Fully Polarized[a]	632.8, 514	Crystalline Orientation	ν_1PO_4,ν_2PO_4,ν_3PO_4, ν_4PO_4, ν_1CO_3, OH	Carbonation preserves the orientation of enamel crystals. Vibrational modes of enamel rods are reconciled to theory.	(51)
Human tooth enamel	Confocal Microscope, 10x objective	Fully Polarized	830	Caries and Lesions	ν_1PO_4	Depolarization ratio and anisotropy of ν1PO4 changes between sound enamel and caries	(52)
Sheep tendon, Fixed Human femur	Confocal Microscope, 100x objective NA=0.8	Not Reported	633	Collagen Fiber Distribution along Osteon Radius, and bone rotation	ν_3PO_4/ν_1PO_4,Amide I/ Amide III, and Amide III ratio (1271/1243)	Polarization-sensitive peak ratios varied with distance from haversian canal	(29)
Rat Tail Tendon Collagen Fibrils	Confocal Microscope, 60x NA=1.0 objective,	Fully Polarized	785	Mechanical Stress	Amide I , Amide III	Stress changes orientation distribution but not vibration frequencies of collagen	(49)
Whole and Powdered Mouse tibia	Custom Confocal Raman Microprobe, various objectives	Fully Polarized	785	Osteogenesis Imperfecta (oim)	ν_1PO_4, Amide I	Orientation Distribution of mineral and collagen differ in oim mice.	(30)
Collagen from Bovine Achilles Tendon	Confocal Microscope 60x objective NA=0.75	Collection Arm Polarized	633	Collagen Fiber Orientation	Amide I, Amide III, and Amide III ratio (1245/1268)	Amide III doublet is sensitive to orientation.	(33)

Turkey Leg Tendon, Embedded Mouse Femurs	Confocal Microscope, 60x NA=1.0, 20x NA=0.4	Fully Polarized	785	Orientation of Cut, Depolarization	ν_1PO_4/AmideI, ν_2PO_4/AmideIII, Carbonate/ν_2PO_4	Tissue age affects Raman Polarization. Collagen orientation obtained from Polarized mapping	(19)
Embedded Human femur Osteons	Confocal Microscope, 100x NA= 0.9	Not Reported	532	Tissue Type and Orientation	ν_1PO_4/Amide I ν_2PO_4,/Amide III ν_4PO_4/ Amide III	Tissue types have differential polarization sensitivity.	(28, 36)
Femoral Head Spongy Bone	Confocal Microscope, 50x objective NA=0.5	Fully Polarized	785	Specimens from Osteoporotic Fracture Patients.	ν_1PO_4/Amide I, ν_2PO_4,/Amide III ν_4PO_4/Amide III Carbonate/ ν_1PO_4	Polarized Raman helps determine the location of Collagen fibers within trabeculae.	(53)
Human Femur	Confocal Microscope, 50x objective NA=0.75, 20x objective NA=0.4	Inherent Polarization	785	Tissue Type and Orientation	Various	Polarization sensitivity inherent in peaks and Raman instrumentation can be minimized by optimizing peak phase.	Current Study

[a] Fully Polarized indicates the use of polarizing optics in the input and collection arm

3.3 Methods

3.3.1 Specimen Preparation

Transverse human cortical bone specimens from the lateral femur midshaft were prepared as per previously published methods [18]. Briefly, bone samples were mounted to slides using cyanoacrylate and ground on silicon carbide papers of sequential grit, then polished with 0.05 µm alumina beads in solution to an ultimate surface area of ~8mm x ~8mm and thickness of approximately 4 mm. One sample from each of 6 donors was used (4 males ages 48, 80, 82 and 94, 2 females ages 86 and 95). To generate a control sample, a human molar was embedded in polymethylmethacrylate; a thick section was cut in the longitudinal direction; and the surfaced polished as previously described [18].

3.3.2 Raman Instrumentation

To fully examine the influence of instrument polarization and bone structure on collected Raman spectra, we conducted several experiments, each with a different collection protocol or degree of polarization. Raman spectra were acquired from the polished surface of the bone tissue in air using a standard confocal Raman microscope (Ramanscope Mark III and InVia Raman Microscope, Renishaw, Hoffman Estates, IL) equipped with Renishaw EasyConfocal, a 35 µm slit opening, and a spectral resolution of $1cm^{-1}$, equipped with a 785 nm laser diode source with a polarization extinction ratio (PER) of 200:1 (Innovative Photonic Solutions, Monmouth Junction, NJ). To eliminate grating bias according to Renishaw specifications, the polarization was aligned upright within the instrument (left-right when operator faces stage), confirmed with known polarizers and silicon standard intensity. Placing a mirror in the sample plane, the PER was also

measured as 20:1 after the dichroic and 17:1 after the grating. Additional optics increased polarization of the Raman microscope, such that the system operated in a highly polarized regime. An isolator (NIR linear polarizer, 1000:1 extinction ratio, Thorlabs, Newton, NJ) was used to isolate a polarization angle of input laser light prior to sample incidence. An analyzer (additional linear polarizer, same specifications) isolates a particular polarization angle of light reflected off the sample. A quartz wedge depolarizer (AR coated achromatic depolarizer DPU-25-B, Thorlabs, Newton, NJ) effectively scrambles the polarization state of light in space prior to the spectral grating to prevent instrumentation bias by transmitting a pseudo-random polarized beam. Removal of the analyzer (1000:1 extinction ratio) decreased system polarization sensitivity, but retaining the input polarizer provided an "input polarization regime". In this regime, the bone sample is rotated to examine bias and the depolarizer remains in the system to minimize instrumentation bias of the grating. Without added optics, the system retains a degree of inherent polarization sensitivity, henceforth referred to as an "unaltered polarization regime".

To preserve system throughput across experiments despite differences in added optics, spectral acquisition exposure times were scaled to ensure 480 mW*s apparent exposure at the sample. This provided a signal to noise ratio for the low intensity Proline peak in excess of 10:1 in highly polarized experiments, translating to at least 25:1 in unaltered experiments. Unless otherwise stated, spectra were obtained with 3 accumulations after 5 seconds photobleaching. Spectra were then binned to a resolution of 3 cm^{-1} , and processed via least squares modified polynomial fit [34] and smoothed for noise using an 2nd order Savitsky-Golay filter [26, 35]. After fluorescence subtraction, a linear baseline subtraction (based on derivative zero-crossings neighboring the peak) was conducted on peaks that overlap with other constituents to ensure no

residual fluorescence, namely Proline, Hydroxyproline, ν1 Phosphate, and Carbonate. Spatial resolution for each objective used was approximated via edge detection on a polished silicon standard. System Raman shift calibration was accomplished using a neon lamp and a silicon standard with Renishaw software to account for grating motion. Silicon measurements before and after each beam path change and at system "startup" ensured wavenumber calibration consistency.

Since dentin has less heterogeneity in collagen fibril orientation than bone, we collected Raman spectra from the same site as a human tooth rotated from 0 to 180 degrees in 20 degree increments in order to characterize the polarization sensitivity of our RS instrument without additional polarization optics. In these dentin measurements, known polarization sensitive peaks oscillated through rotation with percent changes in mean normalized intensity of 6.6% and 22.6% for ν1 Phosphate and Amide I, respectively.

3.3.3 Experimental Design

3.3.3.1 Highly Polarized Analyzer Rotation

Polarization analysis used known bias from previous work [19, 28, 36] to confirm the ability of Malus's law to model phase and amplitude of Raman peaks. In effect, our first experiment was designed to evaluate phase oscillation for sensitive RS peaks. To account for within sample variation, five osteons and neighboring interstitial sites were selected from a single bone sample [18]. In brief, selected osteons were spaced evenly over the surface and distributed by osteon size and pore size. Using upright input polarization through our 50x, NA=0.75 objective (lateral resolution 3-4 μm, as measured by edge detection) and stationary bone orientation, the analyzer

was rotated at each site from 0 to 180 degrees in 20 degree increments. This study used an adaptation of Porto's notations based on microscope translation stage directions since Porto's notations traditionally depend on sample crystallographic axis [37, 38], which varies within cortical bone. In this adaptation, the polarization regime is Z(XB)-Z, where B denotes analyzer rotation relative to instrument input X (always left-to-right as viewed by operator). Intensity for each of the prominent peaks in the bone spectrum was then modeled as a function of polarization angle B to compare the degree of oscillation between quantities.

3.3.3.2 Bone Rotation for Two Polarization Regimes

Next, spectra were collected as a function of bone orientation to evaluate peak and peak ratio sensitivity in less polarization sensitive systems. We analyzed a single osteon and neighboring interstitial site from each of three bones under both input polarized (added isolator and depolarizer) or unaltered (no added optics) polarization regimes. As was done with tooth, the bone sample was rotated around the optical axis using a custom stage to preserve collection location while obtaining spectra (50x, NA= 0.75 objective) from 0 to 180 degrees rotation in 20 degree increments. The polarization regime is Z(Xx)-Z, where x denotes bone rotation around Z relative to instrument input X (left-to-right as viewed by operator).

3.3.3.3 Spectral Mapping of Bone Tissue Rotation

Using the unaltered polarization regime, we acquired confocal Raman maps of spatial heterogeneity to demonstrate the effects of phase-matching on compositional discrimination of known osteonal and interstitial tissue differences. Phase-matching of peak ratios is defined as minimizing the phase difference of the ratio components, effectively choosing peaks that have the most similar rotation angle of maximum intensity, subsequently reducing the impact of

rotation angle upon the observed ratio intensity. One osteon and the neighboring interstitial area (20x, NA= 0.4 objective, lateral resolution of 12 μm) from each of three bones was mapped using unaltered instrumentation at a pixel size of 8 x 8 μm for 0, 45 and 90 degree rotations of the bone sample about the optical axis. To analyze discrimination of osteonal from interstitial tissue, intensity maps were generated for selected peak ratios applying a uniform scale based upon full intensity range, such that a polarization insensitive spectral constituent will show the same intensity image in all three acquisitions. Instrument polarization in direction X is denoted with X-Y stage directions in each figure panel. For one bone, the mapping process was repeated using the 50x objective for an osteonal-interstitial border within the original 20x map to demonstrate Raman maps of polarization bias with a smaller sample volume.

3.3.4 Data modeling and Statistics

Data modeling and statistics were performed on peak heights extracted from each processed spectrum (Figure 3.1 A). Peak intensities were modeled to Malus' Law [39, 40] (intensity varies with polarization angle as a function of cosine squared) for phase and amplitude of oscillation (Figure 3.1 B). The custom algorithm employed a least squares fit for amplitude nested inside a mean squared error driven optimization (Matlab implementation of Nelder-Mead simplex [41], Mathworks, Natick, MA), outputting peak phase, amplitude, and mean intensity as illustrated in Figure 3.1 B. The degree of orientation sensitivity across the three generated polarization regimes was quantified for each prominent peak as a function of oscillation amplitude normalized to mean peak intensity. For less sensitive peaks, individual sample oscillations could become noisy or undetectable, such that data fails the underlying assumptions

of the Malus' Law model. Modeled data were excluded from quantitative analysis if the model fit was not significant ($p<0.05$) via ANOVA regression (all fits shown in figures and tables are significant). For each peak, the number of samples with statistically significant models and the observable percent change in intensity measurements of the same quantity were recorded.

3.4 Results

3.4.1 Phase differences in Raman peaks of bone under highly polarized light

Acquired under a highly polarized regime, RS biomarker peaks exhibited differential polarization behavior in both degree and relative phase of intensity oscillation. For the most part, relative phase varied insignificantly between osteonal and interstitial tissue types for any given peak. However, phase oscillation varied distinctly between different peaks representing the same bone compositional element (i.e. Amide I at 1666 cm^{-1} vs. Amide III at 1247 cm^{-1}, both biomarkers of collagen in Figure 3.2). In reference to the ν1 Phosphate peak (961 cm^{-1}), the strongest spectral signal for bone mineral, Proline (854 cm^{-1}) was found to have the best phase match for the generation of a mineral to collagen ratio, a metric commonly used as an indicator of bone quality.

Building upon our previous findings [18], the observed difference between osteonal and interstitial tissue composition (Figure 3.3) was small (2-30% difference) relative to intensity change as a function of polarization angle (100-300% difference). However, under the traditional calculation of a mineral to collagen ratio using ν1 Phosphate (mineral) and Amide I (collagen) as biomarkers, different quantities would be observed at different polarization angles (e.g., 60 vs. 140 degrees in Figure 3.3 A). As an alternative mineral to collagen ratio that still utilizes the

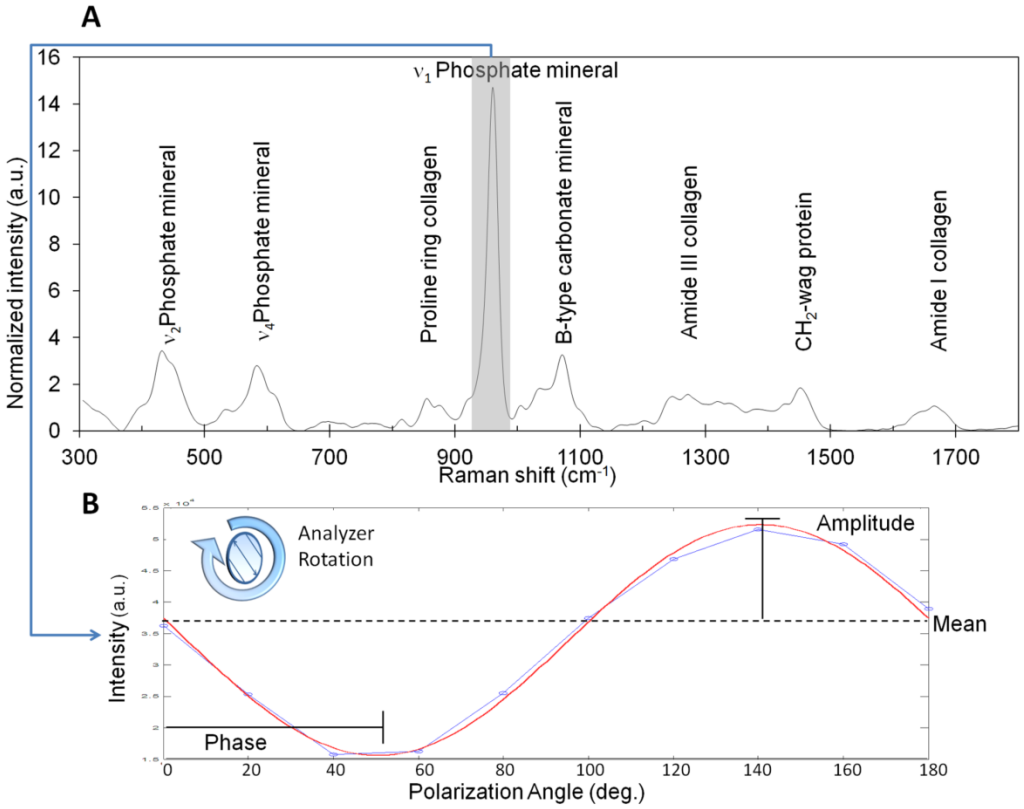

Figure 3.1: Diagram of representative labeled Raman Spectrum of bone shows feature extraction. (**A**) v1 Phosphate peak intensity is extracted from a wavenumber range and baselined. (**B**) Actual data from highly polarized osteon analysis shows v1 Phosphate intensity for each analyzer rotation (output polarization angle). Data is then modeled to a sinusoidal fit to extract phase, amplitude and mean intensity. Shown here for analyzer rotation, this method was also used in bone rotation experiments.

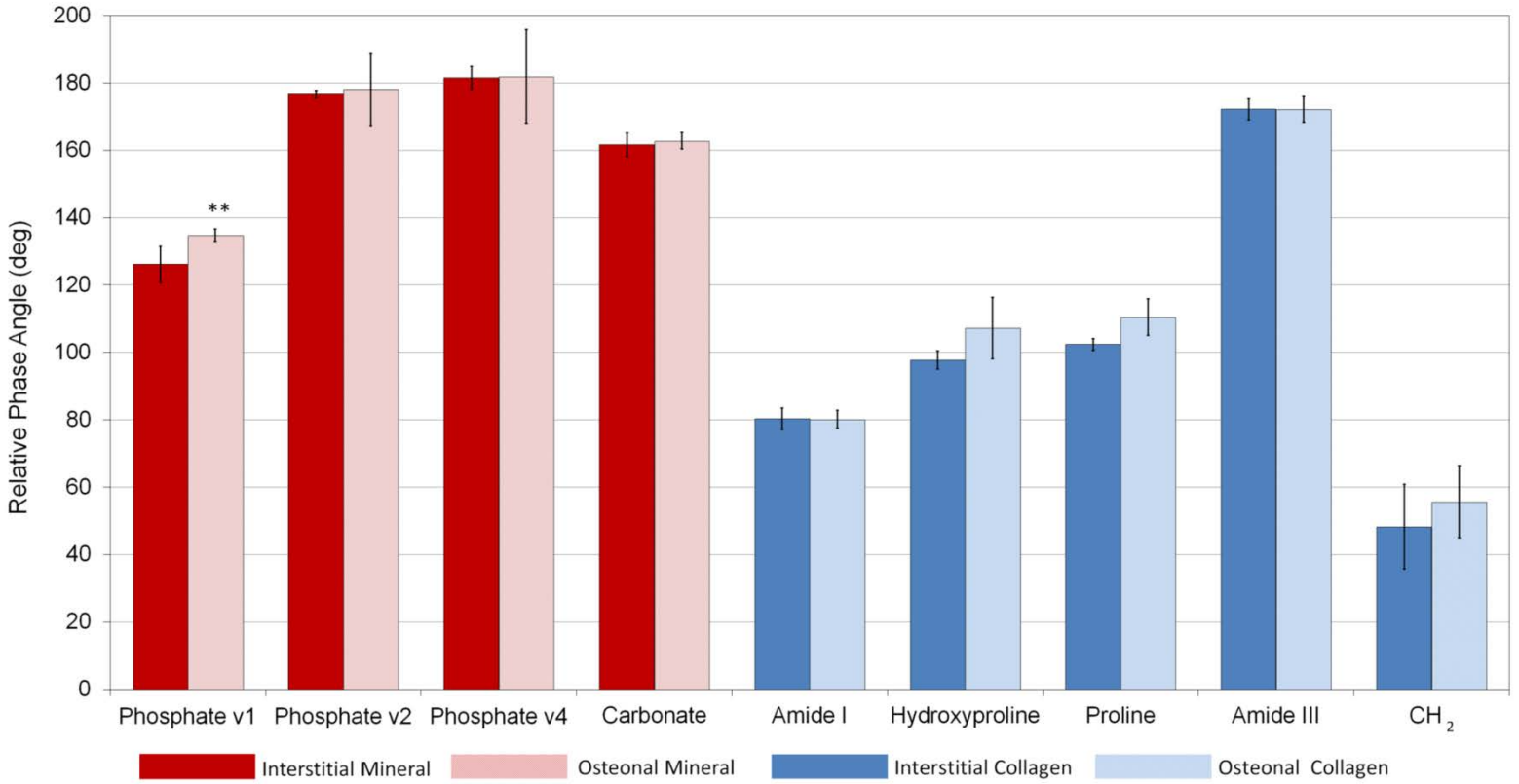

Figure 3.2: Relative phase angle (mean ± SD) from highly polarized analysis of osteons, conducted with analyzer rotation, shows few differences between tissue type but strong compositional element differences in phase angle. The phase range of v1 Phosphate was closest to the phase range of Proline and CH_2-wag. In this regime, Amide I is the collagen peak with the greatest phase difference from v1 Phosphate. ** Only v1 Phosphate had a significant difference $p<0.05$ in phase between osteonal and interstitial tissue types by two sided Student's t-test.

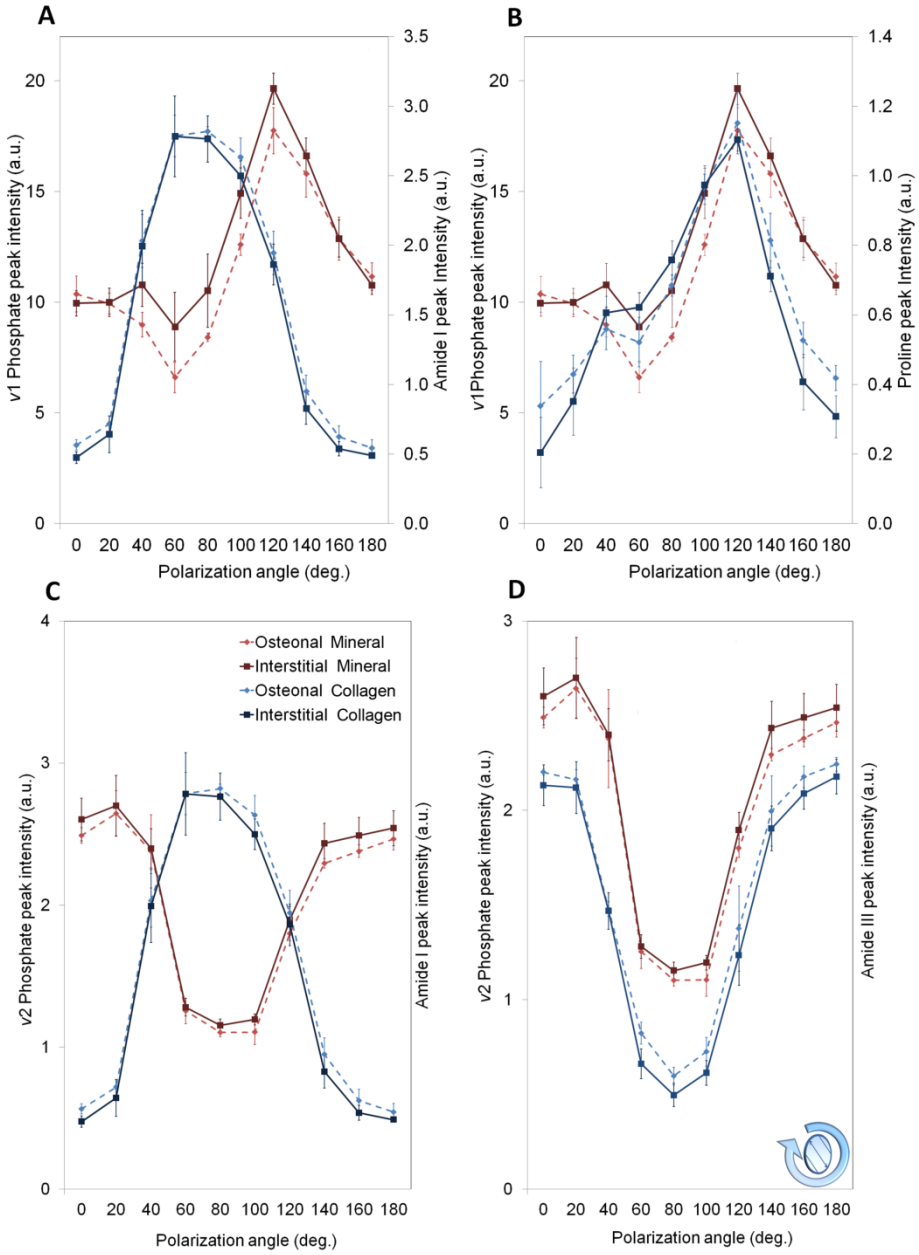

Figure 3.3: Phase mismatch of peak intensity versus polarization angle (v1 Phosphate and Amide I, **A**) leads to polarization bias of mineral to collagen ratio that can be eliminated by using Proline to represent collagen (**B**). Alternative biomarkers of mineral to collagen ratio can also be phase matched (v2 Phosphate and Amide III, **D**) to eliminate Amide I polarization bias (**C**). This phase matching prevents spurious conclusions about osteonal and interstitial differences due to polarization angle.

signal strength of ν1 Phosphate, the phase matched Proline peak can be used to represent collagen (Figure 3.3 B). Also, as indicated by Kazanci et al. [28], other RS mineral quantities can be substituted for ν1 Phosphate (Figure 3.3 C&D). The distinct phase mismatch between ν2 Phosphate and Amide I (Figure 3.3 C) was reversed by using Amide III for collagen (Figure 3.3 D).

3.4.2 Susceptibility of certain Raman peaks to polarization bias

When defined as the model amplitude normalized to mean peak intensity, the peak sensitivity to polarization decreased from the highly polarized regime to the input polarized and unaltered polarized regimes (Figure 3.4). Hydroxyproline (870 cm^{-1}) and Amide I, the two most sensitive peaks in the highly polarized regime, remained polarization sensitive in the input polarized regime. Despite the fact that spectra were acquired from different bone samples, the oscillation sensitivity trends among most peaks remain consistent between the highly polarized and input polarized regimes. Comparing input polarized and unaltered polarization regimes (paired measurements of the same sample locations at the same rotation increments), polarization sensitivity dropped off markedly for some peaks like Carbonate and Hydroxyproline (Figure 3.4). However, for other peaks like Amide I and ν1 Phosphate, degree of oscillation amplitude remains relatively unchanged. In the unaltered polarization regime, less sensitive peaks like Amide III fell into the noise floor, as evidenced by decrease in number of significant model fits by ANOVA regression (Table 3.2).

An RS surface plot for a single osteon acquired with unaltered polarization (Figure 3.5 A) illustrates that ν1 Phosphate peak intensity fluctuations (Figure 3.5 B) were out of

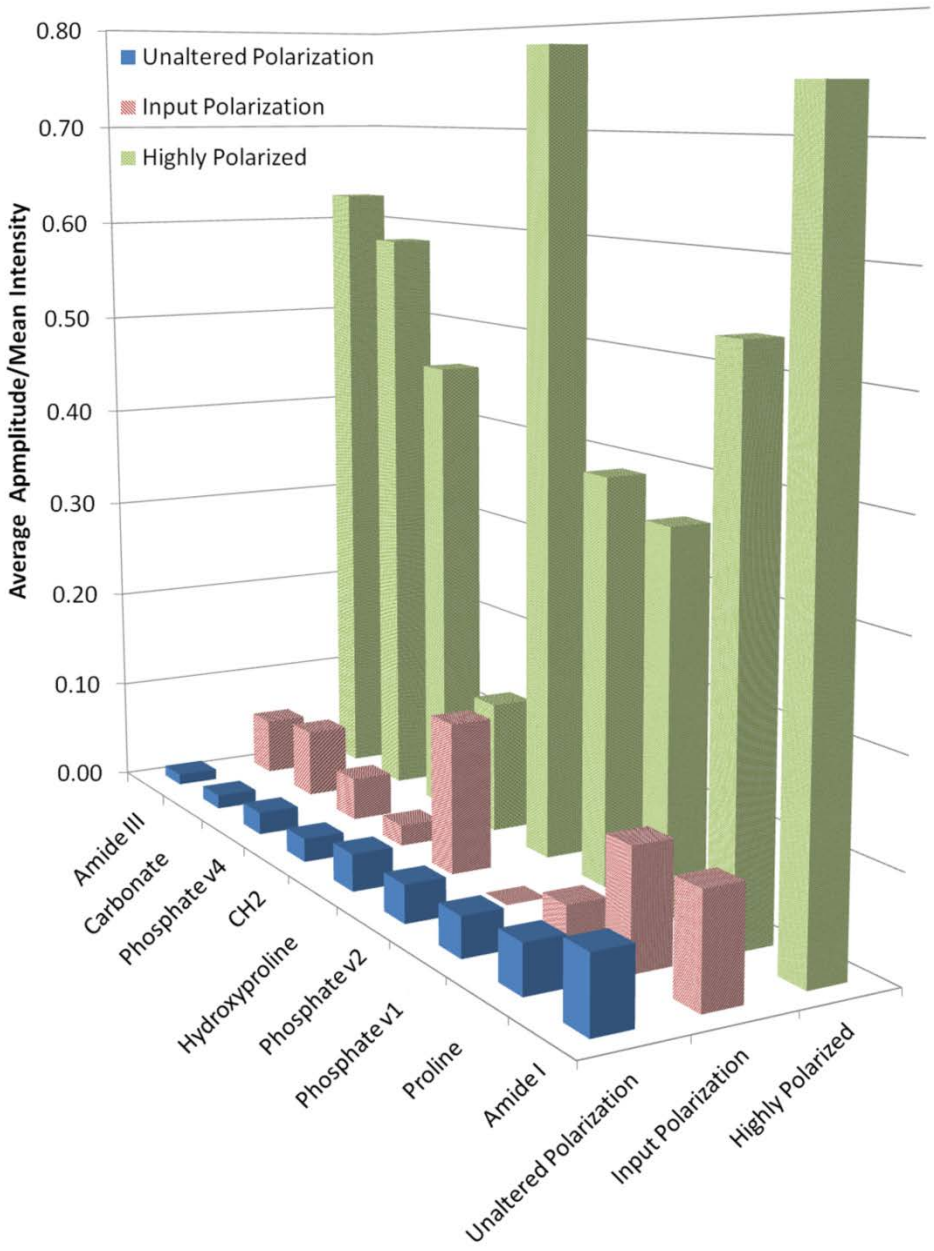

Figure 3.4: Average model amplitude normalized to mean intensity shows a preservation of peak oscillation trends with decreasing polarization. Highly polarized data (**green**) shows greater sensitivity than input polarized data (**red**). Less sensitive peaks like Amide III continue to drop in sensitivity in the unaltered polarization regime (**blue**), whereas more sensitive peaks like Amide I show consistent sensitivity.

Table 3.2: Peak sensitivity ranking as a percent change in intensity during bone rotation shows that some peaks still oscillate with unaltered system polarization.

	Highly Polarized[a]		*Input Polarized*		*Unaltered Polarization*	
Raman Peak[b]	% Change[c]	Sig. Models[d]	% Change	Sig. Models	% Change	Sig. Models
Amide III	125.2	9/10	11.2	4/6	2.2	1/6
Carbonate	116.5	10/10	13.5	5/6	2.8	1/6
ν_4 Phosphate	91.7	9/10	8.4	1/6	4.4	2/6
CH_2	26.0	10/10	4.1	2/6	4.6	1/6
Hydroxyproline	156.0	8/10	29.4	5/6	7.3	1/6
ν_2 Phosphate	77.9	8/10	N/A[e]	0/6	7.4	2/6
ν_1 Phosphate	71.9	10/10	6.2	5/6	7.8	3/6
Proline	106.7	8/10	22.7	5/6	9.5	4/6
Amide I	149.1	10/10	21.2	6/6	14.4	5/6

[a] Derived from separate samples. [b] Rank is based on the degree of mean normalized intensity fluctuation for unaltered polarization. [c] % Change is defined as the range of observed intensities normalized to the mean intensity observed during specimen rotation (Unaltered and Input Polarized) or during analyzer rotation (Highly Polarized) for significant (sig.) model fits. When more than one model fit is significant, the mean is given. [d] Number of significant models. Significance of model fit is defined as $p<0.05$ of the ANOVA regression (goodness of fit). [e] N/A: No significant models.

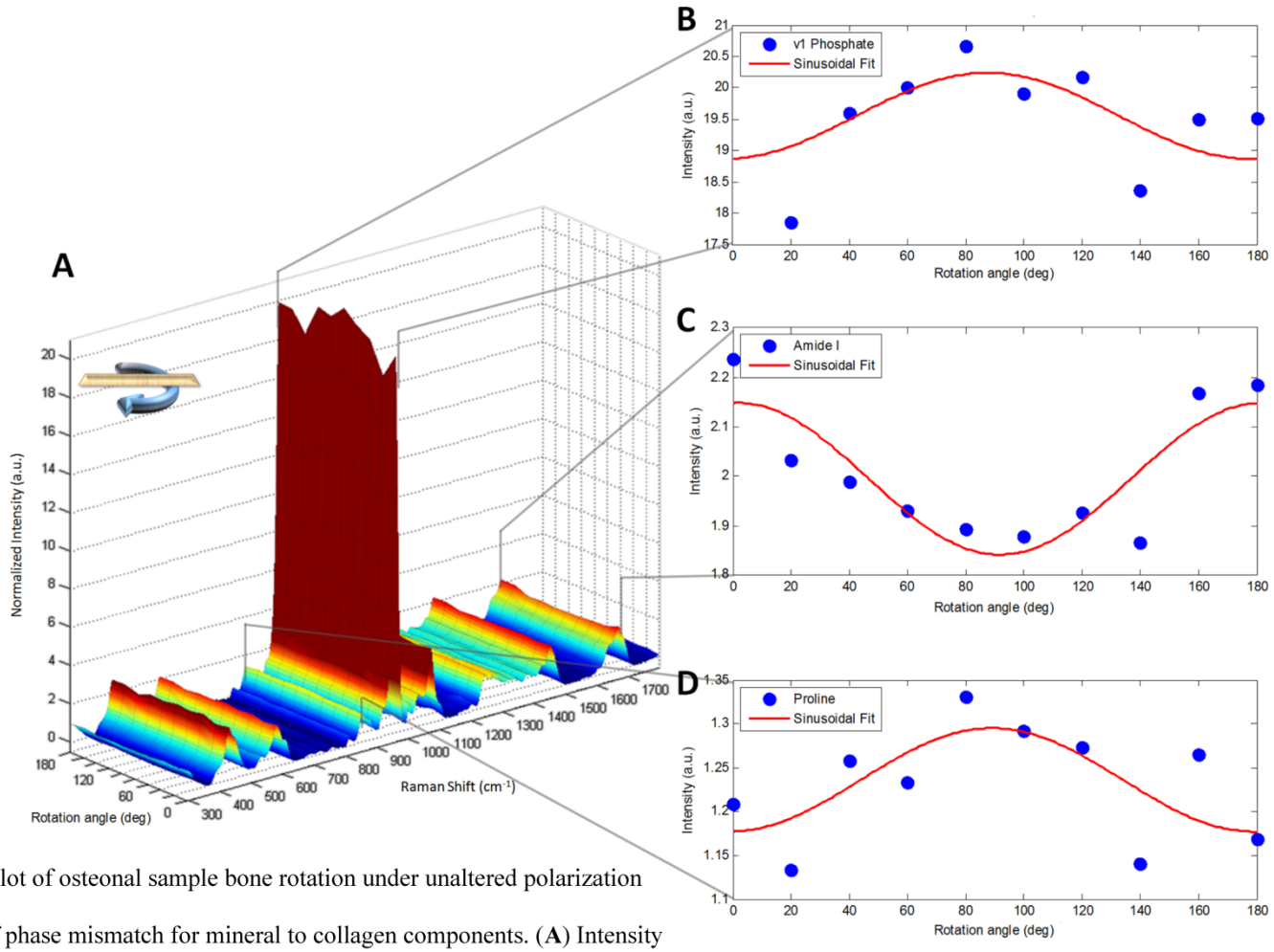

Figure 3.5: Surface plot of osteonal sample bone rotation under unaltered polarization setup indicates persistence of phase mismatch for mineral to collagen components. (**A**) Intensity colored surface plot shows spectral variance due to rotation angle. Cutaways show v1 Phosphate peak intensity (**B**) is out of phase with Amide I (**C**) while in phase with Proline (D)**.**

phase with Amide I intensity fluctuations (Figure 3.5 C) but matched to the fluctuations of Proline (Figure 3.5 D). Although noise has a significant impact on model fit in the unaltered regime, the trends of polarization phase between mineral and collagen peaks (Figure 3.5) remained consistent with trends observed when the analyzer was rotated with the bone sample stationary (Figure 3.3). Phase mismatch trends of RS biomarkers from highly polarized data persisted in unaltered polarization.

3.4.3 Performance of phase-matched ratios for compositional differences

RS maps demonstrate how phase mismatch in RS peak ratios confounds the consistent measurement of spatial heterogeneity, even in an unaltered polarization regime (Figure 3.6). Expected differences in mineral to collagen ratio between an osteon and surrounding interstitial tissue is not maintained throughout bone rotation for polarization sensitive ν1 Phosphate / Amide I (Figure 3.6 B); whereas, ν2 Phosphate / Amide III (Figure 3.6 C) shows consistent overall intensity differences between the tissue types despite rotation. Yet, this latter image is noisier than the former image due to significantly lower signal to noise ratio (SNR) of the ν2 Phosphate and Amide III peaks, relative to ν1 Phosphate. Maps of ν1 Phosphate / Proline (Figure 3.6 D) illustrate a relatively consistent image of compositional heterogeneity throughout rotation, differentiating the osteonal tissue from the more mineralized interstitial tissue. This peak ratio map is independent of bone rotation because of the low phase difference between ν1 Phosphate and Proline (Table 3.3).

Figure 3.7 shows how numerical aperture and subsequent differences in sample volume averaging affect the apparent sensitivity of mineral to matrix calculations to tissue type. The

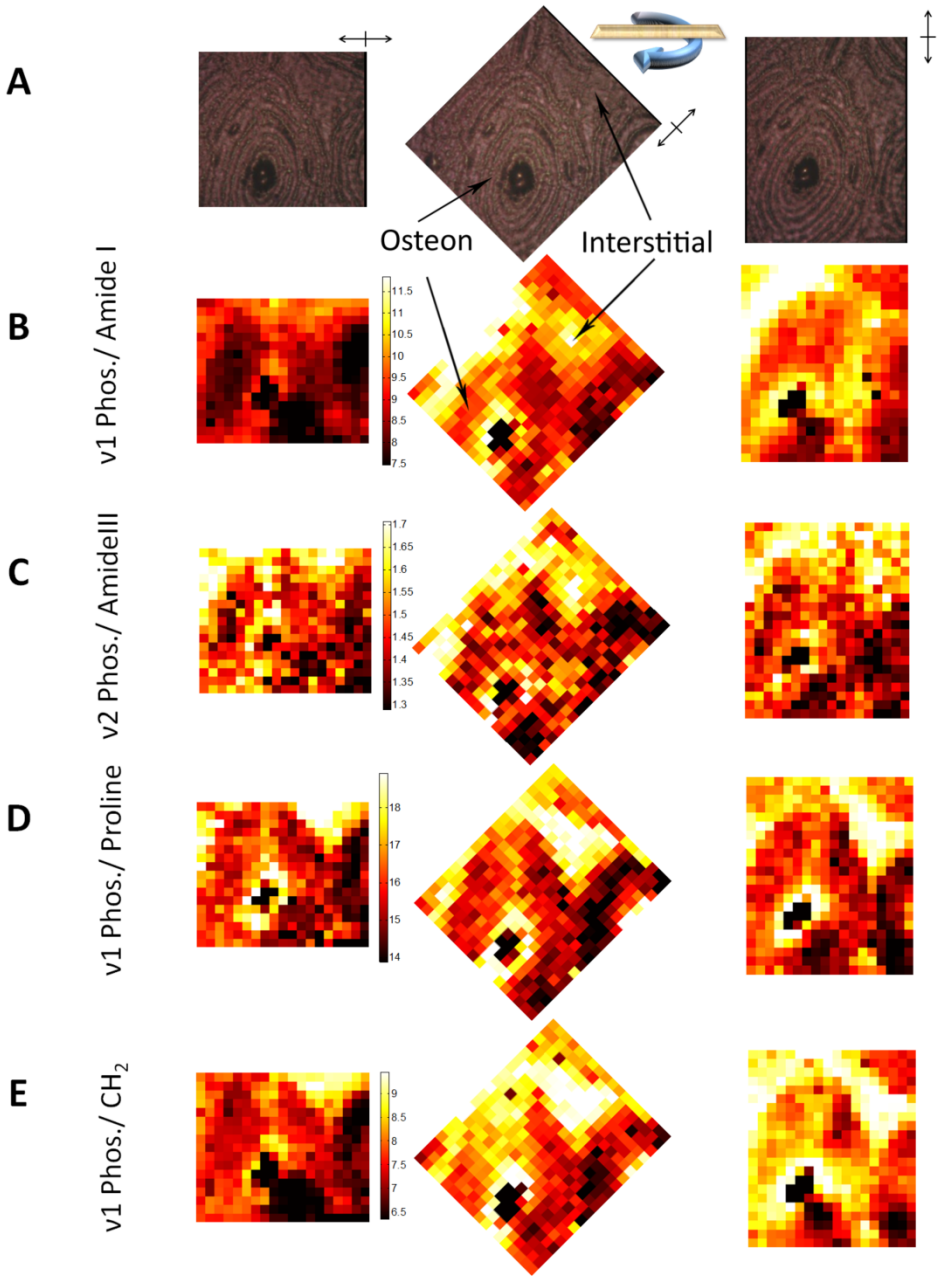

Figure 3.6: Mineral to collagen biomarker heat maps of derived peak ratios validate differential rotational consistency. (**A**) Bright field images reference the rotation of the osteon in 45 ° increments from left to right. Color maps are set to universal scale within each quantity and frames are rotated so that same image should be apparent under a lack of polarization sensitivity. (**B**) ν1 Phosphate / Amide I shows greatest rotational dependence. (**C**) ν2 Phosphate / Amide III consistency is masked by noise due to lower peak intensities. (**D**) ν1 Phosphate / Proline shows rotational consistency with a lower noise floor.

Table 3.3: Paired phase difference between selected Raman peak ratios and overall variance of peak ratios were estimated for bone and tooth rotation using the unaltered polarization instrument.

		Bone Samples		*Dentin Control*	
Peak Ratio	Representation	Phase difference (degrees)[a]	Coefficient of variation[b]	Phase Difference (degrees)	Coefficient of variation
ν1 Phosphate/ Amide I	mineral:collagen	69.9	0.073	85.5	0.110
ν2 Phosphate / Amide III	mineral:collagen	N/A[c]	0.0004	0.1	0.021
ν1 Phosphate / Proline	mineral:collagen	2.2	0.023	9.2	0.040
ν1 Phosphate / CH_2	mineral: protein	62.8	0.038	85.2	0.054
Carbonate / ν1 Phosphate	carbonate substitution	0.1	0.020	3.1	0.009
Carbonate/ ν2 Phosphate	carbonate substitution	N/A[c]	0.025	6.5	0.016
Carbonate/ ν4 Phosphate	carbonate substitution	31.6	0.022	9. 3	0.022

[a] To obtain phase difference, the difference in phase between paired peaks (same spectra for the same site of rotation) was averaged among the multiple sites of data collection in which model fit was significant for both peaks. [b] To obtain coefficient of variation, the standard deviation per mean of the peak ratio for a given rotation was averaged across multiple sites of data collection. [c] N/A: No ratio could be generated from significant models within the same sample. Significance of model fit is defined as $p<0.05$ of the ANOVA regression (goodness of fit).

calculations compare ν1 Phosphate / Amide I sensitivity to the phase matched ν 1 Phosphate / Proline using a map at 20x magnification and a 50x map of a portion of the same area (panel A). The polarization sensitive Amide I ratio produced a distinct intensity change at 50x magnification in the 45 degree map (Figure 3.7 C) that was less pronounced but arguably still apparent at 20x (Figure 3.7 B). The mineral to matrix ratio with Proline (Figure 3.7 D and E) was relatively consistent throughout.

3.5 Discussion

Development of Raman spectroscopy methods towards bone diagnostics requires a firm understanding of which RS measures are sensitive to bone tissue composition and which are sensitive to bone tissue organization. While the potential for highly polarized RS to discriminate bone organization is known (Table 3.1), the present study provides a thorough characterization of the contribution of polarization bias in a standard Raman microscope to RS measurements of bone. When the goal of RS analysis is to assess compositional differences in bone, polarization bias adds uncertainty to the measurements. The addition of polarization optics, even to reduce polarization bias, leads to increased data collection time. Therefore, this study characterized peak and peak ratio specificity without altering instrumentation and found that polarization bias exists in a standard microscope and needs to be addressed.

Consistent with findings from the highly polarized RS analysis of mouse bone by Raghavan et al. [30], polarization bias can persist for a low numerical aperture objective (NA= 0.4) (Figure 3.7) that effectively averages the signal over larger spatial volumes than a 50x objective with a NA of 0.75. Nonetheless, matching polarization-orientation phase, effectively matching

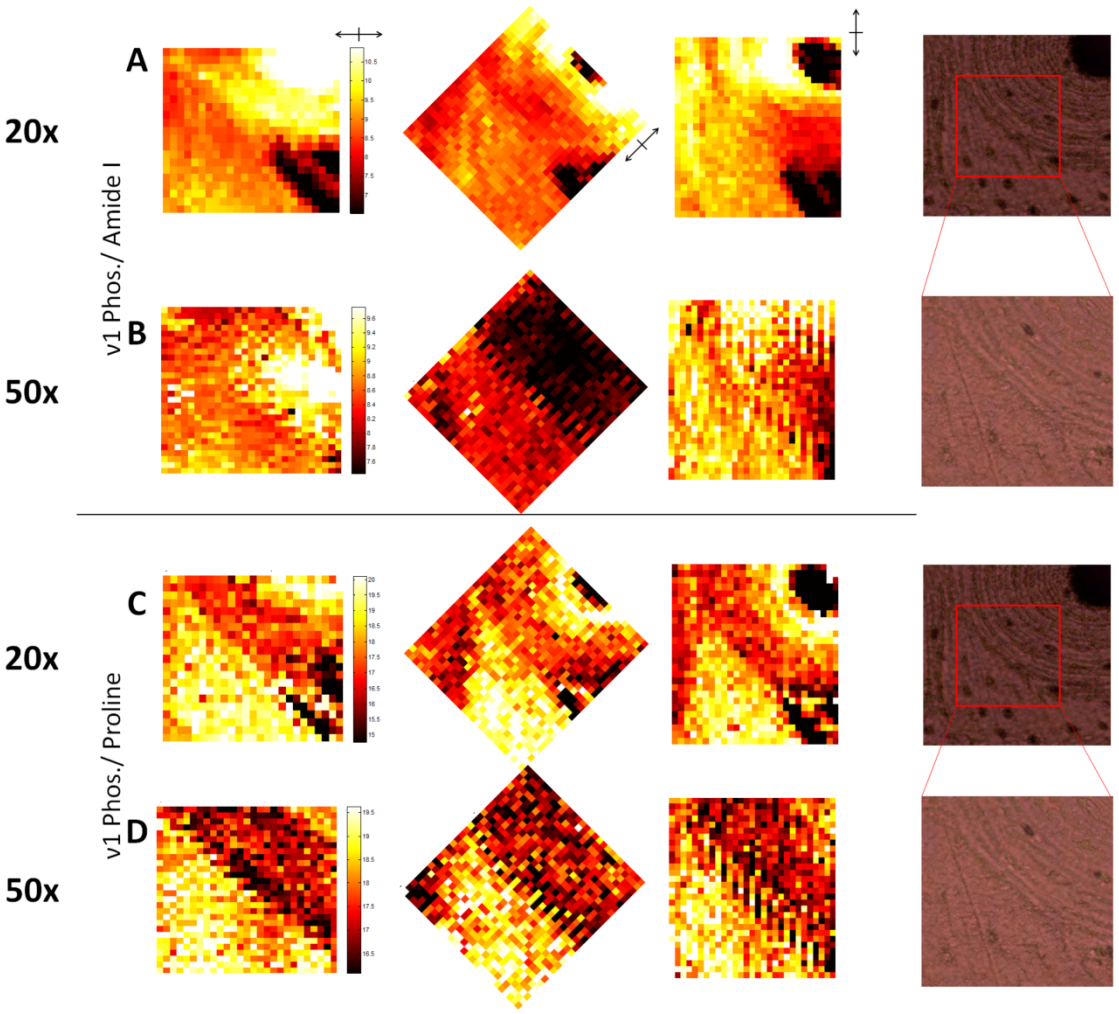

Figure 3.7: Heat Maps of Derived Peak Ratios retain polarization sensitivity when rotated, even with reduction of objective numerical aperture. (**A**) Bright field images reference the scanned areas at 20x (NA= 0.4) and 50x (NA= 0.75). Color maps are set to universal scale within each quantity. (**B**) ν1 Phosphate / Amide I maps at 20x show mild intensity changes under rotation at the border between osteonal and interstitial tissue. (**C**) The effect on ν1 Phosphate / Amide I increases with increased numerical aperture in the 50x maps (**D**) ν1 Phosphate / Proline shows no notable intensity changes with rotation at 20x. (**E**) ν1 Phosphate / Proline shows no notable intensity changes with rotation at 50x, but noise is increased.

the organizational component of RS peaks, allows for consistent measures of composition (Figure 3.3 B and 3 D as well as Figure 3.7 C and 7 D). This study used spectral maps of spatial heterogeneity within bone (Figure 3.6) to establish that peak ratio sensitivity identified by polarized Raman Spectroscopy studies (Table 3.1) remains in unaltered polarization regimes (i.e., standard confocal RS instruments). In effect, polarization phase can be exploited to distinguish compositional heterogeneity from organizational heterogeneity. Finally, throughput costs of added optics can be avoided by using less sensitive peaks and phase-optimized peak ratios.

Spectral fingerprints of disease may rely upon organization of collagen and mineral as much as the relative composition of these constituents. This is of particular importance because bone disorders and disease states including osteoporosis and osteogenesis imperfecta can involve deleterious changes in bone organization [30]. Moreover, the organization of the constituents of bone tissue influences the fracture resistance of bone [42-46]. The observations of phase difference (Figure 3.2) from our modeling of spectral data as a function of analyzer rotation is consistent with findings from previous highly polarized studies [19, 28, 36], as well as recent theoretical models of collagen orientation within osteons [47]. The phase differences between RS biomarker peaks arise from the organization of mineral crystals and collagen fibrils, such that information encoded within polarization phase may provide new insight for future disease diagnosis or fracture risk assessments. However, clear associations of phase and bone's fracture resistance remain to be established. Nonetheless, as RS matures toward clinical use, consistency in discriminating composition from organization may contribute to accurate assessment of fracture risk.

Alternatively, RS could prove especially effective in the diagnosis of bone diseases that are pathologically based upon bone composition, including diabetes, chronic kidney disease, and the discrimination of grades of osteogenesis imperfecta. Recent investigations employing spatial sampling regimens to average out polarization bias concur that alternative mineral to collagen ratios (Figure 3.6) exhibit increased sensitivity to known osteonal and interstitial differences in composition [18, 48]. Specifically, improvement in mineral to collagen ratio variance and microstructure delineation when utilizing Proline instead of Amide I as a collagen component can be explained by a decrease in underlying polarization phase difference between ν1 Phosphate (mineral constituent) and Proline (collagen constituent) (Table 3.3).

RS acquisition of bone spectra often spans a range of 300- 1800 cm^{-1} to cover prominent peaks, though it is expanded in some studies to 3000 cm^{-1} to capture a CH peak. Collecting Proline, ν1 Phosphate, and Carbonate would require spanning only 300 cm^{-1}, further reducing necessary instrumentation, data processing, and collection time. Despite the availability of commercial systems, RS instrumentation differs largely between research groups and studies, implying that polarization bias from orientation sensitive peaks may vary between studies.

Changes in Raman spectra as the bone or tooth rotates relative to the incident laser light reveal the persistence of a polarization-orientation bias for sensitive peaks like Amide I even within less sensitive unaltered RS setups. Polarization sensitivity trends (Figure 3.4) are conserved among prominent peaks in both the highly polarized regime and in the input polarized regime, despite the fact that spectra were acquired from different bone samples. Phase trends seen in highly polarized acquisition of bone appear to persist in unaltered instrumentation as well (Figure 3.5). Phase matched peak ratios of mineral to collagen ratio demonstrate lower

coefficients of variation and therefore greater consistency (Table 3.3). When determined from the same site of bone rotation and then averaged across the various sites, the phase difference between ν1 Phosphate and Proline was 2.2 degrees for bone and 9 degrees for more highly organized dentin (Table 3.3), suggesting that these trends in phase difference may be conserved between tissues and anatomical locations. Despite the low intensity of Proline, the high intensity of the ν1 Phosphate peak may make ν1 Phosphate / Proline a more practical compositional metric than ν2 Phosphate / Amide III, which also has a low paired phased difference (Table 3.3). In addition, the use of peak phase difference confirmed the compositional nature of carbonate substitution (Table 3.3). While results suggest optimal metrics for bone composition and caution against possible inconsistent use of other metrics, the polarization-orientation information of RS biomarkers may have greater implications for future clinical bone diagnostics.

Consistent use of less polarization sensitive peaks or phase-matched ratios may allow for clearer comparisons between instruments and studies. RS sensitivity to glucocorticoid-treatment in rheumatoid arthritis bone shows compositional difference despite normalization to Amide I when using a fiber optic (polarization insensitive) system [26]. These biomechanical correlations are likely separate and distinct from RS correlations to collagen tension changes seen in formal polarization analysis [49]. Given low instrument polarization and results from less polarization sensitive carbonate and Amide III bands, analysis of bone from osteoarthritic patients on different load bearing surfaces can be interpreted as a largely compositional effect [50]. Phase mismatch of v1 Phosphate / CH2 (see Figure 3.2 and Figure 3.6 E) may have contributed to biomechanical correlation due to use of a commercial confocal system [24], thereby indicating a predominantly organizational phenotype. Interpretation of results from these and future studies

in light of instrument polarization may help to define consistent Raman signatures for compositional and structural disease.

3.6 Conclusions

Polarization–orientation information in bone biomarkers, as seen in highly polarized studies involving Raman Spectroscopy, persists in unaltered commercial systems with lower inherent sensitivity to polarization. Modeling this consistent bias shows that matched phase information between peaks yields biomarker ratios that are less sensitive to polarization-orientation, without the loss of throughput necessitated by additional optics. Bias in compositional measures can be minimized by phase matching; specifically, findings support using ν1 Phosphate / Proline for mineral to collagen and Carbonate / ν1 Phosphate for carbonate substitution. In the diagnosis of organizational phenotypes, polarization-orientation can be maximized by phase mismatch (i.e. ν1 Phosphate / Amide I) without necessarily including polarization optics. Optimizing polarization in the instrument and in biomarkers should help to increase discrimination and consistency in future studies of bone.

3.7 Acknowledgements

This material is based upon work supported by the Department of Veterans Affairs, Veterans Health Administration, Office of Research and Development, Biomedical Laboratory Research and Development. The authors would also like to acknowledge financial support from NSF Grant 7074068.

3.8 References:

1. Amin, S., Kopperdhal, D.L., Melton, L.J., 3rd, Achenbach, S.J., Therneau, T.M., Riggs, B.L., Keaveny, T.M. and Khosla, S., "Association of hip strength estimates by finite-element analysis with fractures in women and men," J Bone Miner Res **26**(7), 1593-1600 (2011)
2. Kanis, J.A., McCloskey, E., Johansson, H., Oden, A. and Leslie, W.D., "FRAX((R)) with and without bone mineral density," Calcif Tissue Int **90**(1), 1-13 (2012)
3. Matousek, P., Clark, I.P., Draper, E.R., Morris, M.D., Goodship, A.E., Everall, N., Towrie, M., Finney, W.F. and Parker, A.W., "Subsurface probing in diffusely scattering media using spatially offset Raman spectroscopy," Applied spectroscopy **59**(4), 393-400 (2005)
4. Morris, M.D. and Mandair, G.S., "Raman assessment of bone quality," Clinical orthopaedics and related research **469**(8), 2160-2169 (2011)
5. Schulmerich, M.V., Cole, J.H., Dooley, K.A., Morris, M.D., Kreider, J.M., Goldstein, S.A., Srinivasan, S. and Pogue, B.W., "Noninvasive Raman tomographic imaging of canine bone tissue," Journal of biomedical optics **13**(2), 020506 (2008)
6. Schulmerich, M.V., Cole, J.H., Kreider, J.M., Esmonde-White, F., Dooley, K.A., Goldstein, S.A. and Morris, M.D., "Transcutaneous Raman spectroscopy of murine bone in vivo," Applied spectroscopy **63**(3), 286-295 (2009)
7. Schulmerich, M.V., DOOLEY, K.A., Morris, M.D., Vanasse, T.M. and Goldstein, S.A., "Transcutaneous fiber optic Raman spectroscopy of bone using annular illumination and a circular array of collection fibers," Journal of biomedical optics **11**(6), 060502 (2006)
8. McCreadie, B.R., Morris, M.D., Chen, T.C., Sudhaker Rao, D., Finney, W.F., Widjaja, E. and Goldstein, S.A., "Bone tissue compositional differences in women with and without osteoporotic fracture," Bone **39**(6), 1190-1195 (2006)
9. Awonusi, A., Morris, M.D. and Tecklenburg, M.M., "Carbonate assignment and calibration in the Raman spectrum of apatite," Calcif Tissue Int **81**(1), 46-52 (2007)
10. Yerramshetty, J.S. and Akkus, O., "The associations between mineral crystallinity and the mechanical properties of human cortical bone," Bone **42**(3), 476-482 (2008)
11. Yerramshetty, J.S., Lind, C. and Akkus, O., "The compositional and physicochemical homogeneity of male femoral cortex increases after the sixth decade," Bone **39**(6), 1236-1243 (2006)
12. Timlin, J.A., Carden, A., Morris, M.D., Rajachar, R.M. and Kohn, D.H., "Raman spectroscopic imaging markers for fatigue-related microdamage in bovine bone," Anal Chem **72**(10), 2229-2236 (2000)

13. Ramasamy, J.G. and Akkus, O., "Local variations in the micromechanical properties of mouse femur: the involvement of collagen fiber orientation and mineralization," J Biomech **40**(4), 910-918 (2007)

14. Akkus, O., Adar, F. and Schaffler, M.B., "Age-related changes in physicochemical properties of mineral crystals are related to impaired mechanical function of cortical bone," Bone **34**(3), 443-453 (2004)

15. Draper, E.R., Morris, M.D., Camacho, N.P., Matousek, P., Towrie, M., Parker, A.W. and Goodship, A.E., "Novel assessment of bone using time-resolved transcutaneous Raman spectroscopy," J Bone Miner Res **20**(11), 1968-1972 (2005)

16. Matousek, P., Draper, E.R., Goodship, A.E., Clark, I.P., Ronayne, K.L. and Parker, A.W., "Noninvasive Raman spectroscopy of human tissue in vivo," Applied spectroscopy **60**(7), 758-763 (2006)

17. Patil, C.A., Kalkman, J., Faber, D.J., Nyman, J.S., van Leeuwen, T.G. and Mahadevan-Jansen, A., "Integrated system for combined Raman spectroscopy-spectral domain optical coherence tomography," Journal of biomedical optics **16**(1), 011007 (2011)

18. Nyman, J.S., Makowski, A.J., Patil, C.A., Masui, T.P., O'Quinn, E.C., Bi, X., Guelcher, S.A., Nicollela, D.P. and Mahadevan-Jansen, A., "Measuring differences in compositional properties of bone tissue by confocal Raman spectroscopy," Calcif Tissue Int **89**(2), 111-122 (2011)

19. Gamsjaeger, S., Masic, A., Roschger, P., Kazanci, M., Dunlop, J.W., Klaushofer, K., Paschalis, E.P. and Fratzl, P., "Cortical bone composition and orientation as a function of animal and tissue age in mice by Raman spectroscopy," Bone **47**(2), 392-399 (2010)

20. Juang, C.B., Finzi, L. and Bustamante, C.J., "Design and application of a computer-controlled confocal scanning differential polarization microscope," Rev. Sci. Instr. **59**(11), 2399-2408 (1988)

21. Gourion-Arsiquaud, S., Faibish, D., Myers, E., Spevak, L., Compston, J., Hodsman, A., Shane, E., Recker, R.R., Boskey, E.R. and Boskey, A.L., "Use of FTIR spectroscopic imaging to identify parameters associated with fragility fracture," J Bone Miner Res **24**(9), 1565-1571 (2009)

22. Gadaleta, S.J., Camacho, N.P., Mendelsohn, R. and Boskey, A.L., "Fourier transform infrared microscopy of calcified turkey leg tendon," Calcif Tissue Int **58**(1), 17-23 (1996)

23. Gadaleta, S.J., Landis, W.J., Boskey, A.L. and Mendelsohn, R., "Polarized FT-IR microscopy of calcified turkey leg tendon," Connect Tissue Res **34**(3), 203-211 (1996)

24. Szabo, M.E., Zekonyte, J., Katsamenis, O.L., Taylor, M. and Thurner, P.J., "Similar damage initiation but different failure behavior in trabecular and cortical bone tissue," J Mech Behav Biomed Mater **4**(8), 1787-1796 (2011)

25. Nyman, J.S., Lynch, C.C., Perrien, D.S., Thiolloy, S., O'Quinn, E.C., Patil, C.A., Bi, X., Pharr, G.M., Mahadevan-Jansen, A. and Mundy, G.R., "Differential effects between the

loss of MMP-2 and MMP-9 on structural and tissue-level properties of bone," J Bone Miner Res **26**(6), 1252-1260 (2011)

26. Maher, J.R., Takahata, M., Awad, H.A. and Berger, A.J., "Raman spectroscopy detects deterioration in biomechanical properties of bone in a glucocorticoid-treated mouse model of rheumatoid arthritis," Journal of biomedical optics **16**(8), 087012 (2011)

27. Gevorkian, B.Z., Arnotskaia, N.E. and Fedorova, E.N., "[Study of bone tissue structure using polarized Raman spectra]," Biofizika **29**(6), 1046-1052 (1984)

28. Kazanci, M., Roschger, P., Paschalis, E.P., Klaushofer, K. and Fratzl, P., "Bone osteonal tissues by Raman spectral mapping: orientation-composition," Journal of structural biology **156**(3), 489-496 (2006)

29. Falgayrac, G., Facq, S., Leroy, G., Cortet, B. and Penel, G., "New method for Raman investigation of the orientation of collagen fibrils and crystallites in the Haversian system of bone," Applied spectroscopy **64**(7), 775-780 (2010)

30. Raghavan, M., Sahar, N.D., Wilson, R.H., Mycek, M.A., Pleshko, N., Kohn, D.H. and Morris, M.D., "Quantitative polarized Raman spectroscopy in highly turbid bone tissue," Journal of biomedical optics **15**(3), 037001 (2010)

31. Long, D.A., "Intensities in Raman Spectra. I. A Bond Polarizability Theory," Proceedings of the Royal Society of London. Series A, Mathematical and Physical Sciences **217**(1129), 203-221 (1953)

32. Placzek, G., "Rayleigh-Streuung und Raman-Effekt," in Handbuch der Radiologie E. Marx, Ed., pp. 205-374, Akademische Verlagsgesellschaft, Leipzig, Germany (1934).

33. Bonifacio, A. and Sergo, V., "Effects of sample orientation in Raman microspectroscopy of collagen fibers and their impact on the interpretation of the amide III band," Vib Spec **53**(2), 314-317 (2010)

34. Lieber, C.A. and Mahadevan-Jansen, A., "Automated method for subtraction of fluorescence from biological Raman spectra," Applied spectroscopy **57**(11), 1363-1367 (2003)

35. Robichaux-Viehoever, A., Kanter, E., Shappell, H., Billheimer, D., Jones, H. and Mahadevan-Jansen, A., "Characterization of Raman Spectra Measured in Vivo for the Detection of Cervical Dysplasia," Applied spectroscopy **61**(9), 986-993 (2007)

36. Kazanci, M., Wagner, H.D., Manjubala, N.I., Gupta, H.S., Paschalis, E., Roschger, P. and Fratzl, P., "Raman imaging of two orthogonal planes within cortical bone," Bone **41**(3), 456-461 (2007)

37. Porto, S., Giordmaine, J. and Damen, T., "Depolarization of Raman Scattering in Calcite," Physical Review **147**(2), 608-611 (1966)

38. Levenson, M.D., "Polarization techniques in coherent Raman spectroscopy," J Raman Spec **10**(1), 9-23 (1981)

39. Hecht, E. and Zaj*ac, A., Optics, Addison-Wesley Pub. Co., Reading, Mass. (1987).

40. Malus, E., "Mémoires de Physique et de Chimie de la Société d'Arcueil," (1809).

41. Nelder, J.A. and Mead, R., "A Simplex Method for Function Minimization," The Computer Journal **7**(4), 308-313 (1965)

42. Ascenzi, A. and Bonucci, E., "The tensile properties of single osteons," Anat Rec **158**(4), 375-386 (1967)

43. Ascenzi, M.G. and Lomovtsev, A., "Collagen orientation patterns in human secondary osteons, quantified in the radial direction by confocal microscopy," Journal of structural biology **153**(1), 14-30 (2006)

44. Martin, R.B. and Boardman, D.L., "The effects of collagen fiber orientation, porosity, density, and mineralization on bovine cortical bone bending properties," J Biomech **26**(9), 1047-1054 (1993)

45. Martin, R.B. and Ishida, J., "The relative effects of collagen fiber orientation, porosity, density, and mineralization on bone strength," J Biomech **22**(5), 419-426 (1989)

46. Martin, R.B., Lau, S.T., Mathews, P.V., Gibson, V.A. and Stover, S.M., "Collagen fiber organization is related to mechanical properties and remodeling in equine bone. A comparison of two methods," J Biomech **29**(12), 1515-1521 (1996)

47. Wagermaier, W., Gupta, H.S., Gourrier, A., Burghammer, M., Roschger, P. and Fratzl, P., "Spiral twisting of fiber orientation inside bone lamellae," Biointerphases **1**(1), 1-5 (2006)

48. Bi, X., Patil, C.A., Lynch, C.C., Pharr, G.M., Mahadevan-Jansen, A. and Nyman, J.S., "Raman and mechanical properties correlate at whole bone- and tissue-levels in a genetic mouse model," J Biomech **44**(2), 297-303 (2011)

49. Masic, A., Bertinetti, L., Schuetz, R., Galvis, L., Timofeeva, N., Dunlop, J.W., Seto, J., Hartmann, M.A. and Fratzl, P., "Observations of multiscale, stress-induced changes of collagen orientation in tendon by polarized Raman spectroscopy," Biomacromolecules **12**(11), 3989-3996 (2011)

50. Buchwald, T., Niciejewski, K., Kozielski, M., Szybowicz, M., Siatkowski, M. and Krauss, H., "Identifying compositional and structural changes in spongy and subchondral bone from the hip joints of patients with osteoarthritis using Raman spectroscopy," Journal of biomedical optics **17**(1), 017007 (2012)

51. Leroy, G., Penel, G., Leroy, N. and Brès, E., "Human Tooth Enamel: A Raman Polarized Approach," Applied spectroscopy **56**(8), 1030-1034 (2002)

52. Ko, A.C.T., Choo-Smith, L.-P.i., Hewko, M., Sowa, M.G., Dong, C.C.S. and Cleghorn, B., "Detection of early dental caries using polarized Raman spectroscopy," Opt. Express **14**(1), 203-215 (2006)

53. Kozielski, M., Buchwald, T., Szybowicz, M., Blaszczak, Z., Piotrowski, A. and Ciesielczyk, B., "Determination of composition and structure of spongy bone tissue in human head of femur by Raman spectral mapping," Journal of materials science. Materials in medicine **22**(7), 1653-1661 (2011)

CHAPTER 4

THE LOSS OF ACTIVATING TRANSCRIPTION FACTOR 4 (ATF4) REDUCES BONE TOUGHNESS AND FRACTURE TOUGHNESS

Work described in this Chapter is published in:

Makowski, A.J., Uppuganti, S., Wadeer, S.A., Whitehead, J.M., Rowland, B.J., Granke, M., Mahadevan-Jansen, A., Yang, X. and Nyman, J.S., "The loss of activating transcription factor 4 (ATF4) reduces bone toughness and fracture toughness," Bone 62, 1-9 (2014)

4.1 Abstract

Even though age-related changes to bone tissue affecting fracture risk are well characterized, only a few matrix-related factors have been identified as important to maintaining fracture resistance. As a gene critical to osteoblast differentiation, activating transcription factor 4 (ATF4) is possibly one of these important factors. To test the hypothesis that the loss of ATF4 affects the fracture resistance of bone beyond bone mass and structure, we harvested bones from *Atf4*+/+ and *Atf4*-/- littermates at 8 and 20 weeks of age (n≥9 per group) for bone assessment across several length scales. From whole bone mechanical tests in bending, femurs from *Atf4*-/- mice were found to be brittle with reduced toughness and fracture toughness compared to femurs from *Atf4*+/+ mice. However, there were no differences in material strength and in tissue

hardness, as determined by nanoindentation, between the genotypes, irrespective of age. Tissue mineral density of the cortex at the point of loading as determined by micro-computed tomography was also not significantly different. However, by analyzing local composition by Raman Spectroscopy (RS), bone tissue of *Atf4-/-* mice was found to have higher mineral to collagen ratio compared to wild-type tissue, primarily at 20 weeks of age. From RS analysis of intact femurs at 2 orthogonal orientations relative to the polarization axis of the laser, we also found that the organizational-sensitive peak ratio, ν1Phosphate per Amide I, changed to a greater extent upon bone rotation for Atf4-deficient tissue, implying bone matrix organization may contribute to the brittleness phenotype. Target genes of ATF4 activity are not only important to osteoblast differentiation but also maintaining bone toughness and fracture toughness.

4.2 Introduction

The age-related increase in fracture risk is not solely due to a loss in bone mineral density [1], and by extension a decline in bone strength, leading to the idea that the inherent quality of bone tissue is an important attribute of fracture resistance. With respect to the apparent material properties of bone, there is a greater loss in cortical bone toughness with aging than in bone strength [2] (-8.7% per decade vs. -4.7% per decade [3]). In addition to the age-related decrease in post-yield energy dissipation [4], the capacity of human cortical bone to resist crack growth (fracture toughness) diminishes with advancing age as determined by strain energy release rate (G_c), critical stress intensity factor (K_c), J-integral, and R-curve behavior (crack propagation toughness) [5-9]. Despite the critical role of collagen as a determinant of bone toughness (i.e., lack of brittleness) [10-

12] and fracture toughness [13-15], there is an incomplete understanding of what exactly regulates these material properties of bone.

Recent analyses of long bones from different genetic mouse models have started to identify genes that may be important in promoting the ability of the bone tissue to resist fracture, beyond influencing bone strength. For example, deletion of the proteolysis genes, matrix metalloproteinase (MMP)-9 and MMP-13 separately, produced a brittle bone phenotype (e.g., low post-yield deflection) [16,17]. Deletion of non-collagenous proteins, namely osteopontin (OPN) and osteocalcin (OCN) separately or concurrently, resulted in bones with lower fracture toughness in relation to long bones from wild-type mice [18,19]. Acquiring femurs from genetic and transgenic mice in which transforming growth factor-beta (TGF-β) signaling was either low, normal or high, Balooch et al. [20] provided the first link between a growth factor and fracture toughness: resistance to crack growth was inversely proportional to TGF-β signaling.

The activating transcription factor 4 (ATF4) is another possible gene important to promoting the toughness and fracture toughness of bone. Transcription factors determine cell fate, and in the case of osteoblasts, ATF4 activity promotes the expression of the aforementioned OCN [21]. Moreover, osteoblasts lacking ATF4 do not fully mature and do not adequately synthesize type 1 collagen as amino acid transport is diminished in ATF-deficient osteoblasts (in vitro) [21]. Thus, *Atf4-/-* mice have smaller bones and less trabecular bone volume fraction than *Atf4+/+* mice. To date, there is scant evidence that transcription factors regulate the fracture resistance of bone from the perspective of

energy dissipation during fracture. Understandably, toughening mechanisms are multifactorial given the hierarchical organization of bone's constituents. Nonetheless, evidence that the loss of a transcription factor affects bone toughness or fracture toughness opens avenues of research into novel therapeutic targets that go beyond stimulating more bone (or preventing loss of bone) to generating better bone tissue with high resistance to fracture. Toward this end, we hypothesized that the loss of ATF4 lowers bone's resistance to fracture through changes in the matrix, not necessarily due to deficits in bone structure and mineral density.

4.3 Materials and Methods

4.3.1 Tissue Collection

Mice lacking 1 copy of ATF4 were re-derived onto a FVB background from an existing colony [21] (C57BL/6 background) because bones from the C57BL/6 strain have relatively low ash fraction [22,23] and do not readily snap during load-to-failure tests in the three point bending configuration when acquired from young mice. Breeding *Atf4*+/- mice generated *Atf4*+/+ ($n \geq 12$ per age group) and *Atf4*-/- littermates (n=9 per age group) that were euthanized at 8 and 20 weeks of age following a protocol approved by the local IACUC. Femurs and the L6 vertebrae were frozen in phosphate buffered saline (PBS) for biomechanical testing, while tibiae were dehydrated in ethanol and embedded in polymethylmethacrylate (PMMA) [24]. For Raman Spectroscopy (RS) and nanoindentation, transverse cross sections were cut at the mid-shaft (~6 mm thick in a region above the tibia-fibula junction) using a diamond embedded band saw (310, EXAKT Technologies, Inc., Oklahoma City, OK). The proximal surface of the embedded

section was ground on successive grits of silicon carbide paper using a precision grinder (400CS, EXAKT Technologies, Inc., Oklahoma City, OK) and then polished on synthetic cloth (MasterTex, Buehler, Lake Bluff, IL) with alumina solution (MasterPrep 0.05 μm, Buehler, Lake Bluff, IL),[16] using a polisher (VibroMet 2, Buehler, Lake Bluff, IL). The posterior side of the right femur from each mouse was micro-notched for fracture toughness testing using first a low speed, diamond-embedded saw, and then a razorblade coated with a diamond solution [18].

4.3.2 Micro-Computed Tomography Analysis

Prior to mechanical testing, the mid-shafts of the un-notched, left femurs and the L6 VBs were scanned (μCT40, Scanco Medical, Brüttisellen, Switzerland) at an isotropic voxel size of 12 μm using the same settings (70 kVp/114 μA; 1000 projections per 360° rotation; and 300 ms integration time) and a hydroxyapatite (HA) phantom calibration with the manufacturer's beam hardening correction. To calculate structural properties (Ct.Th, Ct.Ar, I_{min}, etc.) and tissue mineral density of cortical bone (Ct.TMD), contours were fit to the outer cortex. To calculate the architectural properties (BV/TV, Tb.N, Conn.D, etc.) and TMD of trabecular bone (Tb.TMD), contours were drawn by hand inside the cortical shell of the VB for each slice between the endplates. The segmentation procedure was consistent among all scans per bone type: global thresholds (and a Gaussian filter to suppress image noise) of 715.2 mgHA/cm^3 (sigma=0.8 with support of 2) for cortical and 421.3 mgHA/cm^3 (sigma=0.3 with support of 1) for trabecular bone. The central mid-shaft of the notched, right femurs were scanned at an isotropic voxel size of 6 μm using the same scanner and scan conditions. Contours were fit to the outer cortex above and below the notched region to determine the mean centroid, cortical thickness (Ct.Th), mean

radius of the cortex ((c_{min} + c_{max})/2), and Ct.TMD. The notched region was evaluated to ensure proper size and to determine the angle of the notch (2θ).

4.3.3 Whole-Bone Biomechanical Testing

Three point bending tests of hydrated, un-notched [16] and notched femurs [5] were conducted using a bench-top, material testing system (Dynamight 8841, Instron, Canton, OH). For the un-notched bones, the span (L) and loading rate were 8 mm and 3 mm/min, respectively. For the notched femurs, the span was 4 times the mean outer anterior-posterior diameter (i.e., in the direction of loading) of each group. The loading rate of these femurs was 0.06 mm/min. Force vs. displacement data were recorded at 50 Hz from a 100 N load cell (Honeywell, , OH) and the linear variable displacement transducer.

In mechanical analysis of the un-notched femur, whole bone stiffness was the slope of the initial linear portion of the curve and strength was the peak force (P_f) endured by the mid-shaft. Using the moment of inertia (I_{min}) of the mid-shaft and the distance between the centroid and the bone surface in the anterior-posterior direction (c_{min}) from μCT, we estimated the modulus and strength from standard flexural equations [25]. The yield point was deemed to occur when the secant stiffness was 15% less than the initial stiffness. Post-yield deflection (PYD) was then defined as the displacement at fracture minus the displacement at yielding, and post-yield toughness was defined as the area under the force vs. displacement curve after yielding divided by the bone cross-sectional area (Ct.Ar) [26]. K_c was quantified assuming the stress intensity at the micro-notch root is similar to that of a circumferential through-wall crack in a thin-wall cylinder subjected to bending [27]:

$$K_c = F_b \frac{P_f L R_0}{\pi(R_o^4 - R_i^4)} \sqrt{\pi R_m \theta_c} \qquad \text{Eq. 3.1}$$

where the outer, inner, mean radius (Ro, Ri, and Rm) of the bone cortex, and the half-crack angle (θ) were determine using μCT. Confirming the ratio Rm/Ct.Th was less than 80.5 and greater than 1.5 and that θinit was less than 110° and greater than 0, the geometry factor (Fb) was calculated using the equation published by Takahashi [28]. In addition, scanning electron microscopy (SEM) imaging of the fracture surface after fracture toughness testing was used to determine the θ at which crack propagation transitioned from stable to instable (θ_{inst}). The instability K ($K_{c,inst}$) was calculated using the final force at fracture for θ_{inst} (Eq.3.1).

Each hydrated VB was subjected to axial compression at 3 mm/min in which the supporting platen had a rough surface and a moment relief to minimize slippage and off-axis loading, respectively. Moreover, all tests were recorded with a high-resolution camera (Canon E6, Canon, Melville, NY) with a macro lens. We observed that 2 VBs were not tested properly as they moved laterally during compression. Data from these two bones were not included in the analysis.

4.3.4 Tissue-level Assessment

Prior to nanoindentation, 9 spectra (spaced around the cross section) were acquired from each embedded bone using a standard confocal Raman microscope (Renishaw InVia Raman Microscope, Renishaw, Hoffman Estates, IL) equipped with a 50x (NA=0.75) objective, a 35 μm slit opening, and a 785 nm laser diode source (Innovative Photonic Solutions, Monmouth Junction, NJ). Each spectrum consisted of 5 accumulations of 30 s integration time to yield a high signal to noise ratio (SNR) from 300 to 1800 cm^{-1} (Hydroxyproline SNR in excess of 25:1).

Spectra were processed via least squares modified polynomial fit [29] and smoothed for noise using an 2nd order Savitsky-Golay filter [30]. Custom Matlab software (Mathworks, Natick, MA) extracted the intensity and wavenumber of the prominent spectral. There was no spectral binning in this analysis.

Twelve indents (4 per side) were attempted throughout the tibia cross-section using a nanoindenter (XP, MTS, Eden Prairie, MN) equipped with a Berkovich diamond tip. Loading at a constant strain rate to a depth of 1 μm and then unloading after a 30 s dwell, nanoindentation modulus and hardness of the tissue (0.25 μm resolution) were calculated from the slope of the upper unloading portion of the force vs. displacement curve and the peak force, respectively, as described by Oliver and Pharr [31]. Data was excluded if either the force displacement curve or post-hoc optical examination of the indent site revealed the presence of sub-surface pores.

Prior to fracture toughness testing, the anterior side of the right femoral mid-shaft was placed under the 50x objective of the Raman InVia microscope. Using mid-shaft vessel perforations as landmarks to consistently select the site of analysis across bones, spectra were collected at two intact bone orientations: 0° and 90° relative to the polarization axis of the incident laser, which had an approximate extinction ratio of 1:200 (i.e., light was not fully polarized by adding optics). Laser power and exposure time were optimized to achieve SNR similar to embedded samples. Co-localization of spectral collection sites was accomplished manually by registering fine structural features in the bright field.

To determine differences in composition among the experimental groups, we averaged the Raman measurements per bone. The Raman properties of interest included: ν1Phosphate ($961 - 962\ cm^{-1}$) per Amide I ($1667 - 1670\ cm^{-1}$), ν1Phosphate per Proline ($855 - 858\ cm^{-1}$),

ν2Phosphate (430 − 431 cm^{-1}) per Amide III (1248 − 1252 cm^{-1}), Carbonate (1072 – 1073 cm^{-1}) per ν1Phosphate, and the inverse of the full-width at half maximum of ν1Phosphate peak ($[FWHM]^{-1}$). Because ν1Phos/AmI is sensitive to polarization bias (i.e., collagen fibril orientation) while ν1Phos/Proline and ν2Phos/AmIII are less so [24,32], we examined how a change in bone orientation shifted the regression lines among the mineral to collagen ratios (MCR) for each genotype as a way to infer differences in matrix organization.

4.3.5 Statistical analysis

A two-way analysis of variance (ANOVA) determined whether age and genotype affected each property. Pair-wise comparisons were then tested for significance using either Student's t-test (parametric) or Mann-Whitney (non-parametric) depending on normality and homoscedasticity of each data set. Differences were deemed significant at a p-value adjusted by the Šidák correction for multiple hypothesis testing. Analysis of Covariance determined whether linear relationships (i.e., intercept and slope) between peak force and moment of inertia were different between genotypes. To examine the effect of bone rotation on the MCR relationships, the data were pooled across age groups within genotype and then bootstrapped in order to fit general linear models with the initial independent variables being peak ratio, orientation, and their interaction. Equations were recorded for models with the highest possible R2 value. Statistical analysis was performed using Stata (v11, StataCorp, College Station, TX).

4.4 Results

4.4.1 ATF4 deletion affected trabecular bone architecture and cortical bone structure

Verifying that the rederivation of the Atf4+/- mice on a different background strain did not affect the published phenotype, trabecular bone volume fraction of the L6 VB was much lower for the Atf4-/- than for the Atf4+/+ mice, irrespective of age (Table 4.1). There were also architectural differences between the genotypes with Atf4-deficient VBs having fewer trabeculae, thinner trabeculae, and lower connectivity density (Table 4.1). Tissue mineral density of the trabecular bone however was not different between the genotypes. Still, the low BV/TV was sufficient enough that Atf4-/- VBs were weaker in compression than the Atf4+/+ VBs.

Loss of ATF4 affected cortical bone structure as well in that the null femurs had a thinner cortex, smaller medullary volume, and a lower moment of inertia, regardless of age (Table 4.2). As with the trabecular bone, Ct.TMD increased with age for each genotype, but the difference between genotypes was not strictly significant (Table 4.2). Nonetheless, matching the trends in bone structure, the femurs from the knock-out mice were less stiff and weaker in bending than those from wild-type mice. Moreover, at 20 wk of age, the ability of the Atf4-/- bone to deform after yielding was nearly half that of the Atf4+/+ bone (Table 4.2).

4.4.2 Loss of ATF4 decreased bone toughness with no effect on material strength

Upon factoring out the structural contribution to whole bone strength as determined by peak force, we found that the estimated material strength of the mid-shaft was not different

Table 4.1. Mean ± SD of selected properties of the L6 vertebra as determined by μCT analysis and compression testing (unadjusted p-values provided for *Atf4+/+* vs. *Atf4-/-* within age group).

		8 wk			20 wk		
Property	Unit	Atf4+/+	Atf4-/-	p-value	Atf4+/+	Atf4-/-	p-value
BV/TV	–	0.247 ± 0.032	0.147 ± 0.030	<0.001	0.238 ± 0.049	0.131 ± 0.041	<0.001
Tb.N[a]	1/mm	5.32 ± 0.43	4.58 ± 0.42	0.001	4.95 ± 0.59	3.80 ± 0.40	<0.001
Tb.Th	mm	0.046 ± 0.003	0.039 ± 0.003	<0.001	0.048 ± 0.003	0.041 ± 0.005	<0.001
Tb.Sp[b]	mm	0.190 ± 0.015	0.220 ± 0.023	<0.001	0.205 ± 0.029	0.267 ± 0.028	<0.001
Conn.D[a]	$1/mm^3$	330.5 ± 48.0	275.0 ± 70.7	0.013[NS]	223.3 ± 46.7	133.8 ± 30.4	<0.001
Tb.TMD[a]	$mgHA/cm^3$	898 ± 17	882 ± 26	0.104[NS]	939 ± 23	924 ± 23	0.119[NS]
Peak force	N	32.6 ± 6.4	15.3 ± 4.2	<0.001	35.9 ± 8.7	21.3 ± 5.8	<0.001

[a]There were significant differences between age groups, irrespective of genotype; [b]There was a significant difference between age groups within the knock-out mice; [NS]Not-significant: To control for the family-wise error-rate, statistically significant differences occurred at p-values < 0.013 (Šidák correction).

Table 4.2. Mean ± SD or *median (25%, 75% quartile)* of selected properties of the femur mid-shaft as determined by calipers, µCT analysis and three point bending tests (unadjusted p-values provided for *Atf4+/+* vs. *Atf4-/-* within age group).

		8 wk			20 wk		
Property	Unit	Atf4+/+	Atf4-/-	p-value	Atf4+/+	Atf4-/-	p-value
Length	mm	13.7 ± 0.5	12.2 ± 0.8	<0.001	14.5 ± 0.6	12.9 ± 0.5	<0.001
Tt.Ar[b]	mm^2	*1.84 (1.74, 1.95)*	*1.31 (1.26, 1.71)*	0.027[NS]	*1.99 (1.92, 2.13)*	*1.55 (1.40, 1.68)*	*<0.001*
Ct.Ar[b]	mm^2	0.797 ± 0.078	0.680 ± 0.194	0.013[NS]	0.928 ± 0.073	0.707 ± 0.077	<0.001
Imin[b]	mm^4	0.135 ± 0.023	0.097 ± 0.056	0.007	0.165 ± 0.023	0.092 ± 0.022	<0.001
Ma.V	mm^3	1.17 ± 0.15	0.96 ± 0.29	0.011	1.20 ± 0.10	0.93 ± 0.21	0.001
Ct.Th[b]	mm	0.180 ± 0.015	0.169 ± 0.020	0.119[NS]	0.206 ± 0.014	0.180 ± 0.019	0.001
Ct.TMD[a]	$mgHA/cm^3$	1147 ± 33	1173 ± 25	0.025[NS]	1263 ± 22	1290 ± 22	0.020[NS]
Stiffness[a]	N/mm	104 ± 23	72 ± 26	<0.001	139 ± 19	98 ± 17	<0.001
Peak force[b]	N	18.5 ± 3.5	13.0 ± 3.5	<0.001	24.1 ± 2.9	15.5 ± 3.0	<0.001
PYD	mm	0.317 ± 0.152	0.259 ± 0.145	0.258[NS]	0.341 ± 0.111	0.161 ± 0.087	0.001

[a]There were significant differences between age groups, irrespective of genotype; [b]There was a significant difference between age groups within the wild-type mice; [NS]Not-significant: To control for the family-wise error-rate, statistically significant differences occurred at p-values < 0.013 (Šidák correction).

between Atf4+/+ and Atf4-/- mice (Figure 4.1). This observation concurs with the lack of a demonstrable difference in Ct.TMD between the genotypes. To further confirm that the difference in whole bone strength was primarily due to a structural difference between the genotypes, not differences in tissue properties, we compared the slopes and y-intercepts of the regression lines for each genotype's peak force versus moment of inertia relationship. As shown for 20 wk bones, there were no differences in the regression parameters (Figure 4.1). The Atf4-/- femurs were clearly more brittle with substantially lower post-yield work-to-fracture per bone cross-sectional area (Fig 1). The difference in post-yield toughness was more pronounced at 20 wks of age than at 8 wks of age. As further confirmation of fracture resistance phenotype unrelated to material strength, the fracture toughness was lower for the 20 wk old Atf4-/- mice than for the 20 wk old Atf4+/+ mice (Figure 4.2).

4.4.3 ATF4 deletion had differential effects on tissue-level properties between age groups

Nanoindentation of the embedded bone tissue did not reveal differences in modulus and hardness between the genotypes, although there was a trend of a lower modulus for the ATF4-deficient tissue at 8 wk (Table 4.3). The significant age-related increase in these properties for both genotypes was likely related to the age-related increase in mineralization (Table 4.2). Interestingly, the MCR, as determined by the polarization (organization)-sensitive ν1Phos/AmI was less in the Atf4-/- tibia than in the Atf4+/+ tibia (Table 4.3). This peak ratio increased more with age for the knock-out mice than for the wild-type mice. As such, the genotype difference at 20 wk of age trended toward ν1Phos/AmI being higher, not lower, in the ATF4-deficient tissue. The polarization-insensitive ν2Phos/AmIII acquired from the tibia cross-section was not different

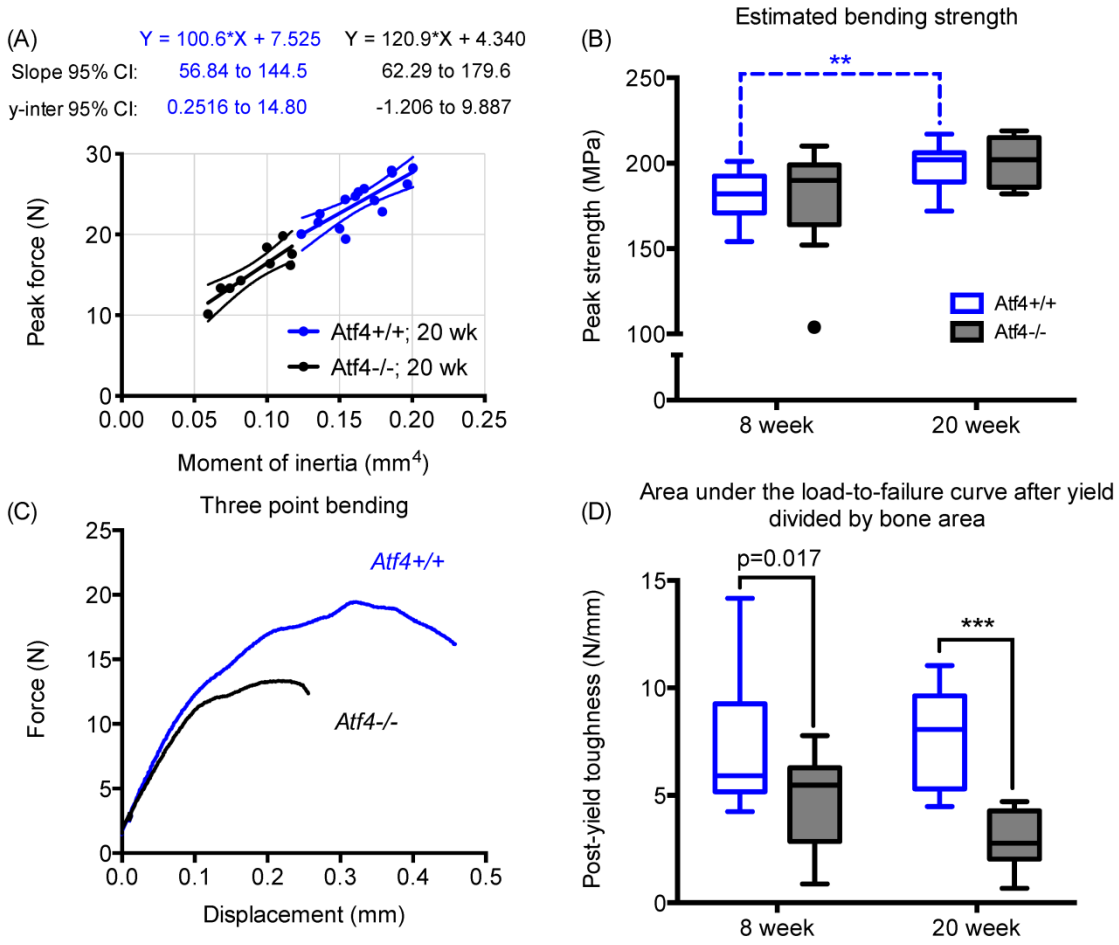

Figure 4.1. Effect of ATF4 deletion on the biomechanical properties of cortical bone. Because they are narrower in cross-section, the femur mid-shafts from *Atf4-/-* mice were structurally weaker than those from wild-type mice **(A)**. However, when accounting for structure, there was no difference in the estimated material strength between genotypes **(B)**. Strikingly, ATF4-deficient bones sustained much less post-yield deformation **(C)** and thus were brittle **(D)**. **p<0.005, ***p<0.0005; otherwise uncorrected p-value.

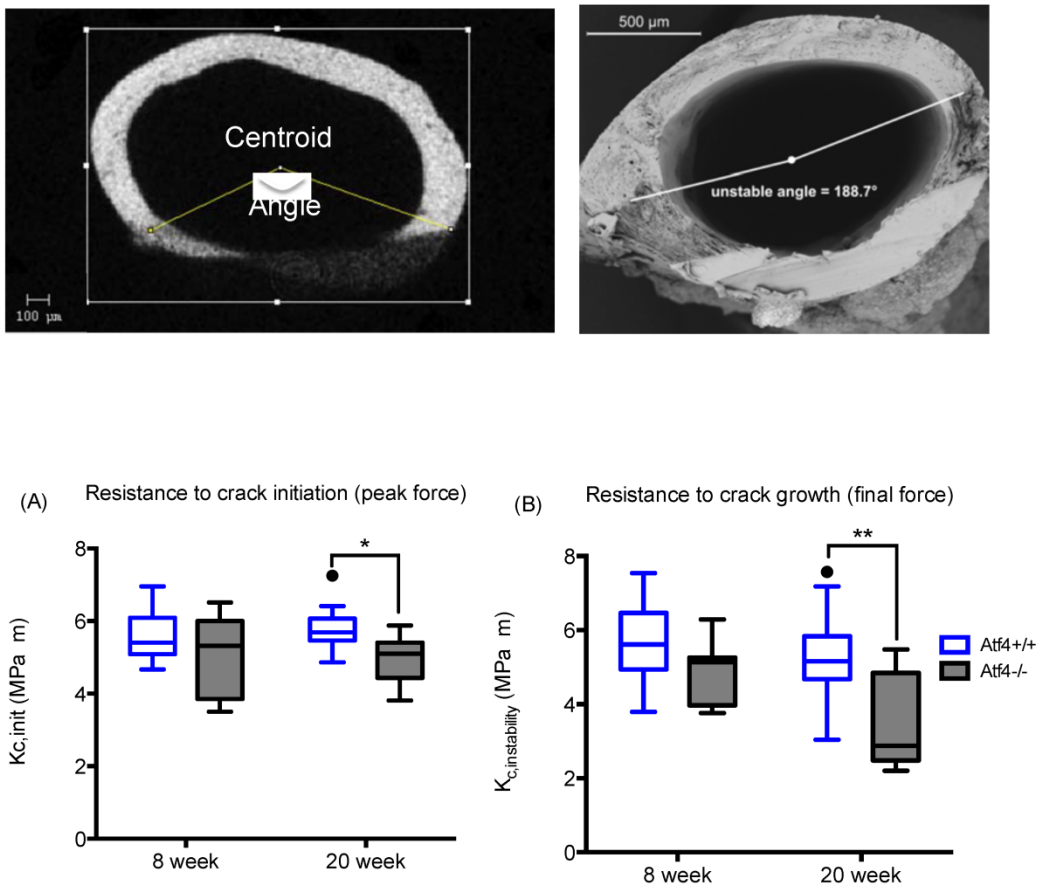

Figure 4.2. Effect of ATF4 deletion on the fracture toughness of cortical bone. Whether determined for the initial notch angle using µCT **(A)** or for the angle at which crack propagation became instable **(B)** using SEM, the fracture toughness of bone was less for *Atf4*-/- than for *Atf4*+/+ mice by 20 weeks of age. *p<0.05, **p<0.005

at 8 wk between genotypes but was greater in the ATF4-deficient tissue suggesting a compositional difference in the mineral relative to the collagen existed between Atf4-/- and Atf4+/+ mice with skeletal maturity (Table 4.3). Other differential effects of ATF4-deficiency between age groups include higher type B carbonate substitution (Carb/ν1Phos) and lower crystallinity ($[FWHM]^{-1}$) with the loss of ATF4 in only the 8 wk group (no differences in the 20 wk group; Table 4.3).

4.4.4 ATF4 deletion possibly affected matrix organization in addition to composition

To identify the potential origins of the brittle bone phenotype of the Atf4-/- mice, we compared the effect of ATF4-deficiency on the volumetric TMD of the mid-shaft cortex (by μCT) to its effect on MCR (by RS), acquired from the same intact femur mid-shaft (i.e., the notched femurs prior to testing). As was observed for the un-notched bone, Ct.TMD was greater for femurs from 20 wk than from 8 wk mice with little difference between genotypes at each age (Figure 4.3A). In contrast, the Raman-derived MCR measurements (ν1Phos/Proline, ν2Phos/AmIII, and ν1Phos/AmI) from the outer cortex of the mid-shaft (anterior side) did not increase with age in the Atf4+/+ bone and had a modest increase with age in the Atf4-/- bone (Figure 4.3B). This suggests that the amount of mineral relative to collagen in the cortex did not vary between 8 wk and 20 wk of age in wild-type mice. In contrast, there was more mineral relative to collagen (or less collagen relative to mineral) with the loss of ATF4 by 20 wk (Figure 4.3B).

Table 4.3. Mean ± SD or *median (25%, 75% quartile)* of selected tissue properties acquired from the tibia cross-section as determined by Raman spectroscopy and nanoindentation (unadjusted p-values provided for Atf4+/+ vs. Atf4-/- within age group).

		8 wk			20 wk		
Property	Unit	Atf4+/+	Atf4-/-	p-value	Atf4+/+	Atf4-/-	p-value
Modulus[a]	GPa	27.2 ± 2.3	25.1 ± 3.7	0.029[NS]	30.7 ± 1.7	29.6 ± 2.1	0.337[NS]
Hardness[a]	*GPa*	*1.03 (0.96, 1.10)*	*0.94 (0.83, 1.06)*	0.173[NS]	*1.12 (1.03, 1.17)*	*1.13 (1.08, 1.20)*	0.429[NS]
ν1Phos/AmI[c]	–	11.2 ± 1.0	10.4 ± 0.7	0.006	11.6 ± 0.7	12.3 ± 0.6	0.025[NS]
ν2Phos/AmIII[c]	–	*1.88 (1.84, 1.91)*	*1.85 (1.66, 1.90)*	0.262[NS]	*1.90 (1.85, 1.98)*	*1.99 (1.98, 2.05)*	0.009
Carb/ν1Phos[b]	–	*0.154 (0.151, 0.161)*	*0.166 (0.157, 0.185)*	0.007	*0.175 (0.167, 0.179)*	*0.178 (0.176, 0.179)*	0.270[NS]
[FWHM]$^{-1}$	–	*0.0630 (0.0620, 0.0632)*	*0.0628 (0.0567, 0.0692)*	0.010	*0.0630 (0.0627, 0.0631)*	*0.0627 (0.0625, 0.0627)*	0.123[NS]

[a]There were significant differences between age groups, irrespective of genotype; [b]There was a significant difference between age groups within the wild-type mice; [c]There was a significant difference between age groups within the knock-out mice; [NS]Not-significant: To control for the family-wise error-rate, statistically significant differences occurred at p-values < 0.013 (Šidák correction)

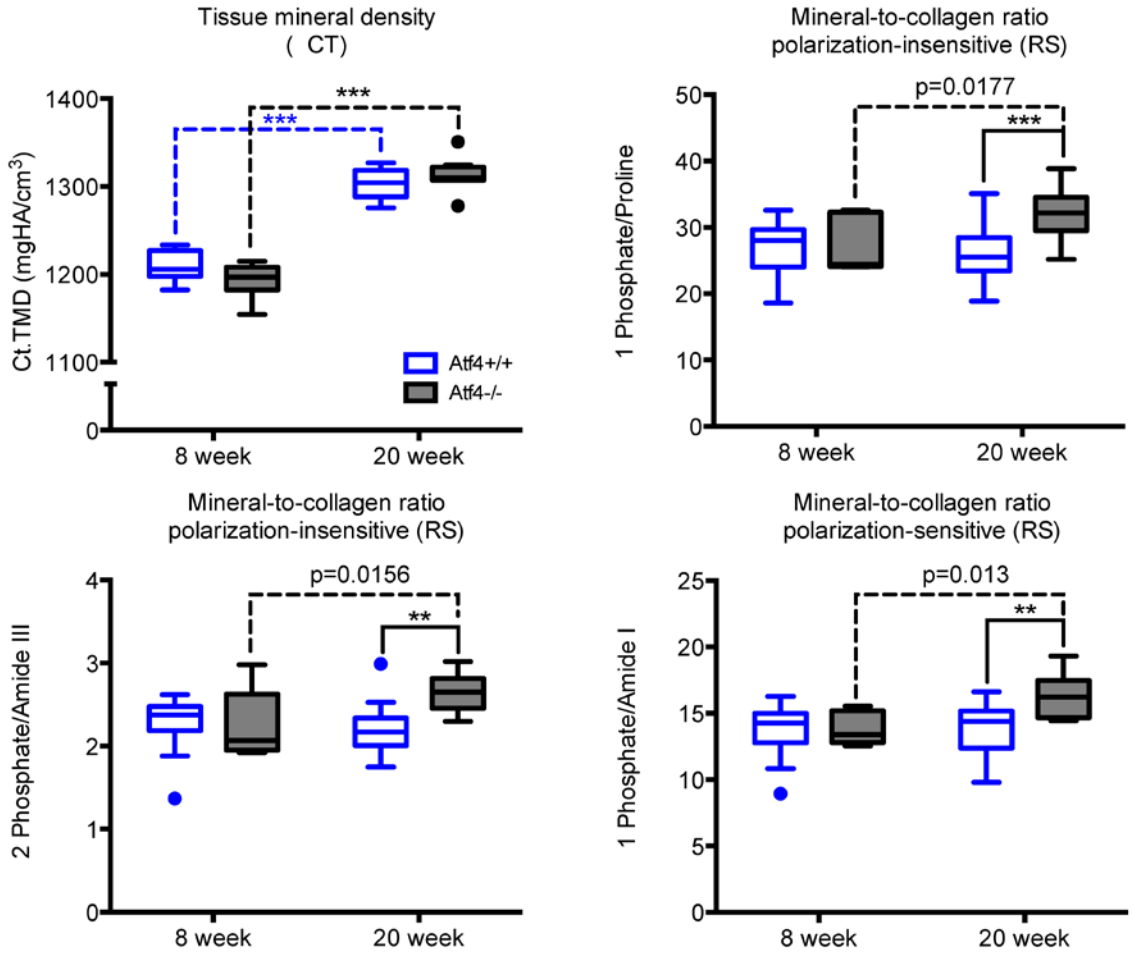

Figure 4.3. Effect of ATF4 deletion on mineralization. As determined by μCT analysis of the notched femur **A**, there was an age-related increase in tissue mineral density but no difference between genotypes. Regardless of whether the peak ratio from RS analysis of notched femur (anterior side) is not sensitive to polarization bias **(B & C)** or is sensitive **(D)**, the mineral relative to collagen was greater in ATF4-deficient tissue at 20 weeks of age. *p<0.05, **p<0.005, ***p<0.0005; otherwise uncorrected p-value.

To gain further insight into whether differences in tissue organization existed between the genotypes, we examined the effect of rotating the intact femur on the relationships among the three peak ratios representing MCR (Figure 4.4). As expected, the regression line for the longitudinal orientation overlapped that of the orthogonal orientation when plotting ν2Phos/AmIII versus ν1Phos/Proline, irrespective of genotype (Figure 4.4A & 4B) because these peak ratios are relatively insensitive to polarization bias [32,33]. When plotting each insensitive peak ratio versus the polarization-sensitive ν1Phos/AmI (Figure 4.4C & 4E), there was a shift in the regression line for the wild-type bone such that the y-intercept, but not the slope, depends on orientation of the bone relative to the polarization angle of the incident light (Table 4.4). Interestingly, the slope of these regression lines changes upon bone rotation from the longitudinal to the orthogonal orientation (Figure 4.4D & 4F) for only the Atf4-/- bone (Table 4.4). The differential effect of bone orientation on MCR regressions between genotypes suggests an underlying tissue organizational phenotype exists with loss of ATF4.

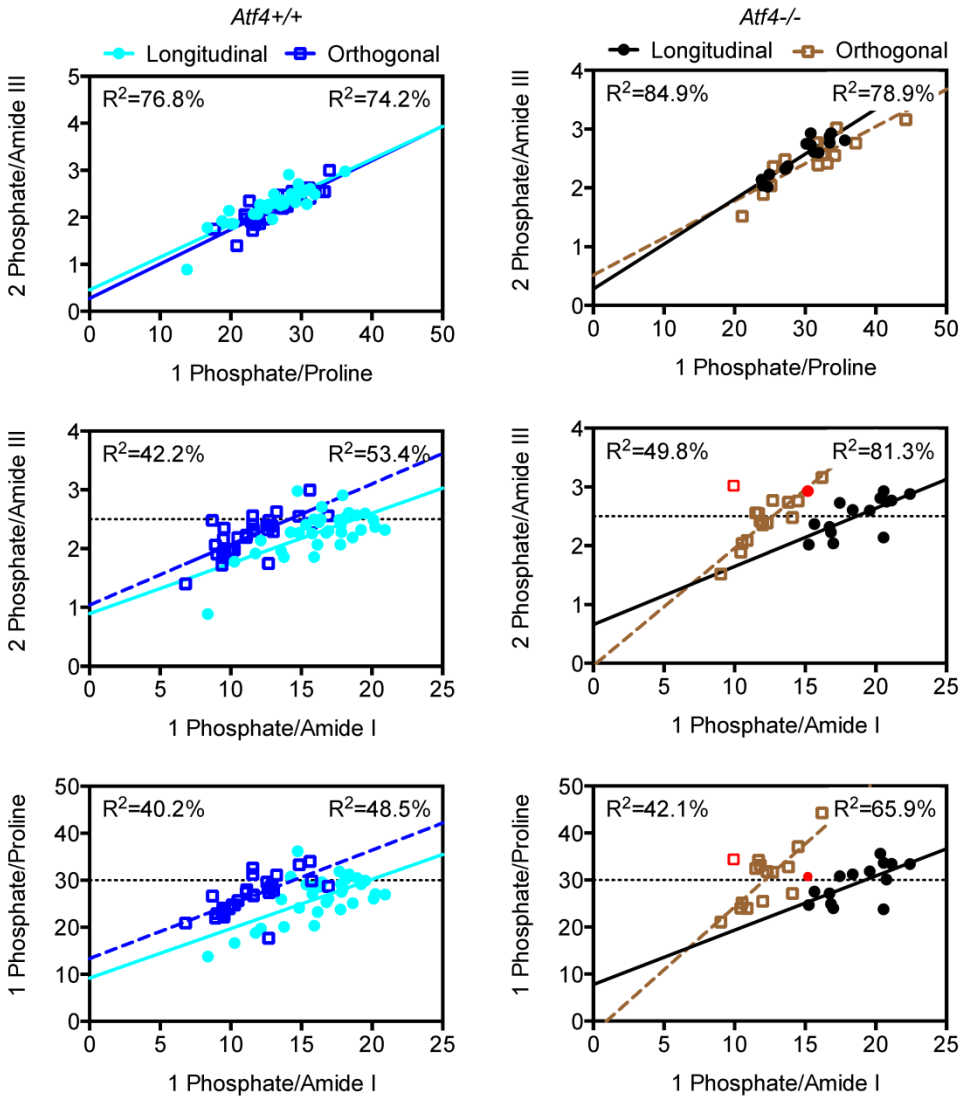

Figure 4.4. Effects of bone orientation relative to light polarization on peak ratio relationships. Rotating the bone by 90° has little effect on the relationship between two different polarization-insensitive peak ratios (regression lines overlap in A and B). However, bone rotation does affect the relationships between a polarization-insensitive peak ratio and the polarization-sensitive peak ratios of MCR **(C – D)**. The shift in the regression line for the Atf4+/+ bone **(C & E)** is less than the shift in regression line for Atf4-/- bone **(D & F)**. Data from 8 wk and 20 wk mice were pooled. Data from 1 bone (red symbols) was removed from regression analyses because ν1Phos/AmI was an outlier in both orientations.

Table 4.4. General linear equations of the best-fit models to 3 different peak ratio combinations of the mineral to collagen ratio for each genotype in which orientation of the bone relative to polarization axis changed by 90 ° (L – longitudinal and O – orthogonal).

Atf4+/+			*Atf4-/-*		
Best-fit Regression Model	Orientation p-value	R^2	Best-fit Regression Model	Orientation p-value	R^2
ν2Phos/AmIII = 0.42 + 0.071 x ν1Phos/Prol if L or O	0.105	75.9	ν2Phos/AmIII = 0.62 + 0.065 x ν1Phos/Prol if L ν2Phos/AmIII = 0.46 + 0.065 x ν1Phos/Prol if O	0.005	80.7
ν1Phos/Proline = 12.52 + 0.85 x ν1Phos/AmI if L ν1Phos/Proline = 16.82 + 0.85 x ν1Phos/AmI if O	0.006	43.3	ν1Phos/Proline = 16.78 + 0.68 x ν1Phos/AmI if L ν1Phos/Proline = 2.64 + 2.26 x ν1Phos/AmI if O	0.038[a]	58.5
ν2Phos/AmIII= 0.92 + 0.084 x ν1Phos/AmI if L ν2Phos/AmIII= 1.26 + 0.084 x ν1Phos/AmI if O	0.014	47.2	ν2Phos/AmIII= 1.08 + 0.076 x ν1Phos/AmI if O ν2Phos/AmIII= 0.36 + 0.17 x ν1Phos/AmI if L	0.059[a]	70.1

[a] p-value for the interaction between orientation and peak ratio.

4.5 Discussion

Strength is not the only property that characterizes the ability of bone to resist fracture. Fracture risk can increase because bone loses the ability i) to sustain deformation after the on-set of permanent deformation (i.e., yield point), ii) to minimize microdamage accumulation, or iii) to resist crack growth. As with other materials subjected to dynamic loads, fracture resistance of bone depends on several properties such as i) toughness, ii) fatigue endurance, and iii) fracture toughness, respectively. Although aging and certain diseases affect these characteristics (e.g., rheumatoid arthritis [34], duration of high fat diet [35,36], and osteogenesis imperfect [37]), there is little known about critical regulators of the bone matrix that promote toughening mechanisms. Presently, we provide evidence that a transcription factor important to osteoblast differentiation influences both the toughness and the fracture toughness of bone (at the material level) in addition to proper cortical bone structure and trabecular bone architecture (at the whole bone level).

The reduction in bone toughness and fracture toughness in the Atf4-/- mice compared to the Atf4+/+ mice could be due to an imbalance of mineral accumulation relative to the organic matrix. As determined by μCT in mgHA/cm3, there was little difference in the TMD between the genotypes (Table 4.1, Table 4.2, and Figure 4.3) with TMD increasing with skeletal maturation or age in both genotypes. However, as determined by Raman spectroscopy on embedded tibia cross-sections and intact femurs, the relative amount of mineral to the amount of collagen did not vary between 8 weeks and 20 weeks of age in wild-type mice but did so in knock-out mice (Table 4.3 and Figure 4.3B, 3C, & 3D). Taken together, these observations suggest that normal mineral accumulation outpaced reduced collagen deposition [21] in the ATF4-deficient bones

with respect to wild-type bones. Of note, bone formation rate is lower with the loss of ATF4 [21] suggesting tissue age, a determinant of the degree of mineralization, varied between the genotypes. In general, mineral density and collagen are the primary determinants of material strength and toughness, respectively [38], but bones with higher degree of mineralization (or ash fraction) have lower toughness than bones with lower mineralization [39]. Thus, matching the trends in tissue composition (no difference in TMD but greater MCR with ATF4 deficiency), there was not a significant difference in peak bending strength between the genotypes (Figure 4.1), but the post-yield deflection (Table 4.2) and fracture toughness (Figure 4.2) were lower for bones from the 20 wk Atf4-/- mice.

The deletion of ATF4 also appeared to affect tissue organization. Although we do not have direct measurements of fibril orientation, we can infer organization-related differences by examining the effect of bone rotation on the regressions among the RS-derived MCRs. This is possible because bone tissue is a birefringent material, and ν1Phos/AmI is sensitive to polarization when the RS instrument does not depolarize the laser light (diode lasers are inherently polarized even without added optics)[33]. That is, for the same location with a given MCR and collagen fibril orientation, ν1Phos/AmI depends on the predominant angle of the polarized light relative to the predominant direction of the collagen fibrils. If the collagen fibrils at the site of measurement are randomly orientated (i.e., isotropic), then ν1Phos/AmI would have minimal change upon rotation. However, mineralized collagen fibrils of bone typically have preferentially orientation that can shift from region to region [40,41]. Thus, there is a shift in the regression line for ν1Phos/AmI versus ν1Phos/Proline, a polarization-insensitive peak ratio, going from longitudinal to orthogonal bone orientation (Figure 4.4). Interestingly, the shift is

greater for the ATF4-deficient bone (see horizontal lines in Figure 4.4). This could be due to an overall difference in fibril direction or a difference in the net distribution of the collagen fibrils (anisotropy) between the genotypes. With respect to the latter possibility, the greater shift suggests the tissue anisotropy was greater or organizational heterogeneity was less for ATF4-deficient bone. This remains to be confirmed.

Identifying the origins of bone brittleness is challenging because toughening mechanism exist at multiple length scales. Thus, there could be other explanations for why bones from Atf4-/- have lower toughness and fracture toughness than bones from control littermates. Surveying reports of other bone brittleness phenotypes, cortical bone from osteopontin (OPN)-deficient mice has local regions of hyper-mineralization and more anisotropic collagen fibrils compared to the tougher bones from Opn+/+ mice [18]. Similarly, in comparison to wild-type mice with higher bone toughness and fracture toughness, the cortical bone from Mmp13-/- mice has local regions of hyper-mineralized tissue as well as increases in non-enzymatic collagen crosslinks and disrupted birefringent lamellar bands [17]. Thus, a common theme in genetic models with a bone brittleness phenotype is a disruption in normal mineralization and collagen organization. As is the case with these previous studies in which the gene was deleted in all cells, we cannot definitively conclude that the regulation of matrix properties by ATF4 is solely osteoblast-specific.

Given that a major downstream target of ATF4 is Ocn gene [21,42] [43,44], the biomechanical phenotype of OCN-deficient mice could be similar to that of ATF4-deficient mice. With respect to toughness, there is similarity in that the bone from Ocn-/- mice have a lower propagation toughness than bone from wild-type mice [19]. Being a charged molecule

with Ca2+ binding sites, OCN may directly promote resistance to cracking [19] by acting as a sacrificial bond between mineralized collagen fibrils [45,46]. There are no reports of whether the loss of OCN reduces post-yield deflection of cortical bone, but there is evidence that OCN-deficiency does not lower the structural strength of whole bones in intact mice [47]. This is different than what we observe for the bone of Atf4-/- mice (Table 4.2). In addition, unlike the effect of ATF4 deficiency on MCR, there was no difference in the mineral to matrix ratio [48] as determined by Fourier transformed infrared spectroscopy or in ν1Phos/AmI as determined by RS [49] between adult (6 mo. and 12 mo.) Ocn-/- and Ocn+/+ mice. Thus, while ATF4 activity may certainly regulate bone brittleness through OCN , other proteins under ATF4 control are likely influencing the fracture resistance of bone.

With respect to its role in bone, ATF4 was initially discovered to be the other transcription factor, along with Runx2, that binds the promoter region of the osteocalcin gene [21]. ATF4 is a downstream target of two important factors in bone maintenance: transforming growth factor beta (TGF-β) and intermittent parathyroid hormone (PTH) [44,50]. Among other actions in bone, TGF-β signaling preserves the osteoprogenitor pool at the expense of differentiation [51], and we previously found that suppressing TGF-β with a neutralizing antibody increased trabecular bone volume in Atf4+/+ mice but not in Atf4-/- mice [50]. Similarly in an earlier study, Yu et al. [52] found that the anabolic effect of intermittent recombinant parathyroid hormone (hPTH(1-34)) on bone was abrogated in growing Atf4-/- mice as well as mature, ovariectomized Atf4-/- mice relative to PTH-treated littermate controls. As further evidence of the interest in ATF4 as a critical mediator of bone maintenance, high expression of a microRNA (miR-214) was recently found to be associated with fractures, and

miR-214 was shown to down-regulate ATF4, thereby inhibiting osteoblast activity [53]. The findings of the present study suggest that suppressing ATF4 does more than reduce bone formation: suppression or specifically the loss of ATF4 can lead to bone brittleness.

4.6 Conclusions

The loss of ATF4 results in a brittle bone phenotype that becomes more severe with skeletal maturity and includes a loss in fracture toughness but no decrease in material strength. Accompanying the difference in bone toughness between Atf4-/- and Atf4+/+ mice is a higher mineral to collagen ratio and more fibril anisotropy with ATF4 deficiency. The lack of a difference in material strength (independent of structure) between the genotypes concur with the lack of significant difference in tissue mineral density, making the ATF4-null model a strong candidate for examination of the underlying mechanisms of toughness, as well as for the evaluation of therapeutics that target bone toughness and resistance to crack propagation.

4.7 Acknowledgements

This material is based upon work supported by the Department of Veterans Affairs, Veterans Health Administration, Office of Research and Development. We thank George M. Pharr and Erick G. Herbert for access to their nanoindenter.

4.8 References

[1] Kanis JA, Johnell O, Oden A, Dawson A, De Laet C, Jonsson B. Ten year probabilities of osteoporotic fractures according to BMD and diagnostic thresholds. Osteoporos Int 2001;12:989–95.

[2] Burstein AH, Reilly DT, Martens M. Aging of bone tissue: mechanical properties. J Bone Joint Surg Am 1976;58:82–6.

[3] Zioupos P, Currey JD, Hamer AJ. The role of collagen in the declining mechanical properties of aging human cortical bone. J Biomed Mater Res 1999;45:108–16.

[4] Nyman JS, Roy A, Tyler JH, Acuna RL, Gayle HJ, Wang X. Age-related factors affecting the postyield energy dissipation of human cortical bone. J Orthop Res 2007;25:646–55.

[5] Yeni YN, Brown CU, Norman TL. Influence of bone composition and apparent density on fracture toughness of the human femur and tibia. Bone 1998;22:79–84.

[6] Zioupos P, Currey JD. Changes in the stiffness, strength, and toughness of human cortical bone with age. Bone 1998;22:57–66.

[7] Zioupos P. Accumulation of in-vivo fatigue microdamage and its relation to biomechanical properties in ageing human cortical bone. J Microsc 2001;201:270–8.

[8] Nalla RK, Kruzic JJ, Kinney JH, Ritchie RO. Effect of aging on the toughness of human cortical bone: evaluation by R-curves. Bone 2004;35:1240–6.

[9] Zimmermann EA, Schaible E, Bale H, Barth HD, Tang SY, Reichert P, et al. Age-related changes in the plasticity and toughness of human cortical bone at multiple length scales. Proceedings of the National Academy of Sciences 2011;108:14416–21.

[10] Currey JD, Foreman J, Laketić I, Mitchell J, Pegg DE, Reilly GC. Effects of ionizing radiation on the mechanical properties of human bone. J Orthop Res 1997;15:111–7.

[11] Wang X, Bank RA, TeKoppele JM, Agrawal CM. The role of collagen in determining bone mechanical properties. J Orthop Res 2001;19:1021–6.

[12] Unger S, Stefan U, Blauth M, Michael B, Schmoelz W, Werner S. Effects of three different preservation methods on the mechanical properties of human and bovine cortical bone. Bone 2010;47:1048–53.

[13] Mitchell EJ, Stawarz AM, Kayacan R, Rimnac CM. The effect of gamma radiation sterilization on the fatigue crack propagation resistance of human cortical bone. J Bone Joint Surg Am 2004;86-A:2648–57.

[14] Yan J, Daga A, Kumar R, Mecholsky JJ. Fracture toughness and work of fracture of hydrated, dehydrated, and ashed bovine bone. Journal of Biomechanics 2008;41:1929–36.

[15] Barth HD, Zimmermann EA, Schaible E, Tang SY, Alliston T, Ritchie RO. Characterization of the effects of x-ray irradiation on the hierarchical structure and mechanical properties of human cortical bone. Biomaterials 2011;32:8892–904.

[16] Nyman JS, Lynch CC, Perrien DS, Thiolloy S, O'quinn EC, Patil CA, et al. Differential effects between the loss of MMP-2 and MMP-9 on structural and tissue-level properties of bone. J Bone Miner Res 2011;26:1252–60.

[17] Tang S, Herber R-P, Ho S, Alliston T. Matrix metalloproteinase-13 is required for osteocytic perilacunar remodeling and maintains bone fracture resistance. J Bone Miner Res 2012.

[18] Thurner PJ, Chen CG, Ionova-Martin S, Sun L, Harman A, Porter A, et al. Osteopontin deficiency increases bone fragility but preserves bone mass. Bone 2010;46:1564–73.

[19] Poundarik AA, Diab T, Sroga GE, Ural A, Boskey AL, Gundberg CM, et al. Dilatational band formation in bone. Proceedings of the National Academy of Sciences 2012;109:19178–83.

[20] Balooch G, Balooch M, Nalla RK, Schilling S, Filvaroff EH, Marshall GW, et al. TGF-beta regulates the mechanical properties and composition of bone matrix. Proc Natl Acad Sci USA 2005;102:18813–8.

[21] Yang X, Matsuda K, Bialek P, Jacquot S, Masuoka HC, Schinke T, et al. ATF4 is a substrate of RSK2 and an essential regulator of osteoblast biology; implication for Coffin-Lowry Syndrome. Cell 2004;117:387–98.

[22] Jepsen KJ, Pennington DE, Lee YL, Warman M, Nadeau J. Bone brittleness varies with genetic background in A/J and C57BL/6J inbred mice. J Bone Miner Res 2001;16:1854–62.

[23] Jepsen KJ, Akkus OJ, Majeska RJ, Nadeau JH. Hierarchical relationship between bone traits and mechanical properties in inbred mice. Mamm Genome 2003;14:97–104.

[24] Nyman JS, Makowski AJ, Patil CA, Masui TP, O'quinn EC, Bi X, et al. Measuring differences in compositional properties of bone tissue by confocal Raman spectroscopy. Calcif Tissue Int 2011;89:111–22.

[25] Turner CH, Burr DB. Basic biomechanical measurements of bone: a tutorial. Bone 1993;14:595–608.

[26] Ritchie RO, Koester KJ, Ionova S, Yao W, Lane NE, Ager JW III. Measurement of the toughness of bone: A tutorial with special reference to small animal studies. Bone 2008;43:798–812.

[27] Ritchie RO, Koester KJ, Ionova S, Yao W, Lane NE, Ager JW. Erratum: Measurement of the toughness of bone: a tutorial with special reference to small animal studies. Bone 2008;43:798–812.

[28] Takahashi Y. Evaluation of leak-before-break assessment methodology for pipes with a circumferential through-wall crack. Part I: stress intensity factor and limit load solutions. International Journal of Pressure Vessels and Piping 2002;79:385–92.

[29] Lieber CA, Mahadevan-Jansen A. Automated method for subtraction of fluorescence from biological Raman spectra. Appl Spectrosc 2003;57:1363–7.

[30] Maher JR, Takahata M, Awad HA, Berger AJ. Raman spectroscopy detects deterioration in biomechanical properties of bone in a glucocorticoid-treated mouse model of rheumatoid arthritis. J Biomed Opt 2011;16:087012.

[31] Oliver WC, Pharr GM. Improved technique for determining hardness and elastic modulus using load and displacement sensing indentation experiments. J Mater Res 1992.

[32] Kazanci M, Roschger P, Paschalis EP, Klaushofer K, Fratzl P. Bone osteonal tissues by Raman spectral mapping: orientation-composition. J Struct Biol 2006;156:489–96.

[33] Makowski AJ. Polarization control of Raman spectroscopy optimizes the assessment of bone tissue. J Biomed Opt 2013;18:055005.

[34] Inzana JA, Maher JR, Takahata M, Schwarz EM, Berger AJ, Awad HA. Bone fragility beyond strength and mineral density: Raman spectroscopy predicts femoral fracture toughness in a murine model of rheumatoid arthritis. Journal of Biomechanics 2013;46:723–30.

[35] Ionova-Martin SS, Wade JM, Tang S, Shahnazari M, Ager JW, Lane NE, et al. Changes in cortical bone response to high-fat diet from adolescence to adulthood in mice. Osteoporos Int 2011;22:2283–93.

[36] Ionova-Martin SS, Do SH, Barth HD, Szadkowska M, Porter AE, Ager JW, et al. Reduced size-independent mechanical properties of cortical bone in high-fat diet-induced obesity. Bone 2010;46:217–25.

[37] Davis MS, Kovacic BL, Marini JC, Shih AJ, Kozloff KM. Increased susceptibility to microdamage in Brtl/+ mouse model for osteogenesis imperfecta. Bone 2012;50:784–91.

[38] Burr DB. The contribution of the organic matrix to bone's material properties. Bone 2002;31:8–11.

[39] Currey JD. Effects of differences in mineralization on the mechanical properties of bone. Philos Trans R Soc Lond, B, Biol Sci 1984;304:509–18.

[40] Giraud-Guille MM. Twisted plywood architecture of collagen fibrils in human compact bone osteons. Calcif Tissue Int 1988;42:167–80.

[41] Reznikov N, Almany-Magal R, Shahar R, Weiner S. Three-dimensional imaging of collagen fibril organization in rat circumferential lamellar bone using a dual beam electron microscope reveals ordered and disordered sub-lamellar structures. Bone 2013;52:676–83.

[42] Schinke T, Karsenty G. Characterization of Osf1, an osteoblast-specific transcription factor binding to a critical cis-acting element in the mouse Osteocalcin promoters. J Biol Chem 1999;274:30182–9.

[43] Xiao G, Jiang D, Ge C, Zhao Z, Lai Y, Boules H, et al. Cooperative interactions between activating transcription factor 4 and Runx2/Cbfa1 stimulate osteoblast-specific osteocalcin gene expression. J Biol Chem 2005;280:30689–96.

[44] Yu S, Franceschi RT, Luo M, Zhang X, Jiang D, Lai Y, et al. Parathyroid hormone increases activating transcription factor 4 expression and activity in osteoblasts: requirement for osteocalcin gene expression. Endocrinology 2008;149:1960–8.

[45] Fantner GE, Hassenkam T, Kindt JH, Weaver JC, Birkedal H, Pechenik L, et al. Sacrificial bonds and hidden length dissipate energy as mineralized fibrils separate during bone fracture. Nat Mater 2005;4:612–6.

[46] Zappone B, Thurner PJ, Adams J, Fantner GE, Hansma PK. Effect of Ca2+ ions on the adhesion and mechanical properties of adsorbed layers of human osteopontin. Biophysical Journal 2008;95:2939–50.

[47] Ducy P, Desbois C, Boyce B, Pinero G, Story B, Dunstan C, et al. Increased bone formation in osteocalcin-deficient mice. Nature 1996;382:448–52.

[48] Boskey AL, Gadaleta S, Gundberg C, Doty SB, Ducy P, Karsenty G. Fourier transform infrared microspectroscopic analysis of bones of osteocalcin-deficient mice provides insight into the function of osteocalcin. Bone 1998;23:187–96.

[49] Kavukcuoglu NB, Patterson-Buckendahl P, Mann AB. Effect of osteocalcin deficiency on the nanomechanics and chemistry of mouse bones. Journal of the Mechanical Behavior of Biomedical Materials 2009;2:348–54.

[50] Lian N, Lin T, Liu W, Wang W, Li L, Sun S, et al. Transforming Growth Factor β Suppresses Osteoblast Differentiation via the Vimentin Activating Transcription Factor 4 (ATF4) Axis. J Biol Chem 2012;287:35975–84.

[51] Janssens K, Dijke ten P, Janssens S, Van Hul W. Transforming growth factor-beta1 to the bone. Endocr Rev 2005;26:743–74.

[52] Yu S, Franceschi RT, Luo M, Fan J, Jiang D, Cao H, et al. Critical role of activating transcription factor 4 in the anabolic actions of parathyroid hormone in bone. PLoS ONE 2009;4:e7583.

[53] Wang X, Guo B, Li Q, Peng J, Yang Z, Wang A, et al. miR-214 targets ATF4 to inhibit bone formation. Nat Med 2013;19:93–100.

CHAPTER 5

POLARIZATION IN RAMAN SPECTROSCOPY HELPS EXPLAIN BONE BRITTLENESS IN GENETIC MOUSE MODELS

5.1 Abstract

Raman spectroscopy (RS) has been used extensively to characterize bone composition; however, the link between bone biomechanics and RS measures is not well established. Here we leveraged the sensitivity of RS polarization to organization, thereby assessing whether RS can explain differences in bone toughness in genetic mouse models for which traditional RS peak ratios are not informative. In the selected mutant mice – ATF4 or MMP9 knock-outs − toughness is reduced but differences in bone strength do not exist between wild-type and knock-out littermates. To incorporate differences in the RS of bone occurring at peak shoulders, a multivariate approach was used. Full spectrum principal components analysis of two paired, orthogonal bone orientations (relative to laser polarization) improved genotype classification and correlation to bone toughness when compared to traditional peak ratios. Applied to femurs from wild-type mice at 8 and 20 weeks of age (maturation), principal components of orthogonal bone orientations improved age classification but not the explanation of the maturation-related increase in strength. Overall, increasing polarization information by collecting spectra from two

bone orientations improves the ability of multivariate RS to explain variance in bone toughness, likely due to polarization sensitivity to organization changes in both mineral and collagen.

5.2 Introduction

The loss of bone fracture resistance, as occurs in osteoporosis and with aging, is not solely due to a decrease in bone mass but likely involves deleterious changes to tissue organization, including both the mineral phase and the organic matrix. Current X-ray based diagnostics predominantly assess bone strength through analysis of mineral density[1, 2] and macro-structure or micro-architecture[3]. However, changes to other material properties including toughness and fracture toughness may also contribute to fracture risk. In fact, Burstein et al. found that the age-related decrease in human bone toughness is greater than the age-related decrease in material strength at the apparent-level[4] suggesting that brittleness, not just weakness, lowers fracture resistance with age. To complement existing clinical diagnostics, many in the optics field have begun to explore the use of Raman Spectroscopy (RS) due to its potential to noninvasively quantify the biochemical signature of both mineral and collagen concurrently[5]. However, RS is traditionally limited to biochemical content without directly assessing matrix organization. Recently, the link inherent between polarization of the Raman phenomenon and structural organization of crystals and birefringent molecules[6, 7] has been extended to tissue[8], and specifically the collagen matrix[9, 10]. Polarization RS may overcome the traditional structural limitations and improve the ability of RS to explore the underlying mechanisms that influence fracture resistance.

The effect of genetic disease on bone is often studied using rodent models as a means to understand the mechanisms linking cellular action to tissue biomechanics [11-13]. Osteogenesis Imperfecta (OI) is perhaps the best characterized human disease of brittle bone; is known to be a disease of collagen organization[14-16]; and the RS peaks of OI mouse models change with polarization[17]. This is perhaps not too surprising, given a growing body of evidence that polarized Raman intensity varies with collagen direction[10, 18] and can even be used to determine collagen orientation in bone[19]. Other genetic mouse models have also demonstrated brittle bone phenotypes that are not necessarily explained by composition but related to matrix organization[20-22], hence may benefit from polarization RS. We recently reported that polarization changes in the RS peak ratios of bones lacking the activating transcription factor 4 (ATF4) imply an organizational component to the phenotype that includes toughness loss and decreased fracture toughness[23], but it is unclear to what extent these polarization RS changes are predictive of mechanical bone quality. This is especially interesting given that mice lacking the matrix metalloproteinase (MMP9) exhibit no changes in standard RS peak ratios even though they too have low bone toughness[24].

In translucent pure media, polarization changes in RS intensities can be quantified relative to theory using a depolarization ratio ($I_{perpendicular}/I_{parallel}$) to assess molecular orientation[6]; however, in turbid media like bone this is confounded by the light scattering properties of tissue. Therefore, the effect of specific optics instrumentation, including degree of confocality[17], on RS peaks needed to be characterized prior to implementing assessment of bone organization with polarization RS. For different objectives (NA = 0.75 and NA= 0.4), we previously showed that observable changes in Raman intensity in polarization sensitive peaks with bone orientation

occur across microstructural features of human tissue samples[25], such that the ν1 Phosphate peak is regularly out of phase with Amide I. However, traditional peak ratios only report a small portion of the known spectral changes that occur with polarization as previously characterized by others[8, 18, 26-28]. Moreover, limiting analysis to established peak ratios may overlook crucial aspects of complex toughness phenotypes if they manifest as subtle peak widening or shifting.

RS analyses of bone are often limited to a set of strong peak intensities and validated peak ratios[29], including only the characteristic frequencies and relative composition of bone. In the absence of tissue complexity, RS is often applied to pure crystalline and polymeric materials i) to analyze stress and strain using Raman shift changes[30, 31]; ii) to determine orientation as a function of peak polarization[32]; and iii) to assess crystal quality and deformation using peak width[33]. While each would require significant empirical support to extend mechanistically to turbid bone tissue, unsupervised multivariate analysis allows for the influence of these known RS sensitivities to mechanical outcomes without spurious mechanistic suppositions. Indeed, recent applications of multivariate RS analyses to bone have helped explain the fracture toughness of bone in a model of rheumatoid arthritis[34] as well as partial mechanical improvement of OI mouse bones after human stem cell transplant[35].

Therefore, we investigated the potential of full spectrum multivariate analysis with a "bottom-up" design built upon the principal directions of Raman variance between test groups. Using multiple published mouse models in which peak ratios alone did not fully explain the mechanical phenotype, we hypothesized that analysis of all wavenumbers within the RS "fingerprint region", while including polarization information, would improve the ability of RS to classify knockout mice of a brittle phenotype (versus wild-type of the same strain) and

subsequently improve RS correlation to mechanical measures of toughness. However, this may not be the case for mechanical properties like strength that can be attributed to composition more than organization. To this end, we scanned excised intact femurs of both *Atf4*-/- and *Mmp9*-/- mice and their corresponding controls prior to mechanical testing at the same location for two different orientations at consistent anatomical marker on the anterior midshaft.

5.3 Methods

5.3.1 Study Design

All procedures were approved by the Institutional Animal Care and Use Committee (IACUC) at Vanderbilt University Medical Center. Femurs were harvested from young adult male mice (unless otherwise noted), stripped of musculature and stored frozen at -20˚C in phosphate buffered saline until analysis. Freeze thaw cycles were minimized and retained consistent among samples within a study to prevent known[36] degradation of Raman signals. Contamination from modeling clay used for temporarily mounting samples and any notable mechanical damage (stress fractures or scratches) to femurs were grounds for exclusion from the study, such that a total of 6 femurs were excluded. To provide a known profile of toughness loss, 15 *Atf4*+/+ and 9 *Atf4*-/- male mice at 20 weeks of age were sacrificed as part of a previously published study[23]. A study of *Mmp9* male mice[24] was utilized to provide 7 *Mmp9*+/+ and 6 *Mmp9*-/- femurs at 16 weeks of age. A larger study of *Mmp9* mice including both genders (7 wild-type and 5 knockout males and 7 wild-type and 9 knockout females), published here for the first time, was used to validate the methods in spite of the possible confounding factor of gender on the complex Raman signatures. Finally wild-type mice from the same colony as the

Atf4 study at both 8 weeks of age (n=18) and 20 weeks of age (n=15) were used to conduct a control for toughness. Because bone strength (which is frequently associated with compositional changes) increases during maturation, but toughness remains constant, RS polarization specificity to organization changes postulated to affect toughness are examined further.

5.3.2 Micro-Computed Tomography (μCT) scans

Prior to mechanical testing, the femoral mid-shafts were scanned (μCT40, Scanco Medical, Brüttisellen, Switzerland) at an isotropic voxel size of 12 μm using consistent settings (70 kVp/114 μA; 1000 projections per 360° rotation; and 300 ms integration time), calibrated to a hydroxyapatite (HA) phantom and corrected for beam hardening using manufacturer's specifications. The outer cortex was contoured to calculated tissue mineral density of cortical bone (Ct.TMD) as well as the structural properties[23]. The consistent segmentation procedure entailed a global threshold of 715.2 mgHA/cm^3 and a Gaussian noise filter (sigma=0.8 with support of 2).

5.3.3 Mechanical Testing Protocol

Three point bending tests of hydrated, intact femurs[24] were conducted using a bench-top, material testing system (Dynamight 8841, Instron, Canton, OH) with a span (L) of 6 times the mean outer anterior-posterior diameter (i.e., in the direction of loading) of each group (~8mm) and a loading rate of 3 mm/min. Force data were recorded at 50 Hz from a 100 N load cell (Honeywell, OH) while the linear variable displacement transducer recorded displacement. Whole bone strength was the peak force (P_f) endured by the mid-shaft. Using the moment of inertia (I_{min}) of the mid-shaft and the distance between the centroid and the bone surface in the

anterior-posterior direction (c_{min}) from μCT, we estimated the material strength from standard flexural equations[37]. Toughness was defined as the area under the force vs. displacement curve divided by the bone cross-sectional area[38].

5.3.4 Raman Spectroscopy

Raman spectra were acquired from the anterior midshaft of the intact extracted femurs of each animal femur prior to mechanical testing using a standard confocal Raman microscope (Renishaw InVia Raman Microscope, Renishaw, Hoffman Estates, IL) set to a 35 μm slit opening at 1 cm^{-1} spectral resolution, and equipped with a 50x (NA=0.75) objective and a model locked TEM (0,0) 785 nm laser diode source (Innovative Photonic Solutions, Monmouth Junction, NJ), and a 1800 grates/mm holographic grating. Laser power was measured daily before and after measurements at the sample to ensure consistent exposure to 35 mW laser power. To eliminate grating bias according to Renishaw specifications, the polarization was aligned upright within the instrument (left-right when operator faces stage), confirmed with known polarizers and silicon standard intensity. Laser polarization was then confirmed to have an approximate extinction ratio of 1:200 (light was not further polarized by additional optics). Spot size was approximated at 1.5 μm and Gaussian via edge detection on a polished silicon standard[39]. System Raman shift calibration was accomplished using a neon lamp and a silicon standard with Renishaw software to account for grating motion. Daily silicon measurements before and after data collection ensured consistency of wavenumber calibration and collection arm throughput.

The third distal mid-shaft vessel perforation was used as a landmark to consistently select the site of analysis across bones[40]. Bones were thawed to room temperature and then mounted on a standard microscope slide using modeling clay, then attached to a rotation stage (accurate to 5 arcsec) to ensure that the plane of the anterior midshaft would be normal to the incident laser beam. Spectra were collected at two intact bone orientations such that the long bone axis was oriented either parallel (termed the longitudinal orientation) or perpendicular (termed the orthogonal orientation) to the polarization axis of the incident laser. Co-localization of collection sites before and after rotation was accomplished manually by registering fine structural features in the bright field. Each spectrum consisted of 5 accumulations of 10 s integration time to yield a high signal to noise ratio (SNR) from 300 to 1800 cm^{-1} (Hydroxyproline SNR in excess of 25:1). Spectra were processed via least squares modified polynomial fit[41] and smoothed for noise using an 2nd order Savitsky-Golay filter[42]. Custom Matlab software (Mathworks, Natick, MA) extracted the intensity and wavenumber of the prominent spectral peaks. There was no spectral binning in this analysis. After fluorescence subtraction, a linear baseline subtraction (based on derivative zero-crossings neighboring the peak) was conducted on peaks that overlap with neighboring constituents to ensure no residual fluorescence, namely Proline, Hydroxyproline, ν1 Phosphate, and Carbonate. This data was then used to generate markers of bone composition for mineralization (ν1 Phosphate/ Amide I), carbonate substitution (Carbonate/ ν1 Phosphate) and crystallinity (crystal grain size and perfection, determined by the inverse full-width at half maximum intensity of the ν1 Phosphate peak).

5.3.5 Multivariate Data Analysis and Statistics

Multivariate analysis of Raman Spectroscopy was used to analyze spectral wavenumbers beyond validated peak ratios that are usually reported. Principal components analysis (PCA) was selected due to its unsupervised nature of computing fundamental uncorrelated directions of variance using eigenvectors, accomplished using a package with options tailored for spectroscopy (Eigenvector Research Inc., package for Matlab 7). Prior to PCA, data was "auto scaled", which is the same as "z-scoring" or running PCA on the correlation matrix, such that each variable or wavenumber was set to zero mean and unit variance. This is essential in PCA of Raman spectra where certain peaks (like ν1 phosphate in bone) have a much higher intensity than others, which could inaccurately skew the ability or PCA to predict mechanical properties of bone. Because the Raman signal of bone likely contains much more information than that which relates to mechanics, PC's are selected for analysis by screening for those that significantly separate genotype or class. PC's were first screened by F-Test of variance and Lillefor's test for normality. Failing normality in all cases, nonparametric Mann-Whitney U tests were used to test significance at $\alpha=0.05$ ($p<0.05$). For PC's significantly separating data class, Sparse Multinomial Logistic Regression (SMLR; Duke University) was used to test for best classification. SMLR is an iterative multivariate weighting technique that allows for sparsity, or the exclusion of features (or in this case PC's) that do not help discriminate class. Briefly, SMLR was run with a Laplacian prior, a direct kernel, no bias, no normalization, component –wise updates, and leave-one-sample-out cross-validation. The algorithm was run for various weights for sparsity index ($\lambda=0.1, 1, 10, 50$) to ensure optimal classification. In all cases single principal components yielded better classification than multiple principal components in the same SMLR

computation; therefore, Spearman's correlations were run on single PC's to test explanation of bending strength and toughness.

5.4 Results

5.4.1 Differences in Raman Spectra between genotypes become apparent upon bone rotation (Polarization)

Despite the strong toughness reduction in *Atf4*-/- mice (Supplemental Figure 5.1), only slight changes in RS peaks (Figure 5.1 A-C) are seen at any one orientation. To investigate whether differences exist between the genotypes in ways beyond traditional peaks and peak ratios, the effect of bone rotation on the Raman spectra of bone was examined (Figure 5.1 D&E). Upon bone rotation with respect to laser polarization, both *Atf4* +/+ (Figure 5.1D) and *Atf4*-/- (Figure 5.1E) RS profiles changed at previously identified polarization-sensitive regions including the shoulder of ν4 Phosphate (590 cm^{-1}), the ν3 Phosphate peak (1045cm^{-1})[8], the Amide III δ(NH) band (1273 cm^{-1})[27, 43], and Amide I band[9]. The spectra of *Atf4*-/- bone had smaller variance than *Atf4*+/+ bone at Amide III δ(NH) band and the Amide I band, yielding greater separation between orientations than its wild-type counterpart.

5.4.2 Classification of brittle bone genotypes improves with inclusion of full spectrum polarization information

To determine whether the principal components derived from polarization-influenced Raman spectra improves the ability of RS to classify brittle bone, we performed sparse multinomial logistic regression (SMLR) on PCA output and traditional peak ratios. The impact of increasing polarization information (Figure 5.2) was examined using models including all

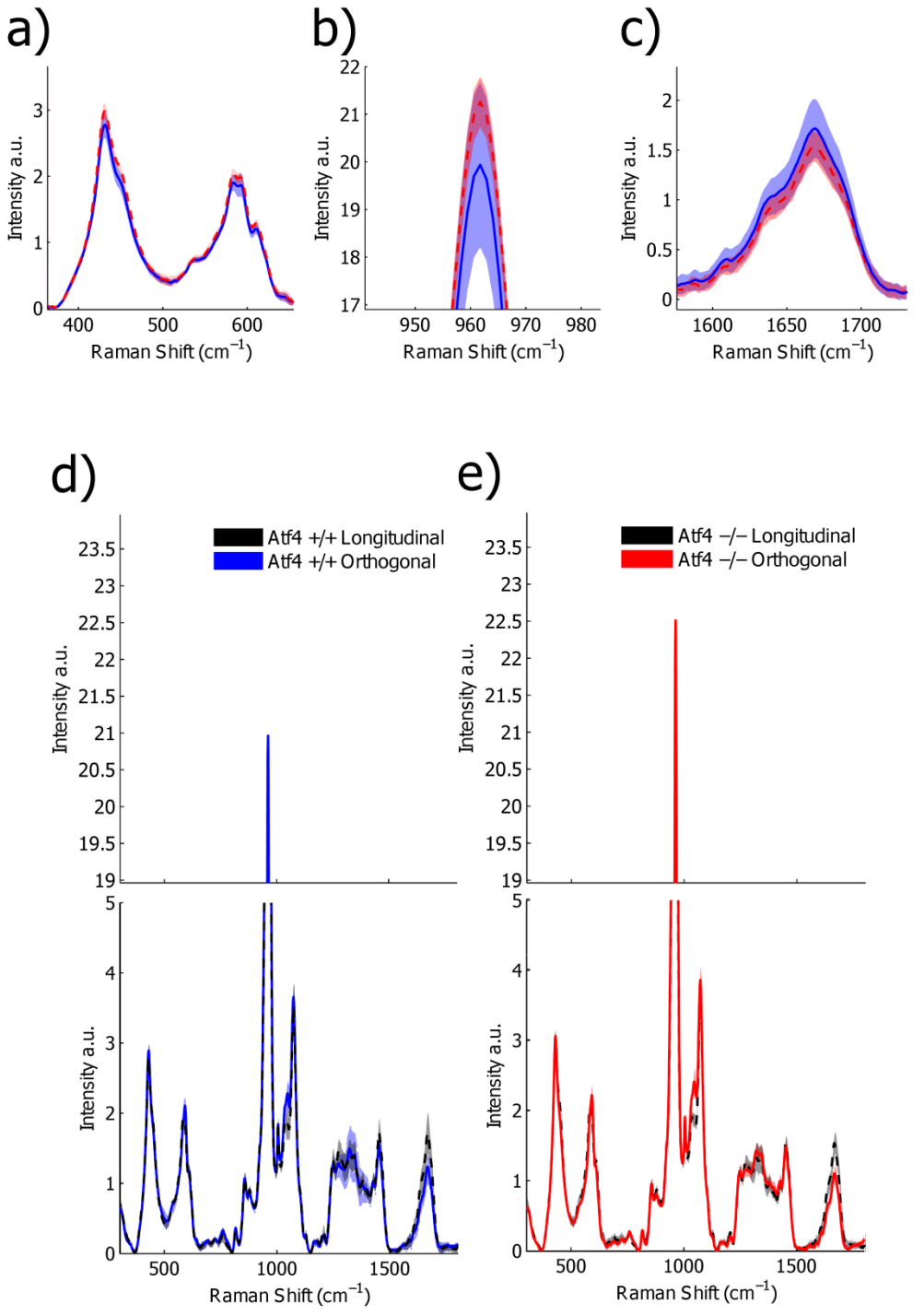

Figure 5.1 Polarization changes in the Raman Spectrum are more intense in brittle bone, but not apparent in any one bone orientation. Peaks from the orthogonal orientation bone spectrum show slight trends that do not separate for **a)** v2 and v4 phosphate, **b)** v1 phosphate, or **c)** Amide I. **d)** Raman spectra (mean ± standard deviation) show more exaggerated differences between orientations for *Atf4*-/- **(e)** than *Atf4* +/+ **(d)**.

principal components that significantly separated *Atf4*-/- from *Atf4*+/+ (Mann-Whitney U; $p<0.05$). SMLR using PCA output from only the orthogonal bone orientation (Figure 5.2A) classified the genotype for 70.8% of the mice (Table 5.1), misclassifying only 2 *Atf4*-/- bones. However, using spectra from both orthogonal (O) and longitudinal (L) orientations in the PCA improves SMLR-based classification capabilities as evident by the increase in the samples correctly classified and the improvement in class posterior probability (Figure 5.2B). Thus, *Atf4*-/- and *Atf4*+/+ bones have different degrees of polarization changes in RS upon bone rotation, and including multiple orientations to capture this polarization-based RS phenotype improves genotype classification (Table 5.1). This finding implies that tissue organization underlies the brittleness difference between *Atf4+/+* and *Atf4-/-* mice.

Improved classification with the inclusion of paired spectra from two bone orientations was consistent across studies involving genetic knock-out mice with a brittle bone phenotype (see Supplemental Figure 5.1 for differences in bone toughness between *Mmp9+/+* and *Mmp9-/-* mice). Unlike the ATF4 study, μCT-derived tissue mineral density (TMD) was significantly different between genotypes for the MMP9 study involving only males, but similar to the ATF4 study, TMD had poor classification accuracy (Table 5.1). With the exception of ν1 Phosphate/Amide I for the *Mmp9* male data set, none of the peak ratios from either bone orientation appropriately classified knockout bones as determined by SMLR (i.e. 0% sensitivity), such that all bones classified as wild-type. Use of the full spectrum as PCA input for either the O or L bone orientation improved SMLR classification sensitivity for all 3 studies (Table 5.1) with the two different bone orientations yielding different classification results. Including both

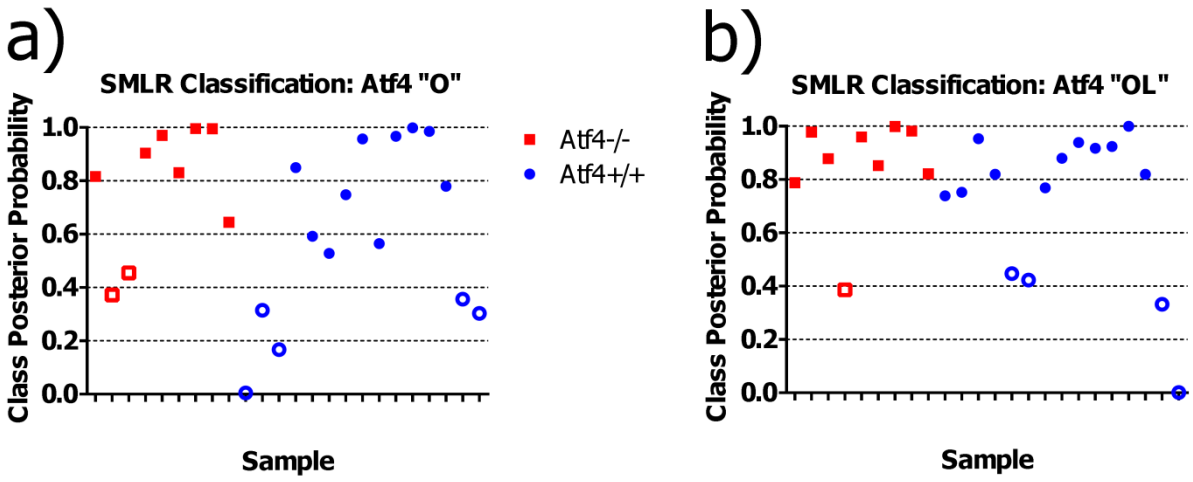

Figure 5.2 Classification accuracy and posterior probability improve with increasing RS polarization information. **a)** SMLR classification for wild-type and knockout bone from the *Atf4* study misclassifies 2 knockout and 5 wild-type samples when using only the orthogonal orientation. **b)** SMLR classification including both orientations misclassifies 1 knockout and 4 wild-type and posterior probability increases for many samples.

Table 5.1 Multivariate expression of increasing polarization information improve classification over common peak ratios

Genotype	Rotation	SMLR Input	Value (Mean ±SD) WT	Value (Mean ±SD) KO	Genotype Separation Pvalue [a]	Correctly Classified	Specificity	Sensitivity
Atf4	-	µCT TMD	1303 ± 16.6	1313 ± 19.2	NS	15/24	100.0%	0.0%
	O	MCR (v1/Aml)	11.450 ± 2.876	13.200 ± 1.549	NS	15/24	100.0%	0.0%
	L	MCR (v1/Aml)	16.330 ± 3.147	19.410 ± 2.253	p =0.017	15/24	100.0%	0.0%
	O	Carb Sub	0.157 ± 0.006	0.151 ± 0.007	NS	15/24	100.0%	0.0%
	L	Carb Sub	0.155 ± 0.006	0.151 ± 0.005	NS	15/24	100.0%	0.0%
	O	Crystallinity	0.0649 ± 0.0008	0.0646 ± 0.0009	NS	15/24	100.0%	0.0%
	L	Crystallinity	0.0646 ± 0.0009	0.0645 ± 0.0008	NS	15/24	100.0%	0.0%
	O	PC Score	8.576 ± 23.730	-14.290 ± 8.013	p =0.015	17/24	66.7%	77.8%
	L	PC Score	8.435 ± 21.420	-14.060 ± 10.350	p =0.001	16/24	53.3%	88.9%
	[O,L]	PC Score	12.030 ± 26.090	-20.050 ± 11.230	p =0.0007	19/24	73.3%	88.9%
Mmp9	-	µCT TMD	1458 ± 14.8	1474 ± 16.1	p =0.004	7/15	0.0%	100.0%
	O	MCR (v1/Aml)	14.530 ± 1.189	12.430 ± 1.270	p =0.009	11/15	71.4%	75.0%
	L	MCR (v1/Aml)	19.930 ± 2.543	18.010 ± 2.040	NS	8/15	42.9%	62.5%
	O	Carb Sub	0.153 ± 0.005	0.154 ± 0.004	NS	7/15	100.0%	0.0%
	L	Carb Sub	0.152 ± 0.006	0.152 ± 0.005	NS	7/15	100.0%	0.0%
	O	Crystallinity	0.0645 ± 0.0005	0.0653 ± 0.0007	p =0.029	7/15	100.0%	0.0%
	L	Crystallinity	0.0650 ± 0.0005	0.0654 ± 0.0006	NS	7/15	100.0%	0.0%
	O	PC Score	-15.330 ± 12.090	13.420 ± 12.120	p =0.001	12/15	71.4%	87.5%
	L	PC Score	-11.120 ± 21.850	9.730 ± 11.690	NS	10/15	57.1%	75.0%
	[O,L]	PC Score	-19.750 ± 20.680	17.280 ± 14.080	p =0.0006	13/15	85.7%	87.5%
Mmp9 Gender	-	µCT TMD	1310 ± 19.0	1235 ± 328	NS	13/26	100.0%	0.0%
	O	MCR (v1/Aml)	11.820 ± 1.901	11.470 ± 1.380	NS	13/26	100.0%	0.0%
	L	MCR (v1/Aml)	18.280 ± 1.962	17.950 ± 3.087	NS	13/26	100.0%	0.0%
	O	Carb Sub	0.152 ± 0.006	0.156 ± 0.004	p =0.034	13/26	100.0%	0.0%
	L	Carb Sub	0.150 ± 0.007	0.152 ± 0.004	NS	13/26	100.0%	0.0%
	O	Crystallinity	0.0653 ± 0.0011	0.0651 ± 0.0009	NS	13/26	100.0%	0.0%
	L	Crystallinity	0.0650 ± 0.0007	0.0653 ± 0.0010	NS	13/26	100.0%	0.0%
	O	PC Score	9.638 ± 23.610	-9.638 ± 15.360	p =0.016	19/26	76.9%	69.2%
	L	PC Score	-5.882 ± 16.030	10.720 ± 20.970	NS	18/26	76.9%	61.5%
	[O,L]	PC Score	7.300 ± 23.440	-13.510 ± 17.720	p =0.022	21/26	76.9%	84.6%

[a]Genotype separation is determined by Mann Whitney U test, significance at $p<0.05$.

orientations as separate variables for PCA (denoted as [O,L]) provided further improvement in overall classification accuracy in both MMP9 studies, despite the confounding factor of gender.

5.4.3 Principal components have a stronger correlation with toughness than traditional compositional RS measurements

Expanding upon the multivariate classification of genotype, we analyzed whether RS polarization information improves mechanical bone quality characterization using Spearman's correlation coefficients (Table 5.2). Peak ratios did not correlate with toughness except for longitudinal MCR in the ATF4 study, the only study where μCT-derived TMD also correlated significantly (Table 5.2). PC1 from either orientation correlated with toughness in the ATF4 and MMP9-gender studies, again with differing results between orientations. The inclusion of both orientations in the PCA strengthened correlation in all three studies. Notably, none of the peak ratios or the genotype separating PC's from toughness models yielded a significant correlation to bending strength. Figure 5.3 shows linear regressions between PC1 from the [O,L] analysis of both orientations and toughness for each genotype. As one of few PCs to significantly separate genotype (Mann-Whitney U; $p<0.05$), PC1 was consistently the only PC observed to significantly explain toughness variance (Figure 5.3). As such, PC1 had a significant linear relationship to toughness for each study (F test: slope $\neq 0$; $p<0.05$), although the slope of this relationship was not positive for all studies. The additional MMP9 study including both male and female femurs exhibited a significant linear regression despite marked overlap in toughness values between the genotypes. That is, there is a notably smaller toughness difference (Supplemental Figure 5.1H) in this study than in the MMP9 male only study, but PC1 still explains the toughness variance. While regression statistics (R^2 values and correlation

Table 5.2 Multivariate Raman spectroscopy signatures provide consistent improved correlation to bone toughness.

Orientation	Property	Atf4[a] Toughness	Mmp9[a] Toughness	Mmp9 Gender[a] Toughness
-	µCT TMD	-0.42	NS	NS
O	MCR (v1/AmI)	NS	NS	NS
L	MCR (v1/AmI)	-0.50	NS	NS
O	Carb Sub	NS	NS	NS
L	Carb Sub	NS	NS	NS
O	Crystallinity	NS	NS	NS
L	Crystallinity	NS	NS	NS
O	PC1 Score	0.53	NS	0.53
L	PC1 Score	0.66	NS	0.57
[O,L]	PC1 Score	0.62	-0.64	0.60

[a] Spearman's correlation coefficient, significance given by using exact test that the correlation is significantly non zero.

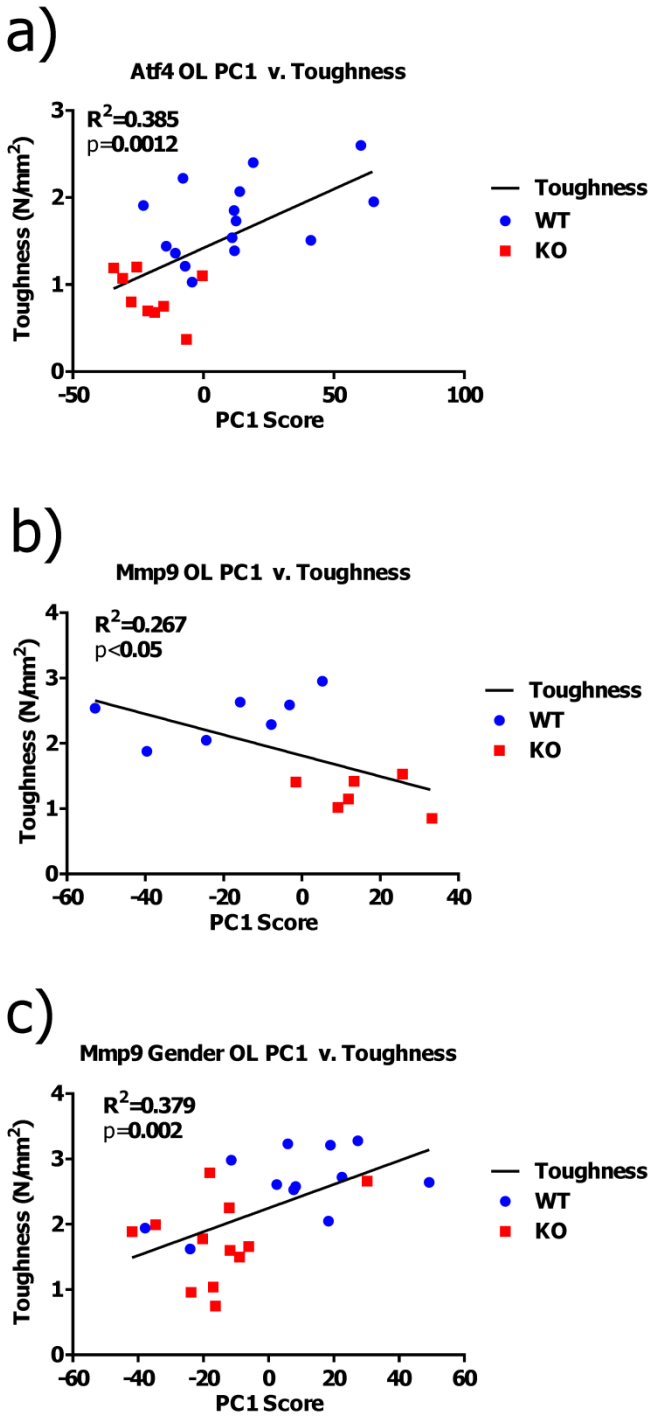

Figure 5.3 Linear regressions of Principal Component scores significantly explain a portion of bone toughness. **a)** PC1 score explains toughness and separates genotype in *Atf4*.**b)** Despite small sample size, PC1 score explains over 20% of variance in toughness of *Mmp9* samples. **c)** Despite overlap due to gender, PC1 score significantly explains over 35% of *Mmp9* toughness.

coefficients) indicate that only a small percentage (<40%) of the total variance was explained, it is important to note that full spectrum polarization information improves genotype classification and correlation to toughness in all three studies when compared to standard RS peak ratios or μCT derived TMD.

5.4.4 Multivariate analysis of full Raman spectra improves classification of young and mature bone, but does not improve correlation to strength

To establish the link between RS polarization information and toughness of bone, a study of strength differences served as a negative control. Strength can often be attributed to changes in composition, as seen with the pronounced increase in cortical tissue mineral density (TMD) that occurs with bone maturation (Supplemental Figure 5.1 J, L). Indeed, μCT-derived TMD separates age significantly (Table 5.3) and correlates to bending strength (Spearman's $\rho = 0.60$; $p<0.05$). Neither MCR nor crystallinity demonstrates SMLR classification sensitivity to maturation or correlation to bending strength. Despite decreased specificity in classifying age, carbonate substitution is the only peak ratio to significantly, albeit weakly, correlate with bending strength ($\rho = 0.42$ for O and $\rho = 0.48$ for L). While PC classification of young and mature bone was more accurate than peak ratios, the correlation to strength was slightly weaker ($\rho = -0.38$ for O, $\rho = -0.37$ for L) than the aforementioned peak ratio. The PC correlation with strength was insignificant when including both orientations. Notably, there were similar results for the 2 orientations with respect to both classification (Table 5.3) and correlation with strength. Unlike models of toughness, adding RS polarization information via full spectrum analysis did not improve explanation of strength in the maturation model, and in general, RS measures do not outperform TMD.

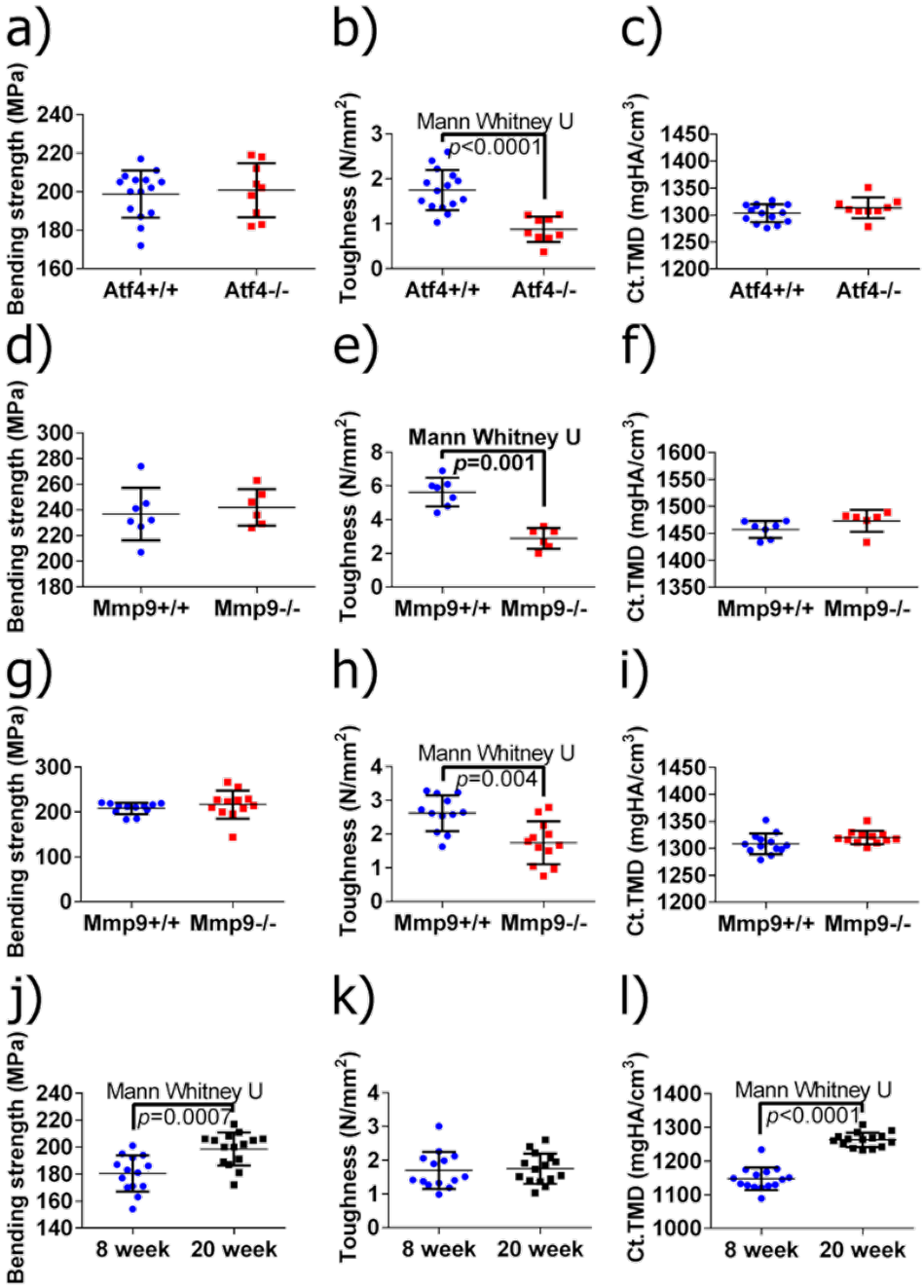

Supplemental Figure 5.1 Toughness differences in *Atf4* and *Mmp9*, unlike strength changes in maturation, are not associated with changes in tissue mineral density (TMD). *Atf4* demonstrates isolation of toughness loss **(b)** without significant changes in strength **(a)** or TMD**(c)**. *Mmp9* males **(d-f)** demonstrate similar mechanical profile of isolated toughness loss **(e)**. *Mmp9* study of both genders illustrates statistically significant but less pronounced difference in toughness **(h)**. Maturation **(j-l)** shows an opposite profile where strength differences **(j)** associate with TMD **(l)** but not toughness **(k)**.

Table 5.3 Multivariate RS expressions of maturation also improve classification accuracy over common peak ratios.

Rotation	SMLR Input	Value (Mean ±STDEV) 8 week	Value (Mean ±STDEV) 20 week	Genotype Separation[a] Pvalue	% Correctly Classified	Specificity	Sensitivity
-	µCT TMD	1147 ± 33.42	1263 ± 21.57	$p<$ 0.0001	18/33	0%	100%
O	MCR (v1/AmI)	11.27 ± 1.741	11.45 ± 2.876	NS	18/33	0%	100%
L	MCR (v1/AmI)	16.3 ± 2.712	16.33 ± 3.147	NS	18/33	0%	100%
O	Carb Sub	0.1457 ± 0.0056	0.1568 ± 0.0061	$p<$ 0.0001	15/33	0%	100%
L	Carb Sub	0.1445 ± 0.0045	0.1552 ± 0.0064	$p<$ 0.0001	15/33	0%	100%
O	Crystallinity	0.0642 ± 0.0006	0.0649 ± 0.0008	p = 0.0094	18/33	0%	100%
L	Crystallinity	0.064 ± 0.0007	0.0646 ± 0.0009	NS	18/33	0%	100%
O	PC4 Score	4.174 ± 5.921	-5.008 ± 9.431	p = 0.004	29/33	87%	89%
L	PC5 Score	3.076 ± 4.628	-3.691 ± 6.797	p = 0.003	28/33	87%	83%
[O,L]	PC3 Score	7.47 ± 15.09	-8.964 ± 15.75	p = 0.0007	28/33	73%	94%

[a] Genotype separation is determined by Mann Whitney U test, significance at $p<0.05$.

5.4.5 Principal components loadings from RS of brittle bone phenotypes suggest conserved elements that are not seen in PCs distinguishing bone maturity

Examining spectral loadings of the principal components may identify elements of RS signatures that explain material property differences. Figure 5.4 compares principal component loadings from the [O,L] PCA that used spectra from both bone orientations and that represents the greatest explanation of variance. In the ATF4 model of toughness loss, strong negative weights of PC1 (differed between genotypes; $p<0.05$) for both orientations occurred at all the mineral peaks, including ν2 Phosphate (430 cm^{-1}), ν4 Phosphate (590 cm^{-1}), ν1 Phosphate shoulders (960 cm^{-1}), and Carbonate (1074 cm^{-1}). Strong positive weights occurred at collagen peaks including Proline (857cm^{-1}), Hydroxyproline (878cm^{-1}), Amide I (1668cm^{-1}), and Amide III (1248cm^{-1}). For several peaks, weights differ between O and L bone orientations, including Amide I and CH_2 (1454cm^{-1}). PC1 of the MMP9 male study, responsible for best genotype classification and correlation to toughness, shows strikingly similar weights to those seen for the ATF4 study with strong negative weights on mineral peaks and strong positive weights on collagen peaks.

While principal components explaining toughness display some conserved spectral features, the principal components that separate maturation illustrate stark contrast from RS signatures of toughness. In Figure 5.4C, PC3 from the maturation experiment did not significantly correlate to strength (note that none of the PC's in the [O,L] input correlated); however, the 11% of the variance explained by this PC offers the best observed separation of class. For both orientations, carbonate was negatively weighted. Surprisingly, very little to no weight was placed on the Amide I peak. Most of the peaks were weighted differently between

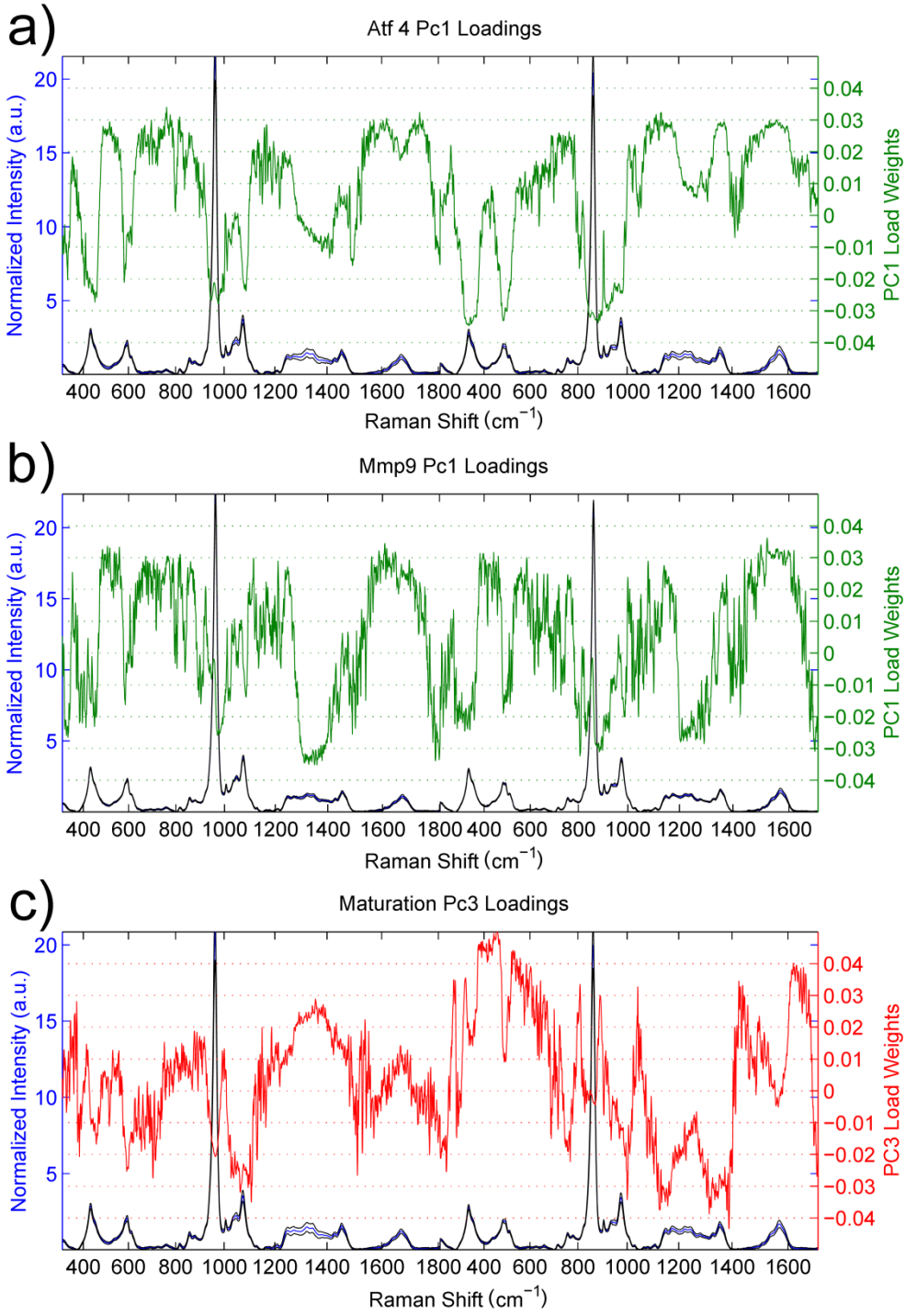

Figure 5.4 PC's that explain toughness demonstrate consistent loadings among studies. **a)** PC1 of *Atf4* demonstrates strong positive collagen and strong negative mineral loadings **b)** Similar positive collagen weights and negative mineral weights explain toughness in PC1 of *Mmp9*. **c)** PC3 of maturation provides best separation of class, but demonstrates strong differences in loading when compared to components from brittleness models.

the two orientations. In summary, mouse genetic models of reduced toughness (loss of ATF4 or MMP9) have a similar RS polarization profile in the principal components that explain toughness; however, separation of maturation based changes have strong differences in orientation that do not correlate to strength, and are loaded differently than RS profiles of toughness.

5.5 Discussion

This paper presents a multivariate analysis of polarization information in Raman Spectroscopy that improves genotype classification and correlation to bone toughness − using bones from 2 genetic mouse models − over peak ratios in traditional RS analyses. As this technique is further developed, it may help establish the interplay between biochemical composition and tissue organization as a factor in bone's fracture resistance.

These experiments confirm that traditional peak ratio analysis is not always sufficient to explain bone mechanical quality. When classifying genotypes for which there is a difference in bone brittleness, only the polarization-sensitive ν1 Phosphate/ Amide I partially identified knockout bones (Table 5.1) and weakly correlated with toughness (Table 5.2). Overall, univariate and even bivariate analysis of RS factors were insufficient to explain genetic-related differences in brittleness, characteristics that depends on defects in matrix organization in addition to abnormal biochemical composition. Full spectrum analysis of principal components derived from a single bone orientation improved classification when compared to single peak ratios (Table 5.1), suggesting that additional RS information assists in the explanation of these complex mechanical phenotypes. Notable differences in RS intensity between orthogonal bone

orientations (Figure 5.1E) occur mostly at locations previously reported by the Penel group[8, 27] to be sensitive to polarization: ν3 Phosphate (1045 cm^{-1}), Amide III δ(NH) band (1273 cm^{-1})[43], and Amide I (1668 cm^{-1}). The most striking differences occur at peak shoulders, and would therefore be overlooked by many standard analyses. Moreover, these orientation effects on Raman spectra were more pronounced in brittle bones than wild-type counterparts (compare Figure 5.1D to Figure 5.1E), suggesting that polarization RS is sensitive to the orientation and subsequently organizational changes underlying toughness loss that occurs with the deletion of ATF4.

While full spectrum analysis improved classification in these models, data from a single orientation alone was insufficient to produce consistent classification and correlation to toughness. In Table 5.1, this manifests as disparate classification accuracy when comparing principal components of results from longitudinal and orthogonal bone orientations. However, use of polarization RS from both bone orientations improves overall classification in all three sets of wild-type and corresponding mutant mice (Table 5.1) and improved class posterior probabilities (Figure 5.2C vs. 2D). In bones lacking MMP9, this additional organization information also improved correlation of RS to toughness.

Principal components analysis identified the RS signatures of brittle phenotypes, and as an unsupervised "bottom up" approach to full spectrum analysis, it lends credence to the reliability of mechanical correlation of these biochemical signatures. In each of the ATF4 and MMP9 studies, the 1st principal direction of variance explained only 25-30% of the total variance of the Raman spectrum, yet it significantly separated genotype and correlated to toughness, explaining over 25% of this mechanical variance (Figure 5.3). Utilizing unsupervised multivariate analysis potentially runs the risk of over-fitting the data, but sensitivity of the

method was validated with two different genetic mouse models and by repeating the MMP9 study on a different data set. Even when the toughness overlaps between genotypes in the additional MMP9 study, which included both genders (Figure 5.3 C), the 1st principal component still significantly explained toughness.

When considering other mechanical properties and potential RS correlation, tissue organization (provided by polarization) may not play as much of a role. Using growing wild-type mice as a model for strength increase with no change in toughness, peak bending stress and μCT-derived tissue mineral density (TMD) increased with age (Supplemental Figure 5.1). Despite this, carbonate substitution was the only peak ratio that correlated with strength, despite lower classification accuracy than other compositional properties (Table 5.3). Considering the numerous endocrine and cellular changes that occur during maturation, it is not entirely unexpected that more bone changes exist in the Raman spectrum than those that explain strength. As such, an increase in the amount of Raman wavenumbers sampled improved classification accuracy, but did not increase correlation to strength (Table 5.3). Moreover, the PCA of the RS data from the individual orientations of bone seem to yield consistent classifications and correlations to strength, which is strikingly different from the orientation and polarization-specific outcomes observed in models of brittleness. Since strength and toughness can be diametrically opposed in many materials, including bone in certain instances[44, 45], it is perhaps not surprising that organizational information from the polarization RS specifically aids the explanation of toughness differences between genotypes but not the strength differences between age groups. Notably, since ATF4 influences collagen synthesis[46] and since MMP-9 is a gelatinase that processes denatured collagen[24], these genes likely influence matrix organization.

On the other hand, secondary mineralization accompanies skeletal maturity[47] from 8 weeks to 20 weeks of age in mice, increasing strength but not toughness.

Although principal components only represent one straightforward and simple application of multivariate analysis to RS, the use of a "bottom up" study design that build upon inherent, uncorrelated dimensions of variance allows for the distinct advantage of analyzing underlying biochemical signatures for consistency between models. Different component loadings (data not shown) between the orthogonal and longitudinal orientations of the same bones within each study imply the necessity of different orientations, and subsequently organizational information, to explain toughness. There are differences in significant principal components between the 2 models of bone brittleness and the model of skeletal maturation (Figure 5.4), noting especially heavy weightings for Amide I bands (~1600-1720 cm^{-1}) in *Atf4* (Figure 5.4A) and *Mmp9* studies (Figure 5.4B) but not for maturation (Figure 5.4C). Strong consistency between the first principal components (PC1) of *Atf4* and *Mmp9* models includes heavy positive weights for Amide III (1235-1280 cm^{-1}) and Amide I bands and heavy negative weights for ν2 phosphate (430 cm^{-1}) and ν4 phosphate (590 cm^{-1}). While the mechanistic significance of these trends remains to be tested, the data imply some conserved elements in the Raman signature of toughness loss (Figure 5.4A and 4B). Note that there is no evidence that ATF4 is upstream or downstream of MMP9 activity to date. By correlating RS to bone material properties, we are effectively assuming an inherent relationship between biochemistry and biomechanics. While the additional RS polarization information allows for a more direct link between toughness and tissue organization, the relationship may not always be clear. This is the

case in bone maturation, where improved classification with full spectrum analysis did not result in an explanation of the age-related increase in strength.

While polarization effects of the Raman phenomenon have been characterized since Placzek[48] and the application of vibrational spectroscopy to the characterization of bone has been conducted for decades (see Boskey[49] and Morris[5, 50] for review), relatively little has been investigated at the union of these two fields, until recently. Pioneers in the bone field showed that crystalline structure was highly organized in enamel and bone[8]; that the orientation of collagen fibers in bone could be extracted from polarization RS[19] and aligned with theory[51]; and that the effect of the polarization phenomenon on bone RS could be augmented or minimized by appropriate instrumentation choices[17]. Traditionally, RS probes tissue biochemistry with a high degree of molecular specificity, but polarization analysis can be sensitive to differences in tissue organization such that RS can then be used to analyze the interaction between bone composition and organization. The additional layer of full spectrum multivariate analysis extends RS interpretation beyond the relative composition implied by peak ratios.

Since the goal of the study was to compare the performance of standard peak ratio analysis to multivariate expressions of RS polarization in their ability to explain bone mechanical quality, Raman spectra were acquired from anatomically consistent surfaces without preparation in the region of mechanical testing, and as such, this anterior midshaft site might not yield the strongest polarization difference seen in bone. The consistent, observed sensitivity of this method to bone mechanical quality is surprising considering vast under-sampling with less than 15 μm^3 sampled per bone. To make an accurate comparison between standard measurements of peak ratios and full spectrum analysis that includes polarization information, the instrument was left at

its inherent polarization extinction ratio. Therefore, further optimization of the Raman instrument may offer continued improvement in the explanation of bone mechanical quality. However, the current configuration makes the method readily available for any lab with a confocal RS instrument and a rotation stage.

In the present study, the subtle spectral changes that occur with polarization sensitivity in RS to matrix organization coincides with the loss of mechanical toughness and not changes in material strength. Thus, polarization RS shows promise as a novel tool to explore the dynamic and subtle underpinnings of the mechanisms behind bone mechanical quality. However, there is indubitably more to the RS signature of bone than a complex explanation of mechanics. In addition, there are likely contributors to mechanical quality to which RS is not sensitive. Near infrared RS, used for clinical relevance, is tuned to be largely insensitive to water, and bound and pore water have a significant contribution to the fracture resistance of bone[52]. RS will not have the resolution of atomic force microscopy to map collagen d spacing[53], nor the SNR of 2 photon fluorescence to examine collagen fiber orientation[54]. Nonetheless, the inherent interplay between chemical composition and tissue organization in RS polarization may prove useful in explaining changes in the fracture resistance of complex human microstructures. Ascenzi showed such complexity as mechanical properties of osteons for different loading modes (i.e., compression vs. tension) were related to the primary collagen orientation relative to the directionality of the haversian canals[55-57]. Both polarized light[58] and polarization RS[59] are sensitive to osteonal lamellae. As such, if the organizational information in polarization RS continues to explain mechanical integrity of bone as it is applied to human bone, this technique could be used to

explain how microstructural heterogeneity and composition affect bone mechanical quality, ultimately producing an RS profile for healthy bone tissue.

5.6 Conclusions

Multivariate analysis of Raman spectrum at two bone orientations (enhancing polarization sensitivity) assisted in the explanation of a toughness loss in genetic mouse models involving 2 different genes (a transcription factor and an enzyme). Across 3 sets of wild-type and knockout bones, mineral-to-collagen ratio, which is often used to characterize compositional differences, did not explain the difference in bone toughness between genotypes. This was effectively achieved with Raman spectral analysis (300 cm^{-1} to 1800 cm^{-1}) using principal components acquired from two orthogonal bone orientations such that the first and largest direction of variance consistently separated the brittleness phenotypes and significantly correlated with bone toughness. Using the same technique on bones from a mouse model of skeletal maturation did not improve the explanation in the age-related increase in strength when compared a univariate approach. This implies that multivariate analysis of Raman spectra is not simply providing more information, but rather the organizational information provided by polarization may specifically aid in explaining variance in toughness but not strength. If the observed Raman profiles scale to complex organization of human bone, polarization in Raman spectroscopy may have clinical utility for bone quality assessment.

5.7 Acknowledgements

This material is based upon work supported by the Department of Veterans Affairs, Veterans Health Administration, Office of Research and Development (1I01BX001018).

Additional funding to support research was received from NIAMS/NIH (AR063157) and NSF (1068988). Lastly, the micro-computed tomography scanner was supported by NIH/NIRR (1S10RR027631) and matching funds from the Vanderbilt Office of Research.

5.8 References

1. B. Ettinger, D. B. Burr and R. O. Ritchie, "Proposed pathogenesis for atypical femoral fractures: Lessons from materials research," Bone **55**(2), 495-500
2. E. M. Lochmuller, et al., "Radius bone strength in bending, compression, and falling and its correlation with clinical densitometry at multiple sites," Journal of bone and mineral research : the official journal of the American Society for Bone and Mineral Research **17**(9), 1629-1638 (2002)
3. X. S. Liu, et al., "Individual trabecula segmentation (ITS)-based morphological analyses and microfinite element analysis of HR-pQCT images discriminate postmenopausal fragility fractures independent of DXA measurements," J Bone Miner Res **27**(2), 263-272 (2012)
4. A. H. Burstein, D. T. Reilly and M. Martens, "Aging of bone tissue: mechanical properties," J Bone Joint Surg Am **58**(1), 82-86 (1976)
5. M. D. Morris and G. S. Mandair, "Raman assessment of bone quality," Clinical orthopaedics and related research **469**(8), 2160-2169 (2011)
6. S. Porto, J. Giordmaine and T. Damen, "Depolarization of Raman Scattering in Calcite," Physical Review **147**(2), 608-611 (1966)
7. M. D. Levenson, "Polarization techniques in coherent Raman spectroscopy," J Raman Spec **10**(1), 9-23 (1981)
8. G. Leroy, et al., "Human Tooth Enamel: A Raman Polarized Approach," Applied spectroscopy **56**(8), 1030-1034 (2002)
9. M. Kazanci, et al., "Bone osteonal tissues by Raman spectral mapping: orientation-composition," Journal of structural biology **156**(3), 489-496 (2006)
10. A. Masic, et al., "Observations of multiscale, stress-induced changes of collagen orientation in tendon by polarized Raman spectroscopy," Biomacromolecules **12**(11), 3989-3996 (2011)
11. T. E. Uveges, et al., "Alendronate treatment of the brtl osteogenesis imperfecta mouse improves femoral geometry and load response before fracture but decreases predicted material properties and has detrimental effects on osteoblasts and bone formation," Journal of bone and mineral research : the official journal of the American Society for Bone and Mineral Research **24**(5), 849-859 (2009)

12. X. Li, et al., "Targeted Deletion of the Sclerostin Gene in Mice Results in Increased Bone Formation and Bone Strength," Journal of Bone and Mineral Research **23**(6), 860-869 (2008)

13. J. Ndong, et al., "Asfotase-alpha improves bone growth, mineralization and strength in mouse models of neurofibromatosis type-1.," Nature Medicine. In press (2014)

14. N. P. Camacho, W. J. Landis and A. L. Boskey, "Mineral changes in a mouse model of osteogenesis imperfecta detected by Fourier transform infrared microscopy," Connect Tissue Res **35**(1-4), 259-265 (1996)

15. E. Miller, et al., "Abnormal mineral-matrix interactions are a significant contributor to fragility in oim/oim bone," Calcified tissue international **81**(3), 206-214 (2007)

16. M. Vanleene, et al., "Ultra-structural defects cause low bone matrix stiffness despite high mineralization in osteogenesis imperfecta mice," Bone **50**(6), 1317-1323 (2012)

17. M. Raghavan, et al., "Quantitative polarized Raman spectroscopy in highly turbid bone tissue," Journal of biomedical optics **15**(3), 037001 (2010)

18. S. J. Gadaleta, et al., "Fourier transform infrared microscopy of calcified turkey leg tendon," Calcif Tissue Int **58**(1), 17-23 (1996)

19. S. Gamsjaeger, et al., "Cortical bone composition and orientation as a function of animal and tissue age in mice by Raman spectroscopy," Bone **47**(2), 392-399 (2010)

20. P. J. Thurner, et al., "Osteopontin deficiency increases bone fragility but preserves bone mass," Bone **46**(6), 1564-1573 (2010)

21. A. A. Poundarik, et al., "Dilatational band formation in bone," Proceedings of the National Academy of Sciences **109**(47), 19178-19183 (2012)

22. S. Y. Tang, et al., "Matrix metalloproteinase–13 is required for osteocytic perilacunar remodeling and maintains bone fracture resistance," Journal of Bone and Mineral Research **27**(9), 1936-1950 (2012)

23. A. J. Makowski, et al., "The loss of activating transcription factor 4 (ATF4) reduces bone toughness and fracture toughness," Bone **62**(1-9 (2014)

24. J. S. Nyman, et al., "Differential effects between the loss of MMP-2 and MMP-9 on structural and tissue-level properties of bone," J Bone Miner Res **26**(6), 1252-1260 (2011)

25. A. J. Makowski, et al., "Polarization control of Raman spectroscopy optimizes the assessment of bone tissue," Journal of biomedical optics **18**(5), 55005 (2013)

26. G. Penel, et al., "MicroRaman Spectral Study of the PO4 and CO3 Vibrational Modes in Synthetic and Biological Apatites," Calcified tissue international **63**(6), 475-481 (1998)

27. G. Falgayrac, et al., "New method for Raman investigation of the orientation of collagen fibrils and crystallites in the Haversian system of bone," Applied spectroscopy **64**(7), 775-780 (2010)

28. B. Z. Gevorkian, N. E. Arnotskaia and E. N. Fedorova, "[Study of bone tissue structure using polarized Raman spectra]," Biofizika **29**(6), 1046-1052 (1984)

29. J. S. Nyman, et al., "Measuring differences in compositional properties of bone tissue by confocal Raman spectroscopy," Calcif Tissue Int **89**(2), 111-122 (2011)

30. L. S. Schadler and C. Galiotis, "Fundamentals and applications of micro Raman spectroscopy to strain measurements

in fibre reinforced composites," International Materials Reviews **40**(3), 116 (1995)

31. O. de Carmejane, et al., "Bone chemical structure response to mechanical stress studied by high pressure Raman spectroscopy," Calcif Tissue Int **76**(3), 207-213 (2005)

32. S. Michielsen, "Application of Raman Spectroscopy to Organic Fibers and Films," in Handbook of Raman Spectroscopy I. R. Lewis and H. G. M. Edwards, Eds., pp. 749-798, Marcel Dekker, New York (2001).

33. D. C. Smith and C. Carabtos-Nedelec, "Raman spectroscopy applied to Crystals: Phenomena and Principles,

Concepts and Coventions," in Handbook of Raman Spectroscopy I. R. Lewis and H. G. M. Edwards, Eds., pp. 349-422, Marcel Dekker, New York (2001).

34. J. A. Inzana, et al., "Bone fragility beyond strength and mineral density: Raman spectroscopy predicts femoral fracture toughness in a murine model of rheumatoid arthritis," J Biomech **46**(4), 723-730 (2013)

35. M. Vanleene, et al., "Transplantation of human fetal blood stem cells in the osteogenesis imperfecta mouse leads to improvement in multiscale tissue properties," Blood **117**(3), 1053-1060 (2011)

36. J. D. McElderry, M. R. Kole and M. D. Morris, "Repeated freeze-thawing of bone tissue affects Raman bone quality measurements," Journal of biomedical optics **16**(7), 071407 (2011)

37. C. H. Turner and D. B. Burr, "Basic biomechanical measurements of bone: a tutorial," Bone **14**(4), 595-608 (1993)

38. R. O. Ritchie, et al., "Measurement of the toughness of bone: a tutorial with special reference to small animal studies," Bone **43**(5), 798-812 (2008)

39. J. M. Khosrofian and B. A. Garetz, "Measurement of a Gaussian laser beam diameter through the direct inversion of knife-edge data," Applied optics **22**(21), 3406 (1983)

40. P. Popesko, V. Rajtová and J. Horák, A Colour Atlas of the Anatomy of Small Laboratory Animals, Saunders (2002).

41. C. A. Lieber and A. Mahadevan-Jansen, "Automated method for subtraction of fluorescence from biological Raman spectra," Applied spectroscopy **57**(11), 1363-1367 (2003)

42. J. R. Maher, et al., "Raman spectroscopy detects deterioration in biomechanical properties of bone in a glucocorticoid-treated mouse model of rheumatoid arthritis," Journal of biomedical optics **16**(8), 087012 (2011)

43. M. Janko, et al., "Anisotropic Raman scattering in collagen bundles," Optics letters **35**(16), 2765-2767 (2010)

44. A. Carriero, et al., "How Tough Is Brittle Bone? Investigating Osteogenesis Imperfecta in Mouse Bone," Journal of Bone and Mineral Research **29**(6), 1392-1401 (2014)

45. J. G. Ramasamy and O. Akkus, "Local variations in the micromechanical properties of mouse femur: the involvement of collagen fiber orientation and mineralization," J Biomech **40**(4), 910-918 (2007)

46. X. Yang, et al., "ATF4 is a substrate of RSK2 and an essential regulator of osteoblast biology; implication for Coffin-Lowry Syndrome," Cell **117**(3), 387-398 (2004)

47. O. Akkus, F. Adar and M. B. Schaffler, "Age-related changes in physicochemical properties of mineral crystals are related to impaired mechanical function of cortical bone," Bone **34**(3), 443-453 (2004)

48. G. Placzek, "Rayleigh-Streuung und Raman-Effekt," in Handbuch der Radiologie E. Marx, Ed., pp. 205-374, Akademische Verlagsgesellschaft, Leipzig, Germany (1934).

49. A. Boskey and R. Mendelsohn, "Infrared analysis of bone in health and disease," Journal of biomedical optics **10**(3), 031102 (2005)

50. A. Carden and M. D. Morris, "Application of vibrational spectroscopy to the study of mineralized tissues (review)," Journal of biomedical optics **5**(3), 259-268 (2000)

51. W. Wagermaier, et al., "Spiral twisting of fiber orientation inside bone lamellae," Biointerphases **1**(1), 1-5 (2006)

52. R. A. Horch, et al., "Non-invasive predictors of human cortical bone mechanical properties: T(2)-discriminated H NMR compared with high resolution X-ray," PLoS One **6**(1), e16359 (2011)

53. J. M. Wallace, et al., "Distribution of type I collagen morphologies in bone: relation to estrogen depletion," Bone **46**(5), 1349-1354 (2010)

54. D. Aït-Belkacem, "Microscopic structural study of collagen aging in isolated fibrils using polarized second harmonic generation," Journal of biomedical optics **17**(8), 080506 (2012)

55. M. Portigliatti Barbos, et al., "Collagen orientation in compact bone: II. Distribution of lamellae in the whole of the human femoral shaft with reference to its mechanical properties," Metab Bone Dis Relat Res **5**(6), 309-315 (1984)

56. A. Boyde, et al., "Collagen orientation in compact bone: I. A new method for the determination of the proportion of collagen parallel to the plane of compact bone sections," Metabolic Bone Disease and Related Research **5**(6), 299-307 (1984)

57. M. G. Ascenzi and A. Lomovtsev, "Collagen orientation patterns in human secondary osteons, quantified in the radial direction by confocal microscopy," Journal of structural biology **153**(1), 14-30 (2006)

58. T. G. Bromage, et al., "Circularly polarized light standards for investigations of collagen fiber orientation in bone," Anatomical record **274**(1), 157-168 (2003)

59. M. Kazanci, et al., "Raman imaging of two orthogonal planes within cortical bone," Bone **41**(3), 456-461 (2007)

CHAPTER 6

MICROSTRUCTURAL HETEROGENEITY OF COMPOSITION AND ORGANIZATION JOINTLY EXPLAIN THE AGE-RELATED DECREASE IN BONE FRACTURE TOUGHNESS

6.1 Abstract

The complex organizational hierarchy of bone makes the accurate assessment of human fracture risk a difficult endeavor; thus, the underlying mechanisms that facilitate a loss of fracture toughness with disease or aging are not completely defined. Loss of microstructural heterogeneity has been implicated as an important factor in the age-related decrease in bone fracture toughness. To assess heterogeneity at this length scale, we employed polarization Raman Spectroscopy for its sensitivity to both composition and organization. Single edge notched beam specimens were generated from the distal lateral midshaft of 62 cadaveric femurs matched for age and gender. Raman spectra were collected at 9 different locations in the intended crack path prior to mechanical testing. A progressive, loading scheme in a three-point bending configuration was used to assess the rising R-curve behavior of each specimen. Then, using a non-linear elastic

fracture mechanics approach, three fracture toughness properties were determined. Average peak ratios from this initial analysis did not correlate with fracture toughness outcomes. Therefore, subset of 33 specimens was then selected for Raman mapping of a single osteonal-interstitial border at 2 polarization states. As observed qualitatively from the maps, microstructural heterogeneity of both organization-sensitive and composition-sensitive peak ratios across the osteonal-interstitial border were positively associated with superior fracture toughness outcomes using standard Raman peak ratios. To assess the explanatory power of the technique, image heterogeneity was quantified for contrast and energy using prominent peaks and principal components of the spectra. Canonical spectral signatures of image energy and contrast explain 25-75% of the age-related decrease in fracture toughness outcomes. Analysis of weightings and component loadings demonstrate interplay between compositional and organizational heterogeneity, and imply that opposing biochemical influences on heterogeneity maybe driving crack initiation toughness and overall crack growth resistance (J-integral). The evidence is not only compelling for the explanation of human fracture risk, but polarization Raman spectroscopy shows promise as a means to assess the relationship between heterogeneity and fracture toughness for complex organic composites.

6.2 Introduction

As an organic composite material, bone tissue has exceptional mechanical properties, especially given the combination of low weight, high Young's modulus, and significant post yield toughness. Many of the landmark findings about bone, notably Wolff's Law[1] and Ascenzi's analysis of osteons[2, 3], associate its remarkable load bearing ability to its complexity. However,

the complex organizational hierarchy of bone makes the accurate assessment of human fracture risk a difficult endeavor. Thus, the underlying mechanisms behind age, disease, and even treatment related loss of fracture resistance are not completely defined. A growing body of evidence suggests that bone fracture resistance depends upon both bone strength, the ability of material to withstand stress without failure, and fracture toughness, the resistance to crack formation and propagation arising from inherent flaws. While the clinical loss of bone strength is well characterized by areal bone mineral density (aBMD) via dual X-ray absorptiometry, BMD is not an accurate assessment of fracture risk[4, 5]. In fact, there is a lack of clinical surrogates that are sensitive to fracture toughness properties. Understanding the underlying mechanisms for fracture toughness could benefit the design and application of both diagnostics for early fracture risk assessment and advanced biocompatible materials.

Investigations into the fracture mechanics of bone and hard tissue, spearheaded largely by Bonfield, Vashishth and Ritchie, suggest that there are several tissue level mechanisms by which bone resists damage accumulation, crack initiation, and subsequent crack propagation. As a crack propagates, damage accumulated in the plastic zone preceding the crack tip and the peritubular region leads to microcracks, often visible at pores and canals, and intrinsic toughening[6, 7]. Several other mechanisms have also been observed including: extrinsic unbroken ligament crack bridging[8, 9], crack deflection around osteons[10], and even time-dependent crack blunting[11]. While the observed mechanisms vary distinctly in which length-scales are involved, each is based upon the fact that cracks follow the path of least resistance, and that deflection due to damage or material boundaries consumes energy. Therefore, these mechanisms could logically lead to the hypothesis that increased heterogeneity in microstructure directly impacts the fracture

toughness of bone. In fact, in other materials, local structural and compositional boundaries, like metallic grain boundaries, promote fracture toughness[12]. However it is unclear to what extent differences in tissue heterogeneity may drive these observed mechanisms and the role they play in the pathological decrease in fracture toughness[13]. Moreover, current evidence suggests that the effects of heterogeneity on fracture risk are strongly context dependent. A recent study examining heterogeneity in the femoral neck of fracture patients and cadaveric controls using FTIR spectroscopy found that fragility fracture was associated with decreased heterogeneity in distributions of mineral to collagen ratio (MCR) as well as carbonate substitution[14]. However, the same study found that fracture was associated with greater heterogeneity in crystallinity. Adding to the dichotomy, a qBEI (quantitative backscattered electron imaging) study associated alendronate treatment with restoration of normal heterogeneity in the bone mineralization density distribution after long-term treatment (contrary to previous results indicating decreased heterogeneity during early treatment)[15]. Finally, bisphosphonate use in both dogs[16] and humans[17] has been associated with decreased tissue microstructural heterogeneity of mineral composition as measured by FTIRI[16], and may be linked to the incidence of atypical femoral fractures[17, 18].

The myriad of techniques used, length scales examined, and definitions of heterogeneity for different pathologies may attribute to these dichotomous results. Specifically, it is unclear whether heterogeneity at the microstructural level is more strongly influenced by local compositional variance (e.g., degree of mineralization) or organizational variance (e.g., distribution of collagen fibril orientation). In addition to the compositional heterogeneity examined in association with atypical fractures, it is known through the work of Ascenzi et al. that lamellar collagen orientation is associated with resistance to different mechanical forces,

such that different osteon types (defined by collagen fibril orientation) dominate different anatomical quadrants[19-22]. To this end, Raman spectroscopy provides a unique opportunity to concurrently examine both compositional heterogeneity, due to its inherent sensitivity to chemical bonds[23] , as well as organizational heterogeneity, due to polarization sensitivity to mineral and collagen direction[24, 25]. The nondestructive measure from Raman spectroscopy caused by inelastic scattering allows for the quantitative analysis of mineral to collagen ratios (MCR), type-B carbonate substitution, and mineral crystallinity[23]. Studies have associated changes in Raman spectra with tissue aging[26-28], mechanical damage[29, 30], collagen cross-linking[30], and osteoporotic fracture[31], among other bone pathologies. The polarization in Raman spectroscopy is consistent between samples[25], reveals tissue microstructure including variance in osteonal lamellae and differences in osteonal-interstitial tissue types[32, 33], and has been linked to animal models of diseases with phenotypic loss of mechanical integrity[34-37]. To provide a more detailed analysis of the link between heterogeneity and fracture toughness, we investigated the correlation between the age-related decrease in fracture toughness and microstructural tissue heterogeneity as measured by polarization Raman spectroscopy. Prior to fracture toughness testing, Raman spectra were collected from various microstructures in the intended crack path to examine heterogeneity of neighboring microstructures, and polarization mapping of a single osteonal-interstitial border at two orthogonal orientations was used to measure heterogeneity within microstructures.

6.3 Methods

6.3.1 Study Design

Fresh frozen human cadaveric femur specimens from 62 age and gender matched donors (30 male donors, aged 21 – 98 years old, mean ± standard deviation: 63.5 ± 23.7 years; and 32 female donors, aged 23 -101 years old, 64.4 ± 21.3 years) were obtained from the Musculoskeletal Transplant Foundation (Edison, NJ), the Vanderbilt Donor Program (Nashville, TN), and the National Disease Research Interchange (Philadelphia, PA). Exclusion criteria included total hip arthroplasty, joint replacement, diagnosed bone disease, use of bisphosphonates, chronic kidney disease, cancer, and infectious cause of death. The lateral quadrant of the distal femoral midshaft cortical bone was extracted via low-speed diamond osteotomy saw (South Bay Technologies, San Clemente, CA) and machined into a single-edged notched beam (SENB) sample with an endocortical notch oriented in the radial direction, such that crack propagation occurred normal to osteon direction (Figure 6.1A). Briefly after extraction, low torque, low-speed hydrated machining with an end mill was used to remove the endosteal and periosteal surfaces producing a uniform beam specimen with dimensions proportional to donor cortical thickness (nominally: 1.9–3.3 mm height x 4–6.8 mm width x 19–31 mm length). To reach ASTM E1820[38] size standards, the sample was ground on successive grades of sandpaper on a plane parallel surface grinder (EXAKT Technologies, Oklahoma City, OK) and then polished in one micron alumina solution on a vibratory polisher (Buehler, Lake Bluff, IL). A micro-notch was generated to just below ASTM specifications using a low-speed, irrigated osteotomy saw equipped with diamond embedded wafering blade after which ASTM specified notch length (a_0 = 0.9-1.9 mm) was achieved by polishing the crack tip with a

razorblade irrigated with 1μm diamond polishing solution. The samples were briefly sonicated to remove any solution, and then the bone was frozen in PBS at -20°C until taken for scanning. Care was taken to track the freeze thaw cycles of each bone to ensure that each freeze thaw cycle lasted less than eight hours and fewer than 4 cycles occurred[39] prior to mechanical testing and Raman mapping. Micro-computed tomography (μCT) scanning (Figure 6.1B) was used to confirm the initial notch length (Scanco Medical, Switzerland). Raman spectroscopy measurements were acquired prior to crack propagation to examine heterogeneity of local features in the intended crack path (Figure 6.1C). The bone was stored frozen until thawed and subjected to cyclic three-point bend fracture toughness testing. After testing, a randomly selected half of the specimen was chosen for Raman mapping (Figure 6.1G) and transferred to 70% ethanol for 48 hours followed by air drying for 72 hours in a sterile environment, after which the specimen was stored sealed in plastic under a vacuum until Raman acquisition.

6.3.2 Fracture toughness testing

All fracture toughness tests were conducted in adherence to ASTM E1820 standards[38] with SENB samples subjected to cyclic three-point bending, by an axial servo-hydraulic testing apparatus (Instron, Norwood, MA) run in displacement control with progressive load (+0.07 mm at 0.01 mm/s)-unload (-0.04 mm at 0.015 mm/s)-dwell cycles (Figure 6.1D). Force and displacement data were acquired at 50 Hz from a 1000N load cell and a linear-variable displacement transducer, respectively. Scaled photomicrographs were acquired during each dwell with a macro lens at 4x magnification (pixel size: ~144 μm^2). Oblique lighting was used to

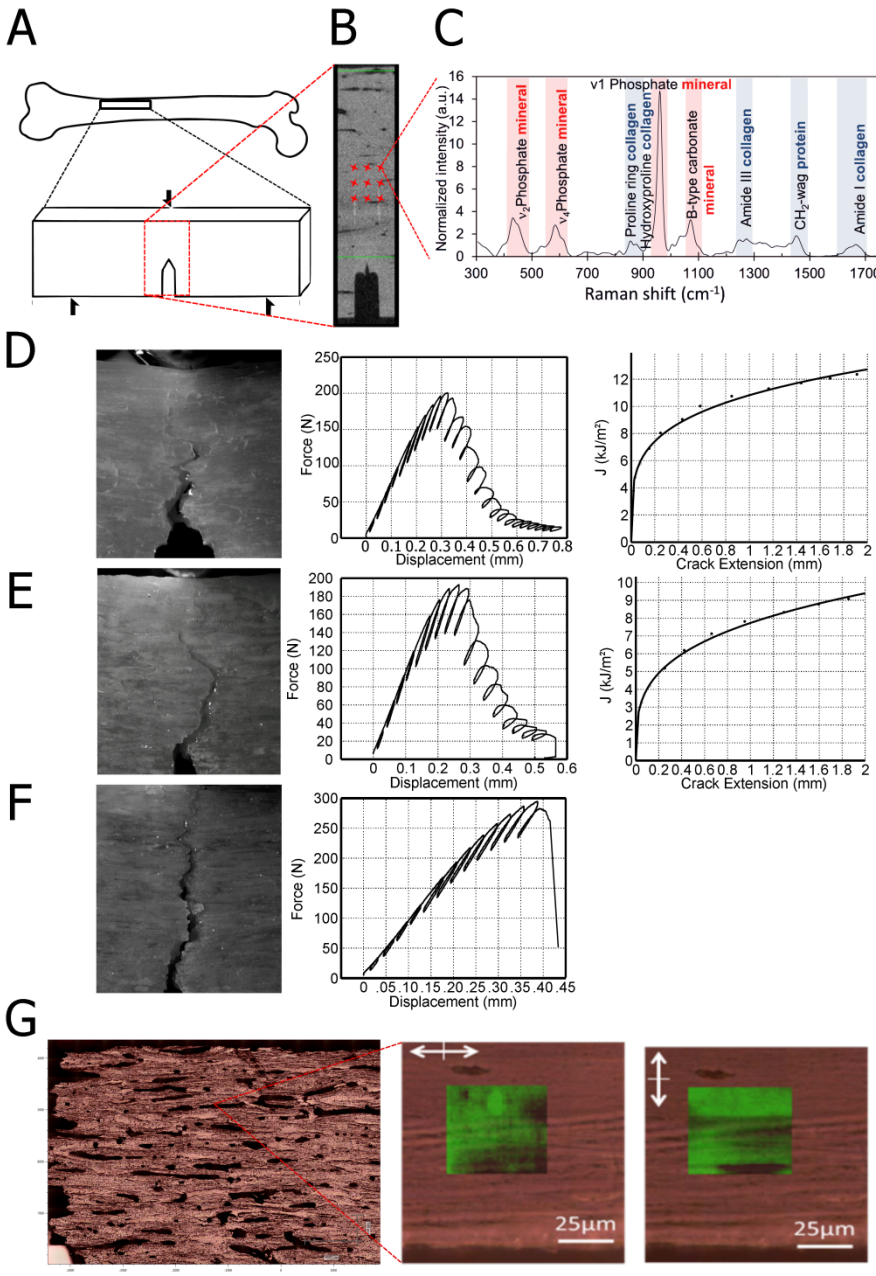

Figure 6.1 A) Extraction of bone sample from distal lateral femoral midshaft that was machined to ASTM E1820 fracture toughness standard **B)** µCT scan demonstrates notch length as well as representative Raman collection locations. **C)** Typical Raman spectrum of human cortical bone demonstrates mineral and collagen peak assignments. **D)** High fracture toughness sample demonstrates a high degree of tortuosity and crack propagation. Force-displacement curve shows several stable crack extensions. R-curve fit shows expected "rising" behavior. **E)** Lower fracture toughness samples demonstrate arguably less crack tortuosity, fewer crack extensions. **F)** Very low fracture toughness samples demonstrate little to no tortuosity or appreciable crack extension, and therefore no R-curve can be calculated. **G)** Osteon oriented along the bone's long axis, and registered Raman maps of carbonate intensity demonstrating variable feature contrast.

highlight crack propagation and qualitatively confirm compliance-based crack growth, as well as assess stability and tortuosity of the crack path.

Processing of fracture toughness data included generating the rising R-curve to appropriately encompass the elastic-plastic mechanical behavior of human cortical bone.[40-42] Crack growth was computed from the unloading compliance data as per ASTM E1820[38]. The analysis produces measurements of the crack initiation toughness (K_{init}), crack growth toughness (K_{grow}), and overall crack growth resistance (J-Integral) such that the potential energy of crack growth is measured with respect to the **elasto-plastic** stress and strain fields around the crack tip (i.e., a non-linear, elastic fracture mechanics approach). Details for the calculations are as per Granke et al. [36]. K_{grow} could not be calculated for specimens when no appreciable stable crack propagation is recorded due to brittle instability. This was the case for 11 samples out of total 62, and 5 of which mapped by polarization RS.

6.3.3 Raman Spectroscopy: Data Acquisition

All Raman spectra were acquired using a confocal Raman microscope (Renishaw InVia Raman Microscope, Renishaw, Hoffman Estates, IL) set to a 35 μm slit at 1 cm^{-1} spectral resolution, equipped with a 50x (NA=0.75) near infrared objective and a model locked TEM (0,0) 785 nm laser diode (Innovative Photonic Solutions, Monmouth Junction, NJ), dispersed by an 1800 lines/mm holographic grating. Laser polarization was aligned upright according to Renishaw specifications and confirmed with known polarizers and silicon standard intensity. Laser specifications were tested to have a 1 μm Gaussian spot and a polarization extinction ratio of 1:200. Raman shift calibration was accomplished using Renishaw software and supplied

standards to account for grating motion. Daily silicon measurements before and after data collection ensured wavenumber calibration and light throughput.

To prevent spurious influence on multivariate analyses, the presence of any cosmic rays were removed using custom Matlab software (Mathworks, Natick, MA). Spectra were then processed via modified polynomial fit[43] and smoothed for noise using a Savitsky-Golay filter[34]. Custom Matlab software extracted the intensity and wavenumber of spectral peaks. After fluorescence subtraction, a linear baseline subtraction was conducted on peaks that overlap with neighboring constituents to ensure no residual fluorescence, namely Proline, Hydroxyproline, ν1 Phosphate, and Carbonate. This data was then used to generate peak ratio biomarkers of bone composition for mineral-to-collagen ratio (MCR: ν1 Phosphate/ Amide I, ν1 Phosphate/ Proline, ν2 Phosphate/ Amide III), Type-B carbonate substitution (Carbonate/ ν1 Phosphate) and crystallinity (crystal grain size and perfection, determined by the inverse full-width at half maximum intensity of the ν1 Phosphate peak)[44].

For measurements of multiple microstructural features in the crack path prior to fracture toughness testing, the bone was aligned with the long axis parallel to laser polarization. A 3 x 3 grid with ~250 μm linear spacing between each location was centered over the intended crack propagation region directly between the notch tip and the periosteal edge. At each of the 9 sites, 7 accumulations of 10 seconds exposure time were acquired for the fingerprint region from 300-1800 cm^{-1} (Figure 6.1C). The osteonal and interstitial nature of each location was balanced during site selection. Laser power was measured daily before and after measurements at the sample to ensure exposure to 35 mW laser power.

For polarization Raman mapping, the bone was mounted to a plastic slide using cyanoacrylate subsequently attached to a custom rotation stage, again oriented with the bone long axis parallel to laser polarization. A single osteonal-interstitial border of an osteon running parallel to the long axis of the bone was chosen with the site no less than 3 mm away from visible damage. Proprietary Renishaw Streamline software utilized line scan optics to acquire 32x 32 pixel raster maps of the selected region (Figure 6.1G). Pixel spacing was set to the system resolution of 1.4 μm in each dimension. To capture the fingerprint region, two static grating map scans were required, with the grating centered at 930 cm^{-1} and 1350 cm^{-1}, respectively. Corresponding spectra from each location for both grating positions were then overlaid and stitched together to encompass the entire 300-1800 cm^{-1} fingerprint region at the 1 cm^{-1} system resolution. Total dwell time per pixel was set to 180 seconds. Total laser power for the entire line was measured at 45mW, and checked for consistency between maps. The bone was then rotated 90 degrees about the optical axis. Minor error was corrected by manually registering fine structural features in the bright field. The accuracy of this method was confirmed to be within system tolerance by using Matlab mutual information registration of bright field photomicrographs before and after rotation on several samples. After rotation and fine registration, the map acquisition protocol was repeated for this orthogonal orientation. For multivariate analyses, coregistered pixels from each orientation are then concatenated so that both orientations belonging to a single physical location are analyzed as one observation.

6.3.4 Statistical Analysis

For Raman spectra collected prior to fracture toughness testing on hydrated bone, the average value and coefficient of variation for standard peak ratios were used to conduct correlations to mechanical outcomes. Univariate analyses were conducted using Matlab and GraphPad Prism (GraphPad Software, San Diego, CA). Upon failing the F-test of normality, Spearman's correlations were used with significance at a *p*-value less than 0.05 for the null hypothesis of the slope of the correlation is zero. For Raman mapping of dried bone, average and coefficient of variation of peak ratios were examined similarly as correlates to fracture toughness. Principal components analysis (PCA) was run on the correlation matrix of the full spectrum, effectively the same as "z-scoring" each wavenumber, using Matlab built-in functions. The scree plot technique was used to screen the cumulative sum of variance to limit further analysis to principal components that contain a relevant proportion of the underlying variance[45]. The elbow of the scree plot indicated that 39 principal components should be used, accounting for approximately 70% of the total variance of the Raman spectra.

To perform an accurate analysis of whether heterogeneity plays a role in fracture toughness, heterogeneity needed to be defined from the Raman map data, such that a one-to-one correspondence existed between heterogeneity and mechanical outcomes. To quantify heterogeneity, image processing methods called texture analysis were employed. Specifically, the gray level co-occurrence matrix was calculated for each peak and principal component. The gray level co-occurrence matrix (glcm) bins an image and calculates the relative frequency of neighboring pixels for each possible intensity pair, subsequently used to calculate image texture[46]. Baraldi et al. showed that commonly used metrics for texture homogeneity were in fact

a complex combination of both image energy and contrast, each with its own interpretation[47]. Contrast is practically defined as a quantification of spatial frequency and the range of values in the image[46]:

$$Contrast = \sum_{i,j} |i-j|^2 p(i,j) \qquad \text{Eq. 6.1}$$

where i,j represent all possible pixel intensities and p(i,j) is the corresponding element in the glcm. Energy is commonly defined as the evenness of the intensity field or the presence of regular periodic intensities[46]:

$$Energy = \sum_{i,j} p(i,j)^2 \qquad \text{Eq. 6.2}$$

Because both energy and contrast are negatively correlated with homogeneity and uncorrelated to each other, image heterogeneity and it's driving factors are best interpreted using the energy and contrast of the glcm[47]. Texture analysis parameters, as well as the mean and coefficient of variation (COV), were calculated from peak ratios and principal component scores of Raman maps.

More information likely exists in the Raman signatures of bone microstructure than that which explains fracture toughness; therefore, the canonical correlation of image heterogeneity and fracture toughness was then calculated. Canonical correlation finds the variance output explained by the input by maximizing the linear redundancy between the two data sets, weighting by singular value decomposition[48]. To prevent over-fitting and to weight each input

evenly, image heterogeneity data is Z-scored prior to analysis. Accuracy of the analysis as measured by percent redundancy and Bartlett's chi-squared approximation tests for correlation significance. Then weighting vectors were applied to the original data (before Z-scoring) to examine the true amount of variance explained. Separate analyses were run for energy and contrast. Since canonical correlation does not allow for data sparsity and 5 samples have no valid K_{grow} data, separate analyses were run for K_{grow}. Canonical correlation requires data matrices to be "full rank", therefore when fewer observations from the dependent target matrix (fracture toughness) exist relative to the number of input metrics (Raman peaks or PCs), Matlab built-in algorithms choose data metrics by orthogonal triangular decomposition of rank order to generate a full rank matrix (other metrics are subsequently given a zero weight).

6.4 Results

6.4.1 Average composition alone is insufficient to explain the age-related decrease in fracture toughness

Fracture toughness decreases with age in this mixed gender cohort; however, correlations show that age and biochemical parameters with association to age explain only a small percentage of the variance in the fracture toughness properties (Figure 6.2), resulting in correlations with limited, if any, meaning.. Examining the average of selected RS properties among multiple microstructures, Type-B carbonate substitution (Figure 6.2E) directly, albeit weakly, correlates with age ($R^2 = 0.3$), a relationship initially observed for small sample size by Akkus et al.[49]. Compositional v1 Phosphate/Proline (Figure 6.2D) and crystallinity (Figure 6.2F) do not vary with age. However, despite the seeming association with age, Type-B carbonate did

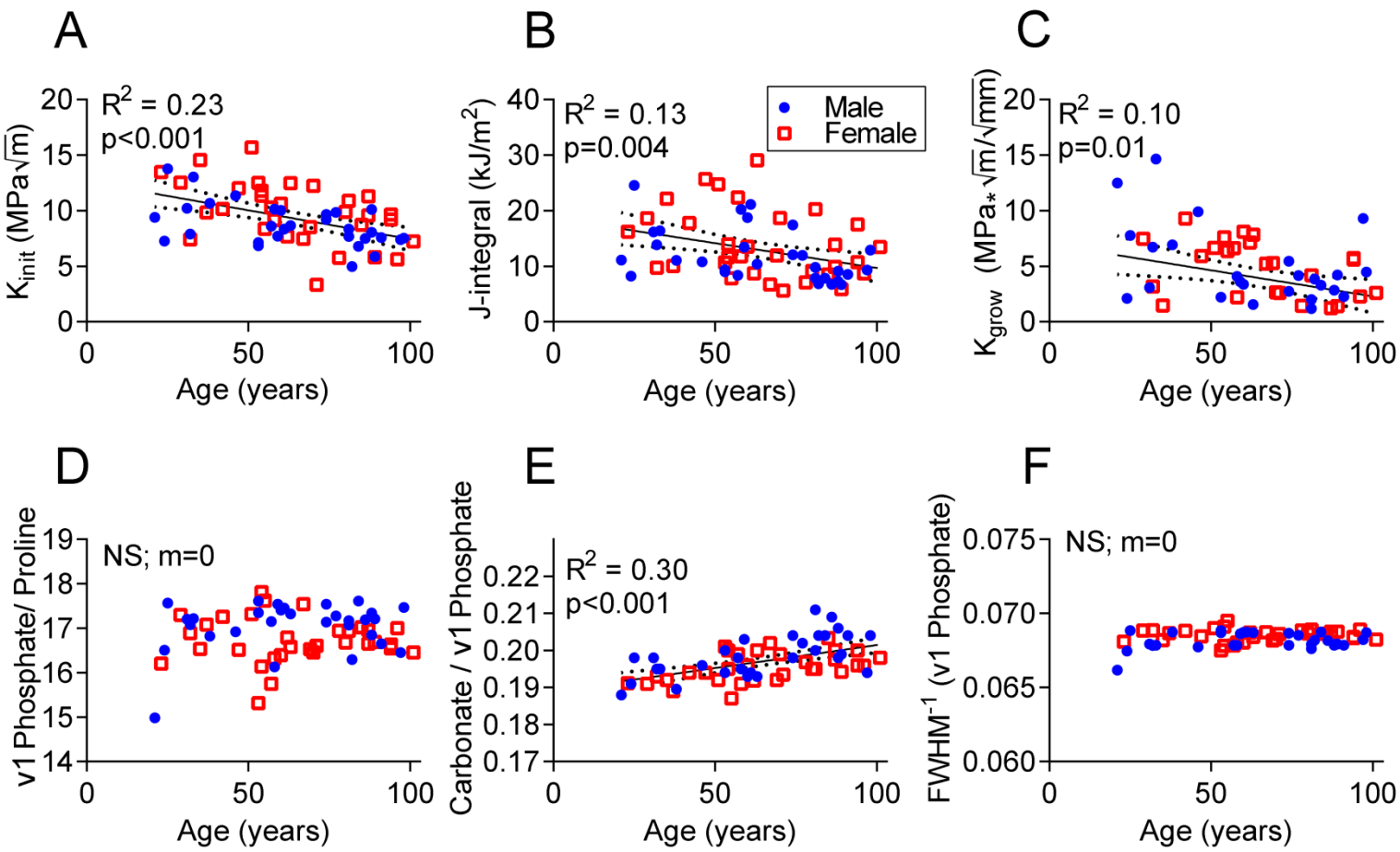

Figure 6.2

Fracture toughness properties decrease with age; however, correlation shows that only age loosely correlates with K_{init} **(A)**, J-integral **(B)**, and K_{grow} **(C)**. Carbonate substitution also correlates with age **(E)** but the compositional mineral to collagen ratio v1 Phosphate/ Proline **(D)** and crystallinity do not **(F)**.

not have a significant, meaningful correlation with fracture mechanics outcomes (Figure 6.3B, E, H), explaining only 7% of the variance in K_{grow}. In fact, none of the typical average peak ratios explain even 12% of the variance in any fracture toughness outcome (including compositional MCR ν1 Phosphate/Proline and ν2 Phosphate/Amide III, data not shown). As a preliminary measure of heterogeneity at this length scale, the coefficient of variation (COV) was calculated for each of the standard peak ratios, however, no significant correlations were found for any fracture toughness outcomes. The only statistically significant representation of MCR to explain fracture toughness was the mean of organization-sensitive ν1 Phosphate/Amide I (Figure 6.3 A, D) suggesting that the interplay between organization and composition merits investigation. However, average compositional changes are not driving the observed difference in fracture toughness.

6.4.2 Peak ratio intensity maps indicate microstructural heterogeneity as a driving force of fracture toughness

Examining RS maps, microstructural heterogeneity observed at the osteonal-interstitial border appears to associate with the age-related loss of fracture toughness. Compositional MCR ν1 Phosphate/Proline maps show sharp contrast between the less mineralized osteon and the more mineralized interstitial tissue, at least for the specimens with high fracture toughness (Figure 6.4A). Samples with lower K_{init} and J- integral display a distinct loss of visual heterogeneity such that the osteonal-interstitial border is not distinguishable as it is for specimens with higher K_{init} and J- integral. Mirror image trends in contrast across osteonal and interstitial tissue are seen for carbonate substitution maps (Figure 6.4B) in which the amount of crystalline lattice substitutions in hydroxyapatite appear to become more similar between the tissue types as

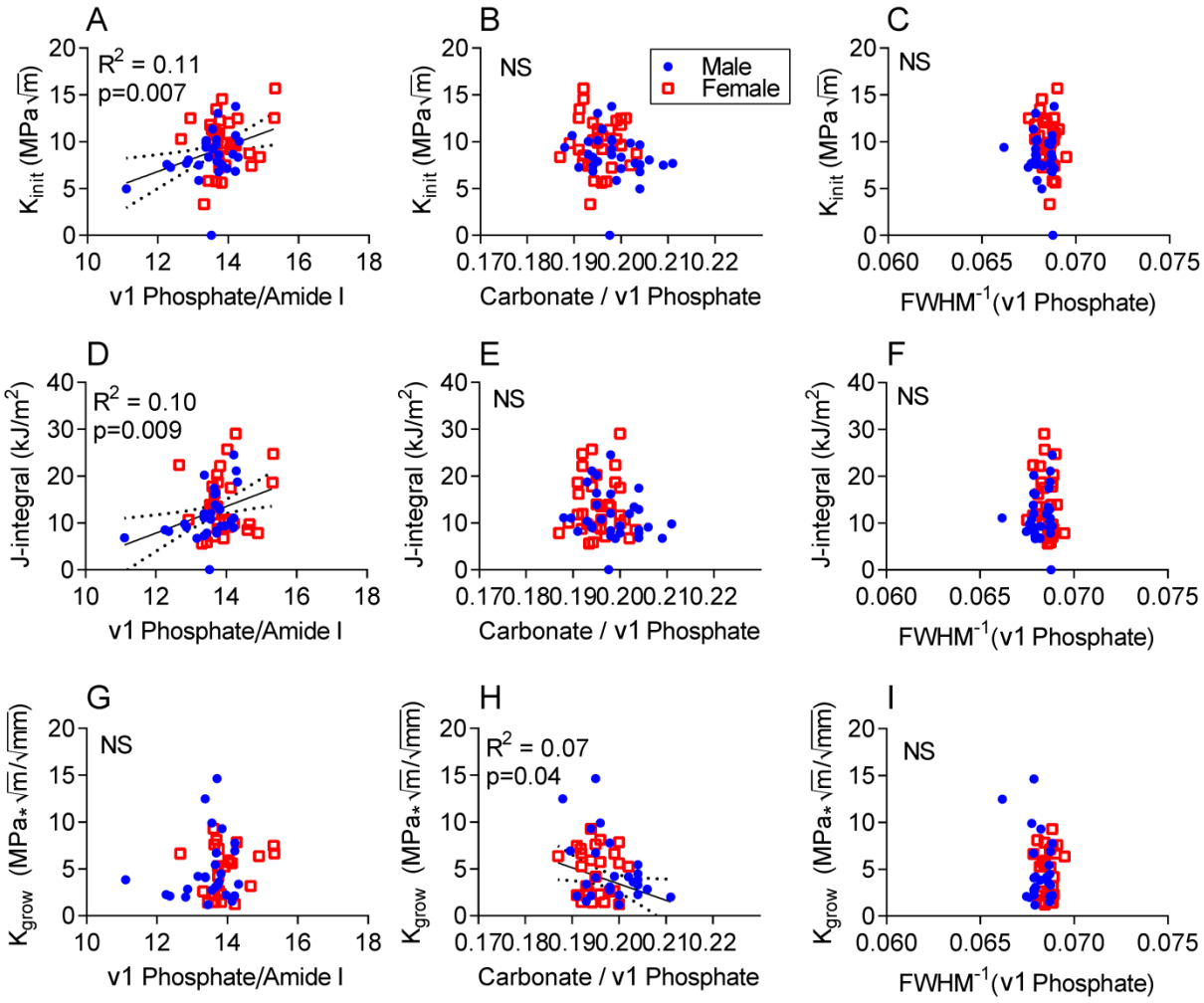

Figure 6.3

Prominent Raman peak ratios alone show no meaningful correlation with fracture toughness. Only the polarization sensitive ν1 Phosphate/ Amide I one show slight albeit statistically significant correlation to K_{init} **(A)** and J-integral **(D)**. Carbonate substitution shows slight albeit statistically significant correlation to K_{grow} **(H)**. Other mineral to collagen ratios (data not shown) ν1 Phosphate/ Proline and ν2 Phosphate/ Amide III do not show significant correlations to any fracture toughness outcomes.

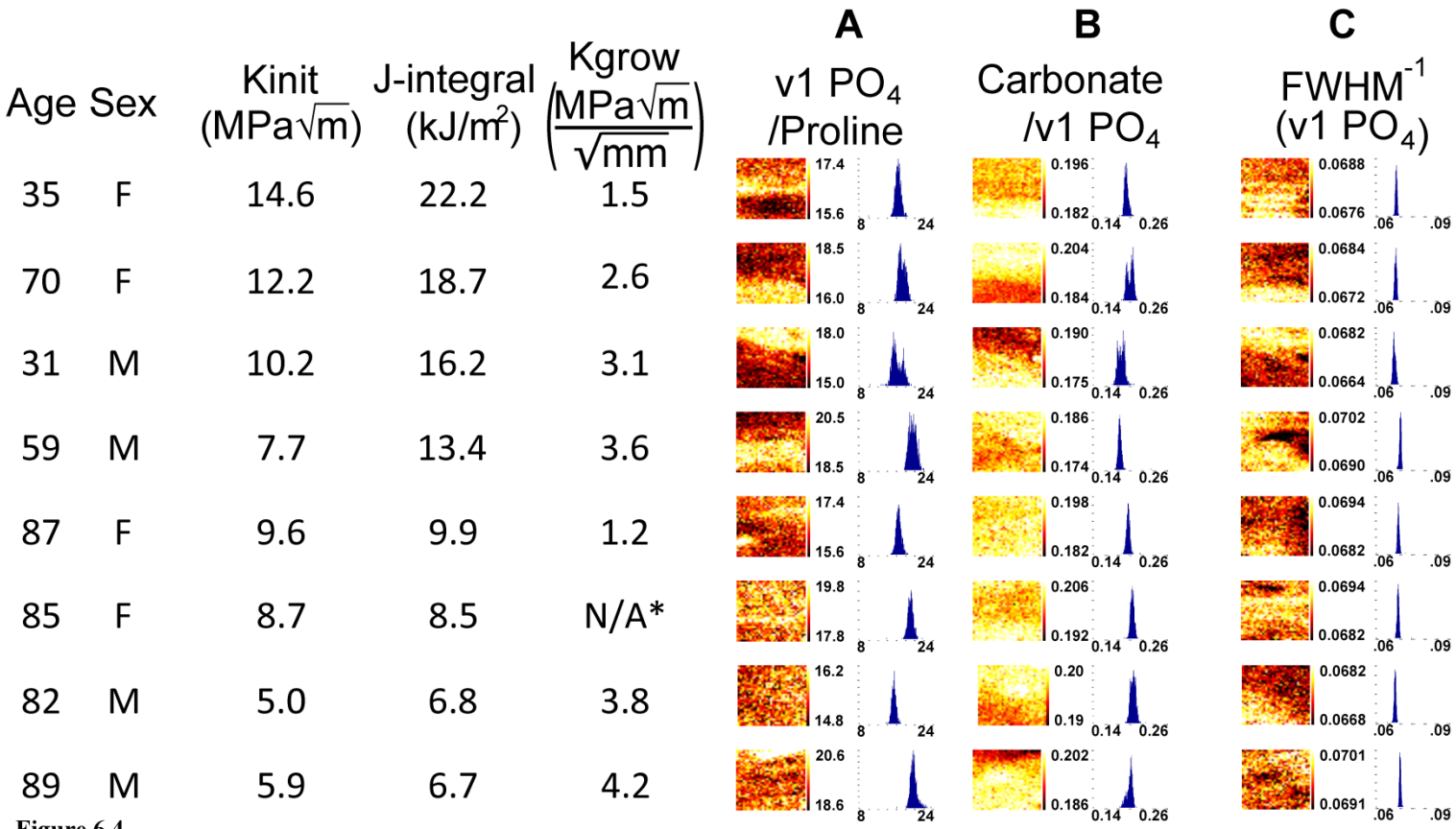

Figure 6.4

Raman maps of peak ratios demonstrate microstructural heterogeneity of composition is associated with superior fracture toughness. Representative samples from both genders at high and low fracture toughness were sorted by decreasing K_{init} and J-integral. Maps are scaled 5 – 95% within each sample to demonstrate within sample microstructural heterogeneity. Histograms are set to a uniform scale across all bones for comparing distributions between bones. Note that not all osteons are located above the interstitial space.**A)** v1 Phosphate/ Proline demonstrates clear osteonal-interstitial heterogeneity at high fracture toughness at the border becomes indistinguishable due to homogeneity at low fracture toughness. **B)** Carbonate substitution appears as the mirror image of **(A)** but with less of an osteonal-interstitial heterogeneity trend. **C)** Crystallinity shows evidence of mild lamellar contrast, but only at high fracture toughness values.

the fracture toughness of the bone specimen decreases. Crystallinity demonstrates that lamellar contrast in the osteonal region is also associated with the age-related loss in fracture toughness (Figure 6.4D). Noise in this measurement is due to system wavenumber resolution limitations, effectively discretizing measureable step size. Each of the major RS outcomes (MCR, carbonate, and crystallinity) used to characterize bone quality shows its own association with compositional heterogeneity at the microstructural level and the age-related loss of fracture toughness.

Analysis of the ν1 Phosphate/Amide I peak ratio expands upon the role of compositional heterogeneity to utilize RS polarization sensitivity and also captures the role of organizational heterogeneity. While ν1 Phosphate/Amide I is sensitive to collagen fiber orientation under polarized conditions[32], it is still a mineral to collagen ratio and therefore also sensitive to composition. For specimens with high fracture toughness, both composition and organizational heterogeneity are observed across osteonal-interstitial borders. In addition, osteonal lamellae are visible when the polarization axis of the laser is orthogonal to the bone long axis (Figure 6.5A), such that the trend fades to only osteonal-interstitial contrast for low fracture toughness specimens. In the histograms (Figure 6.5B), these changes in contrast manifests as a decrease in distribution width and kurtosis, and a general shift towards decreased mineralization with a decrease in fracture toughness. However, in the longitudinal orientation, contrast across the border at the cement line, not among lamellae, occurs in the specimens with superior fracture toughness. The osteonal-interstitial border consistently remains visible in specimens at low fracture toughness, but maps are bit noisier. These qualitative assessments indicate a role for organizational heterogeneity in explaining the age-related decrease in fracture toughness, but the bivariate histograms make the quantification of heterogeneity by standard methods (e.g.,

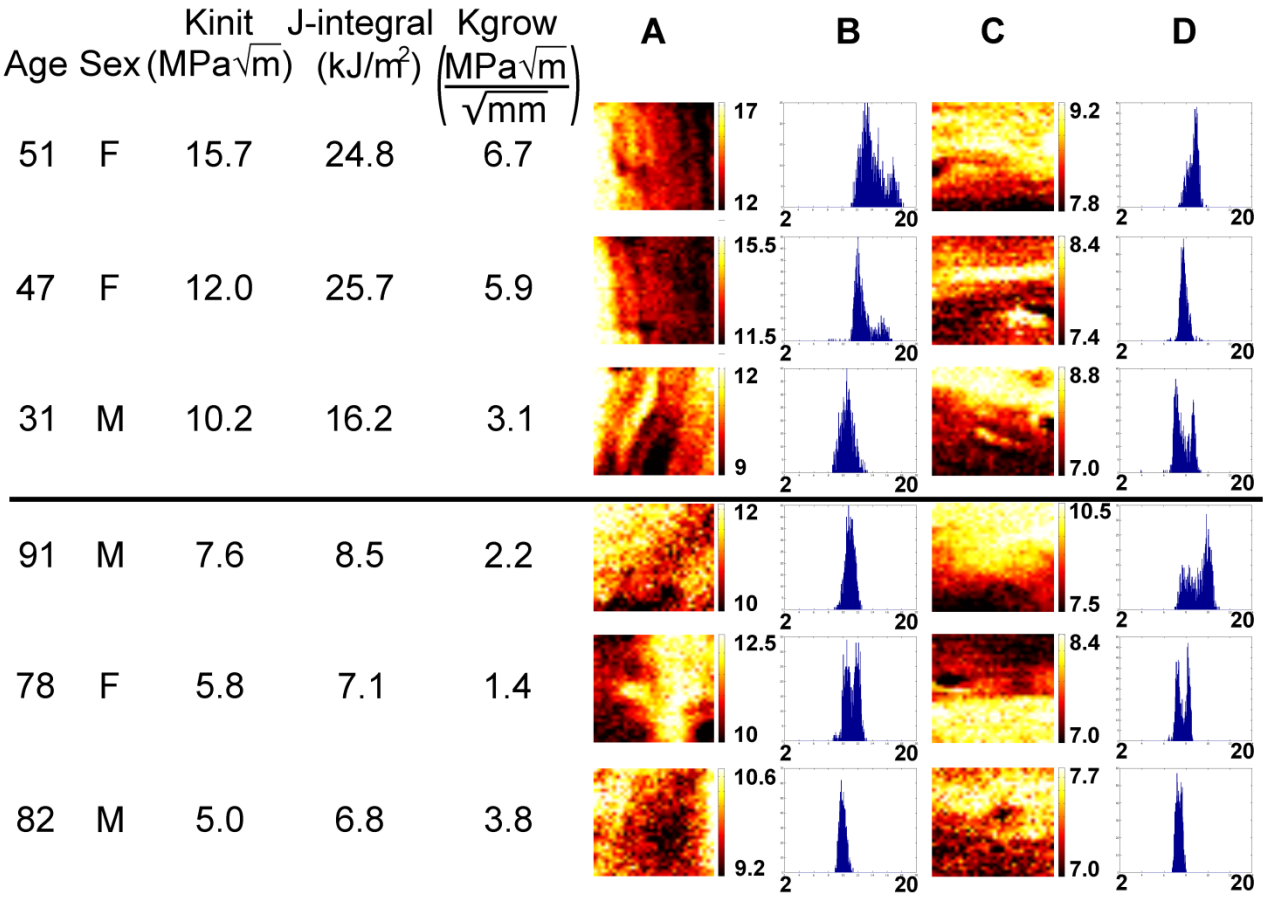

Figure 6.5

Polarization sensitive mineral to collagen ratio ν1 Phosphate/ Amide I shows lamellar contrast and osteonal-interstitial contrast for only specimens with high fracture toughness values. Maps are scaled 5 – 95% for each orientation. Histograms are set to uniform scale for comparing distributions between bones and orientations. **A)** Organizational lamellar contrast of high fracture toughness fades to osteonal-interstitial (compositional) contrast with lower fracture toughness. **B)** Histograms show a shift to less mineralization and a tighter leptokurtotic distribution. **C)** Higher fracture toughness values show contrast of the cement line that is not visible in low fracture toughness maps. **D)** Kurtosis and mean value shows no trends with histograms of longitudinal orientation.

standard deviation, full-width-at-half-max, or kurtosis) intractable. Also, the mixed mode contrast of organizational and compositional heterogeneity as well as differences between orthogonal bone orientations preclude definitive correlations with the fracture toughness properties.

6.4.3 Heterogeneity of organization and composition jointly improve explanation of the age-related decrease in fracture

To overcome these issues and better establish the relative contributions of organizational and compositional heterogeneity, image-based quantifications of heterogeneity (Energy and Contrast) were determined for Raman maps by using principal components and the following prominent peak ratios at each orientation: ν1 Phosphate/ Amide I, Carbonate/ ν1 Phosphate, FWHM-1 (ν1 Phosphate). Univariate correlations were determined for individual peak ratios and principal components, showing weak but statistically significant correlations to fracture toughness outcomes (Table 6.1; Spearman's rho r=0.3-0.45) for both heterogeneity and mean value. Heterogeneity values showed only slight improvement over the information offered by mean and coefficient of variation (COV) of peak ratio maps. Individual peak ratios only explained a maximum of 20% of the variance in J-integral, and only 9% of the variance in crack growth toughness (K_{grow}).

We previously showed in mouse models of brittle bone (Chapter 5) that using principal components of the Raman Spectrum identified underlying directions of variance that are associated with mechanical changes. Recall that principal components represent a series of uncorrelated underlying directions of variance in data, essentially composite traits of the spectrum that are unsupervised. While these were genetically altered models, and not aging as

Table 6.1 Peak ratio heterogeneity correlates with fracture toughness

Image Value	Peak Ratio	Orientation	Fracture Toughness Outcome	r*	p**
Contrast	v1 Phosphate/ Amide I	Longitudinal	J-Integral	0.414	0.017
Contrast	v1 Phosphate/ Amide I	Longitudinal	K_{grow}	0.336	0.080
Contrast	v1 Phosphate/ Proline	Longitudinal	K_{init}	-0.348	0.047
Energy	v1 Phosphate/ Amide I	Longitudinal	K_{init}	-0.309	0.080
Energy	v1 Phosphate/ Amide I	Longitudinal	J-Integral	-0.452	0.008
COV	v1 Phosphate/ Amide I	Longitudinal	J-Integral	0.3479	0.047
Mean	Carbonate/ v1 Phosphate	Longitudinal	J-Integral	-0.3519	0.045

*Spearman's correlation coefficient between canonical variates and fracture toughness

** p-value for signficance of correlation such that slope of correlation is zero.

seen here, it was notable that PCA often weighted areas outside traditional peaks and ratios that were associated with polarization based changes in tissue organization (Figure 5.4). Therefore, principal components of paired spectra in the map may help determine the biochemical signature of age-related changes in fracture toughness, and to what degree polarization RS improves upon average composition. Table 6.2 illustrates how mean, COV, and imaged-based quantifications of heterogeneity derived from PC maps correlate to fracture toughness outcomes. Again there are weak, but statistically significant correlations between different measurements of heterogeneity. In addition to heterogeneity, the average value of several single principal components explained as much as 23% of the variance in either K_{init} or K_{grow}. Notably, the contrast of principal component 11 explains 28% of crack growth toughness. Although an improvement over individual peak ratios, this is still not a compelling explanation of fracture toughness.

Given the complexity of human aging, it is unreasonable to consider only a single biochemical peak ratio or underlying spectral signature in attempting to capture the age-related changes in fracture toughness. However, the use of multiple peak ratios or orientations would multiply the influence of individual peaks, resulting in over fitting. Therefore, canonical correlation was used to compare sets of RS data to the set of fracture toughness outcomes, comparing the explanatory power of heterogeneity relative to average compositional value using either the set of peaks above, or principal components selected by scree analysis (PC1-39). The single value decomposition underlying canonical correlation decreases the risk of overfitting associated with iterative methods. Mimicking traditional RS analysis of bone (Figure 6.3), the average value of multiple peak intensities acquired at either orthogonal or longitudinal polarization (Table 6.3) explained up to 35% of the variance in fracture toughness, performing

Table 6.2 Principal component scores and score heterogeneity correlate with fracture toughness

Image Value	Principal Component	Fracture Toughness Outcome	r*	p**
Energy	11	K_{grow}	-0.4176	0.03
Energy	18	K_{grow}	0.3962	0.0408
Energy	37	K_{grow}	0.4585	0.0162
Energy	2	J-Integral	-0.3576	0.041
Energy	9	J-Integral	0.3917	0.0242
Energy	2	K_{init}	-0.3804	0.029
Contrast	11	K_{grow}	0.533	0.0042
Contrast	37	K_{grow}	-0.4035	0.0369
Contrast	2	J-Integral	0.3579	0.0408
Contrast	9	J-Integral	-0.4223	0.014
Contrast	2	K_{init}	0.3549	0.0427
Contrast	6	K_{init}	-0.4429	0.0098
COV	7	K_{grow}	0.4145	0.0316
COV	22	K_{grow}	-0.4029	0.0372
COV	7	J-Integral	0.3632	0.0378
COV	11	J-Integral	0.4187	0.0153
COV	23	J-Integral	0.3779	0.0301
COV	2	K_{init}	0.381	0.0287
COV	7	K_{init}	0.4173	0.0157
COV	22	K_{init}	-0.3625	0.0382
COV	34	K_{init}	0.4492	0.0087
Average	15	K_{grow}	0.3816	0.0495
Average	18	K_{grow}	-0.4835	0.0106
Average	23	K_{grow}	0.4567	0.0166
Average	8	J-Integral	-0.415	0.0163
Average	9	J-Integral	-0.3956	0.0227
Average	3	K_{init}	-0.3521	0.0445
Average	9	K_{init}	-0.3705	0.0338
Average	17	K_{init}	0.4076	0.0185
Average	20	K_{init}	0.4414	0.0101
Average	22	K_{init}	0.4544	0.0079
Average	26	K_{init}	-0.3585	0.0405
Average	31	K_{init}	-0.4934	0.0035

* Spearman's correlation coefficient between canonical variates and fracture toughness

** p-value for signficance of correlation such that slope of correlation is zero.

Table 6.3 Canonical variate expressions of full spectrum tissue heterogeneity provide the best explanation of fracture toughness.

		K_{init} ($MPa\sqrt{m}$)		J-integral (kJ/m^2)		K_{grow} $\left(\frac{MPa\sqrt{m}}{\sqrt{mm}}\right)$	
		r*	p**	r*	p**	r*	p**
Orthogonal Polarization Peaks‡	Average	0.59	3.00E-04	0.57	5.00E-04	0.55	2.00E-03
	Energy	0.54	1.00E-03	0.50	3.00E-03	0.50	6.00E-03
	Contrast	0.51	2.00E-03	0.44	1.00E-02	0.48	1.00E-02
Longitudinal Polarization Peaks‡	Average	0.57	5.00E-04	0.54	1.00E-03	0.50	6.00E-03
	Energy	0.59	3.00E-04	0.63	8.00E-05	0.69	4.00E-05
	Contrast	0.51	3.00E-03	0.45	9.00E-03	0.52	5.00E-03
PC1:39	Average	NS	NS	NS	NS	NS	NS
	Energy	NS	NS	NS	NS	0.74	6.00E-06
	Contrast	0.68	1.00E-05	0.73	1.00E-06	0.86	4.00E-09

*Pearson's correlation coefficient between canonical variates and fracture toughness.

** p-value for signficance of correlation such that slope of correlation is zero.

‡Peaks Include: Amide I, Amide III, Proline, CH , Hydroxyproline, v1 Phosphate, Carbonate, v2 Phosphate ,v4 Phosphate.

comparably between orientations. However, energy correlations with J-integral and K_{grow} for these peaks were higher for longitudinal than for the orthogonal polarization, while contrast correlations remain similar among the 3 fracture toughness properties. Canonical correlation requires independent variables. Since not all peaks are strongly affected by polarization, combining the two orthogonal sets of peaks as variables in one analysis would falsely inflate the degrees of freedom, resulting in over-fitting. Moreover, the selection of RS peaks with currently established biochemical assignments is inherently biased based. To avoid these risks of over-fitting while ensuring that canonical correlation accesses the entire spectrum, the average value, energy, and contrast of the fundamentally uncorrelated principal components were used. The canonical representation of average PC value did not correlate with fracture toughness, yet contrast of the underlying direction of variance greatly improves correlation to K_{init}, J-integral, and K_{grow} (see Figure 6.6) with few notable outliers. Interestingly, energy was only found to be significant in its correlation to K_{grow}, explaining over 50% of the variance. In canonical analyses of principal components, direct quantification of heterogeneity demonstrates a stronger correlation to the age-related decrease in fracture toughness than average compositional values (Table 6.3). Examining weights for each of the principal component correlations between image heterogeneity in fracture toughness, there appear to be significant differences in the weightings that optimally explain each aspect of fracture toughness. Heavy weights in principal components with low numbers indicate stability and reliability of these findings, since fracture toughness is driven by heterogeneity in the largest directions of RS variance. Interestingly, several principal components including PC3, 7, 9, and 12 were weighted oppositely between K_{init} and J-integral.

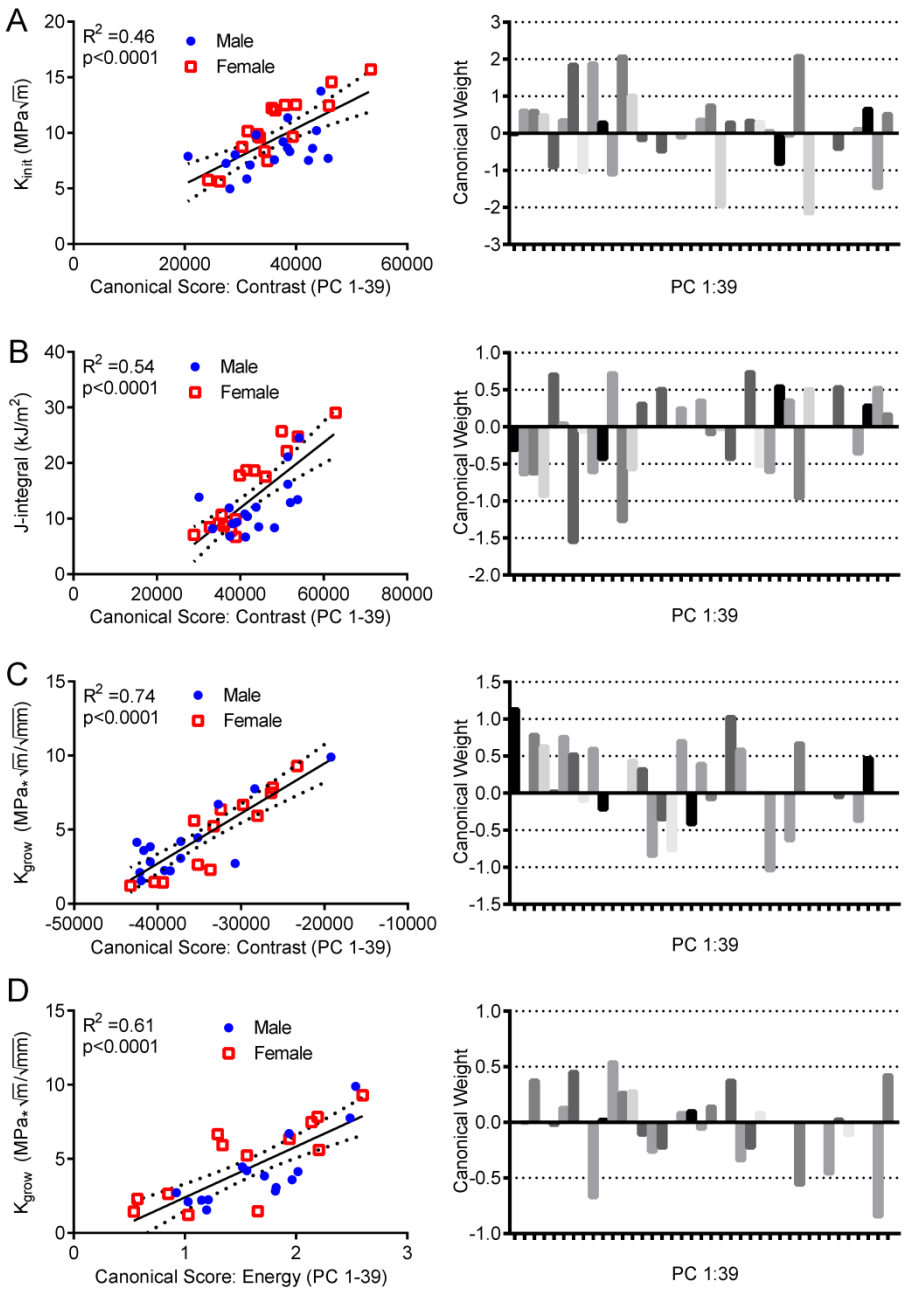

Figure 6.6

Canonical correlations of heterogeneity values from principal components significantly explain each aspect of fracture toughness. **A)** PC contrast explains 46% of the variance K_{init}, heavily weighting PC 7, 9, and 12. **B)** Separate canonical weights for PC contrast explain 54% of the variance in J-integral, such that many PCs are waited oppositely from K_{init}. **C)** Canonical weights for PC contrast explain 74% of the variance in K_{grow} with weightings differing from either K_{init} or J-integral. **D)** Canonical representation of PC energy also significantly explains 61% of K_{grow}, conserving several principal component weights from PC contrast explanation of K_{grow}.

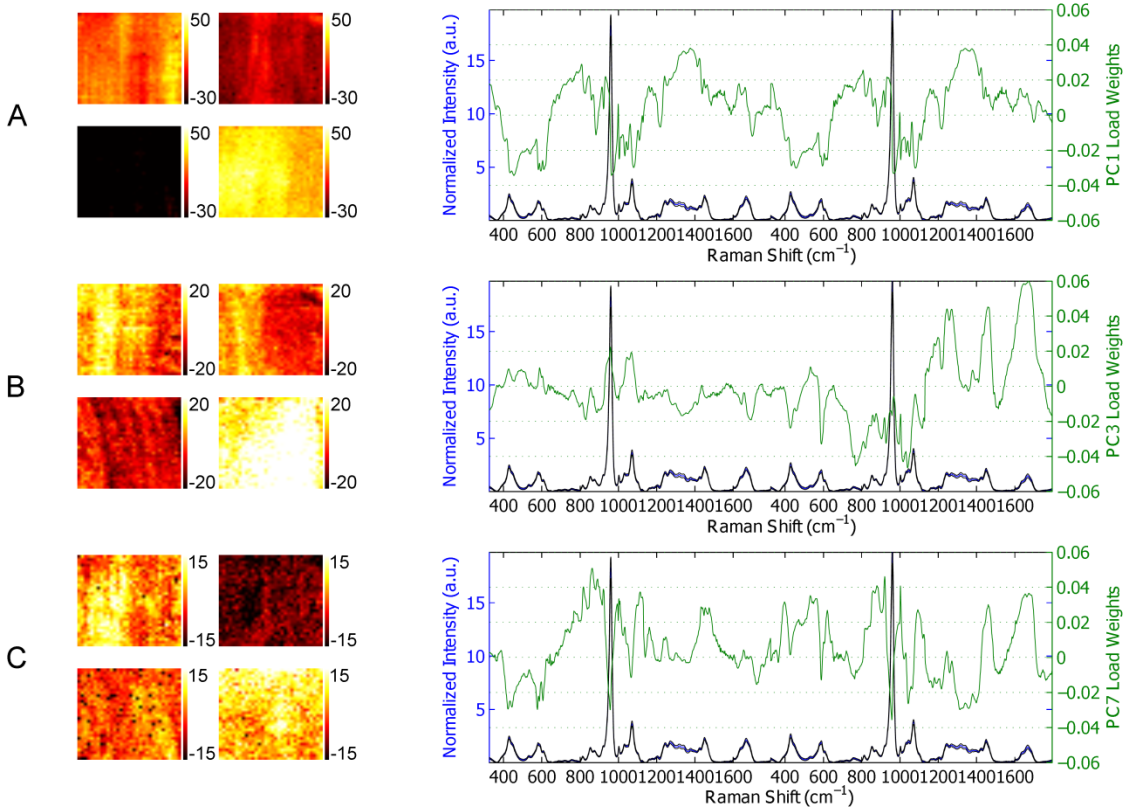

Figure 6.7

Principal component maps and loadings implicate both organizational and compositional heterogeneity in explaining age-related fracture toughness loss. Representative maps for specimens (two with high fracture toughness outcomes and two with low fracture toughness outcomes) are uniformly scaled. **A)** Maps for PC1 emphasize cement line contrast when representing high fracture toughness. Strong negative weights are placed on all Phosphate peaks, with positive weights on Amide III and CH_2 compositional contrast. **B)** PC3 maps indicate a presence of both lamellar contrast and an osteonal-interstitial border at high fracture toughness values. At low fracture toughness values, either the two contrast mechanisms can be lost. PC3 heavily loads polarization sensitive Amide I, v3 Phosphate, Amide III, and v1 Phosphate. **C)** PC7 maps show few features but a higher range of contrast at high fracture toughness values. Loadings indicate a complex compositional mineral to collagen ratio that appears to eliminate the influence of polarization and heavily weight carbonate.

Several the PCs weighted strongly in the explanation of K_{grow} exhibit only energy characteristics, but others were weighted in several canonical analyses (Figure 6.7).

In-depth analysis of principal component loadings indicates that both compositional and organizational heterogeneity contribute to fracture toughness. Compositional contrast of the cement line is associated with high fracture toughness values (Figure 6.7A; PC1), such that higher cement line collagen content (relative to neighboring tissue) is associated with higher resistance to crack propagation (K_{grow}); however, the same contrast has a negative impact on J-integral. Concurrent organizational lamellar contrast and compositional osteonal-interstitial border contrast (Figure 6.7B; PC3) is associated with superior critical stress intensity for both crack initiation(K_{init}) and propagation (K_{grow}); however, observation of lower fracture toughness specimens indicates that low PC3 scores can be driven by a loss of either organizational or compositional heterogeneity. Despite a lack of visual features, PC 7 maps that have a higher range of contrast in carbonate composition is positively associated with K_{init} and negatively associated with J-integral (Figure 6.7C).

6.5 Discussion

The work herein represents the first quantitative evidence that the microstructural heterogeneity of both composition and organization in bone (as observed in polarization-influenced Raman spectra) is a determinant of fracture toughness, alternative to the idea that bulk compositional properties alone explain age-related changes in bone fracture resistance. Indeed, the measurement of local compositional properties (with high sampling at the osteonal-interstitial border) provided correlations to fracture toughness for individual peak ratios and PCs, However,

quantification of the loss in microstructural heterogeneity as measured by canonical signatures accounts for a greater proportion of the age-related decrease in crack propagation toughness, such that preservation of microstructural heterogeneity observed in young bone could preserve fracture toughness and subsequently bone mechanical quality throughout aging. Prominent peak ratios (ν1 Phosphate / Proline, ν1 Phosphate/ Amide I , Carbonate / ν1 Phosphate and $FWHM^{-1}$(ν1 Phosphate)) showed qualitative association between microstructural heterogeneity of both organization and composition and fracture toughness, and subsequent quantification of image heterogeneity established the complexity of these observations of heterogeneity as well as a role for heterogeneity in the loss of fracture toughness, with multivariate signatures of heterogeneity outperforming average tissue composition as well as the coefficient of variation (COV). It is important to note that measurements of image texture, like energy and contrast, incorporate spatial heterogeneity, unlike the distribution heterogeneity of COV or full-width-at-half-maximum. Also, the supervised nature and bias of choosing peaks, combined with the potential for over fitting, makes the uncorrelated, unsupervised principal component results more reliable. Finally, principal components of polarization RS defined spectral signatures of both composition and organization that explain fracture toughness.

Landmark observations by von Meyer[1, 50] and Ascenzi[19, 22] about the complex organizational hierarchy of bone suggest, by the principle of Occam's razor, that heterogeneity plays a crucial role in bones mechanical integrity. Otherwise, it would not be preserved during remodeling. Surprisingly, evidence to evaluate this hypothesis has only recently been uncovered, and is largely limited to compositional heterogeneity as it relates to the incidence of pathological fracture[14] or the extended use of bisphosphonate treatment[17], which impairs natural remodeling.

However this does not imply that an increase in heterogeneity is always beneficial to the fracture toughness of bone. Fracture toughness, like bone mass, probably exists on a normally distributed continuum such that changes outside the optimal window of heterogeneity could be detrimental. Specifically, insufficient spatial heterogeneity could reduce crack-deflecting boundaries, and excess spatial heterogeneity could lead to strain concentration and thereby a more definitive crack path through weak interfaces. This is evidenced by the strong dichotomy of heterogeneity weighting between the canonical explanations of critical stress intensity for crack initiation K_{init} and that of strain energy release rate J-integral, much in the same way that Ritchie et al. demonstrated the inherent conflict between strength and toughness[51]. This may also be the case in the dichotomy relating heterogeneity and fragility fracture, such that there was insufficient heterogeneity in carbonate substitution but excess heterogeneity in crystallinity[14], or bone mineral density distribution[15] as observed by qBEI. Regardless, current evidence suggests that proper heterogeneity is crucial to fracture resistance.

While these data support the influence of heterogeneity on the age-related decrease in fracture toughness, many aspects of bone heterogeneity remain unexplored. This analysis was limited to microstructural heterogeneity of cortical bone, leaving questions about the implications of nanoscale and mesoscale heterogeneity. Heterogeneity of composition between neighboring features was probed, but no trends were observed. To emphasize study size, only one osteonal-interstitial border was mapped, undersampling the fracture toughness specimen as a whole. Strong trends suggest that the loss of microstructural heterogeneity would be observed across many osteons, but a more thorough analysis may help determine the relative contribution of entropy-based microdamage accumulation[52-54] versus cell-based imbalanced remodeling [18, 28,

[55] as a potential biological mechanisms for these findings, ultimately helping to direct and screen future therapeutics.

These findings are especially encouraging given the broad applicability of polarization Raman spectroscopy. With its nondestructive near infrared capabilities, Raman spectroscopy is shown promise clinically in its diagnosis of cancer[56] and osteomyelitis[57]. Heterogeneity measures could be conducted on a bone biopsy, or a custom polarization-preserving probe could be inserted through the skin. The current study was limited in correlation due to sample size and rank limitations of the canonical correlation analysis; however, a large patient bank could establish fracture risk predictors to complement DXA or FRAX[58]. Because of RS inherent sensitivity to local dipolar bonds, it would not be surprising if certain RS components correlate strongly to other potential fracture toughness surrogates, including bound water and pore water[36], or collagen cross-linking and advanced glycation end products[59]. Once RS signatures of bone mechanical quality are fully established, nondestructive measures could determine optimal allograft quality and guide surgical resection and fixation decisions.

The current work also extends to the greater study of the fracture mechanics of materials. Highly polarized RS is already used to study protein conformation and fiber orientation in organics like silks and electrospun polymers[60, 61], but this study shows that inherent levels of polarization can be used to study organization in turbid fibrous composites, allowing for concurrent analysis of organizational and compositional heterogeneity. These techniques could be used to design, validate, or even optimize manufacture of composite polymers and organic scaffolds to match desired mechanical specifications. In the study of fracture toughness of composite polymers, polarization RS could be used to identify structural and compositional

boundaries, or even for quality assurance and fabrication processes for structural materials. In patient tailored medicine, an accurate RS assessment of mechanical integrity could allow implant heterogeneity to be tuned to match mechanical properties of existing tissue, preventing wear and stress shielding[62]. Polarization Raman spectroscopy may provide a powerful tool for assessing fracture toughness, overcoming the practical limitations associated with quantitative analysis of impure biological materials.

6.6 Conclusions

Microstructural heterogeneity partially explained the age-related decrease in fracture toughness. Analysis by Raman spectroscopy implicates both organizational heterogeneity and compositional heterogeneity as significant contributing factors to fracture toughness. In a constrained multivariate expression of RS, image heterogeneity outperforms average composition, finding that the interplay between organization and composition is crucial for a reliable, robust explanation of fracture toughness. Finally, the observation of opposing forces driving the critical stress intensity of crack initiation and the strain energy release rate suggest a balancing phenomenon in optimal fracture toughness, a common theme in the biomechanical mechanisms of bone. These findings not only provide deeper insight into the pathological progression age-related bone disease, but the use of polarization Raman spectroscopy to concurrently examine composition and organization may prove to be a crucial tool for assessing and validating optimal bone therapeutics, and applying our knowledge of nature for improved synthetic material manufacture.

6.7 References

1. Wolff, J., Das Gesetz der Transformation der Knochen, von Dr Julius Wolff, A. Hirschwald, Berlin (1892).
2. Boyde, A., Bianco, P., Portigliatti Barbos, M. and Ascenzi, A., "Collagen orientation in compact bone: I. A new method for the determination of the proportion of collagen parallel to the plane of compact bone sections," Metab Bone Dis Relat Res **5**(6), 299-307 (1984)
3. Portigliatti Barbos, M., Bianco, P., Ascenzi, A. and Boyde, A., "Collagen orientation in compact bone: II. Distribution of lamellae in the whole of the human femoral shaft with reference to its mechanical properties," Metab Bone Dis Relat Res **5**(6), 309-315 (1984)
4. Johnell, O., Kanis, J.A., Oden, A., Johansson, H., De Laet, C., Delmas, P., Eisman, J.A., Fujiwara, S., Kroger, H., Mellstrom, D., Meunier, P.J., Melton, L.J., 3rd, O'Neill, T., Pols, H., Reeve, J., Silman, A. and Tenenhouse, A., "Predictive value of BMD for hip and other fractures," J Bone Miner Res **20**(7), 1185-1194 (2005)
5. Kanis, J.A., Johnell, O., Oden, A., Dawson, A., De Laet, C. and Jonsson, B., "Ten year probabilities of osteoporotic fractures according to BMD and diagnostic thresholds," Osteoporos Int **12**(12), 989-995 (2001)
6. Vashishth, D., Tanner, K.E. and Bonfield, W., "Contribution, development and morphology of microcracking in cortical bone during crack propagation," Journal of Biomechanics **33**(9), 1169-1174 (2000)
7. Vashishth, D., Tanner, K.E. and Bonfield, W., "Experimental validation of a microcracking-based toughening mechanism for cortical bone," Journal of Biomechanics **36**(1), 121-124 (2003)
8. Nalla, R.K., Kinney, J.H. and Ritchie, R.O., "Mechanistic fracture criteria for the failure of human cortical bone," Nature materials **2**(3), 164-168 (2003)
9. Zimmermann, E.A., Schaible, E., Bale, H., Barth, H.D., Tang, S.Y., Reichert, P., Busse, B., Alliston, T., Ager, J.W., 3rd and Ritchie, R.O., "Age-related changes in the plasticity and toughness of human cortical bone at multiple length scales," Proceedings of the National Academy of Sciences of the United States of America **108**(35), 14416-14421 (2011)
10. Ritchie, R.O., "How does human bone resist fracture?," Ann N Y Acad Sci **1192**(72-80 (2010)
11. Nalla, R.K., Kruzic, J.J., Kinney, J.H. and Ritchie, R.O., "Mechanistic aspects of fracture and R-curve behavior in human cortical bone," Biomaterials **26**(2), 217-231 (2005)
12. Gao, Y., Ritchie, R., Kumar, M. and Nalla, R., "High-cycle fatigue of nickel-based superalloy ME3 at ambient and elevated temperatures: Role of grain-boundary engineering," Metallurgical and Materials Transactions A **36**(12), 3325-3333 (2005)

13. Donnelly, E., Lane, J.M. and Boskey, A.L., "Research perspectives: The 2013 AAOS/ORS research symposium on Bone Quality and Fracture Prevention," Journal of Orthopaedic Research **32**(7), 855-864 (2014)

14. Gourion‐Arsiquaud, S., Lukashova, L., Power, J., Loveridge, N., Reeve, J. and Boskey, A.L., "Fourier transform infrared imaging of femoral neck bone: Reduced heterogeneity of mineral‐to‐matrix and carbonate‐to‐phosphate and more variable crystallinity in treatment‐naive fracture cases compared with fracture‐free controls," Journal of Bone and Mineral Research **28**(1), 150-161 (2013)

15. Roschger, P., Lombardi, A., Misof, B.M., Maier, G., Fratzl-Zelman, N., Fratzl, P. and Klaushofer, K., "Mineralization density distribution of postmenopausal osteoporotic bone is restored to normal after long-term alendronate treatment: qBEI and sSAXS data from the fracture intervention trial long-term extension (FLEX)," Journal of Bone and Mineral Research **25**(1), 48-55 (2010)

16. Gourion-Arsiquaud, S., Allen, M.R., Burr, D.B., Vashishth, D., Tang, S.Y. and Boskey, A.L., "Bisphosphonate treatment modifies canine bone mineral and matrix properties and their heterogeneity," Bone **46**(3), 666-672 (2010)

17. Donnelly, E., Meredith, D.S., Nguyen, J.T., Gladnick, B.P., Rebolledo, B.J., Shaffer, A.D., Lorich, D.G., Lane, J.M. and Boskey, A.L., "Reduced cortical bone compositional heterogeneity with bisphosphonate treatment in postmenopausal women with intertrochanteric and subtrochanteric fractures," J Bone Miner Res **27**(3), 672-678 (2012)

18. Ettinger, B., Burr, D.B. and Ritchie, R.O., "Proposed pathogenesis for atypical femoral fractures: Lessons from materials research," Bone **55**(2), 495-500 (2013)

19. Boyde, A., Bianco, P., Portigliatti Barbos, M. and Ascenzi, A., "Collagen orientation in compact bone: I. A new method for the determination of the proportion of collagen parallel to the plane of compact bone sections," Metabolic Bone Disease and Related Research **5**(6), 299-307 (1984)

20. Carando, S., Barbos, M.P., Ascenzi, A. and Boyde, A., "Orientation of collagen in human tibial and fibular shaft and possible correlation with mechanical properties," Bone **10**(2), 139-142 (1989)

21. Carando, S., Portigliatti-Barbos, M., Ascenzi, A., Riggs, C.M. and Boyde, A., "Macroscopic shape of, and lamellar distribution within, the upper limb shafts, allowing inferences about mechanical properties," Bone **12**(4), 265-269 (1991)

22. Portigliatti Barbos, M., Bianco, P., Ascenzi, A. and Boyde, A., "Collagen orientation in compact bone: II. Distribution of lamellae in the whole of the human femoral shaft with reference to its mechanical properties," Metabolic Bone Disease and Related Research **5**(6), 309-315 (1984)

23. Morris, M.D. and Mandair, G.S., "Raman assessment of bone quality," Clinical orthopaedics and related research **469**(8), 2160-2169 (2011)

24. Gamsjaeger, S., Masic, A., Roschger, P., Kazanci, M., Dunlop, J.W., Klaushofer, K., Paschalis, E.P. and Fratzl, P., "Cortical bone composition and orientation as a function of animal and tissue age in mice by Raman spectroscopy," Bone **47**(2), 392-399 (2010)

25. Makowski, A.J., Patil, C.A., Mahadevan-Jansen, A. and Nyman, J.S., "Polarization control of Raman spectroscopy optimizes the assessment of bone tissue," Journal of biomedical optics **18**(5), 55005 (2013)

26. Ager, J.W., 3rd, Nalla, R.K., Balooch, G., Kim, G., Pugach, M., Habelitz, S., Marshall, G.W., Kinney, J.H. and Ritchie, R.O., "On the increasing fragility of human teeth with age: a deep-UV resonance Raman study," J Bone Miner Res **21**(12), 1879-1887 (2006)

27. Donnelly, E., Boskey, A.L., Baker, S.P. and van der Meulen, M.C., "Effects of tissue age on bone tissue material composition and nanomechanical properties in the rat cortex," Journal of biomedical materials research **92**(3), 1048-1056 (2010)

28. Gourion-Arsiquaud, S., Burket, J.C., Havill, L.M., DiCarlo, E., Doty, S.B., Mendelsohn, R., van der Meulen, M.C. and Boskey, A.L., "Spatial variation in osteonal bone properties relative to tissue and animal age," J Bone Miner Res **24**(7), 1271-1281 (2009)

29. Dooley, K.A., McCormack, J., Fyhrie, D.P. and Morris, M.D., "Stress mapping of undamaged, strained, and failed regions of bone using Raman spectroscopy," Journal of biomedical optics **14**(4), 044018 (2009)

30. Timlin, J.A., Carden, A., Morris, M.D., Rajachar, R.M. and Kohn, D.H., "Raman spectroscopic imaging markers for fatigue-related microdamage in bovine bone," Anal Chem **72**(10), 2229-2236 (2000)

31. McCreadie, B.R., Morris, M.D., Chen, T.C., Sudhaker Rao, D., Finney, W.F., Widjaja, E. and Goldstein, S.A., "Bone tissue compositional differences in women with and without osteoporotic fracture," Bone **39**(6), 1190-1195 (2006)

32. Kazanci, M., Roschger, P., Paschalis, E.P., Klaushofer, K. and Fratzl, P., "Bone osteonal tissues by Raman spectral mapping: orientation-composition," Journal of structural biology **156**(3), 489-496 (2006)

33. Kazanci, M., Wagner, H.D., Manjubala, N.I., Gupta, H.S., Paschalis, E., Roschger, P. and Fratzl, P., "Raman imaging of two orthogonal planes within cortical bone," Bone **41**(3), 456-461 (2007)

34. Maher, J.R., Takahata, M., Awad, H.A. and Berger, A.J., "Raman spectroscopy detects deterioration in biomechanical properties of bone in a glucocorticoid-treated mouse model of rheumatoid arthritis," Journal of biomedical optics **16**(8), 087012 (2011)

35. Raghavan, M., Sahar, N.D., Wilson, R.H., Mycek, M.A., Pleshko, N., Kohn, D.H. and Morris, M.D., "Quantitative polarized Raman spectroscopy in highly turbid bone tissue," Journal of biomedical optics **15**(3), 037001 (2010)

36. Granke, M., Makowski, A.J., Uppuganti, S., Does, M.D. and Nyman, J.S., "Identifying novel clinical surrogates to assess human bone fracture toughness," Journal of Bone and Mineral Research **(Under Review)**((2014)

37. Makowski, A.J., Pence, I.J., Uppuganti, S., Zein-Sabatto, A., Huzagh, M.C., Mahadevan-Jansen, A. and Nyman, J.S., "Polarization in Raman Spectroscopy helps explain bone brittleness in genetic mouse models," Journal of biomedical optics **(Under Review)**((2014)

38. "ASTM E 1820-05a. Standard Test Method for Measurement of Fracture Toughness," American Society for Testing and Materials International (2005).

39. McElderry, J.D., Kole, M.R. and Morris, M.D., "Repeated freeze-thawing of bone tissue affects Raman bone quality measurements," Journal of biomedical optics **16**(7), 071407 (2011)

40. Launey, M.E., Chen, P.Y., McKittrick, J. and Ritchie, R.O., "Mechanistic aspects of the fracture toughness of elk antler bone," Acta Biomater **6**(4), 1505-1514 (2010)

41. Li, S., Abdel-Wahab, A. and Silberschmidt, V.V., "Analysis of fracture processes in cortical bone tissue," Engineering Fracture Mechanics **110**(448-458 (2013)

42. Koester, K.J., Barth, H.D. and Ritchie, R.O., "Effect of aging on the transverse toughness of human cortical bone: evaluation by R-curves," J Mech Behav Biomed Mater **4**(7), 1504-1513 (2011)

43. Lieber, C.A. and Mahadevan-Jansen, A., "Automated method for subtraction of fluorescence from biological Raman spectra," Applied spectroscopy **57**(11), 1363-1367 (2003)

44. Nyman, J.S., Makowski, A.J., Patil, C.A., Masui, T.P., O'Quinn, E.C., Bi, X., Guelcher, S.A., Nicollela, D.P. and Mahadevan-Jansen, A., "Measuring differences in compositional properties of bone tissue by confocal Raman spectroscopy," Calcif Tissue Int **89**(2), 111-122 (2011)

45. Jackson, D.A., "Stopping rules in principal components analysis: a comparison of heuristical and statistical approaches," Ecology 2204-2214 (1993)

46. Haralick, R.M. and Shapiro, L.G., Computer and robot vision, Addison-Wesley Pub. Co. (1992).

47. Baraldi, A. and Parmiggiani, F., "An investigation of the textural characteristics associated with gray level cooccurrence matrix statistical parameters," Geoscience and Remote Sensing, IEEE Transactions on **33**(2), 293-304 (1995)

48. Hotelling, H., "Relations between two sets of variates," Biometrika 321-377 (1936)

49. Akkus, O., Polyakova-Akkus, A., Adar, F. and Schaffler, M.B., "Aging of microstructural compartments in human compact bone," J Bone Miner Res **18**(6), 1012-1019 (2003)

50. Skedros, J.G. and Brand, R.A., "Biographical sketch: Georg Hermann von Meyer (1815-1892)," Clinical orthopaedics and related research **469**(11), 3072-3076 (2011)

51. Ritchie, R.O., "The conflicts between strength and toughness," Nature materials **10**(11), 817-822 (2011)

52. Brennan, O., Kennedy, O.D., Lee, T.C., Rackard, S.M. and O'Brien, F.J., "Effects of estrogen deficiency and bisphosphonate therapy on osteocyte viability and microdamage accumulation in an ovine model of osteoporosis," Journal of Orthopaedic Research **29**(3), 419-424 (2011)

53. Bigley, R., Singh, M., Hernandez, C., Kazakia, G., Martin, R. and Keaveny, T., "Validity of serial milling-based imaging system for microdamage quantification," Bone **42**(1), 212-215 (2008)

54. Schaffler, M.B., Choi, K. and Milgrom, C., "Aging and matrix microdamage accumulation in human compact bone," Bone **17**(6), 521-525 (1995)

55. Verborgt, O., Gibson, G.J. and Schaffler, M.B., "Loss of osteocyte integrity in association with microdamage and bone remodeling after fatigue in vivo," Journal of bone and mineral research : the official journal of the American Society for Bone and Mineral Research **15**(1), 60-67. (2000)

56. Patil, C.A., Kirshnamoorthi, H., Ellis, D.L., van Leeuwen, T.G. and Mahadevan-Jansen, A., "A clinical instrument for combined raman spectroscopy-optical coherence tomography of skin cancers," Lasers in surgery and medicine **43**(2), 143-151 (2011)

57. Esmonde-White, K.A., Esmonde-White, F.W., Holmes, C.M., Morris, M.D. and Roessler, B.J., "Alterations to bone mineral composition as an early indication of osteomyelitis in the diabetic foot," Diabetes care **36**(11), 3652-3654 (2013)

58. Kanis, J.A., McCloskey, E., Johansson, H., Oden, A. and Leslie, W.D., "FRAX((R)) with and without bone mineral density," Calcif Tissue Int **90**(1), 1-13 (2012)

59. Tang, S.Y. and Vashishth, D., "The relative contributions of non-enzymatic glycation and cortical porosity on the fracture toughness of aging bone," Journal of biomechanics **44**(2), 330-336 (2011)

60. Rousseau, M.E., Lefevre, T., Beaulieu, L., Asakura, T. and Pezolet, M., "Study of protein conformation and orientation in silkworm and spider silk fibers using Raman microspectroscopy," Biomacromolecules **5**(6), 2247-2257 (2004)

61. Richard-Lacroix, M. and Pellerin, C., "Novel method for quantifying molecular orientation by polarized Raman spectroscopy: a comparative simulations study," Applied spectroscopy **67**(4), 409-419 (2013)

62. Kim, H.W., Knowles, J.C. and Kim, H.E., "Hydroxyapatite porous scaffold engineered with biological polymer hybrid coating for antibiotic Vancomycin release," Journal of materials science. Materials in medicine **16**(3), 189-195 (2005)

CHAPTER 7

SUMMARY AND CONCLUDING REMARKS

7.1 Summary of Dissertation Findings

This work has assessed the ability of Raman spectroscopy (RS) to evaluate and explain the mechanical quality of bone by establishing a relationship between biochemical profiles detected by RS and mechanical differences caused by genetic manipulation and aging. Moreover, in this work, I established that the manipulation of polarization in Raman spectroscopy assesses the organization of bone concurrently with its composition. Chapter 3 established that the organization of bone impacts Raman spectroscopy at low, instrument-inherent, polarization states. I established that polarization sensitivity followed optical theory and could be optimized to either eliminate or magnify its influence depending on the desired analysis. These findings were found to be consistent across spatial locations and donors of varying age, thereby offering potential reconciliation for notable inconsistencies in other studies of compromise bone quality. Building upon these findings, the work presented in Chapter 4 (the study of ATF4 bone quality) showed that RS polarization changes were associated with the loss of bone toughness and fracture toughness even when biochemical compositional property measurements by RS were insensitive to the mechanical changes. However, aging the animal model changed the mechanical phenotype and subsequently, compositional Raman spectroscopy peak ratios were then able to

detect the resulting changes in strength. In Chapter 5, correlation between polarization in Raman spectroscopy and bone toughness was confirmed by analyzing brittle knockout models (either ATF4-/- or MMP9-/-). Using multivariate principal components analysis, I showed that the 1st and largest principal component (i.e., underlying direction of variance in the data), significantly explains bone toughness in both models. Moreover, the load profile of RS peaks was similar for both models despite the fundamental difference in genetic mutation. Finally, insensitivity of principal components to strength in the maturation model indicated specificity of polarization Raman spectroscopy as a significant correlation to bone toughness. Combining multivariate analysis with the polarization sensitivity of Raman spectroscopy to the orientation in bone (using techniques developed in Chapters 3-5), the work in Chapter 6 correlated age-related decrease in fracture toughness of human cortical bone to organizational and compositional heterogeneity at the microstructural length scale. Mapping the osteonal-interstitial boundary for two orientations (parallel and orthogonal to the bone long axis) and registering the maps allowed for an organization-sensitive quantification of microstructural heterogeneity. The canonical correlation of image texture analysis quantifications of contrast and energy (both shown to be driving forces in heterogeneity) indicated that a decrease in both compositional and organizational microstructural heterogeneity explained a significant proportion of the age-related decrease in fracture toughness.

The application of polarization Raman spectroscopy has been found by this thesis to explain the biochemical basis of elusive mechanical properties of toughness and fracture toughness not otherwise explained by conventional Raman measurements of composition could not. Note that unlike strength, neither of these mechanical properties is explained by currently

established clinical techniques that assess patient fracture risk. The primary implication of my dissertation findings is that polarization content of Raman spectroscopy facilitates concurrent analysis of composition and organization of bone mineral and collagen, which was not possible in other nondestructive analyses.

7.2 Major Conclusions

- Refuting common practice, the influence of polarization on Raman spectroscopy for organized samples like bone is present in commercial confocal microscope systems, even at lower magnifications (and numerical apertures) due to the inherent polarization bias generated by laser sources, dichroic mirrors, and holographic gratings.
- The polarization of Raman peaks follows Malus's law in the absence of explicit depolarization, despite the confounding factors of tissue turbidity and multiple scattering. Therefore the amplitude and phase of peak polarization can be modeled. Peaks in bone were ranked for polarization sensitivity by amplitude, such that the assessment of composition and organization can be optimized by comparing peak phase when defining peak ratios.
- Peak phase and ratio sensitivity to polarization (and subsequently organization) are both consistent among microstructures and across bones from multiple donors of varying age, in accordance with bone birefringence and current theories of mineral and collagen organization in bone.
- In the analysis of animal bone from genetically modified rodent models, RS measures of changes in bone composition are usually indicative of changes in mechanical strength, and

are not found in prominent models of bone brittleness. Instead, polarization-sensitive RS measurements of bone organization are associated with these brittle phenotypes.

- When performing polarization Raman spectroscopy measurements for multiple orientations of a turbid birefringent material, it is best practice to include all the variables as individual features, rather than attempt to mathematically combine paired observation at each wavenumber. The former allows for data reduction by principal components analysis, while the latter produces spurious results due to the inappropriate rescaling of data variance.
- The first (and largest) principal component of polarization RS variance significantly correlates to toughness in multiple animal models of bone brittleness, suggesting that the interplay between orientation and composition that results in bone brittleness has consistent elements and comprises the majority of biochemical differences in these altered tissues.
- In the analysis of human cortical bone, only a small portion of the age-related decrease in fracture toughness can be explained by bulk compositional properties. Quantification of image heterogeneity over osteonal-interstitial bone tissue generated from the principal components of Raman maps significantly explains the age-related loss of fracture toughness, including stress intensity factors for crack initiation and growth, as well as the strain energy release rate J-integral.
- The weight of principal components generated from the Raman maps of osteonal-interstitial bone tissue suggest a significant contribution of both composition and organization in the explanation of fracture toughness. There is distinct interplay between organization and composition in the RS signatures of microstructural heterogeneity.

- The relationship between heterogeneity of the principal components and fracture toughness suggest an inherent struggle between critical stress intensity and the release rate of non-linear strain energy, much like the known conflicts between strength and toughness for many situations in bone.

7.3 Implications of This Work and Future Directions

The most prominent potential applications of this work include: application of polarized Raman spectroscopy for the diagnosis and analysis of tissue organization; Raman spectroscopy in general for the measurement of bone quality; the specialized use of multivariate statistics on Raman spectroscopy data for correlation to continuous outcome variables; addressing anatomical differences and concerns in the relationship between bone structure and function; implications for the Raman assessment of the mechanics of materials; the relationship between compositional and structural heterogeneity and fracture mechanics; the clinical and surgical potential and likely limitations of polarization Raman spectroscopy for bone quality; and the greater meaning and potential hypotheses generated by the application of these findings current theories of bone biology and aging.

7.3.1 Raman spectroscopy for the optical diagnosis of mineralized tissue

As a growing optical detection technique, Raman spectroscopy is often touted for superior chemical sensitivity and specificity, as well as the potential for nondestructive measurement with minimal tissue heating. Herein lies the true strength and weakness of Raman spectroscopy as a modality for optical diagnosis: its context-specific versatility. Depending upon a given hypothesis or target tissue, one can modify laser wavelength, delivery system, the sample

volume probed, and —with advances in polarization— even the relative sensitivity to orientation and composition. While this is a fortuitous circumstance for the evaluation of well-posed hypotheses, these variables also imply that inherent differences exist among the myriad of specialized Raman instruments, data acquisition techniques, and protocols may significantly drive scientific findings. Because Raman spectroscopy is inherently sensitive to all dipole moments and changes in tissue optical properties, there is little that can be done to a biological sample without changing its Raman spectrum. This is evidenced by the study performed by McElderry et al (Morris lab) showing that nearly all prominent peaks in the Raman spectrum of bone are altered by as few as 3 to 4 freeze thaw cycles of less than 8 hours each[1]. However, mechanical properties of bone samples show no notable changes with this number of freeze thaw cycles. Not surprisingly, related Raman studies of bone often have seemingly opposed interpretations. In reality, experimental design is usually lacking in at least one of these studies, largely due to unintentional ignorance of at least one context-specific variable that happens to be important. Such was likely the case for the large discrepancy in results of bone studies that attempted to use Raman spectral changes as a biomarker for diseases of decreased bone mechanical quality (see 2.4 Discussion)[2-6]. Those studies finding a significant association between mineral to collagen ratio and diseases of decreased mechanical quality often cited the use of the prominent peak ratio ν1 phosphate/amide I. Others citing no association between mineral to collagen ratio and diseases of decreased bone mechanical quality, happened to be using mineral to collagen ratios of ν2 phosphate/amide III or ν1 phosphate/proline. However, the observation that the mineral collagen ratio ν2 phosphate/amide III showed no differences as a function of disease may be equally valid. In fact, the differences between outcomes, now

examined in light of the results from the thesis, may imply that the results of the two studies agree insofar as the differences in mineral to collagen ratio observed by ν1 phosphate/amide I were driven by changes in local tissue organization and not composition.

Aforementioned discrepancies in research findings may be driven by the fact that the use of Raman spectroscopy for the diagnosis of bone disease is pushing the limits of commercially available RS technologies and systems. The historic use of Raman spectroscopy for chemical quality assurance was based upon the principle that certain peaks would move or be entirely absent under different chemical formulations due to a significant change in the distribution of dipolar bonds. More recent uses of near infrared Raman spectroscopy for the diagnosis of cancer can rely upon the fact that cancer greatly up-regulates amount of nuclear material relative to normal cells. Such a large change in chemical composition is not the case in the use of Raman spectroscopy for the assessment of bone quality because bone only has the three major dipolar chemical components: calcium hydroxyapatite, type I collagen, and water. The relative composition of bone is remarkably stable from the perspective of analytical chemistry. Essentially, to the untrained eye, the Raman spectrum of poor quality mouse bone and healthy adult human bone would appear the same. Rough estimates from data acquired during this thesis indicate that the bulk compositional change of bone with respect to age-related disease is well below 10%. Effectively, the mild progression of age-related bone disease, as well as the heterogeneous presentation of many major genetic bone diseases (including NF1[7], which displays heterogeneous cortical porosity and hypomineralization), implies that the traditional application of Raman spectroscopy may not be optimal for early detection of osteoporosis or heritable skeletal maladies. That said, the findings of this thesis indicate that RS can be

extremely effective as an investigative tool in the laboratory when instrumentation is appropriately modified to evaluate a specific hypothesis.

Rather than examining diseases where compositional change is arguably mild, there are several conditions where strong changes in composition are optimally matched to traditional Raman measurements. The exact compositional changes and mechanisms behind the formation of heterotopic ossification (the presence of mineralized collagenous nodules outside of bone) are still under debate[8]; however, Raman could easily identify the presence of ossified nodules. Infectious disease of bone is a source of major health burden associated with surgical revision and amputation, both for injured soldiers and hospital patients exposed to antibiotic resistant bacteria[9]. Virulent strains of Staphylococcus aureus are especially known for their formation of biofilms in bone, sequestering them from exposure to pharmacological treatment[10]. Early detection of these biofilms could be used to indicate the presence of Staphylococcus aureus and guide treatment decisions. Raman spectroscopy is also ideally suited to tracking and identifying the degradation products of biomaterials used in coatings implants and defect-filling cement. In this application, I envision a library-based function of known degradation products being matched to experimental samples to determine the relevant breakdown and better grasp the degree of material biocompatibility. Osteomyelitis, another example of infectious bone disease, is currently being investigated for detection potential by Raman Spectroscopy at the Morris lab. In the presence of diabetic neuropathy, lesions with specific osteomyelitis involvement contain brushite, mineralized phosphate-based material commonly associated with the exoskeleton of coral. Incidentally, brushite has a distinctly different phosphate peak from bone, allowing high sensitivity of detection[11, 12]. Finally, it may be possible to use Raman spectroscopy to help

investigate the finer points underpinning osteolytic and osteoblastic cancer lesions[13]. While the use of Raman spectroscopy as an early diagnostic technique for metastasis is intractable, given that metastatic lesions theoretically start as single cell entities, understanding exactly what happens compositionally when the cancer manipulates the surrounding bone extracellular matrix may prove to be valuable information when differentiating between potential mechanisms.

Raman Spectroscopy is not ideally sensitive to the presence of water in samples. While Raman shifts for water do exist, they reside beyond the fingerprint region, in high wavenumber bands. Therefore these bands were not included in this thesis. The effects of hydrogen bonding between tissue and water can also be measured with Raman Spectroscopy, but the very low wavenumber shifts are often swamped by specular reflectance of the laser input wavelength. That said, RS measurements may be related to NMR findings from bound and pore water hydrating the bone tissue. Decreased tissue hydration leads to brittleness[14] and a decrease in fracture toughness[15], even at physiological levels. Because artificial dehydration of collagen results in decreased sample volume and a change in the relative spacing between collagen molecules, it is possible that this happens at physiological levels as well. An increase in the local density of collagen molecules could lead to small changes in light throughput, and with confocal Raman, this could alter the content of Raman scattering reflected by each sample. Because Raman is sensitive to mechanical strain[16], observed shifts in wavenumber or subsequent changes in molecular alignment from polarized RS signatures could be the downstream results of changes in tissue hydration. It remains to be seen whether the body has any active mechanisms for controlling the incorporation of bound water into the bone matrix, or if the process is purely a passive component of matrix maturation in an aqueous environment. It will be important to

examine the effect of collagen packing in bone and its relationship to water, especially since the treatment raloxifene is purported to increase matrix hydration[17]. Examining the local heterogeneity of water content and how it corresponds to tissue microstructure could be accomplished by modifying Raman instrumentation and collection protocols to allow for full analysis of the high wavenumber RS signature of water in bone.

7.3.2 Polarization Raman spectroscopy for tissue organization

Traditionally RS is used for measuring chemical composition and to measure large changes in tissue biochemistry; however,information gathered throughout this thesis suggests that polarization in the Raman spectrum of bone has significant implications for the study of bone tissue organization. The polarization trends observed arise from several different factors. Placzek showed that the "Raman effect" is inherently affected by polarization, such that a pair of orthogonally oriented or “crossed” polarizers can be used to generate a depolarization ratio for each particular peak or bond as an inherent measure of the strength of the dipole and molecular chirality. In larger molecules or repeating structures including fibers and crystals, this translates into the inherent sensitivity of Raman polarization to molecular orientation. Because Raman spectroscopy is a scattering phenomenon, tissue birefringence also affects the propagation and subsequently measure of polarized light. Chapter 3 of the thesis shows that while this phenomenon could be effectively eliminated either by modulation of the instrument to depolarize the input laser beam, or by generating ratios of peaks that are matched in their polarization phase, polarization in Raman spectroscopy allows for the concurrent analysis of both composition and organization. Repeating patterns of birefringence and organized fibers and crystalline materials

are in fact common throughout the body, especially given the birefringence of fibrillar collagen molecules that make up a large proportion of the body's structural extracellular matrix. The techniques described in this thesis could also be applied to recognize the organizational structure in other tissues, as well as diagnosing the pathological loss of the interplay between organization and composition. Skeletal and cardiac muscle are composed of fibrous actin and myosin complexes, and are known to demonstrate birefringence. Muscle damage and disease investigations could benefit from the concurrent examination of fiber organization and compositional changes associated with their pathology.

The study of skin wound healing presents another exciting possibility. As skin heals, highly organized scar tissue is formed, and it is known that the degree of orientation, specifically heterogeneity in the directionality of collagen fibers contained within the scar, is associated with the mechanical integrity of the healed tissue. Chemical and burn wounds that denature the collagen of skin are currently examined by polarized light microscopy, such that worse burns show greater loss of tissue birefringence. The more detailed information regarding chemical composition and its interplay with fiber organization may assist in determining better metrics for tissue viability and mechanisms preceding the onset of tissue necrosis. It is important to note, however, that current technology for polarized Raman would be limited to examination of superficial or excised tissue. Polarization is not preserved through multiple scattering events in turbid media (most biological tissues), such that polarization Raman has the best high sensitivity to organization when coupled to confocal open beam microscopes. The use of polarization preserving fibers or other optics could allow access to deeper tissues; however, specific instrument redesign would be necessary in the context of these experiments.

7.3.3 The application of multivariate correlation analysis to Raman spectroscopy

The proper choice among statistical methods forms a crucial part of the effective analysis of any scientific hypothesis, but the analysis of Raman spectroscopy for bone poses its own unique set of problems. The methods employed throughout this thesis demonstrate the application of engineering problem solving methods to preserve data reliability while maximizing analytical power. The primary issue with the statistical analysis of Raman spectroscopy arises from the fact that the number of observations or samples "n" is significantly less than the observed number of variables. The vast majority of available statistical methods are predicated upon the assumption that the opposite is in fact true. Most multivariate statistical analyses are designed for psychological and epidemiological surveys, such that the expected number of samples would exceed the number of variables by several orders of magnitude[18]. To overcome the difficulty that this often poses in the analysis of Raman spectroscopy, spectral binning is employed to reduce the number of wavenumber based variables. Alternatively, the number of variables can be limited to prominent peaks or peak ratios that have previously been assigned a biochemical meaning[19]. However this is not possible in the case of multivariate analysis, especially when attempting to check the subtle changes that often arise outside the maximum peak intensity, as is the case for many of the polarization based changes that represent the organization of bone tissue[20, 21]. Previous works of Madahevan-Jansen {Mahadevan-Jansen, 1998 #238;Mahadevan-Jansen, 1996 #239} , applied multivariate dimension reduction and feature extraction techniques to classify disease states (ordinal outcome variables). This is a different statistical scenario than the continuous outcome variables given by bone biomechanics. Multivariate analysis in this situation can lead to singularities or "Heywood cases"[22] where the

iterative solution of complex multivariate methods may not converge to the correct answer, or to any answer at all.

Engineering a design from the “bottom-up” implies starting with fundamental principles, such that a bottom up statistical analysis would use the fundamental directions of variance or established variables. Alternatively, engineering from the “top-down” implies targeting the ultimate outcome and then choosing the best methods to achieve that outcome. Statistically, top-down designs would weight any variables, no matter how redundant or nonsensical, to achieve the best representation of the desired outcome. Bottom-up design focus on the reliability of results such that statistical analysis by principal components chooses the fundamental uncorrelated directions of variance, offering greater reliability and stability for interpretation at the possible sacrifice of under-explaining the data, as opposed to top-down designs which could potentially over fit the data set. This is especially challenging for bone where subtle changes occurring outside main biochemical peaks were found to associate with profound changes in mechanical outcomes. Recall that RS measures biochemical bond profiles in bone, and as such, indirectly associates with any mechanical changes. Moreover, mechanical changes are not necessarily the only changes associated with the age-related changes in bone biochemistry. Therefore, unlike the diagnosis of cancer where the largest biochemical changes likely correspond to the presence or class of disease, only a small subset of the biochemical changes in aging bone may be responsible for decreased fracture resistance.

This application of engineering design principles to the surplus number of variables in Raman spectroscopy successfully allowed the identification of RS signatures that have classified the bones of brittle animal models as well as correlated to continuous outcomes of fracture

toughness as a function of age. I utilized bottom-up data reduction via principal components constraining the model to the fundamental directions of variance and preventing over-fitting. Classifying bone in Chapter 5, I utilized sparse multinomial logistic regression of the principal components that significantly separate genotype (by a univariate nonparametric analysis) in a top-down iterative classification scheme, with the additional safety factor of leave-one-sample-out cross validation. Correlating image heterogeneity to bone fracture toughness in Chapter 6, we again constrain the statistical model using principal components to prevent over-fitting and bolster the validity of interpretation, while employing a top-down canonical correlation that weights the principal components to maximize linear redundancy and therefore the explanation of fracture toughness. Finally, the benefit of using the bottom-up method of principal components allows the user to view the spectral weightings in order to assign an appropriate biochemical meaning to the result.

Because high spectral resolution is necessary to fully characterize the subtle changes in polarization sensitive peak shoulder and overlapping peaks detailed in this dissertation, as polarization RS techniques improve, attempts should be made to analyze Raman spectra with even higher wavenumber resolution to find more subtle cues about the early underpinnings of progressive disease or slight differences in material properties. However analyses of samples from patients with rare atypical subtrochanteric femoral fractures (associated with long-term bisphosphonate use) and from rare human diseases (like Nf1) are even more precious than those used in this dissertation, further limiting the number of potential specimens. Applying these engineering principles in study design and statistical analysis will help to produce robust and reliable results in the future without sacrificing potentially critical information. Ultimately, the

real power of any statistical analysis is derived from the intelligent interpretation of meaning in light of the hypothesis posed. Nevertheless appropriate planning of a proper statistical design will result in less waste, and fewer spurious interpretations that could arise from the improper design of statistics when employing RS.

7.3.4 Bone heterogeneity across the anatomy: a link to biological mechanisms

The direct link between micro structural heterogeneity and the fracture toughness of bone will pose new hypotheses more than it validates existing ones. This thesis may represent the 1st time a quantitative measure of microstructural heterogeneity has been directly correlated to a quantitative measure of human fracture resistance, especially considering the microstructural heterogeneity of organization herein. The most prominent limitation across the studies was undersampling of anatomical diversity, given the presence and importance of heterogeneity as I observed in the femur. Specifically it will be important to evaluate whether or not microstructural heterogeneity is a strong determinant of fracture toughness throughout the anatomy or just in loadbearing long bones. We know from Wolff's law that bone adapts to the forces encountered, driving biological mechanisms of modeling and remodeling to allow the bone to resist diverse and changing force profiles[23]. The work of Jepsen et al. has shown that sources of anatomical variation have developed over time into specific anatomical traits, and these traits, including bone slenderness, impact how well the same bone from different people withstands similar mechanical forces[24]. Viewed in terms of Frost's mechanostat theory[25], anatomical differences and individual traits would affect the range of mechanical loads considered homeostatic, such that neither bone formation nor resorption would dominate. If this is accurate, the degree of tissue microstructure heterogeneity may be much more valuable to the

fracture resistance of certain individuals. One must also consider the findings of Ascenzi regarding the relationship between collagen orientations in sequential osteonal lamellae as it relates to the predominant mechanical forces encountered by a given region of the bone[26]. Different types and configurations of osteons (i.e. different collagen fibril orientations in sequential lamellae) are known to be found in different quadrants of long bones[27, 28], so it stands to reason that the relative impact of organizational heterogeneity may depend on the loadbearing role of the bone tissue in the body. For example, organizational heterogeneity of osteonal lamellae may be crucial to the fracture toughness of the femur, which is exposed to consistent cyclic heavy loading; however, the heterogeneity of composition may play a more significant role in the fracture toughness of a humerus or radius when experiencing momentary high level forces from an impact or static forces from carrying a burden. Knowledge that the fracture toughness mechanisms of bone are in fact rate-dependent[29, 30] makes this a distinct possibility.

Due to the tissue volume, ease of machining, and established methods of mechanical testing, the results of this thesis were derived almost entirely from the analysis of cortical bone; however, trabecular bone also exists at sites of osteoporotic fracture including the hip, distal radius, and lumbar spine vertebral bodies[31]. Since heterogeneity has already been associated with iliac crest biopsies[32] in the presence of fragility fracture[33, 34], it is likely that the results of microstructural heterogeneity for both composition and organization will translate directly to trabecular bone; however, the analysis of trabecular bone will present its own challenges, given that trabecular bone itself is comprised of heterogeneous features such as plates and rods at levels above the microstructural lamellar features. Therefore individual Raman measurements on one specific feature may be less representative of an entire structure. These hypotheses merit

validation before a direct link can be established between the value of microstructural heterogeneity and clinical osteoporotic fracture risk. The next step in the research process is to validate the heterogeneity findings across additional anatomical sites, specifically those implicated in osteoporosis (distal radius, lumbar spine, iliac crest, and femoral neck). Then it will be possible to determine the minimum sampling rate necessary to capture changes in organizational heterogeneity.

7.3.5 The use of Raman spectroscopy for the evaluation of the mechanical properties of materials

Methods and protocols in this thesis have applications outside of bone biomechanics, and even biological materials. Measurement of material organization using polarization Raman spectroscopy could provide significant new insights into the development of superior man-made materials ranging from biocompatible implant materials that could theoretically match patient specific mechanical properties, to structural composites used in building and manufacturing. Microstructural heterogeneity is known as an important factor in the determinant of material fracture resistance, especially for organic composites[35-38]. In the modern manufacture of lightweight but reliable composites, Raman spectroscopy could be used as a gatekeeper for quality assurance, and as a validation of new designs and manufacturing methods. That said, it is important to keep in mind the true benefits of Raman spectroscopy are twofold. Firstly, RS demonstrates superior sensitivity and specificity to narrowband changes in chemical bonds. Raman is able to detect even slight changes in the material that can be caused by environmental factors or gradual degradation. This can be seen in spectral changes during the fixation of bone[19], as well as the minute changes that happen in the spectrum of bone that undergo gradual

dehydration on the microscope stage. However, specifically because of the sensitivity to minute variation, it is important to note that the advantage of Raman spectroscopy is not statistical power; therefore, the use of RS to predict material properties will likely not reduce the number of samples necessary to complete a study. Rather, the best method to determine the effect of material composition and organization upon mechanical properties would be to build extensive library functions to weight appropriate spectral components with known impacts, necessitating large datasets to yield optimal results.

The second major advantage of using Raman to predict mechanical properties of materials would be its versatility. Specifically, the ability to manipulate RS instrumentation to evaluate different hypotheses makes the development of new protocols and methods more versatile in their application. For example, polarization maintaining fibers could be used to develop a probe that measures both organization and composition concurrently to be inserted deep within materials or the body, while confocal hand-held probes [39] could be used to measure the contribution of changes in heterogeneity from various layered structures, both natural and human-made.

Analysis of the principal components weightings that explained microstructural heterogeneity and the age-related decrease in human fracture toughness (Chapter 6) poses a significant question. Does the observed trend of competition between critical stress intensity (K) and strain energy release rate (J-integral) extends beyond aging to other diseases of bone, to other bodily tissues, or even to other organic composites? If so, these findings have a broader impact on our understanding of the fracture resistance of materials. In our constantly evolving digital society, there is a growing demand for lighter, more durable materials, all while still

increasing biointegration, both for medical implants within our own bodies, and for integration with the surrounding environment. Subsequently, polarization RS could be used in the iterative design of materials, owing largely to its unique capability to analyze the interplay between organization and composition across various length scales.

7.3.6 Discussing the influence of bone tissue heterogeneity on biomechanics

While synthetic materials could be designed to decouple critical stress intensity (K) from the strain energy release rate (J-integral) in the same way that some materials are both strong and tough, the materials comprising bone and biological tissues are fundamentally limited to production capabilities of the body. Therefore, a greater understanding of the relationship between fracture resistance and heterogeneity across the length scales will ultimately lead to better medicine for both diagnosis and improved therapeutics. While Chapter 6 provides quantitative evidence supporting theories suggesting that heterogeneity is a driving factor in the age-related loss of fracture toughness[40], a deeper analysis of the observed trends lends credence to the dichotomy of results observed by others[33, 41]. Examining the mechanics of materials in general, properties describing the maximum value of the load sustained by material until failure are often diametrically opposed to "area under the curve" properties that describe work to failure or energy dissipated. This is evidenced by the inherent conflict between strength and toughness in many natural and basic synthetic materials[42]. For example, polymeric materials like rubber bands have a high degree of toughness but low ultimate strength, while glass is strong yet brittle. The relationship between heterogeneity and fracture toughness, even within the microstructural length scale examined, likely exists on a bell curve distribution, such that there is an optimal

range of heterogeneity to produce the maximum fracture toughness outcomes. Insufficient heterogeneity would lead to a decrease in fracture toughness driven by a lack of compositional and organizational boundaries to deflect and deter crack growth and propagation. Excess heterogeneity would result in such large contrast between neighboring features like lamellae, that there would be a clearly defined path of least resistance along which the crack will propagate based solely upon the amount of energy required.

It is important to note that by the same principle heterogeneity at larger length scales is likely detrimental to bone. Results indicated that in spite of microstructural heterogeneity, average properties from the RS measurements of composition and organization between different microstructures average to the same value, having little correlation with fracture toughness. Changes severe enough to imbalance the average compositional properties of bone observed would likely have catastrophic results. Since the osteonal-interstitial border of only one microstructure in each bone was observed, it is also possible that the loss of microstructural heterogeneity is unique to only a small handful of features within each bone as a function of age. This would translate to a weakest link theory at a higher length scale, such that the osteon displaying a lack of heterogeneity would be the preferred location of crack propagation. Note that these two theories have opposite interpretations regarding the biological origins of age-related fracture toughness loss. Moreover, the current dichotomy of results regarding the impact of heterogeneity on fracture toughness doesn't suggest either of these mechanisms is more likely than the other.

While reality of complex biomechanics likely involves more contributing mechanisms (including the accumulation of microdamage or the shape and frequency of pores that serve as

stress risers), the findings of this thesis may indicate that optimal fracture toughness properties involve balancing J, K, and heterogeneity, effectively conserving mass and mechanical properties. On the other hand, it is also possible that the idea that bone achieves an "optimal" fracture toughness value for healthy individuals is an inherently flawed concept. The structural support the bone provides for the body is only one of its many functions, and in considering the degradation of mechanical properties like fracture toughness, it is easy to overlook imbalances caused by bone's other functions as a regulator of calcium and acid homeostasis, as well as regulation of metabolism through its action on insulin.

7.3.7 The implications for Raman spectroscopy is a diagnostic tool in the orthopedic clinic

This thesis has established the added value of analyzing polarization in Raman spectroscopy to achieve a greater explanation of the fracture resistance of bone; however, this also implies that the standard compositional measurements derived from RS analysis are insufficient on their own. Subsequently a paradigm shift in instrument design and data acquisition might be required for optimal explanation of bone quality. Namely, current Raman instruments for clinical application are built around fiber-optic delivery systems, but the vast majority of fiber optics do not preserve polarization, with systems opting instead for higher light throughput over larger volumes of tissue. This inherently allows for faster data acquisition in the clinic while minimizing the necessary laser exposure, applying a safety factor to established standards for laser irradiation. Moreover, current fiber-optic collection techniques allow for multiple scattering events in the tissue, resulting in a decrease in the preservation of polarization. Given that fracture toughness has been determined by heterogeneity of bone organization as

measured by polarization RS, decreased polarization information is effectively noise in the measurement of bone quality. To accomplish the original goal of using RS to assess bone quality for in situ surgical fixation decisions, special polarization maintaining fibers would be necessary. I propose the following design for a new polarization preserving probe: multiplexing polarization maintaining fibers to both irradiate and collect RS from a significant number of microstructural features simultaneously. Due to inherently small diameter of “panda” and “bowtie” fibers, several dozen be multiplexed into a probe less than 500 μm in diameter. This would allow for in situ imaging on the same length scale as data collected in this dissertation. Fiber lasers should allow for much smaller excitation fibers than current probes while preserving the necessary input power. From a safety aspect, the device would need to be designed with careful attention to fluence (energy per unit area), since the volumes irradiated would decrease drastically relative to current designs. The ultimate goal is to provide the surgeon with a quantitative analog for bone’s mechanical integrity within several seconds, making it easier to decide whether a certain procedure requires surgical pins, plates, or total joint replacement. Such a design could be calibrated for bone quality against the measure of pullout tests used to determine mechanical integrity for screw retention.

Polarization information could be acquired directly from the bone tissue when screening patients; however, this would require the creation of a small incision and the insertion of the Raman probe within a hypodermic needle. The need for sterilization, replaceable parts, local anesthesia and subsequent healing all detract from the normal advantages of Raman spectroscopy, which is touted for being nondestructive, rapid in acquisition, and relatively low cost. Therefore, while this option is feasible from a technological standpoint, human factors limit

the potential applicability of such a diagnostic tool. Even if spectral information would be defined directly from a probe touching the bone surface, the optimal explanation of mechanical bone quality would require the implementation of library functions such that measurements would be compared to population-specific statistics, not unlike the methodology currently used in scoring DXA and FRAX.

The final and perhaps most lofty goal for the application of Raman spectroscopy to bone quality was the development of a high throughput transdermal screening system for the early diagnosis of osteoporosis, such that earlier treatment would have a more significant impact on fracture risk prevention. However, the findings of this thesis strongly implicate the influence of organization and the need to polarize Raman spectroscopy in order to attain valid predictors of bone toughness and fracture toughness. With current RS instrumentation and technology, transdermal acquisition of bone through many layers of tissue requires the process called SORS (Spatially Offset Raman Spectroscopy), wherein distance between the excitation fiber and collection fibers at the surface of the specimen predispose the collection fibers to light that has traveled along a deeper "banana curve" shaped path while scattering through the layers of tissue[43]. The Morris lab has also applied this technology directly to the measure of bone through skin and muscle[44]. Because bone is one of the few tissues with a dominant mineral component and abnormally strong peaks, library functions of known spectra can be fit to collected data to remove the influence of Raman scatter from other tissue layers. However, polarization data is largely lost by multiple scattering events; therefore, the acquisition of organization information from deeper layers of tissues is currently intractable. Therefore Raman spectroscopy may not be the optimal technology for the clinical screening of osteoporosis at this time. In the future, the

reconstruction of polarization information after it has traveled through several layers of tissue may be possible.

7.3.8 Potential mechanisms for the age-related decrease in fracture toughness

Without delving into the application of Raman spectroscopy for future use in orthopedic medicine, the finding that the interplay between tissue organization and composition drives mechanical bone quality in both human aging and in animal models of several genetic diseases may be significant for our understanding of bone biology. Several possible mechanisms could be responsible for the observations in Chapters 5 and 6. The observed decrease in heterogeneity seems to imply a failure in the normal system by which cells maintain the microstructural organization of bone tissue. Under normal circumstances when tissue is damaged, leading theories suggest that osteocyte death signaling begins basic multicellular unit processes of remodeling; however, it is possible that with aging, a downward spiral of functional inequivalence begins. For example, let's suppose that during the formation of the new osteon, osteoblasts require the organization of the matrix to which they are attached in order to correctly organize the new bone matrix that they are currently synthesizing. If the matrix undergoes a large amount of microdamage accumulation resulting in the entropy of organization, this could lead to the failure of mechanosensing. Osteoblasts remodeling the damage would deposit new tissue as inappropriately oriented lamellar. Because we know that lamellar orientation is essential for the appropriate resistance to local forces, these inappropriately oriented lamellae would subsequently sustain more microdamage, and more organizational information would be lost to the next remodeling activity.

Alternatively a downward spiral could also initiate at the osteoblasts themselves, if they lose the ability to sense the organization of the surroundings. This type of failure could occur at any step in the process. A change in the speed of osteocyte turnover could result in a failure of the tissue to appropriately mechanically sense damage, leading to a failure to remodel. While the various redundancies in autocrine and paracrine signaling between bone cells make this option less likely, a specific cell population failure could lead to the uncoupling of remodeling and subsequently a loss of bone mass that also translates into a loss of microstructural heterogeneity. Osteoblasts could be responsible if aging results in a decreased output of collagen and mineral. Osteoclasts could be responsible if the long-term maturation and fusion results in greater enzymatic production capabilities. Since osteocytes are practically required to live for the duration of the bone tissue lifecycle, it is also feasible to hypothesize that osteocytes are more likely with age to undergo inappropriate cell death, such that remodeling is not triggered and damage accumulates.

Discussion of possible cellular mechanisms supported by the findings of this thesis eventually presents a causality dilemma, the proverbial “chicken and the egg”. Just as cells may fail to detect the bone tissue organization properly, it is possible that the bone tissue fails before the cellular damage detection and repair mechanisms. In the study of the extracellular matrix, it is well known that many smaller proteins embedded into the matrix, and degradable byproducts from structural proteins are also cues for cellular signaling, resulting in redundancy that ensures proper matrix growth and maintenance. In the case of bone, the non-collagenous proteins osteocalcin and osteopontin have structural roles in forming dilatational bands[45], local bone cell signaling roles, and systemic signaling as part of bone’s non-structural functions. If non-

collagenous proteins became ineffective, down-regulated, or improperly formed, it would not only mean that bone tissue was more susceptible to the formation of microdamage, but also that the signaling pathways that regulate remodeling processes responsible for repairing that damage would be inhibited. The large number of potential mechanisms discussed could have any number of interactions to explain how the complex structure and functions of bone are compromised in aging and disease; however, the development of polarization Raman Spectroscopy has led to a tool that can be used to help address these hypotheses.

The greater implications of this work stem from the finding that the proper analysis of bone, by Raman spectroscopy requires control of instrument polarization. The elimination of polarization from the instrument allows for pure compositional measurements; however, dissertation findings support the idea that instead of eliminating polarization as noise, it can be used to obtain more detailed information about the structure of bone. The dissertation shows that there is a strong link between the biochemical heterogeneity of tissue and its mechanical resistance. These findings could be leveraged to advance the use of RS in the study of tissue, as detailed above, but they also extend to the study of natural and artificial materials, including bio-mimicry and the tuning of mechanical properties. Insofar as the traditional RS analyses alone did not explain fracture resistance, this dissertation implies that polarization in RS may be necessary for the explanation of biochemical profiles that are associated with material properties. Although polarization microscopy has been used for years to analyze birefringent materials (including bone), polarized RS offers the additional benefit of quantifying organization of specific biochemical moieties. Because I specifically developed the techniques of peak phase matching so that instruments would not need complete elimination of polarization, this also allows for

"first pass" investigation of whether or not organization plays a role in the chemical profile of material mechanics, while still obtaining compositional profiles for which Raman instruments are designed. With careful attention to polarization, better RS analysis of bone and other materials may lead to greater understanding of the chemical changes underlying the resistance to mechanical failure.

7.4 Contributions to the Field and Societal Impact

While the most important aspect of scientific research is arguably making careful observations in order to form well-posed testable hypotheses, the most difficult aspect of research pursuits is indubitably evaluating these hypotheses systematically until the original observations are mechanistically explained in a way that has an impact on the greater body of science and society. In the field of biomedical engineering, this practically amounts to improving our understanding of the human body and disease while developing technology that directly impacts patient diagnosis or treatment. Four years ago, I was brought into a project that was assessing and standardizing the proper preparation methods for human and animal bone to achieve reliable Raman spectroscopy results. This thesis started with the observation that certain Raman metrics of bone composition have abnormally high variation. I tied that observation to the polarization sensitivity of Raman spectroscopy, and then built upon the relatively small body of polarization RS literature to show that trends in sensitivity followed optical theory and were therefore dependable as a metric of organization in birefringent tissue like bone. This knowledge has helped me produce guidelines for the use of standard RS peak ratios to express bone composition and organization, helping to resolve seeming conflict in the interpretation of other

Raman studies when instrument polarization and bone organization were not taken into account. Armed with this new knowledge, I then assessed the relationship between bone mechanical properties and Raman spectroscopy across multiple length scales and species, for both standard mechanical analyses and fracture mechanics. The new polarization technique and protocols of measuring bone at multiple orientations has allowed me to use RS to identify the influence of organization in genetically modified animal models of brittle bone where standard compositional RS measurements were insensitive to the phenotype. Applying these techniques to age-related changes in fracture risk, we saw early on that the bulk composition of bone was not strongly correlated with its fracture toughness, such that the same trend of higher variation in RS data was now observed in association with lower fracture toughness. I associated this variability with an existing body of literature that implicates microstructural heterogeneity as a factor in human fracture risk. Ultimately this led to the finding that polarization RS signatures of microstructural tissue heterogeneity serve as a strong driving force in the age-related decrease in fracture toughness. In the meantime, field leaders with whom I have had regular correspondence regarding heterogeneity, have completed studies suggesting that microstructural heterogeneity is associated with fragility fracture in osteoporosis patients. The findings of this thesis help to tie these observations to a better mechanistic understanding of the progression of this debilitating disease.

Aside from the main novel results of the thesis, several contributions to the field have been made along the way. I participated in standardizing the methods for samples preparation and Raman collection, and have subsequently been contacted by colleagues at other universities to help establish these protocols in their laboratories. Our results in polarization Raman

spectroscopy have resulted in contact from design engineers at Renishaw, a leading manufacturer of Raman spectroscopy devices, soliciting advice on the development of next-generation devices to allow for more flexible analysis of polarization in Raman spectroscopy. Early results in tissue heterogeneity resulted in an invitation to apply for, and subsequently obtain a scholarship to attend the 2013 Bone Quality and Fracture Prevention Research Symposium hosted by the Orthopedic Research Society and the American Academy of Orthopedic Surgeons, where I was given the opportunity to spread the knowledge that fracture risk in bone is more than a question of simply assessing bone strength by x-ray. One-on-one discussions with field leaders and physician-scientists resulted in the inclusion of my ideas on bone heterogeneity in the published report. Since then, I have found multiple articles from attendees with whom I spoke evaluating the impact of tissue microstructural heterogeneity of composition and organization on different aspects of bone quality. The symposium also led to the discussion of tissue microstructural heterogeneity as a possible driving factor behind the atypical femoral fractures associated with long-term use of bisphosphonate therapy in a special session at ORS 2014. At this meeting, a specific call was made expressing the need for better quantification of tissue heterogeneity in relation to this problem.

In order to complete these scientific studies, it was necessary for me to develop methods, protocols, and device components to overcome several technical obstacles. A great deal of technical rigor was required in order to integrate light-tissue interactions and optical theory to advance polarization RS beyond a method that was previously only being used to visualize osteon features and lamellar spacing in the same way this could be accomplished with regular polarized light microscopy. Manufacturer’s recommendations for assembly of RS

instrumentation often mention polarization only briefly as a potential source of variance in data collection, not as a phenomenon that could be exploited to explore organization, so limited technical specifications are available for existing instrument components. Raman sources are marketed and sold without standard reporting of laser polarization extinction ratio. Therefore, before acquiring any valid data, I had to establish the impact of each basic optical component on polarization preservation through the instrument, and then systematically prove that my observations were not simply an artifact of instrument design. In order to validate my theory, I needed to develop custom rotation stages for both the samples and the laser housing. To make my findings usable by the rest of the field, I also established that inherent instrument polarization was sufficient to acquire a measure of bone organization from a minimal data set, requiring only replication of the measurement at 0° and 90° relative to the bone long axis using a set of peak ratios specifically defined based upon their polarization phase. I furthered these techniques to include multivariate analysis, where I had to overcome analysis issues for the new methods of polarization analysis. I attempted various mathematical combinations, but subsequent multivariate data reduction weighted nonsensical components. To use all the wavenumbers from both orientations, I resolved the issue of excessive variables (known as rank deficiency) in full spectrum RS analysis by employing engineering design strategies to balance assumptions about the data. By choosing and evaluating unsupervised data reduction methods, I identified RS signatures of brittle genotypes using established classification algorithms, and explained fracture toughness using canonical correlation. Bottom-up designs also allowed for post-hoc analysis of heavily weighted features to explain the biochemistry underlying these statistical operations.

Throughout this thesis, I have actively spread knowledge of the applicability of Raman spectroscopy as well as the need for better measurements of bone quality that appropriately explain bone mechanics. I assessed the mechanics of bone across multiple length scales using nanoindentation, reference point indentation at the microstructural level, fracture toughness testing, and whole bone biomechanics. I actively developed and validated detailed protocols and standard operating procedures for the preparation of both whole animal bones and human bone samples (single edge notched beams) for fracture toughness testing, even performing a study where I evaluated existing techniques by altering the location of the notch in mouse femurs. Using materials science knowledge I had learned during collaboration with the Pharr lab at UT Knoxville in the preparation for and conducting of nanoindentation testing, I then modified these protocols to include specimen grinding and polishing, eliminating material damage from the machining process and it's known impacts on Raman spectroscopy[46] as a source of noise. I have also applied these methods and protocols outside of the projects directly included in this thesis. I used the technique of polarization Raman spectroscopy to nondestructively analyze the effects of a drug used to treat defects of bone mineralization on the skeleton of mice with NF1 gene ablation, confirming the partial rescue of hypomineralization in a high-profile Nature Medicine study that may help guide future treatment parameters for young children. I'm thankful for the opportunity to have applied these techniques in such high-profile studies that may eventually impact the practice of orthopedic medicine.

7.5 References

1. McElderry, J.D., Kole, M.R. and Morris, M.D., "Repeated freeze-thawing of bone tissue affects Raman bone quality measurements," Journal of biomedical optics **16**(7), 071407 (2011)
2. Masic, A., Bertinetti, L., Schuetz, R., Galvis, L., Timofeeva, N., Dunlop, J.W., Seto, J., Hartmann, M.A. and Fratzl, P., "Observations of multiscale, stress-induced changes of collagen orientation in tendon by polarized Raman spectroscopy," Biomacromolecules **12**(11), 3989-3996 (2011)
3. Maher, J.R., Takahata, M., Awad, H.A. and Berger, A.J., "Raman spectroscopy detects deterioration in biomechanical properties of bone in a glucocorticoid-treated mouse model of rheumatoid arthritis," Journal of biomedical optics **16**(8), 087012 (2011)
4. Buchwald, T., Niciejewski, K., Kozielski, M., Szybowicz, M., Siatkowski, M. and Krauss, H., "Identifying compositional and structural changes in spongy and subchondral bone from the hip joints of patients with osteoarthritis using Raman spectroscopy," Journal of biomedical optics **17**(1), 017007 (2012)
5. Kozielski, M., Buchwald, T., Szybowicz, M., Blaszczak, Z., Piotrowski, A. and Ciesielczyk, B., "Determination of composition and structure of spongy bone tissue in human head of femur by Raman spectral mapping," Journal of materials science. Materials in medicine **22**(7), 1653-1661 (2011)
6. Szabo, M.E., Zekonyte, J., Katsamenis, O.L., Taylor, M. and Thurner, P.J., "Similar damage initiation but different failure behavior in trabecular and cortical bone tissue," J Mech Behav Biomed Mater **4**(8), 1787-1796 (2011)
7. de la Croix Ndong, J., Makowski, A.J., Uppuganti, S., Vignaux, G., Ono, K., Perrien, D.S., Joubert, S., Baglio, S.R., Granchi, D., Stevenson, D.A., Rios, J.J., Nyman, J.S. and Elefteriou, F., "Asfotase-alpha improves bone growth, mineralization and strength in mouse models of neurofibromatosis type-1," Nature medicine **20**(8), 904-910 (2014)
8. Peterson, J.R., Okagbare, P.I., De La Rosa, S., Cilwa, K.E., Perosky, J.E., Eboda, O.N., Donneys, A., Su, G.L., Buchman, S.R. and Cederna, P.S., "Early detection of burn induced heterotopic ossification using transcutaneous Raman spectroscopy," Bone **54**(1), 28-34 (2013)
9. Murray, C.K., Obremskey, W.T., Hsu, J.R., Andersen, R.C., Calhoun, J.H., Clasper, J.C., Whitman, T.J., Curry, T.K., Fleming, M.E., Wenke, J.C. and Ficke, J.R., "Prevention of infections associated with combat-related extremity injuries," The Journal of trauma **71**(2 Suppl 2), S235-257 (2011)
10. Cassat, J.E., Lee, C.Y. and Smeltzer, M.S., "Investigation of biofilm formation in clinical isolates of Staphylococcus aureus," in Methicillin-Resistant Staphylococcus aureus (MRSA) Protocols, pp. 127-144, Springer (2007).

11. Penel, G., Leroy, N., Van Landuyt, P., Flautre, B., Hardouin, P., Lemaitre, J. and Leroy, G., "Raman microspectrometry studies of brushite cement: in vivo evolution in a sheep model," Bone **25**(2 Suppl), 81S-84S (1999)

12. Esmonde-White, K.A., Esmonde-White, F.W., Holmes, C.M., Morris, M.D. and Roessler, B.J., "Alterations to bone mineral composition as an early indication of osteomyelitis in the diabetic foot," Diabetes care **36**(11), 3652-3654 (2013)

13. Bi, X., Sterling, J.A., Merkel, A.R., Perrien, D.S., Nyman, J.S. and Mahadevan-Jansen, A., "Prostate cancer metastases alter bone mineral and matrix composition independent of effects on bone architecture in mice—A quantitative study using microCT and Raman spectroscopy," Bone **56**(2), 454-460 (2013)

14. Nyman, J.S., Roy, A., Shen, X., Acuna, R.L., Tyler, J.H. and Wang, X., "The influence of water removal on the strength and toughness of cortical bone," J Biomech **39**(5), 931-938 (2006)

15. Nalla, R.K., Kinney, J.H., Tomsia, A.P. and Ritchie, R.O., "Role of alcohol in the fracture resistance of teeth," J Dent Res **85**(11), 1022-1026 (2006)

16. Schadler, L.S. and Galiotis, C., "Fundamentals and applications of micro Raman spectroscopy to strain measurements

in fibre reinforced composites," International Materials Reviews **40**(3), 116 (1995)

17. Gallant, M.A., Brown, D.M., Hammond, M., Wallace, J.M., Du, J., Deymier-Black, A.C., Almer, J.D., Stock, S.R., Allen, M.R. and Burr, D.B., "Bone cell-independent benefits of raloxifene on the skeleton: a novel mechanism for improving bone material properties," Bone **61**(191-200 (2014)

18. Sherry, A. and Henson, R.K., "Conducting and interpreting canonical correlation analysis in personality research: A user-friendly primer," Journal of Personality Assessment **84**(1), 37-48 (2005)

19. Nyman, J.S., Makowski, A.J., Patil, C.A., Masui, T.P., O'Quinn, E.C., Bi, X., Guelcher, S.A., Nicollela, D.P. and Mahadevan-Jansen, A., "Measuring differences in compositional properties of bone tissue by confocal Raman spectroscopy," Calcif Tissue Int **89**(2), 111-122 (2011)

20. Falgayrac, G., Facq, S., Leroy, G., Cortet, B. and Penel, G., "New method for Raman investigation of the orientation of collagen fibrils and crystallites in the Haversian system of bone," Applied spectroscopy **64**(7), 775-780 (2010)

21. Leroy, G., Penel, G., Leroy, N. and Brès, E., "Human Tooth Enamel: A Raman Polarized Approach," Applied spectroscopy **56**(8), 1030-1034 (2002)

22. Johnson, R.A., Wichern, D.W. and Education, P., Applied multivariate statistical analysis, Prentice hall Englewood Cliffs, NJ (1992).

23. Wolff, J., Das Gesetz der Transformation der Knochen, von Dr Julius Wolff, A. Hirschwald, Berlin (1892).

24. Jepsen, K.J., Centi, A., Duarte, G.F., Galloway, K., Goldman, H., Hampson, N., Lappe, J.M., Cullen, D.M., Greeves, J. and Izard, R., "Biological constraints that limit compensation of a common skeletal trait variant lead to inequivalence of tibial function among healthy young adults," Journal of Bone and Mineral Research **26**(12), 2872-2885 (2011)

25. Frost, H., "Bone “mass” and the “mechanostat”: a proposal," The Anatomical Record **219**(1), 1-9 (1987)

26. Ascenzi, M.G. and Lomovtsev, A., "Collagen orientation patterns in human secondary osteons, quantified in the radial direction by confocal microscopy," Journal of structural biology **153**(1), 14-30 (2006)

27. Portigliatti Barbos, M., Bianco, P., Ascenzi, A. and Boyde, A., "Collagen orientation in compact bone: II. Distribution of lamellae in the whole of the human femoral shaft with reference to its mechanical properties," Metabolic Bone Disease and Related Research **5**(6), 309-315 (1984)

28. Boyde, A., Bianco, P., Portigliatti Barbos, M. and Ascenzi, A., "Collagen orientation in compact bone: I. A new method for the determination of the proportion of collagen parallel to the plane of compact bone sections," Metabolic Bone Disease and Related Research **5**(6), 299-307 (1984)

29. Nalla, R.K., Stolken, J.S., Kinney, J.H. and Ritchie, R.O., "Fracture in human cortical bone: local fracture criteria and toughening mechanisms," J Biomech **38**(7), 1517-1525 (2005)

30. Kruzic, J.J., Nalla, R.K., Kinney, J.H. and Ritchie, R.O., "Crack blunting, crack bridging and resistance-curve fracture mechanics in dentin: effect of hydration," Biomaterials **24**(28), 5209-5221 (2003)

31. Johnell, O. and Kanis, J.A., "An estimate of the worldwide prevalence and disability associated with osteoporotic fractures," Osteoporos Int **17**(12), 1726-1733 (2006)

32. Donnelly, E., Meredith, D.S., Nguyen, J.T. and Boskey, A.L., "Bone tissue composition varies across anatomic sites in the proximal femur and the iliac crest," Journal of Orthopaedic Research **30**(5), 700-706 (2012)

33. Gourion‐Arsiquaud, S., Lukashova, L., Power, J., Loveridge, N., Reeve, J. and Boskey, A.L., "Fourier transform infrared imaging of femoral neck bone: Reduced heterogeneity of mineral‐to‐matrix and carbonate‐to‐phosphate and more variable crystallinity in treatment‐naive fracture cases compared with fracture‐free controls," Journal of Bone and Mineral Research **28**(1), 150-161 (2013)

34. Donnelly, E., Meredith, D.S., Nguyen, J.T., Gladnick, B.P., Rebolledo, B.J., Shaffer, A.D., Lorich, D.G., Lane, J.M. and Boskey, A.L., "Reduced cortical bone compositional

heterogeneity with bisphosphonate treatment in postmenopausal women with intertrochanteric and subtrochanteric fractures," J Bone Miner Res **27**(3), 672-678 (2012)

35. Sela, N., Ishai, O. and Banks-Sills, L., "The effect of adhesive thickness on interlaminar fracture toughness of interleaved CFRP specimens," Composites **20**(3), 257-264 (1989)

36. Kolednik, O., Predan, J., Fischer, F.D. and Fratzl, P., "Bioinspired Design Criteria for Damage-Resistant Materials with Periodically Varying Microstructure," Advanced Functional Materials **21**(19), 3634-3641 (2011)

37. Munch, E., Launey, M.E., Alsem, D.H., Saiz, E., Tomsia, A.P. and Ritchie, R.O., "Tough, bio-inspired hybrid materials," Science **322**(5907), 1516-1520 (2008)

38. Pukánszky, B. and Maurer, F.H., "Composition dependence of the fracture toughness of heterogeneous polymer systems," Polymer **36**(8), 1617-1625 (1995)

39. Lieber, C.A., Majumder, S.K., Ellis, D.L., Billheimer, D.D. and Mahadevan‐Jansen, A., "In vivo nonmelanoma skin cancer diagnosis using Raman microspectroscopy," Lasers in surgery and medicine **40**(7), 461-467 (2008)

40. Nalla, R.K., Kruzic, J.J., Kinney, J.H., Balooch, M., Ager, J.W. and Ritchie, R.O., "Role of microstructure in the aging-related deterioration of the toughness of human cortical bone," Materials Science & Engineering C-Biomimetic and Supramolecular Systems **26**(8), 1251-1260 (2006)

41. Roschger, P., Lombardi, A., Misof, B., Maier, G., Fratzl‐Zelman, N., Fratzl, P. and Klaushofer, K., "Mineralization density distribution of postmenopausal osteoporotic bone is restored to normal after long‐term alendronate treatment: qBEI and sSAXS data from the fracture intervention trial long‐term extension (FLEX)," Journal of Bone and Mineral Research **25**(1), 48-55 (2010)

42. Ritchie, R.O., "The conflicts between strength and toughness," Nature materials **10**(11), 817-822 (2011)

43. Keller, M.D., Vargis, E., de Matos Granja, N., Wilson, R.H., Mycek, M.A., Kelley, M.C. and Mahadevan-Jansen, A., "Development of a spatially offset Raman spectroscopy probe for breast tumor surgical margin evaluation," Journal of biomedical optics **16**(7), 077006 (2011)

44. Schulmerich, M.V., Cole, J.H., Kreider, J.M., Esmonde-White, F., Dooley, K.A., Goldstein, S.A. and Morris, M.D., "Transcutaneous Raman spectroscopy of murine bone in vivo," Applied spectroscopy **63**(3), 286-295 (2009)

45. Poundarik, A.A., Diab, T., Sroga, G.E., Ural, A., Boskey, A.L., Gundberg, C.M. and Vashishth, D., "Dilatational band formation in bone," Proceedings of the National Academy of Sciences **109**(47), 19178-19183 (2012)

46. Timlin, J.A., Carden, A., Morris, M.D., Rajachar, R.M. and Kohn, D.H., "Raman spectroscopic imaging markers for fatigue-related microdamage in bovine bone," Anal Chem **72**(10), 2229-2236 (2000)